Proceedings of the symposium on threshold meson production in pp and pd interaction

Edited by P. Moskal and M. Wolke

Extended COSY-11 Collaboration Meeting
20 – 24 June 2001
Institute of Physics, Jagellonian University, Cracow

List of Attendees

Heinz-Hermann Adam	adamh@uni-muenster.de
Andrzej Bałanda	balanda@if.uj.edu.pl
Steven D. Bass	sbass@ect.it
Kazimierz Bodek	ufbodek@jetta.if.uj.edu.pl
Andrzej Budzanowski	andrzej.budzanowski@ifj.edu.pl
Saša Ceci	ceci@rudjer.irb.hr
Johann Haidenbauer	j.haidenbauer@fz-juelich.de
Ashot Gasparyan	g.achot@fz-juelich.de
Dieter Grzonka	d.grzonka@fz-juelich.de
Alfons Khoukaz	khoukaz@uni-muenster.de
Lucjan Jarczyk	jarczyk@if.uj.edu.pl
Bogusław Kamys	ufkamys@cyf-kr.edu.pl
Kurt Kilian	k.kilian@fz-juelich.de
Małgorzata Kistryn	mkistryn@if.uj.edu.pl
Stanisław Kistryn	skistryn@if.uj.edu.pl
Frieder Kleefeld	kleefeld@cfif.ist.utl.pt
Wojciech Klimala	klimala@pisa.if.uj.edu.pl
Christian Kolf	c.kolf@fz-juelich.de
Piotr Kowina	p.kowina@fz-juelich.de
Reinhard Kulessa	kulessa@jetta.if.uj.edu.pl
Joanna Kuroś-Żołnierczuk	kuros@if.uj.edu.pl
Norbert Lang	langn@ikp.uni-muenster.de
Andrzej Magiera	magiera@if.uj.edu.pl
Paweł Moskal	ufmoskal@sigma.if.uj.edu.pl
Kanzo Nakayama	nakayama@arches.uga.edu
Walter Oelert	w.oelert@fz-juelich.de
Piotr Salabura	salabura@psja1.if.uj.edu.pl
Georg Schepers	g.schepers@fz-juelich.de
Thomas Sefzick	t.sefzick@fz-juelich.de
Marek Siemaszko	siemaszk@us.edu.pl
Roman Skibiński	skibinsk@modrzew.if.uj.edu.pl
Jerzy Smyrski	smyrski@if.uj.edu.pl
Siegfried Steltenkamp	steltes@math.uni-muenster.de
Elżbieta Stephan	stephan@us.edu.pl
Hans Stockhorst	h.stockhorst@fz-juelich.de
Adam Strzałkowski	ufstrzal@cyf-kr.edu.pl
Antoni Szczurek	szczurek@alf.ifj.edu.pl
Peter Winter	p.winter@fz-juelich.de
Magnus Wolke	m.wolke@fz-juelich.de
Peter Wüstner	p.wuestner@fz-juelich.de
Sławomir Wycech	slawomir.wycech@fuw.edu.pl
Wiktor Zipper	zipper@us.edu.pl

photo: Andrzej Magiera

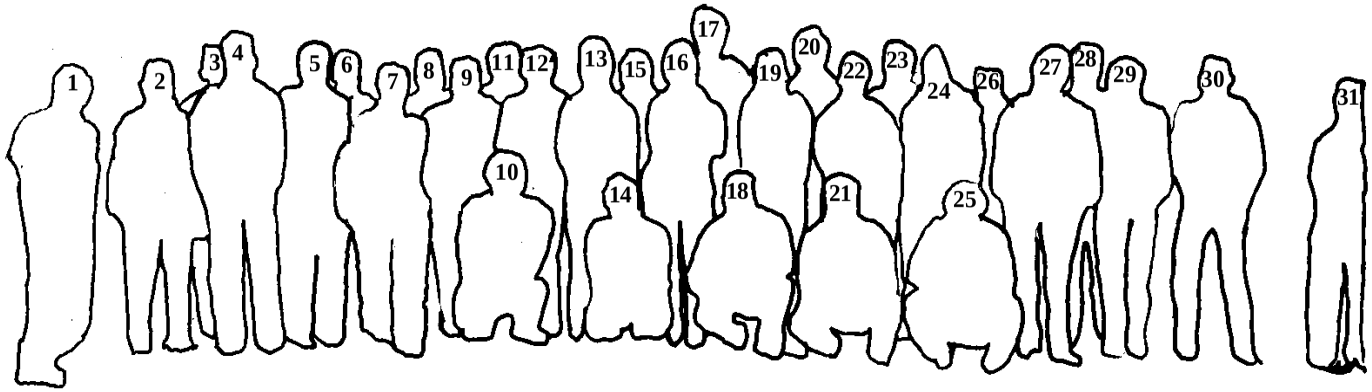

1 Lucjan Jarczyk
2 Hans Stockhorst
3 Peter Winter
4 Piotr Salabura
5 Reinhard Kulessa
6 Christian Kolf
7 Sławomir Wycech
8 Walter Oelert
9 Wiktor Zipper
10 Bogusław Kamys
11 Georg Schepers
12 Stanisław Kistryn
13 Marek Siemaszko
14 Piotr Kowina
15 Dieter Grzonka
16 Frieder Kleefeld
17 Magnus Wolke
18 Paweł Moskal
19 Thomas Sefzick
20 Kurt Kilian
21 Kanzo Nakayama
22 Peter Wüstner
23 Siegfried Steltenkamp
24 Heinz-Hermann Adam
25 Saša Ceci
26 Alfons Khoukaz
27 Steven D. Bass
28 Norbert Lang
29 Johann Haidenbauer
30 Ashot Gasparyan
31 Małgorzata Kistryn

Foreword

Physics at medium energies has been and will continue to be one of the major activities of the Research Centre Jülich. For this purpose the Cooler Synchrotron COSY was built and has received considerable support during the last decade. Only recently the bodies of the Research Center have agreed to upgrade COSY by installing a new injector for the provision of polarized proton and deuteron beams with much higher intensities and better quality.

The present proceedings of the Symposium on Threshold Meson Production in pp and pd Interaction are giving a most impresive testimony of the scientific activities and engagements of one part of a large international community working successfully at COSY, in this particular case the COSY–11 collaboration.

This year the related annual COSY–11 collaboration meeting was hosted by our friends from the Jagellonian University at Cracow who, indeed, have taken a strong part in the successful COSY–11 collaboration as witnessed in this booklet. The latter is giving account of a healthy combination of both experimental and theoretical achievements, interpretation of experimental data and new ideas for future research directions.

I strongly regret that I could not participate at these obviously vivid, interesting and inspiring discussions, which do highlight what has been achieved at this threshold facility of COSY, what are the goals in this particular physics research fields and how it might develop in the future.

I hope that COSY–11, and COSY in general, will continue to work on this exciting road of physics for a better understanding of fundamental aspects in hadron physics.

Richard Wagner
Forschungszentrum Jülich
Jülich, September 17th 2001

Acknowledgements

Results of the investigations reported in this proceedings would be impossible without the financial support which we received from the International Büro and the Verbundforschung of the BMBF, the Polish State Committee for Scientific Research, the FFE grants from the Forschungszentrum Jülich, the Forschungszentrum Jülich directorates, and the European Community - Access to Research Infrastructure action of the Improving Human Potential Programme.

Contents

Gluonic effects in η'-nucleon interactions[1]

Steven D. Bass

European Centre for Theoretical Studies in Nuclear Physics and Related Areas, Villazzano (Trento), Italy

Abstract: We review the theory and phenomenology of the axial U(1) problem with emphasis on the role of gluonic degrees of freedom in the low-energy $pp \to pp\eta$ and $pp \to pp\eta'$ reactions.

1 Introduction

η and η' physics together with polarised deep inelastic scattering provide complementary windows on the role of gluons in dynamical chiral symmetry breaking. Gluonic degrees of freedom play an important role in the physics of the flavour-singlet $J^P = 1^+$ channel [1] through the QCD axial anomaly [2]. The most famous example is the $U_A(1)$ problem: the masses of the η and η' mesons are much greater than the values they would have if these mesons were pure Goldstone bosons associated with spontaneously broken chiral symmetry [3, 4]. This extra mass is induced by non-perturbative gluon dynamics [5, 6, 7, 8] and the axial anomaly [9, 10].

For the first time since the discovery of QCD (and the U(1) problem) precise data are emerging on processes involving η' production and decays. There is presently a vigorous experimental programme to study the $pp \to pp\eta$ and $pp \to pp\eta'$ reactions close to threshold in low-energy proton-nucleon collisions at CELSIUS [11] and COSY [12]. New data on η' photoproduction, $\gamma p \to p\eta'$, are expected soon from Jefferson Laboratory [13] following earlier measurements at ELSA [14]. The light-mass "exotic" meson states with quantum numbers $J^{PC} = 1^{-+}$ observed at BNL [15] and CERN [16] in $\pi^- p$ and $\bar{p}N$ scattering were discovered in decays to $\eta\pi$ and $\eta'\pi$ suggesting a possible connection with axial U(1) dynamics. Further "exotic" studies are proposed in photoproduction experiments at Jefferson Laboratory. At higher energies anomalously large branching ratios have been observed by CLEO for B-meson decays to an η' plus additional hadrons [17] and for the $D_s^+ \to \eta'\rho^+$ [18] process. The B decay measurements have recently been

[1] Invited lecture

confirmed in new, more precise, data from BABAR [19] and BELLE [20]. The LEP data on η' production in hadronic jets is about 40 % short of the predictions of the string fragmentation models employed in the JETSET and ARIADNE Monte-Carlos without an additional η' "suppression factor" [21]. First measurements of $\eta' \to \gamma\gamma^*$ decays have been performed at CLEO [22]. The new WASA 4π detector [23] at CELSIUS will enable precision studies of η and η' decays. Data expected in the next few years provides an exciting new opportunity to study axial U(1) dynamics and to investigate the role of gluonic degrees of freedom in η and η' physics.

In this lecture we focus primarily on η' production in proton-proton collisions together with a brief review of the axial U(1) problem in QCD.

The role of gluonic degrees of freedom and OZI violation in the η'–nucleon system has been investigated through the flavour-singlet Goldberger-Treiman relation [24, 25], the low-energy $pp \to pp\eta'$ reaction [26] and η' photoproduction [27]. The flavour-singlet Goldberger-Treiman relation connects the flavour-singlet axial-charge $g_A^{(0)}$ measured in polarised deep inelastic scattering with the η'–nucleon coupling constant $g_{\eta' NN}$. Working in the chiral limit it reads

$$M g_A^{(0)} = \sqrt{\frac{3}{2}} F_0 \Big(g_{\eta' NN} - g_{QNN} \Big) \tag{1}$$

where $g_{\eta' NN}$ is the η'–nucleon coupling constant and g_{QNN} is an OZI violating coupling which measures the one particle irreducible coupling of the topological charge density $Q = \frac{\alpha_s}{4\pi} G\tilde{G}$ to the nucleon. In eq. 1 M is the nucleon mass and F_0 ($\sim 0.1\,\mathrm{GeV}$) renormalises [26] the flavour-singlet decay constant. The coupling constant g_{QNN} is, in part, related [24] to the amount of spin carried by polarised gluons in a polarised proton. The large mass of the η' and the small value of $g_A^{(0)}$

$$g_A^{(0)}\Big|_{\mathrm{pDIS}} = 0.2 - 0.35 \tag{2}$$

extracted from deep inelastic scattering [28, 29] (about a 50 % OZI suppression) point to substantial violations of the OZI rule in the flavour-singlet $J^P = 1^+$ channel [1]. A large positive $g_{QNN} \sim 2.45$ is one possible explanation of the small value of $g_A^{(0)}|_{\mathrm{pDIS}}$.

It is important to look for other observables which are sensitive to g_{QNN}. OZI violation in the η'–nucleon system is a probe of the role of gluons in dynamical chiral symmetry breaking in low-energy QCD.

Working with the $U_A(1)$–extended chiral Lagrangian for low-energy QCD [30, 31] — see Section 3 below — one finds a gluon-induced contact interaction in the $pp \to pp\eta'$ reaction close to threshold [26]:

$$\mathcal{L}_{\text{contact}} = -\frac{i}{F_0^2}\, g_{QNN}\, \tilde{\mathrm{m}}_{\eta_0}^2\, \mathcal{C}\, \eta_0 \left(\bar{p}\gamma_5 p\right) \left(\bar{p}p\right) \tag{3}$$

Here $\tilde{\mathrm{m}}_{\eta_0}$ is the gluonic contribution to the mass of the singlet 0^- boson and $\mathcal{C}$ is a second OZI violating coupling which also features in $\eta' N$ scattering. The physical interpretation of the contact term (3) is a "short distance" ($\sim 0.2\,\text{fm}$) interaction where glue is excited in the interaction region of the proton-proton collision and then evolves to become an η' in the final state. This gluonic contribution to the cross-section for $pp \to pp\eta'$ is extra to the contributions associated with meson exchange models [32, 33, 34, 35]. There is no reason, a priori, to expect it to be small.

What is the phenomenology of this gluonic interaction?

Since glue is flavour-blind the contact interaction (3) has the same size in both the $pp \to pp\eta'$ and $pn \to pn\eta'$ reactions. CELSIUS [11] have measured the ratio $R_\eta = \sigma(pn \to pn\eta)/\sigma(pp \to pp\eta)$ for quasifree η production from a deuteron target up to 100 MeV above threshold. They observed that R_η is approximately energy-independent $\simeq 6.5$ over the whole energy range — see fig. 1. The value of this ratio signifies a strong isovector exchange contribution to the η production mechanism [11]. This experiment should be repeated for η' production. The cross-section for $pp \to pp\eta'$ close to threshold has been measured at COSY [12]. Following the suggestion in [26] a new COSY-11, Uppsala University Collaboration [36] has been initiated to carry out the $pn \to pn\eta'$ measurement. The more important that the gluon-induced process (3) is in the $pp \to pp\eta'$ reaction the more one would expect $R_{\eta'} = \sigma(pn \to pn\eta')/\sigma(pp \to pp\eta')$ to approach unity near threshold after we correct for the final state interaction between the two outgoing nucleons. (After we turn on the quark masses, the small $\eta - \eta'$ mixing angle $\theta \simeq -18$ degrees means that the gluonic effect (3) should be considerably bigger in η' production than η production.) η' phenomenology is characterised by large OZI violations. It is natural to expect large gluonic effects in the $pp \to pp\eta'$ process.

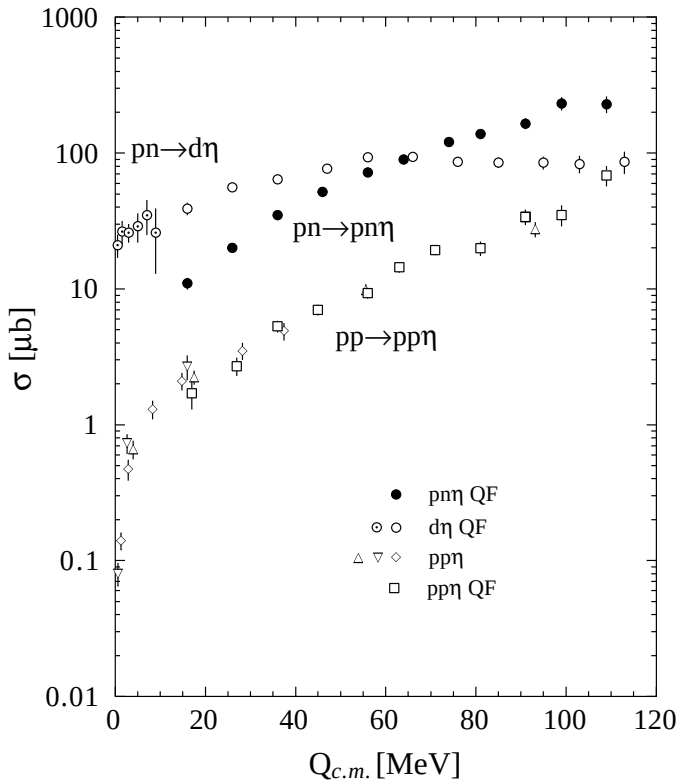

Figure 1:

In Section 2 we give a brief introduction to the U(1) problem. Section 3 introduces the chiral Lagrangian approach and Section 4 makes contact with the experimental data from CELSIUS and COSY.

2 The U(1) problem

In classical field theory Noether's theorem tells us that there is a conserved current associated with each global symmetry of the Lagrangian. The QCD

Lagrangian

$$\mathcal{L}_{QCD} = \sum_q \bar{q}_L \Big(i\hat{D} - g\hat{A} \Big) q_L + \bar{q}_R \Big(i\hat{D} - g\hat{A} \Big) q_R$$
$$- \sum_q m_q \Big(\bar{q}_L q_R + \bar{q}_R q_L \Big) - \frac{1}{2} G_{\mu\nu} G^{\mu\nu} \tag{4}$$

exhibits chiral symmetry for massless quarks: when the quark mass term is turned off the left- and right-handed quark fields do not couple in the Lagrangian and transform independently under chiral rotations.
Chiral $SU(2)_L \otimes SU(2)_R$

$$\begin{pmatrix} u_L \\ d_L \end{pmatrix} \mapsto e^{i\frac{1}{2}\vec{\alpha}.\vec{\tau}\gamma_5} \begin{pmatrix} u_L \\ d_L \end{pmatrix} \quad , \quad \begin{pmatrix} u_R \\ d_R \end{pmatrix} \mapsto e^{i\frac{1}{2}\vec{\beta}.\vec{\tau}\gamma_5} \begin{pmatrix} u_R \\ d_R \end{pmatrix} \tag{5}$$

is associated with the isotriplet axial-vector current $J^{(3)}_{\mu 5}$

$$J^{(3)}_{\mu 5} = \Big[\bar{u}\gamma_\mu\gamma_5 u - \bar{d}\gamma_\mu\gamma_5 d \Big] \tag{6}$$

which is partially conserved

$$\partial^\mu J^{(3)}_{\mu 5} = 2\mathrm{m}_u \bar{u} i\gamma_5 u - 2\mathrm{m}_d \bar{d} i\gamma_5 d \tag{7}$$

The absence of parity doublets in the hadron spectrum tells us that the near-chiral symmetry for light u and d quarks is spontaneously broken. Spontaneous chiral symmetry breaking is associated with a non-vanishing chiral condensate

$$\langle \text{ vac } | \ \bar{q}q \ | \text{ vac } \rangle < 0 \tag{8}$$

The light-mass pion is identified as the corresponding Goldstone boson and the current $J^{(3)}_{\mu 5}$ is associated with the pion through PCAC

$$\langle \text{vac} | J^{(3)}_{\mu 5}(z) | \pi(q) \rangle = -i f_\pi q_\mu e^{-iq.z} \tag{9}$$

Taking the divergence equation

$$\langle \text{vac} | \partial^\mu J^{(3)}_{\mu 5}(z) | \pi(q) \rangle = -f_\pi \mathrm{m}^2_\pi e^{-iq.z} \tag{10}$$

the pion mass-squared vanishes in the chiral limit as $\mathrm{m}^2_\pi \sim \mathrm{m}_q$. This and PCAC [37] are the starting points for chiral perturbation theory [38].

The non-vanishing chiral condensate also spontaneously breaks the axial U(1) symmetry so, naively, one might expect an isosinglet pseudoscalar degenerate with the pion. The lightest mass isosinglet pseudoscalar is the η meson which has a mass of 547 MeV.

The puzzle deepens when one considers SU(3). Spontaneous chiral symmetry breaking suggests an octet of Goldstone bosons associated with chiral $SU(3)_L \otimes SU(3)_R$ plus a singlet boson associated with axial U(1) — each with mass $\mathrm{m}^2_{\mathrm{Goldstone}} \sim \mathrm{m}_q$. If the η is associated with the octet boson then the Gell-Mann Okubo relation

$$\mathrm{m}^2_{\eta_8} = \frac{4}{3}\mathrm{m}^2_K - \frac{1}{3}\mathrm{m}^2_\pi \tag{11}$$

is satisfied to within a few percent. Extending the theory from $SU(3)$ to $SU(3)_L \otimes SU(3)_R \otimes U(1)$ the large strange quark mass induces considerable η-η' mixing. Taking $\mathrm{m}^2_{\mathrm{Goldstone}} \sim \mathrm{m}_q$ the η would be approximately an isosinglet light-quark state $(\frac{1}{\sqrt{2}}|\bar{u}u + \bar{d}d\rangle)$ degenerate with the pion and the η' would be approximately a strange quark state $|\bar{s}s\rangle$ with mass about $\sqrt{2\mathrm{m}^2_K - \mathrm{m}^2_\pi}$. That is, the masses for the η and η' mesons with η-η' mixing and without extra physical input come out about 300-400 MeV too small! This is the axial U(1) problem.

The extra physics which is needed to understand the U(1) problem are gluon topology and the QCD axial anomaly. The (gauge-invariantly renormalised) flavour-singlet axial-vector current in QCD satisfies the anomalous divergence equation [9, 10]

$$\partial^\mu J_{\mu 5} = \sum_{k=1}^{f} 2i\left[\mathrm{m}_k \bar{q}_k \gamma_5 q_k\right] + N_f\left[\frac{\alpha_s}{4\pi} G_{\mu\nu}\tilde{G}^{\mu\nu}\right] \tag{12}$$

where

$$J_{\mu 5} = \left[\bar{u}\gamma_\mu\gamma_5 u + \bar{d}\gamma_\mu\gamma_5 d + \bar{s}\gamma_\mu\gamma_5 s\right] \tag{13}$$

Here $N_f = 3$ is the number of light flavours, $G_{\mu\nu}$ is the gluon field tensor and $\tilde{G}^{\mu\nu} = \frac{1}{2}\epsilon^{\mu\nu\alpha\beta}G_{\alpha\beta}$. The anomalous term $Q(z) \equiv \frac{\alpha_s}{4\pi}G_{\mu\nu}\tilde{G}^{\mu\nu}(z)$ is the topological charge density. Its integral over space $\int d^4z\, Q = n$ measures the gluonic "winding number" [39], which is an integer for (anti-)instantons and which vanishes in perturbative QCD. The exact dynamical mechanism how (non-perturbative) gluonic degrees of freedom contribute to axial U(1) symmetry breaking through the anomaly is still hotly debated [4, 39, 40, 41]: suggestions include instantons [5] and possible connections with confinement [42].

Independent of the detailed QCD dynamics one can construct low-energy effective chiral Lagrangians which include the effect of the anomaly and axial U(1) symmetry, and use these Lagrangians to study low-energy processes involving the η and η'.

3 The low-energy effective Lagrangian

Starting in the meson sector, the building block for the $U_A(1)$-extended low-energy effective Lagrangian [30, 31] is

$$\begin{aligned}\mathcal{L}_{\rm m} = & \quad \frac{F_\pi^2}{4}{\rm Tr}(\partial^\mu U \partial_\mu U^\dagger) + \frac{F_\pi^2}{4}{\rm Tr}\Big[\chi_0\ (U+U^\dagger)\Big] \\ & + \ \frac{1}{2}iQ{\rm Tr}\Big[\log U - \log U^\dagger\Big] + \frac{3}{\tilde{\rm m}_{\eta_0}^2 F_0^2}Q^2\,. \end{aligned} \tag{14}$$

Here

$$U = \exp\left(i\frac{\phi}{F_\pi} + i\sqrt{\frac{2}{3}}2\frac{\eta_0}{F_0}\right) \tag{15}$$

is the unitary meson matrix where $\phi = \sum_k \phi_k \lambda_k$ with ϕ_k denotes the octet of would-be Goldstone bosons (π, K, η_8) associated with spontaneous chiral $SU(3)_L \otimes SU(3)_R$ breaking, η_0 is the singlet boson and Q is the topological charge density; $\chi_0 = {\rm diag}[{\rm m}_\pi^2, {\rm m}_\pi^2, (2{\rm m}_K^2 - {\rm m}_\pi^2)]$ is the meson mass matrix. The pion decay constant $F_\pi = 92.4\,{\rm MeV}$ and F_0 renormalises the flavour-singlet decay constant.

When we expand out the Lagrangian (14) the first term contains the kinetic energy term for the pseudoscalar mesons; the second term contains the meson mass terms before coupling to gluonic degrees of freedom. The $U_A(1)$ gluonic potential involving the topological charge density is constructed to reproduce the axial anomaly (12) in the divergence of the gauge-invariantly renormalised axial-vector current and to generate the gluonic contribution to the η and η' masses. The gluonic term Q is treated as a background field with no kinetic term. It may be eliminated through its equation of motion

$$\frac{1}{2}iQ{\rm Tr}\Big[\log U - \log U^\dagger\Big] + \frac{3}{\tilde{\rm m}_{\eta_0}^2 F_0^2}Q^2 \ \mapsto\ -\frac{1}{2}\tilde{\rm m}_{\eta_0}^2\eta_0^2 \tag{16}$$

making the gluonic mass term clear. After Q is eliminated from the effective Lagrangian via (16), we expand $\mathcal{L}_{\rm m}$ to $\mathcal{O}(p^2)$ in momentum keeping finite

quark masses and obtain:

$$\begin{aligned}
\mathcal{L}_{\rm m} = & \sum_k \frac{1}{2}\partial^\mu\phi_k\partial_\mu\phi_k + \frac{1}{2}\partial_\mu\eta_0\partial^\mu\eta_0\left(\frac{F_\pi}{F_0}\right)^2 - \frac{1}{2}\tilde{\rm m}^2_{\eta_0}\eta_0^2 \\
- & \frac{1}{2}{\rm m}^2_\pi\left(2\pi^+\pi^- + \pi_0^2\right) - {\rm m}^2_K\left(K^+K^- + K^0\bar{K}^0\right) \\
- & \frac{1}{2}\left(\frac{4}{3}{\rm m}^2_K - \frac{1}{2}{\rm m}^2_\pi\right)\eta_8^2 - \frac{1}{2}\left(\frac{2}{3}{\rm m}^2_K + \frac{1}{3}{\rm m}^2_\pi\right)\left(\frac{F_\pi}{F_0}\right)^2\eta_0^2 \\
+ & \frac{4}{3\sqrt{2}}\left({\rm m}^2_K - {\rm m}^2_\pi\right)\left(\frac{F_\pi}{F_0}\right)\eta_8\eta_0 + \ldots
\end{aligned} \tag{17}$$

The value of F_0 is usually determined from the decay rate for $\eta' \to 2\gamma$. In QCD one finds the relation [43]

$$\frac{2\alpha}{\pi} = \sqrt{\frac{3}{2}}F_0\left(g_{\eta'\gamma\gamma} - g_{Q\gamma\gamma}\right) \tag{18}$$

(in the chiral limit) which is derived by coupling the effective Lagrangian (14) to photons. The observed decay rate [44] is consistent [45] with the OZI prediction for $g_{\eta'\gamma\gamma}$ *if* F_0 and $g_{Q\gamma\gamma}$ take their OZI values: $F_0 \simeq F_\pi$ and $g_{Q\gamma\gamma} = 0$. Motivated by this observation it is common to take $F_0 \simeq F_\pi$.

3.1 Glue and the η and η' masses

If we work in the approximation ${\rm m}_u = {\rm m}_d$ and set $F_0 = F_\pi$, then the $\eta - \eta'$ mass matrix which follows from (17) becomes

$$\mathrm{M}^2_{\eta-\eta'} = \begin{pmatrix} \frac{4}{3}{\rm m}^2_K - \frac{1}{3}{\rm m}^2_\pi & -\frac{2}{3}\sqrt{2}({\rm m}^2_K - {\rm m}^2_\pi) \\ -\frac{2}{3}\sqrt{2}({\rm m}^2_K - {\rm m}^2_\pi) & [\frac{2}{3}{\rm m}^2_K + \frac{1}{3}{\rm m}^2_\pi + \tilde{\rm m}^2_{\eta_0}] \end{pmatrix} \tag{19}$$

with η-η' mixing

$$\begin{aligned}
|\eta\rangle &= \cos\theta\,|\eta_8\rangle - \sin\theta\,|\eta_0\rangle \\
|\eta'\rangle &= \sin\theta\,|\eta_8\rangle + \cos\theta\,|\eta_0\rangle
\end{aligned} \tag{20}$$

driven predominantly by the large strange-quark mass. The Gell-Mann Okubo mass formula (11) can be seen in the top left matrix element of the mass matrix (19). Diagonalising the η–η' mass matrix we obtain values for the η and η' masses:

$${\rm m}^2_{\eta',\eta} = ({\rm m}^2_K + \tilde{\rm m}^2_{\eta_0}/2) \pm \frac{1}{2}\sqrt{(2{\rm m}^2_K - 2{\rm m}^2_\pi - \frac{1}{3}\tilde{\rm m}^2_{\eta_0})^2 + \frac{8}{9}\tilde{\rm m}^4_{\eta_0}}\,. \tag{21}$$

If we turn off the gluon mixing term, then one finds $\mathrm{m}_{\eta'} = \sqrt{2\mathrm{m}_K^2 - \mathrm{m}_\pi^2}$ and $\mathrm{m}_\eta = \mathrm{m}_\pi$. Without any extra input from glue, in the OZI limit, the η would be approximately an isosinglet light-quark state ($\frac{1}{\sqrt{2}}|\bar{u}u + \bar{d}d\rangle$) degenerate with the pion and the η' would a strange-quark state $|\bar{s}s\rangle$ — mirroring the isoscalar vector ω and ϕ mesons. Indeed, in an early paper [3] Weinberg argued that the mass of the η would be less than $\sqrt{3}\mathrm{m}_\pi$ without any extra U(1) dynamics to further break the axial U(1) symmetry. Summing over the two eigenvalues in (21) yields [30]

$$\mathrm{m}_\eta^2 + \mathrm{m}_{\eta'}^2 = 2\mathrm{m}_K^2 + \tilde{\mathrm{m}}_{\eta_0}^2 \,. \tag{22}$$

Substituting the physical values of $(\mathrm{m}_\eta^2 + \mathrm{m}_{\eta'}^2)$ in eq. 22 and m_K^2 yields $\tilde{\mathrm{m}}_{\eta_0}^2 = 0.73\,\mathrm{GeV}^2$, which corresponds to $\mathrm{m}_\eta = 499\,\mathrm{MeV}$ and $\mathrm{m}_{\eta'} = 984\,\mathrm{MeV}$. The value $\tilde{\mathrm{m}}_{\eta_0}^2 = 0.73\,\mathrm{GeV}^2$ corresponds to an η-η' mixing angle $\theta \simeq -18$ degrees — which is within the range -17 to -20 degrees obtained from a study of various decay processes in [45, 46]. The physical masses are $\mathrm{m}_\eta = 547\,\mathrm{MeV}$ and $\mathrm{m}_{\eta'} = 958\,\mathrm{MeV}$. Closer agreement with the physical masses can be obtained by taking $F_0 \neq F_\pi$ and including higher-order mass terms in the chiral expansion. Two mixing angles [47, 48] enter the η-η' system when one extends the theory and $\mathcal{L}_\mathrm{m}$ to $O(p^4)$ in the meson momentum. (The two mixing angles are induced by $F_\pi \neq F_K$ due to chiral corrections at $O(p^4)$ [38].)

3.2 OZI violation and the η'–nucleon interaction

The low-energy effective Lagrangian (14) is readily extended to include η–nucleon and η'–nucleon coupling. Working to $O(p)$ in the meson momentum the chiral Lagrangian for meson-baryon coupling is

$$\begin{aligned}
\mathcal{L}_\mathrm{mB} &= \mathrm{Tr}\,\overline{B}(i\gamma_\mu D^\mu - \mathrm{M}_0)B \\
&+ F\,\mathrm{Tr}\Big(\overline{B}\gamma_\mu\gamma_5[a^\mu, B]_-\Big) + D\,\mathrm{Tr}\Big(\overline{B}\gamma_\mu\gamma_5\{a^\mu, B\}_+\Big) \\
&+ \frac{i}{3}K\,\mathrm{Tr}\Big(\overline{B}\gamma_\mu\gamma_5 B\Big)\mathrm{Tr}\Big(U^\dagger\partial^\mu U\Big) - \frac{\mathcal{G}_{QNN}}{2\mathrm{M}_0}\partial^\mu Q\,\mathrm{Tr}\Big(\overline{B}\gamma_\mu\gamma_5 B\Big) \\
&+ \frac{\mathcal{C}}{F_0^4}Q^2\mathrm{Tr}\Big(\overline{B}B\Big)
\end{aligned} \tag{23}$$

Here

$$B = \begin{pmatrix} \frac{1}{\sqrt{2}}\Sigma^0 + \frac{1}{\sqrt{6}}\Lambda & \Sigma^+ & p \\ \Sigma^- & -\frac{1}{\sqrt{2}}\Sigma^0 + \frac{1}{\sqrt{6}}\Lambda & n \\ \Xi^- & \Xi^0 & -\frac{2}{\sqrt{6}}\Lambda \end{pmatrix} \tag{24}$$

denotes the baryon octet and M_0 denotes the baryon mass in the chiral limit. In eq. 23 D_μ is the chiral covariant derivative and $a_\mu = -\frac{1}{2F_\pi}\partial_\mu\phi - \frac{1}{2F_0}\sqrt{\frac{2}{3}}\partial_\mu\eta_0 + ...$ is the axial-vector current operator. The SU(3) couplings are $F = 0.459 \pm 0.008$ and $D = 0.798 \pm 0.008$ [49]. The Pauli-principle forbids any flavour-singlet $J^P = \frac{1}{2}^+$ ground-state baryon degenerate with the baryon octet B. In general, one may expect OZI violation wherever a coupling involving the Q-field occurs.

Following eq. 16, we eliminate Q from the total Lagrangian $\mathcal{L} = \mathcal{L}_{\mathrm{m}} + \mathcal{L}_{\mathrm{mB}}$ through its equation of motion. The Q dependent terms in the effective Lagrangian become:

$$\begin{aligned} \mathcal{L}_Q \;=\; & \frac{1}{12}\tilde{\mathrm{m}}^2_{\eta_0}\Bigg[-6\eta_0^2 - \frac{\sqrt{6}}{\mathrm{M}_0}\,\mathcal{G}_{QNN}\,F_0\,\partial^\mu\eta_0\,\mathrm{Tr}\Big(\bar{B}\gamma_\mu\gamma_5 B\Big) \\ & + \mathcal{G}^2_{QNN}\,F_0^2\,\Big(\mathrm{Tr}\bar{B}\gamma_5 B\Big)^2 + 2\,\mathcal{C}\,\frac{\tilde{\mathrm{m}}^2_{\eta_0}}{F_0^2}\,\eta_0^2\,\mathrm{Tr}\Big(\bar{B}B\Big) \\ & - \frac{\sqrt{6}}{3\mathrm{M}_0F_0}\,\mathcal{G}_{QNN}\,\mathcal{C}\tilde{\mathrm{m}}^2_{\eta_0}\eta_0\,\partial^\mu\mathrm{Tr}\Big(\bar{B}\gamma_\mu\gamma_5 B\Big)\,\mathrm{Tr}\Big(\bar{B}B\Big) + ...\Bigg] \end{aligned} \tag{25}$$

This equation describes the gluonic contributions to the η-nucleon and η'-nucleon interactions. The term $-\frac{\sqrt{6}}{\mathrm{M}_0}\,\mathcal{G}_{QNN}\,F_0\,\partial^\mu\eta_0\,\mathrm{Tr}\Big(\bar{B}\gamma_\mu\gamma_5 B\Big)$ is a gluonic (OZI violating) contribution to the η'–nucleon coupling constant, which is $g_{\eta_0 NN} = \sqrt{\frac{2}{3}}\frac{\mathrm{m}}{F_0}(2D + 2K + \mathcal{G}_{QNN}F_0^2\frac{\tilde{\mathrm{m}}^2_{\eta_0}}{2\mathrm{m}})$ in the notation of (23). The Lagrangian (25) has three contact terms associated with the gluonic potential in Q. We recognise $\mathcal{L}^{(2)}_{\mathrm{contact}} = -\frac{\sqrt{6}}{12\mathrm{m}F_0}\mathcal{G}_{QNN}\tilde{\mathrm{m}}^2_{\eta_0}\,\frac{1}{3}\mathcal{C}\tilde{\mathrm{m}}^2_{\eta_0}\,\eta_0\,\partial^\mu\mathrm{Tr}\Big(\bar{B}\gamma_\mu\gamma_5 B\Big)\,\mathrm{Tr}\Big(\bar{B}B\Big)$ as the gluonic contact term (3) in the low-energy $pp \to pp\eta'$ reaction with $g_{QNN} \equiv \sqrt{\frac{1}{6}}\mathcal{G}_{QNN}F_0\tilde{\mathrm{m}}^2_{\eta_0}$. The term $\mathcal{L}^{(3)}_{\mathrm{contact}} = \frac{1}{6F_0^2}\,\mathcal{C}\,\tilde{\mathrm{m}}^4_{\eta_0}\,\eta_0^2\,\mathrm{Tr}\Big(\bar{B}B\Big)$ is potentially important to η–nucleon and η'–nucleon scattering processes. The contact terms $\mathcal{L}^{(j)}_{\mathrm{contact}}$ are proportional to $\tilde{\mathrm{m}}^2_{\eta_0}$ $(j = 2)$ and $\tilde{\mathrm{m}}^4_{\eta_0}$ $(j = 3)$ which vanish

in the formal OZI limit. Phenomenologically, the large masses of the η and η' mesons means that there is no reason, a priori, to expect the $\mathcal{L}^{(j)}_{\rm contact}$ to be small.

Gluonic $U_A(1)$ degrees of freedom induce several "η'–nucleon coupling constants". The three couplings ($g_{\eta_0 NN}$, $\mathcal{G}_{QNN}$ and $\mathcal{C}$) are each potentially important in the theoretical description of the η'–nucleon and η'–two-nucleon systems. Different combinations of these coupling constants are relevant to different η' production processes and to the flavour-singlet Goldberger-Treiman relation. Testing the sensitivity of η'–nucleon interactions to the gluonic terms in the effective chiral Lagrangian for low-energy QCD will teach us about the role of gluons in chiral dynamics.

4 Proton-proton collisions

How important is the contact interaction $\mathcal{L}^{(2)}_{\rm contact}$ in the $pp \to pp\eta'$ reaction?

The T-matrix for η' production in proton-proton collisions, $p_1(\vec{\rm p}) + p_2(-\vec{\rm p}) \to p + p + \eta'$, at threshold in the centre of mass frame is

$$\mathrm{T}^{\rm cm}_{\rm th}(pp \to pp\eta') = \mathcal{A}\Big[i(\vec{\sigma}_1 - \vec{\sigma}_2) + \vec{\sigma}_1 \times \vec{\sigma}_2\Big] \cdot \vec{\rm p} \tag{26}$$

where $\mathcal{A}$ is the (complex) threshold amplitude for η' production. Measurements of the total cross-section for $pp \to pp\eta'$ have been published by COSY [12] and SATURNE [50] between 1.5 and 24 MeV above threshold – see fig. 2.

The energy dependence of the data are well described by phase space plus proton-proton final state interaction (neglecting any η'-p FSI). Using the model of Bernard et al. [51] treating the pp final state interaction in effective range approximation one finds a good fit to the measured total cross-section data with

$$|\mathcal{A}| = 0.21 \text{ fm}^4 \,. \tag{27}$$

The present (total cross-section only) data on $pp \to pp\eta'$ is insufficient to distinguish between possible production mechanisms involving the (short-range) gluonic contact term (3) and the long-range contributions associated with meson exchange models. Long-range meson exchange contributions to $\mathcal{A}$ involve the exchange of a π^0, η, ω or ρ^0 between the two protons and the emission of an η' from one of the two protons. This process involves $g_{\eta_0 NN}$. The contact term (3) involves the excitation of gluonic degrees of freedom in the interaction region, is isotropic and involves the product of

$\mathcal{G}_{QNN}$ and the second gluonic coupling $\mathcal{C}$. In their analysis of the SATURNE data on $pp \to pp\eta'$ Hibou et al. [50] found that a one-pion exchange model adjusted to fit the S-wave contribution to the $pp \to pp\eta$ cross-section near threshold yields predictions about 30 % below the measured $pp \to pp\eta'$ total cross-section. The gluonic contact term (3) is a candidate for additional, potentially important, short range interaction.

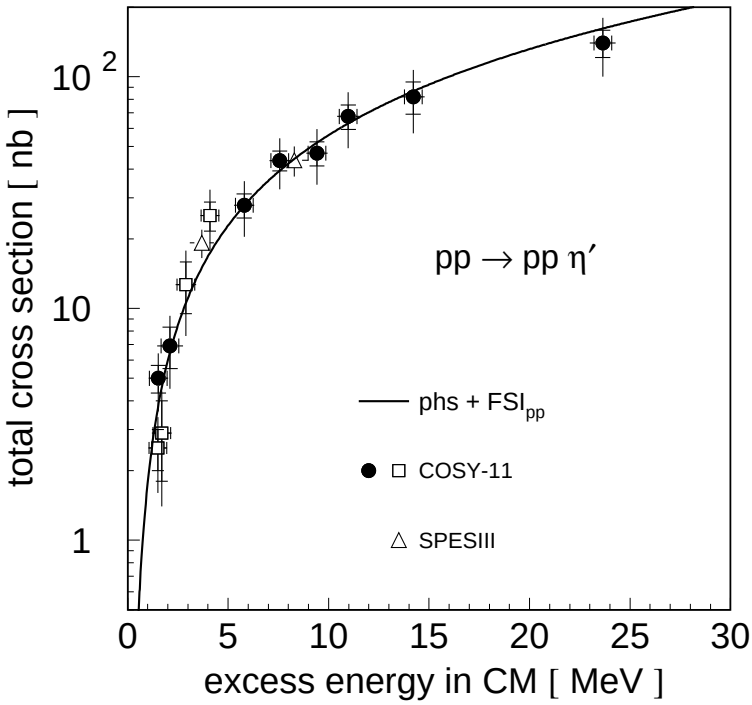

Figure 2: The COSY and SATURNE data on $pp \to pp\eta'$

To estimate how strong the contact term must be in order to make an important contribution to the measured $pp \to pp\eta'$ cross-section, let us consider the extreme scenario where the value of $|\mathcal{A}|$ in eq. 27 is saturated by the contact term (3). If we take the estimate $g_{QNN} \sim 2.45$ (or equivalently $\mathcal{G}_{QNN} \sim +60\,\mathrm{GeV}^{-3}$) suggested by the polarised deep inelastic scattering and the flavour-singlet Goldberger-Treiman relation below eq. 2, then we need $\mathcal{C} \sim 1.8\,\mathrm{GeV}^{-3}$ to saturate $|\mathcal{A}|$. The OZI violating parameter $\mathcal{C} \sim 1.8\,\mathrm{GeV}^{-3}$ seems reasonable compared with $\mathcal{G}_{QNN} \sim 60\,\mathrm{GeV}^{-3}$. To help resolve the different production mechanisms it will be important to

test the isospin dependence of the $pN \to pN\eta'$ process through quasi-free production from the deuteron [26, 36] and to make a partial wave analysis of the η' production process, following the work pioneered by CELSIUS for η production [52]. Here, it is interesting to note that the recent higher-energy ($p_{beam} = 3.7\,\mathrm{GeV/c}$) measurement of the $pp \to pp\eta'$ cross-section by the DISTO collaboration [53] suggests isotropic η' production at this energy.

Acknowledgement. It is a pleasure to thank P. Moskal for organising this stimulating workshop in the beautiful surroundings of Cracow. I thank E. Gabathuler, T. Johansson, S. Kullander, P. Moskal, G. Rudolph, J. Stepaniak and U. Wiedner for helpful communications about experimental data.

References

[1] G. Veneziano, Okubofest: From Symmetries to Strings: Forty Years of Rochester Conferences, Rochester, New York, 4–5 May 1990, Proc. ed. by A. Das, World Scientific (1990) 13 and CERN preprint **TH-5840-90** (1990).

[2] G.M. Shore, Zuoz Summer School on Hidden Symmetries and Higgs Phenomena, Zuoz, Switzerland, Aug 16–22 1998, Proc. ed. by D. Graudenz, PSI–Proceedings–98–02 (1998) 201 and e–Print Archive: hep–ph/9812354.

[3] S. Weinberg, Phys. Rev. **D 11** (1975) 3583.

[4] G. Christos, Phys. Rept. **116** (1984) 251.

[5] G. 't Hooft, Phys. Rev. Lett. **37** (1976) 8; Phys. Rev. **D 14** (1976) 3432.

[6] H. Fritzsch, P. Minkowski, Nuovo Cim. **A 30** (1975) 393.

[7] G. Veneziano, Nucl. Phys. **B 159** (1979) 213; Phys. Lett. **B 95** (1980) 90.

[8] E. Witten, Nucl. Phys. **B 156** (1979) 269.

[9] S.L. Adler, Phys. Rev. **177** (1969) 2426.

[10] J.S. Bell, R. Jackiw, Nuovo Cim. **A 60** (1969) 47.

[11] H. Calén et al., Phys. Rev. Lett. **80** (1998) 2069; Phys. Rev. **C 58** (1998) 2667.

[12] P. Moskal et al., Phys. Rev. Lett. **80** (1998) 3202; Phys. Lett. **B 474** (2000) 416; Phys. Lett. **B 482** (2000) 356; P. Moskal, doctoral thesis, Jagellonian University, Cracow (1998).

[13] CEBAF experiments E-91-008 and E-94-008 (B.G. Ritchie et al.); B.G. Ritchie, CEBAF Mini–Workshop On The Structure Of The Eta-Prime Meson, 8-9 Mar 1996, Las Cruces, New Mexico, Proc. ed. by M. Burkardt et al., World Scientific, Singapore (1997).

[14] R. Plötzke et al., Phys. Lett. **B 444** (1998) 555.

[15] D.R. Thompson et al., Phys. Rev. Lett. **79** (1997) 1630; S.U. Chung et al., Phys. Rev. **D 60** (1999) 092001; G.S. Adams et al., Phys. Rev. Lett. **81** (1998) 5760; E.I. Ivanov et al., Phys. Rev. Lett. **86** (2001) 3977.

[16] A. Abele et al., Phys. Lett. **B 423** (1998) 246.

[17] B.H. Behrens et al., Phys. Rev. Lett. **80** (1998) 3710; T.E. Browder et al., Phys. Rev. Lett. **81** (1998) 1786.

[18] C.P. Jessop et al., Phys. Rev. **D 58** (1998) 052002.

[19] B. Aubert et al., Phys. Rev. Lett. **87** (2001) 221802.

[20] K. Abe et al., Phys. Lett. **B 517** (2001) 309.

[21] R. Barate et al., Phys. Rept. **294** (1998) 1.

[22] J. Gronberg et al., Phys. Rev. **D 57** (1998) 33.

[23] R. Bilger et al., Nucl. Phys. **A 626** (1997) 93c.

[24] G. Veneziano, Mod. Phys. Lett. **A 4** (1989) 1605; G.M. Shore, G. Veneziano, Nucl. Phys. **B 381** (1992) 23.

[25] T. Hatsuda, Nucl. Phys. **B 329** (1990) 376.

[26] S.D. Bass, Phys. Lett. **B 463** (1999) 286; 8th Int. Workshop on Deep Inelastic Scattering and QCD (DIS 2000), Liverpool, England, 25–30 Apr 2000, Proc. ed. by J.A. Gracey, T. Greenshaw, World Scientific (2001) 206 and e–Print Archive: hep–ph/0006348.

[27] S.D. Bass, S. Wetzel, W. Weise, Nucl. Phys. **A 686** (2001) 429.

[28] S.D. Bass, Eur. Phys. J. **A 5** (1999) 17.

[29] R. Windmolders, Nucl. Phys. Proc. Suppl. **79** (1999) 51.

[30] P. Di Vecchia, G. Veneziano, Nucl. Phys. **B 171** (1980) 253.

[31] C. Rosenzweig, J. Schechter, C.G. Trahern, Phys. Rev. **D 21** (1980) 3388; P. Nath, R. Arnowitt, Phys. Rev. **D 23** (1981) 473.

[32] R. Machleidt, K. Holinde, C. Elster, Phys. Rept. **149** (1987) 1.

[33] J.-F. Germond, C. Wilkin, Nucl. Phys. **A 518** (1990) 308.

[34] G. Fäldt, C. Wilkin, Z. Phys. **A 357** (1997) 241; Phys. Scripta **64** (2001) 427.

[35] K. Nakayama, H.F. Arellano, J.W. Durso, J. Speth, Phys. Rev. **C 61** (1999) 024001.

[36] P. Moskal, T. Johansson, *Investigation of the glue content in the η' meson*, COSY Proposal No. 100, April 2001; P. Moskal, contribution to these proceedings.

[37] S.L. Adler, R.F. Dashen, *Current Algebras and Applications to Particle Physics*, Benjamin, New York (1968).

[38] J. Gasser, H. Leutwyler, Nucl. Phys. **B250** (1985) 465.

[39] R.J. Crewther, XVII Int. Universitätswochen für Kernphysik, Schladming, Austria, 21 Feb – 3 Mar 1978, Acta Phys. Austriaca Suppl. **19** (1978) 47.

[40] G. 't Hooft, Phys. Rept. **142** (1986) 357.

[41] E. Witten, Nucl. Phys. **B 149** (1979) 285.

[42] J. Kogut, L. Susskind, Phys. Rev. **D 11** (1975) 3594.

[43] G.M. Shore, G. Veneziano, Nucl. Phys. **B 381** (1992) 3; G.M. Shore, Nucl. Phys. **B 569** (2000) 107.

[44] C. Caso et al., *The Review of Particle Physics*, Eur. Phys. J. **C 3** (1998) 1.

[45] F.J. Gilman, R. Kauffman, Phys. Rev. **D 36** (1987) 2761; (E) **D 37** (1988) 3348.

[46] P. Ball, J.M. Frere, M. Tytgat, Phys. Lett. **B 365** (1996) 367.

[47] H. Leutwyler, Nucl. Phys. Proc. Suppl. **64** (1998) 223; R. Kaiser and H. Leutwyler, Workshop On Methods Of Nonperturbative Quantum Field Theory, Adelaide, Australia, 2–13 Feb 1998, Proc. ed. by A.W. Schreiber, A.G. Williams, A.W. Thomas, World Scientific, Singapore (1998) 15, e–Print Archive: hep–ph/9806336.

[48] T. Feldmann, Int. J. Mod. Phys. **A 15** (2000) 159.

[49] F.E. Close, R.G. Roberts, Phys. Lett. **B 316** (1993) 165.

[50] F. Hibou et al., Phys. Lett. **B 438** (1998) 41.

[51] V. Bernard, N. Kaiser, U.-G. Meißner, Eur. Phys. J. **A4** (1999) 259.

[52] H. Calén et al., Phys. Lett. **B 458** (1999) 190.

[53] A. Balestra et al., Phys. Lett. **B 491** (2000) 29.

Feasibility study of the quasi-free creation of the η' meson in the reaction pn $\rightarrow$ pnη'

P. Moskal[a,b]

[a] *Institute of Physics, Jagellonian University, Kraków, Poland*

[b] *Institut für Kernphysik, Forschungszentrum Jülich, Germany*

Abstract: The feasibility of an investigation of the $pn \rightarrow pn\eta'$ reaction by means of the COSY-11 internal target facility is discussed. Appraisals are based on the assumption of the quasi-free reactions of beam protons, circulating in the cooler synchrotron COSY, with neutrons from a windowless deuteron cluster target.

1 Introduction[1]

In 1984 Maltman and Isgur [2] have argued on the basis of simple geometrical considerations (see figure 1) that at the distances smaller than 2 fm the internucleon potential should begin to be free of meson exchange effects and may be dominated by the residual colour forces. However, as pointed

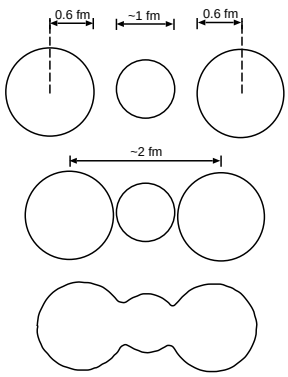

Figure 1: A cartoon illustrating in naive geometrical terms that for $r < 2r_N + 2r_M$ meson exchange is unlikely to be appropriate to the description of the internucleon potential. Figure and caption are taken from reference [2].

out by Nakayama [3], the transition region from the hadronic to constituent quark degrees of freedom does not have a well defined boundary, and at

[1] This part of the talk presents some aspects of the motivation from the COSY Proposal No. 100 [1].

present both approaches should be evaluated in order to test their relevance in the description of close-to-threshold meson production in the collision of nucleons. The authors of reference [4] have shown, that for example the K^+ meson production via the $pp \to pK^+\Lambda$ reaction far from its production threshold can well be described in terms of either the meson-exchange mechanism or the two-gluon exchange model. Thus, a determination of the relevant degrees of freedom for the description of the nucleon-nucleon interaction, especially in case when nucleons are very close together, remains one of the key issues in hadronic physics [5].

Close-to-threshold production of η and η' mesons in the nucleon-nucleon interaction requires a large momentum transfer between the nucleons and hence can occur only at distances smaller than ~ 0.3 fm. This suggests that the quark-gluon degrees of freedom may indeed play a significant role in the production dynamics of these mesons, and especially that the η' meson can be created directly from the glue which is excited in the interaction region of the colliding nucleons [6, 7]. A possibly large glue content of the η' and the dominant flavour-singlet combination of its quark wave function may cause that the dynamics of its production process in the nucleon-nucleon collisions are significantly different from those responsible for the production of the η meson (see figure 2).

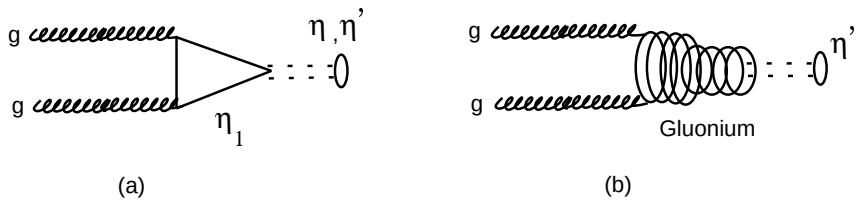

Figure 2: Coupling of η and η' to two gluons through (a) quark and antiquark triangle loop and (b) gluonic admixture. The figure is taken from reference [8].

Figure 3 depicts possible short-range mechanisms which may lead to the creation of the η' meson via a fusion of gluons emitted from the exchanged quarks of the colliding protons [7] or via an exchange of a colour-singlet object made up from glue, which then rescatters and converts into η' [9]. The hadronization of gluons to the η' meson may proceed directly via its gluonic component or through its overwhelming flavour-singlet admixture η_1 (see fig. 2). Contrary to the significant meson exchange mechanisms and the fusion of gluons of graph 3a, the creation through the colour-singlet object proposed by S.D. Bass [9] (graph 3b) is isospin independent, and

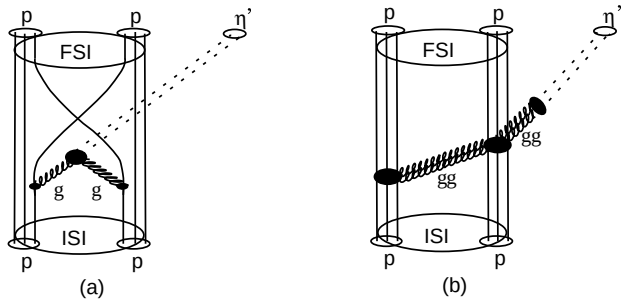

Figure 3: Diagrams depicting possible quark-gluon dynamics of the reaction $pp \to pp\eta'$. (a)— production via a fusion of gluons [7] with rearrangement of quarks. (b)— production via a rescattering of a "low energy pomeron" [9].

hence should lead to the same production yield [2] of the η' meson in both reactions $pp \to pp\eta'$ and $pn \to pn\eta'$ because gluons do not distinguish between flavours. This property should allow to test the relevance of a short range gluonic term [10] by the experimental determination of the cross section ratio $R_{\eta'} = \sigma(pn \to pn\eta')/\sigma(pp \to pp\eta')$, which in that case should be close to unity after correcting for the final and initial state interaction. The other extreme scenario — assuming the dominance of the isovector meson exchange mechanism — should result in the value of $R_{\eta'}$ close to 6.5 as was already established in the case of the η meson [11].

The total cross section for the $pp \to pp\eta'$ reaction has already been measured close to the kinematical threshold by the COSY-11 [12, 13], SPES-III [14] and DISTO [15] collaborations. However, data on the near threshold production of the η' meson in proton-neutron collisions do not exist. Thus as a first step towards the determination of the value of $R_{\eta'}$ the feasibility of the measurement of the $pn \to pn\eta'$ reaction by means of the COSY-11 facility was studied by the Monte-Carlo method and is discussed in the following section.

2 Experimental method: Quasi-free production [3]

In order to measure the $pn \to pn\eta'$ reaction by means of a proton beam it is necessary to use a nuclear target, since a pure neutron target does not

[2] after correcting for the final and initial state interaction between participating baryons.

[3] Results presented in this section constitute an extended experimental part of the COSY Proposal No. 100 [1].

exist. Similar to investigations of the η meson production in the $pn \to pn\eta$ reaction [11, 16, 17], a deuteron will be considered as source of neutrons. Due to the small binding energy of the deuteron ($E_B = 2.2\,\mathrm{MeV}$), the neutron struck by the proton incoming with 2540 MeV kinetic energy may approximately be treated as being a free particle in the sense that the matrix element for quasi-free meson production on a bound neutron is identical to that for the free $pn \to pn\eta$ reaction. Measurements performed at CELSIUS [11, 17] and TRIUMF [18, 19] have proven that the offshellness of the reacting neutron can be neglected and that the spectator proton influences the interaction only in terms of the associated Fermi motion [18]. In this approximation the proton from the deuteron is considered as a spectator which does not interact with the bombarding proton, but rather escapes untouched and hits the detectors carrying the Fermi momentum possessed at the moment of the collision. The momentum spectrum of the nucleons in the deuteron is shown in figure 4a.

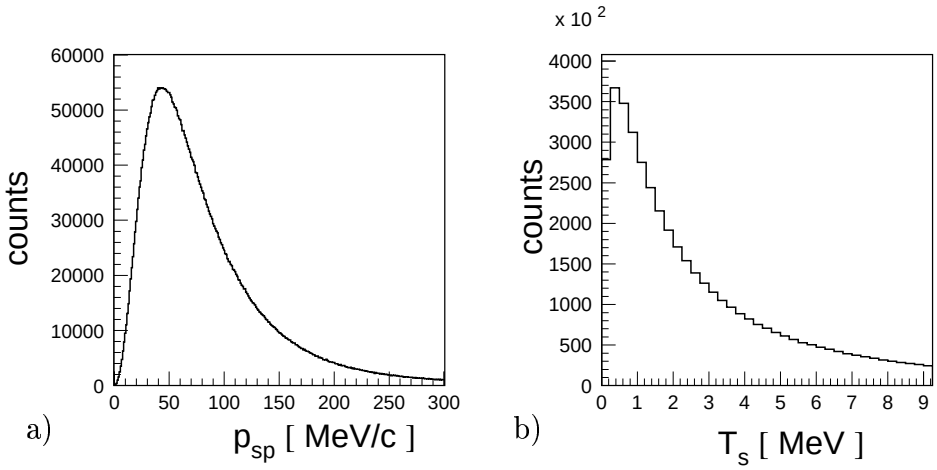

Figure 4: (a) Momentum and (b) kinetic energy distribution of the nucleons in the deuteron, generated according to an analytical parametrization of the deuteron wave function [20, 21] calculated from the PARIS potential [22].

Since the neutron bound inside a deuteron is not at rest, and its momentum may change from event to event, the excess energy in the quasi-free proton-neutron reaction will also vary from event to event. This enables to scan a large range of excess energies with a constant proton beam momen-

tum, but simultaneously requires the determination of this energy for each registered event, which can be done only if the neutron momentum vector is known. This may be realized experimentally either by determining the four-momentum vectors of the outgoing proton, neutron, and η' or by measuring the four-momentum of the spectator proton. Since at present none of the experimental facilities installed at COSY can fulfill the first requirement only the case with the registration of the spectator proton will be considered. From the measurement of the momentum vector of the spectator proton one can infer the momentum vector of the neutron at the time of the reaction, and hence calculate the excess energy. The distribution of the excess energy in a quasi-free $pn \to pn\eta'$ reaction is presented in figure 5a. In the

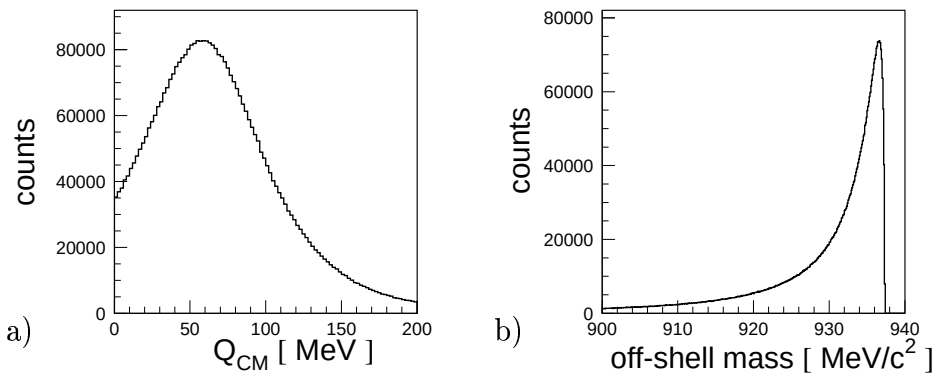

Figure 5: (a) Distribution of the excess energy Q_{CM} for the $pn\eta'$ system originating from the reaction $pd \to p_{sp}pn\eta'$ calculated with a proton beam momentum of 3.350 GeV/c, and the neutron momentum smeared out according to the Fermi distribution shown in figure 4b. The beam momentum of 3.350 GeV/c corresponds to an excess energy of $Q_{CM} = 44.7$ MeV for the free $pn \to pn\eta'$ reaction.
(b) Spectrum of the off-shell mass of the interacting neutron, as calculated under the assumption of the impulse approximation.

framework of the so-called impulse approximation the spectator proton is a physical particle, hence it must be on its mass shell. This implies, however, that the reacting neutron is off its mass shell, and hence the extrapolation from the quasi-free to the free $pn \to pn\eta'$ must be done with care. The distribution of the off-shell mass of the interacting neutron is shown in figure 5b. It can be seen that the maximum of this spectrum differs only by about 3 MeV from the free neutron mass ($m_n = 939.57$ MeV, however on the average it is off by about 9 MeV. Measurements performed at the CEL-

SIUS and TRIUMF accelerators for the $pp \to pp\eta$ [17] and $pp \to d\pi^+$ [18] reactions, respectively, have shown that within the statistical errors there is no difference between the total cross section of the free and quasi-free processes. The quasi-free production was realized utilizing a deuteron target. This observation allows to anticipate that in the case of the planned study of the η' in the $pd \to p_{sp}np\eta'$ reaction, the measured total cross section for the quasi-free $pn \to pn\eta'$ reaction will not differ from the on-shell one. In fact, the difference between off-shell and on-shell cross section of the η' meson production should be even smaller than in the case of the η and π, since in the former case the total energy of the interacting nucleons is much larger than in the latter one, and the mean difference between the off-shell and on-shell neutron mass remains the same.

Other nuclear effects in case of the production on the neutron bound in the nucleus are rather of minor importance. The effect of the reduction of the beam flux on a neutron due to the presence of the proton in the deuteron, referred to as a shadow effect, decreases the total cross section by about 4.5 % in case of η production [16]. Thus it should also have a minor influence on the evaluation of the total cross section for the $pn \to pn\eta'$ reaction. Similarly the reduction of the total cross section due to the reabsorbtion of the produced η' on the spectator proton should be negligible due to the weak [23] proton-η' interaction. Even in case of the η meson, which interacts with protons much more strongly, this effect was found to be only about 3 % [16].

In order to identify the production of the η' meson in a proton-deuteron collision it is necessary either to measure the decay products of the meson or to register the outgoing nucleons and nuclei. At present only the second possibility can be considered at COSY experiments due to the lack of an appropriate detector [4]. The requirement to register the spectator proton excludes the possibility of performing such an experiment by means of any external facility which utilizes liquid or solid targets.

At present, COSY-11 is the only internal facility at COSY, where the outgoing proton and neutron can be measured simultaneously. Since for the proposed study the ratio $R_{\eta'} = \sigma(pn \to pn\eta')/\sigma(pp \to pp\eta')$ has to be determined it would be extremely advisable to perform both the production on protons and on neutrons by means of the same detection system in order to minimize systematical uncertainties.

During the last years close to threshold total cross sections for the $pp \to pp\eta'$ reaction have been succesfully measured at the COSY-11 fa-

[4] A photon detector is planned to be built and installed at the ANKE facility, however, first experiments with this apparatus are foreseen for the end of the year 2004 [24].

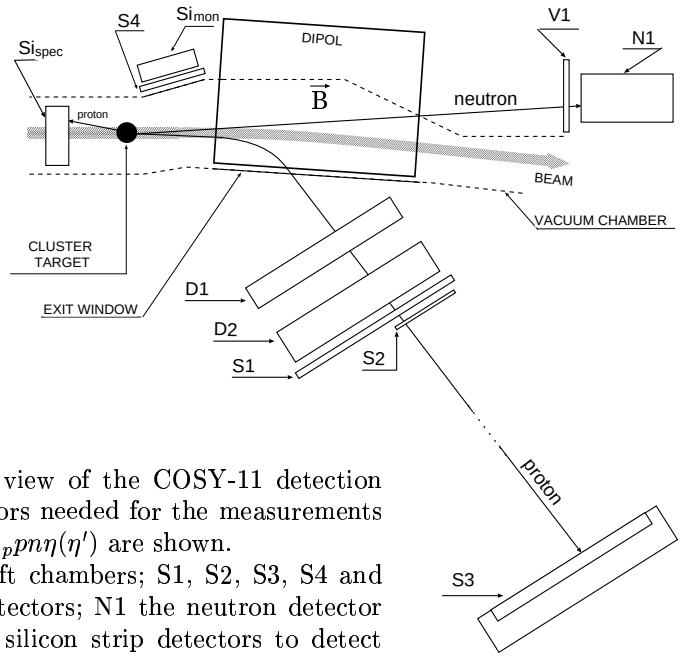

Figure 6: Schematic view of the COSY-11 detection setup[25]. Only detectors needed for the measurements of the reaction $pd \to p_{sp}pn\eta(\eta')$ are shown.
D1, D2 denote the drift chambers; S1, S2, S3, S4 and V1 the scintillation detectors; N1 the neutron detector and Si_{mon} and Si_{spec} silicon strip detectors to detect elastically scattered and spectator protons, respectively.

cility [12, 13]. Thus the proposed investigation is planned to be performed using the COSY-11 detection system with an additional silicon strip detector for the registration of the spectator proton. The shape of the COSY-11 scattering chamber close to the target allows for the installation of the spectator detectors [26] which were already used succesfully at the CELSIUS accelerator for tagging of quasi-free proton-neutron interactions.

In figure 6 a schematic view of the COSY-11 detection system together with the spectator detector is presented. The spectator detector consists of four modules with two layers of 0.3 mm thick silicon strips. Each module is further divided into six parts each of them with 3 strips of 20 mm × 5 mm. The physical properties of the detector were implemented into the COSY-11 Monte-Carlo programme and detailed simulations of the $pd \to p_{sp}pn\eta'$ reaction were performed, taking into account the momentum and dimension spread of the COSY beam [27], as well as the dimensions of the cluster target [28] and the known resolution of the time and position measurements of the standard COSY-11 detectors.

Figure 7a depicts the spectrum of the spectator proton momentum which will be registered in coincidence with the forward flying proton and neutron. The fact that spectator protons with momenta larger than 130 MeV/c will

not be registered has the advantage that events with neutron masses differing much from its on-shell value will be omitted (compare figures 5b and 7c). A

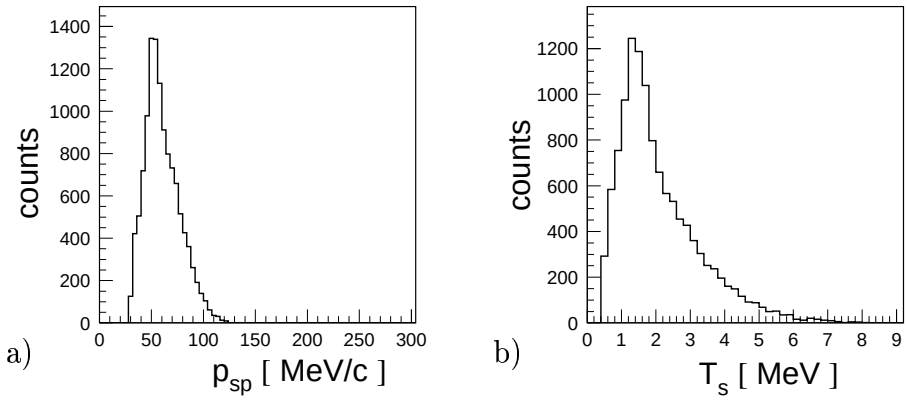

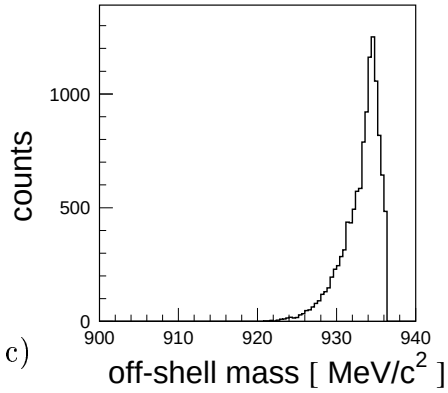

Figure 7: (a) Momentum and (b) kinetic energy distributions of the spectator protons registered in coincidence with the forward scattered neutron and proton. (c) Spectrum of the off-shell mass of the interacting neutron, provided that all nucleons from the $pd \to p_{sp}pn\eta'$ reaction have been measured with the COSY-11 detection system.

300 μm thick silicon detector can absorb protons up to a momentum of about 106 MeV/c corresponding to a kinetic energy of $T_s \approx 6$ MeV. Both layers together can absorb protons up to a momentum of 130 MeV/c ($T_s \approx 9$ MeV), however, protons with momenta lower than 30 MeV/c ($T_s \approx 0.5$ MeV) cannot be distinguished from noise. Thus this detector allows the registration and identification of about 70 % of the spectator protons hitting its sensitive area (see figure 4). On the other hand, figure 7b shows that the fraction of spectator protons having kinetic energy larger than 6 MeV and registered simultaneously with the forward scattered neutron and proton is very small. Consequently, most of the spectator protons will be fully stopped already in the first layer. This gives the opportunity to get rid of the background due to fast protons and pions crossing both layers of the detector, just by

considering in the off-line analysis only those events which have no signal in the second layer.

Both the position of the spectator detector and the proton beam momentum were optimized such that most of the registered events have an excess energy between 0 MeV and 25 MeV. This is the range for which the total cross section of the $pp \to pp\eta'$ has been studied at COSY-11 [13]. Increasing the beam momentum in general shifts the maximum of the excess energy distribution (Fig. 5a) to larger values, but simultaneously installing the spectator detector upstream the target (see figure 6), such that the spectator proton is moving opposite to the proton beam, the excess energy is decreasing, since the neutron is escaping the beam proton. Positioning of the tagger detector upstream the target also reduces drastically its irradiation. The distribution of the excess energy for events registered under the chosen geometry is shown in figure 8a. In the first approximation it reflects the dependence of the COSY-11 acceptance on the excess energy. Figure 8b

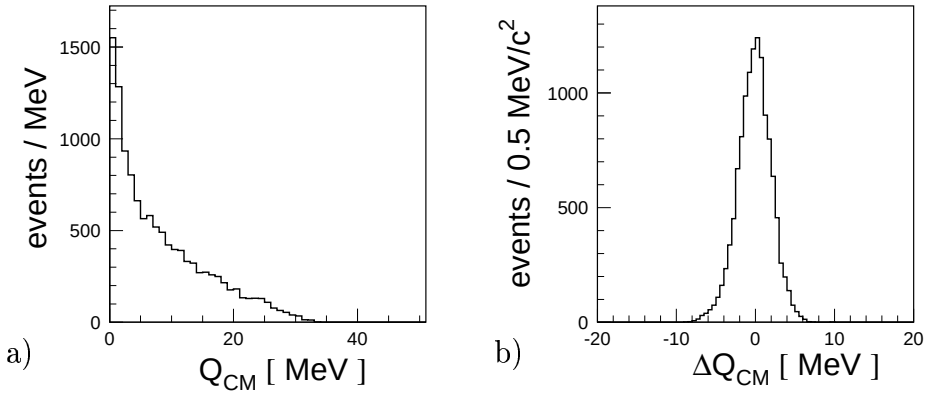

Figure 8: (a) Distributions of the excess energy Q_{CM} for the quasi-free $pn \to pn\eta'$ reaction as it would be measured with the COSY-11 detection system at a beam momentum of 3.350 GeV/c. The shape corresponds roughly to the energy dependence of the detection efficiency. The figure shows the number of reconstructed events per 1 MeV bin out of the $5 \cdot 10^6$ events generated in the target. (b) Difference between the generated and reconstructed excess energy. Calculations were performed assuming a target diameter of 0.9 cm [28], and standard deviations of 0.2 cm and 0.4 cm for the horizontal and vertical beam spread, respectively. The applied values correspond to a realistic estimation of the beam parameters based on the data from previous COSY-11 experiments [27]. The spectator detector modules were positioned behind the target, five centimeters from the beam, as it is indicated in figure 6.

depicts the difference between the generated and reconstructed excess energy. The standard deviation of the obtained resolution amounts to 2 MeV, and is due to the finite dimension of the beam and target and the granularity of the spectator detector. In these simulations the distance between the beam and the detector was adjusted to be 5 cm as an optimum regarding both the coverage of the solid angle and the angular resolution. However, the accuracy of the excess energy reconstruction may be improved significantly if needed, since the scattering chamber allows for the installation of spectator detectors at a distance of 10 cm from the beam. Apart from the excess energy, in order to identify the reaction it is necessary to determine the momentum vectors of the registered protons and neutrons. Proton momenta will be reconstructed by tracking back the proton trajectory to the target point, and the neutron momenta will be determined from the time of flight between the target and neutron detector and the angle defined by the middle of the hit segment. The granularity of the neutron detector allows to determine the horizontal position with an accuracy of ± 4.5 cm. For the time resolution of one segment (11 scintillation and 11 lead plates) a conservative value of 0.5 ns (standard deviation) was assumed. The missing mass spectrum, reconstructed from events for which signals from the spectator detector as well as the forward scattered protons and neutrons were registered, is shown in figure 9. An obtained mass resolution amouts to 7.6 MeV (FWHM) which is only 3 times the resolution of the measurements for the $pp \to pp\eta'$ reaction at an excess energy of 23.6 MeV.

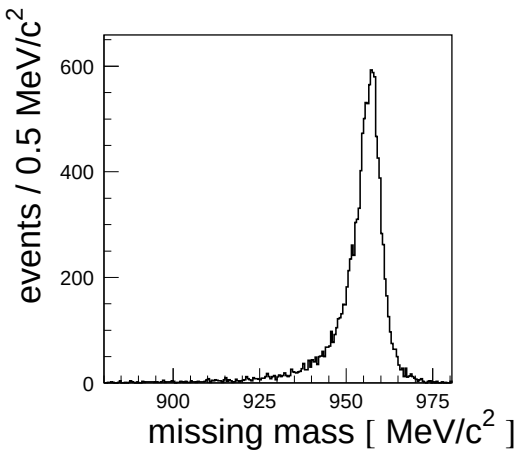

Figure 9: The missing mass distribution with respect to the pn subsystem from the reaction $pn \to pn\eta'$ as reconstructed from the generated events under the described assumptions of the time and position resolution of the COSY-11 detectors.

Assuming a luminosity of $3 \cdot 10^{30}$ cm^{-2} s^{-1}, and taking into account i) the detection efficiency which decreases with excess energy as shown in figure 8a

and ii) the energy dependence of the total cross section as determined for the $pp \to pp\eta'$ reaction, we calculate the number of quasi-free $pn \to pn\eta'$ events which will be measured per day. The calculation can be performed modulo the absolute cross section which in the one extreme scenario should be equal to the cross section of the $pp \to pp\eta'$ reaction, and in the other extreme case should be enhanced by factor of about 6.5, as discussed in the introduction. The estimation results in 30 and 195 measured and reconstructed events per day for the extreme scenarios. The energy dependence of the total cross section is predominantly determined by the nucleon-nucleon final state interaction [3, 29], which approximately has the same influence for η and η' production. Thus, the observation that the excitation function for the $pp \to pp\eta$ and $pn \to pn\eta$ reaction is approximately the same justifies our assumption of the cross section dependence for the estimation of the counting rate.

A natural extension of the experiments with the close to threshold production of η and η' mesons in proton-proton and proton-neutron collisions would be the creation of these mesons in neutron-neutron reactions. This is a challenge for the future, however, a first consideration concerning this possible study by utilizing a double quasi-free reaction has already been described in reference [30].

References

[1] P. Moskal, T. Johansson, *Investigation of the glue content in the η' meson*, COSY Proposal No. 100, April 2001.

[2] K. Maltman, N. Isgur, Phys. Rev. **D 29** (1984) 952.

[3] K. Nakayama, contribution to these proceedings, e–Print Archive: nucl–th/0108032.

[4] F. Kleefeld, M. Dillig, F. Pilotto, Acta Phys. Polon. **B 27** (1996) 2867.

[5] S. Capstick et al., APS Division Of Nuclear Physics Town Meeting On Electromagnetic And Hadronic Physics, Newport News, Virginia, 1-4 Dec 2000, e–Print Archive: hep–ph/0012238.

[6] S.D. Bass, S. Wetzel, W. Weise, Nucl. Phys. **A 686** (2001) 429.

[7] N. Nikolaev, CosyNews **No. 3**, ed. by T. Mayer-Kuckuk, Forschungszentrum Jülich, May 1998.

[8] E. Kou, Phys. Rev. **D 63** (2001) 054027.

[9] S.D. Bass, private communication.

[10] S.D. Bass, contribution to these proceedings, e–Print Archive: hep–ph/0108187.

[11] H. Calén et al., Phys. Rev. **C 58** (1998) 2667.

[12] P. Moskal et al., Phys. Rev. Lett. **80** (1998) 3202.

[13] P. Moskal et al., Phys. Lett. **B 474** (2000) 416.

[14] F. Hibou et al., Phys. Lett. **B 438** (1998) 41.

[15] F. Balestra et al., Phys. Lett. **B 491** (2000) 29.

[16] E. Chiavassa et al., Phys. Lett. **B 337** (1994) 192.

[17] H. Calén et al., Phys. Rev. Lett. **79** (1997) 2642.

[18] F. Duncan et al., Phys. Rev. Lett. **80** (1998) 4390.

[19] H. Hahn et al., Phys. Rev. Lett. **82** (1999) 2258.

[20] M. Lacombe et al., Phys. Lett. **B 101** (1981) 139.

[21] S. Häggström, doctoral thesis, Uppsala University, Acta Universitatis Upsaliensis **13** (1997).

[22] M. Lacombe et al., Phys. Rev. **C 21** (1980) 861.

[23] P. Moskal et al., Phys. Lett. **B 482** (2000) 356.

[24] J. Bacelar et al., *A Photon Detector for COSY*, COSY Proposal No. 83.2, November 2000.

[25] S. Brauksiepe et al., Nucl. Instr. & Meth. **A 376** (1996) 397.

[26] R. Bilger et al., Nucl. Instr. & Meth. **A 457** (2001) 64.

[27] P. Moskal et al., Nucl. Instr. & Meth. **A 466** (2001) 448.

[28] H. Dombrowski et al., Nucl. Instr. & Meth. **A 386** (1997) 228.

[29] F. Kleefeld, contribution to these proceedings, e–Print Archive: nucl–th/0108064.

[30] P. Moskal et al., Phys. Lett. **B 517** (2001) 295.

Study of the η-Meson Production in the Reaction pd $\rightarrow$ ^{3}He η
- Status Report and Outlook -

H.-H. Adam, I. Geck, A. Khoukaz, T. Lister, R. Santo and S. Steltenkamp
Institut für Kernphysik, Westfälische Wilhelms-Universität Münster, Germany

Abstract: The near threshold η meson production in the reaction $pd \rightarrow {}^3He\,\eta$ is investigated at the COSY-11 facility using an internal cluster jet target. A clear identification of emitted ^3He nuclei is achieved and distinct signals of the η production are observed at all studied excess energies between Q = 5 MeV and Q = 40 MeV. Preliminary results will be presented and the status of the data evaluation will be discussed.

Within the COSY-11 experiment a number of detailed measurements on meson and hyperon production in proton-proton reactions have been performed. An obvious extension of these measurements, making use of the approved techniques developed, is to investigate proton-deuteron reactions. The first type of reactions being studied is $pd \rightarrow {}^3He\,X$, where X can be any of η, η', $\pi^+\pi^-$, $\pi^+\pi^-\pi^0$.

Motivation for studying the reaction channel $pd \rightarrow {}^3He\,X$ is the currently poor data base, especially in the near threshold region, in combination with still open questions concerning the underlying production processes. Up to an excess energy of Q $\approx$ 7 MeV relative to the $pd \rightarrow {}^3He\,\eta$ threshold the SPES-II-Collaboration has measured several data points at SATURNE, reporting an isotropic angular distribution for the ejectiles [1]. However at Q $\sim$ 49 MeV there exists a data point from the COSY-GEM-Collaboration, displaying a highly non-isotropic angular distribution [2]. These observed angular distributions and cross sections have initiated two different models to describe the η-production process in pd-collisions, a two-step model proposed by Kilian and Nann [3] calculated by Fäldt and Wilkin [4], and a resonance model, in analogy with the description of the η-production in pp-reactions [2]. The energy dependence of the data measured at SATURNE is consistent with predictions of the two-step model, including a strong ^3He–η final state interaction, but fails to describe the COSY-GEM data point (Fig. 1). To clarify this situation, new data, especially in the intermediate

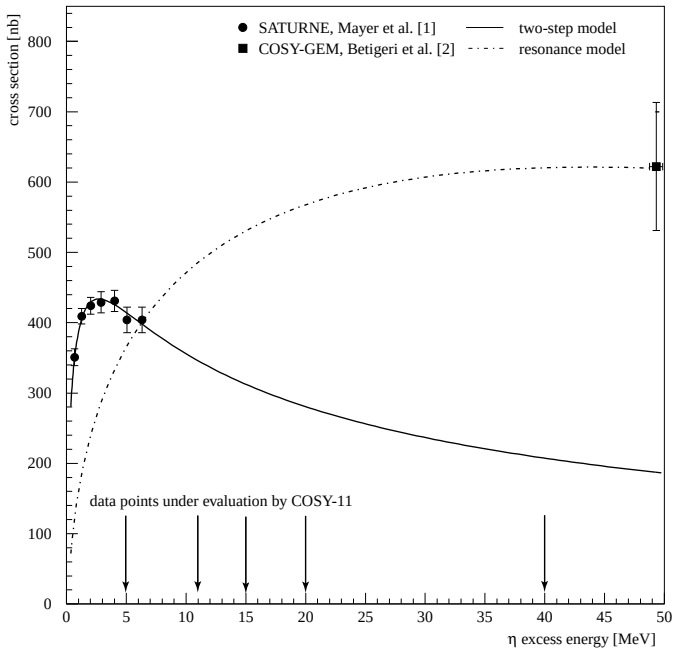

Figure 1: Published data on $pd \to {}^3He\,\eta$ including calculations for two reaction models: two-step model and resonance model. The prediction of the two-step model has been normalized to the SATURNE data while the resonance model calculation was fit to the COSY-GEM data point.

region of excess energies, are needed. Therefore, the reaction $pd \to {}^3He\,\eta$ has been measured at COSY-11 at Q values of 5, 11, 15, 20 and 40 MeV.

The COSY-11 installation makes use of one of the accelerator dipole magnets as a spectrometer magnet. Charged ejectiles of the reaction between the beam protons and the target deuterons are separated from the circulating proton beam by the magnetic field of the dipole and redirected towards the detection system. In case of the $pd \to {}^3He\,X$ reaction the four-momentum vectors of the emitted ${}^3He$ nuclei are determined by means of two drift chambers for track identification and tracking back these particles through the well known magnetic field to the fixed interaction point. By this it is possible to determine the invariant mass of the undetected X-system via a missing mass analysis. Additionally, scintillation detectors are available, acting as start and stop detectors for a time-of-flight measurement, and silicon pad detectors are mounted near the target and inside the COSY-dipole for measuring the elastic proton-deuteron scattering. A clear separation

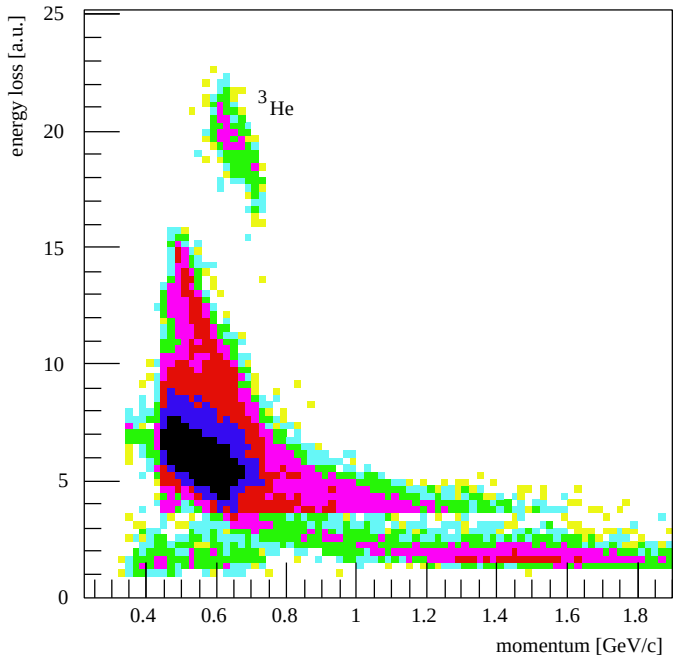

Figure 2: Particle identification by ΔE – p.

of the produced ^3He from background (pions, protons, deuterons) can be achieved by measuring the energy loss ΔE of the detected particle in the scintillation detector S1 as function of the reconstructed momentum (Fig. 2). First studies on the $^3He\eta$ reaction at COSY-11 have been performed at Q = 11 MeV [5]. It has been shown that events of the type $pd \rightarrow {}^3He\,X$ can be clearly separated from background reactions. In the resulting missing mass distribution a clear signal of the η meson production is visible on top of a background (Fig. 3), which can be reproduced by Monte Carlo simulations on multi-pion production channels.

For proton-proton reactions the normalization of the reaction data is routinely performed at COSY-11 by simultaneously measuring the *pp*-elastic scattering and comparing the results to precise *pp*-data available from the EDDA experiment. In the proton-deuteron case normalization is done analogously based on the *pd*-elastic scattering [5, 6]. However, the luminosity determination using the *pd*-elastic scattering is still under evaluation. Therefore, the absolute cross section determined in that thesis [5] has to be understood as a first guess and needs to be re-evaluated as soon as the data

normalization has been done in a more sophisticated way.
Further data on $pd \to {}^3He\,\eta$ were taken at COSY-11 at excess energies of 5, 15, 20 and 40 MeV [6].

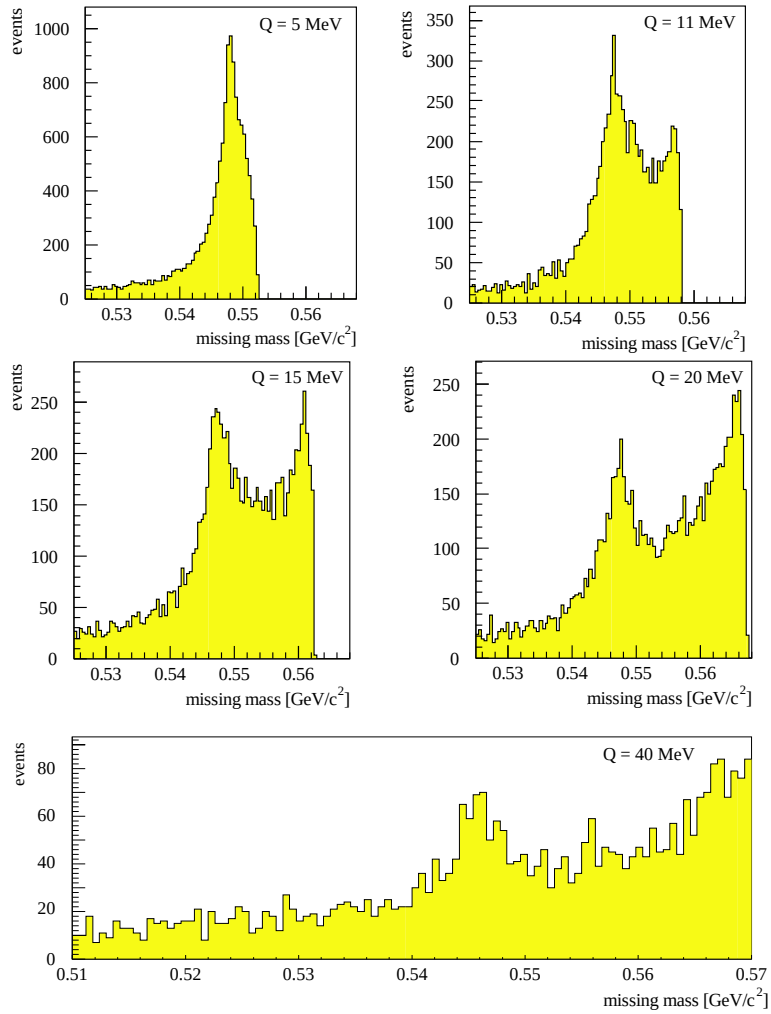

Figure 3: Missing mass spectra for $pd \to {}^3He\,X$ events for η excess energies of 5, 11, 15, 20 and 40 MeV.

For gaining a consistent picture of the energy dependence of either the cross section as well as the angular distribution each analysis had to be revisited, in order to treat data similarly for all the five η energies. Furthermore,

checks on angular distribution as well as on angular resolution have been carried out or are in progress.

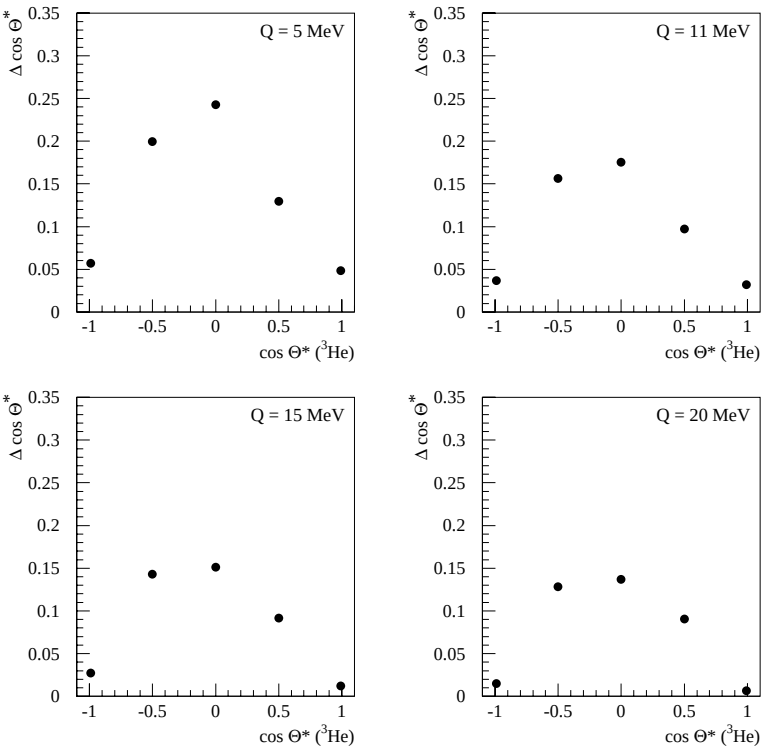

Figure 4: Angular resolution for different center of mass angles at Q values of 5, 11, 15 and 20 MeV.

Studies on the angular resolution (Fig. 4) reveal that a precise momentum determination is limited by multiple scattering of the ^3He nuclei. Therefore, in the determination of angular distributions this has to be taken into account.

For data normalization available data sets on the elastic $pd \to pd$ scattering have been examined and selected data sets have been taken into account for a parameterization, covering a broad range including the energies measured at COSY-11. At low momentum transfers the differential cross section $d\sigma/dt$ can be parameterized by an exponential function of type $exp(a+b\cdot|t|)$. However, at comparatively low energies and momentum transfers larger than $-t = 1.4\,(\mathrm{GeV/c})^2$ this fit deviates from the data. This results in a quite large error when fitting parameter a and slope b as a function of the beam

energy and thus leads to a large deviation of the parameterization for the lower energy data (Fig. 5). Therefore an optimized parameterization for the region of momentum transfers covered by the experiment has to be found. Nevertheless this parameterization already shows, that the differential *pd*-elastic cross section is only weakly energy dependent within the energy range studied at COSY-11.

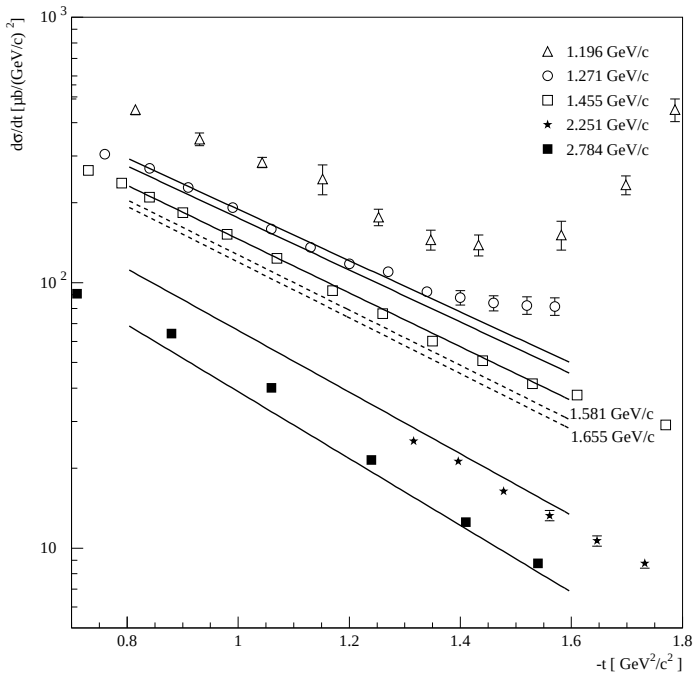

Figure 5: Preliminary parameterization of *pd*-elastic data from literature. The dashed lines represent the highest (Q = 40 MeV) and lowest (Q = 5 MeV) $pd \to {}^3He\,\eta$ excess energies measured at COSY-11.

Another option for data normalization can be performed using the quasi-free *pp*-elastic scattering, where the neutron of the target deuteron acts only as a spectator.

In addition to the reaction $pd \to {}^3He\,\eta$ there will also be investigations on the multi-pion production in $pd \to {}^3He\,\pi^+\pi^-, \pi^+\pi^-\pi^0$ appearing as background reactions to the η production. Besides the measurement on the

η production there have also been first measurements on the η' as X particle in $pd \to {}^3He\,X$ which will be studied in detail in the near future.

References

[1] B. Mayer et al., Phys. Rev. **C 53** (1996) 2068.

[2] M. Betigeri et al., Phys. Lett. **B 472** (2000) 267.

[3] K. Kilian, H. Nann, 1990 Topical Conference On Particle Production Near Threshold, Nashville, Indiana, 30 Sep - 3 Oct 1990, Proc. ed. by H. Nann, E.J. Stephenson, AIP Conf. Proc. **221** (1990) 185.

[4] G. Fäldt, C. Wilkin, Nucl. Phys. **A 587** (1995) 769.

[5] H.-H. Adam, diploma thesis, Universität Münster (2000).

[6] I. Geck, Staatsexamensarbeit, Universität Münster (2000).

Investigation of near–threshold η production in the dp $\rightarrow$ pdη reaction

J. Smyrski

Institute of Physics, Jagellonian University, Kraków, Poland

Abstract: The new proposal of the COSY–11 collaboration to measure the near–threshold η meson production in the $dp \rightarrow pd\eta$ reaction is presented. The effect of the d–η interaction in the Dalitz plot for the p–d–η final system is estimated. Feasibility of measurements of the $dp \rightarrow {}^3He\,\eta$ and $dp \rightarrow {}^3He\,\pi^0$ reactions is discussed.

1 Proposal to measure the dp $\rightarrow$ pdη reaction near threshold

The new proposal of the COSY–11 collaboration to measure the near–threshold η meson production in the $dp \rightarrow pd\eta$ reaction for seven excess energies in the range from 1 MeV to 15 MeV has been accepted by the COSY Program Advisory Committee at the spring 2001 meeting. The experiment will be performed with the COSY–11 facility using the internal deuteron beam of the COSY accelerator. The detection acceptance for measurements with deuteron beams scattered on a proton target ($dp \rightarrow pd\eta$ experiment) is by about one order of magnitude higher compared to the acceptance for measurement with proton beams scattered on a deuteron target ($pd \rightarrow pd\eta$ experiment). Momenta of the final protons will be measured with the existing detector system whereas for the determination of the deuteron momenta an additional detector consisting of a drift chamber, plastic Čerenkov counter and ΔE scintillator is being built. The η mesons will be identified via the missing mass determination. Data on the $dp \rightarrow pd\eta$ reaction are needed in order to contribute to the understanding of the η meson production mechanism in a three nucleon system. They are also important for studies of the low energy η–deuteron interaction, which according to theoretical predictions can be strong enough to form quasi–bound states.

2 Signal of η–d FSI in the Dalitz plot

The proposed measurements will make it possible to study the strength of the η–deuteron interaction on the basis of the energy dependence of the total cross section as well as using the Dalitz plot analysis for the final state particles. In order to estimate the influence of the p–d–η FSI on the measured cross sections it was assumed, that the p–d–η enhancement factor can be factorized into p–d, p–η and d–η enhancement factors:

$$f_{pd\eta} = f_{pd}(\mathrm{q}_{pd}) \cdot f_{p\eta}(\mathrm{q}_{p\eta}) \cdot f_{d\eta}(\mathrm{q}_{d\eta}) \,, \tag{1}$$

where q_{pd}, $\mathrm{q}_{p\eta}$ and $\mathrm{q}_{d\eta}$ are relative momenta in the p–d, p–η and d–η systems, respectively. The enhancement factor for the proton–deuteron FSI was calculated according ref. [1] using effective–range expansion of pd elastic

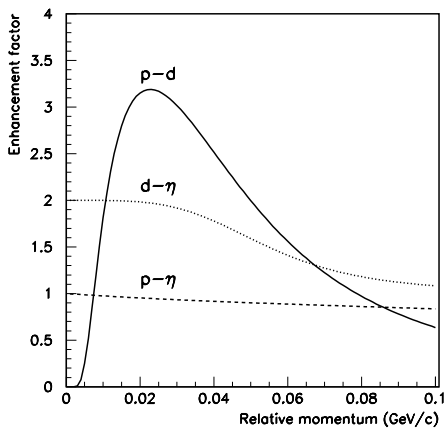

Figure 1: Enhancement factors for p–d, d–η and p–η FSI.

scattering phase shifts in spin doublet and spin quadruplet states and taking into account the Coulomb interaction. The enhancement factor for the η–proton FSI was calculated in the effective–range approximation with the complex η–proton scattering length $a_{\eta p} = 0.717 + i\,0.263$ taken from ref. [2] and the complex η–proton effective range parameter $r_{\eta p} = -1.50 - i\,0.24$ from ref. [3]. The enhancement factor for the η–deuteron interaction was calculated on the basis of the $pn \to d\eta$ near threshold cross sections measured at CELSIUS [4] divided by the two–body phase space volume and parametrized using the following expression:

$$f_{d\eta} = 1. + \frac{0.5}{0.5 + (\mathrm{Q}/5.)^2} \,, \tag{2}$$

where the excess energy Q is calculated in MeV.

Enhancement factors are shown in fig. 1 as a function of relative momentum between the interacting particles. The absolute normalization of the η–proton and proton–deuteron factors is free.

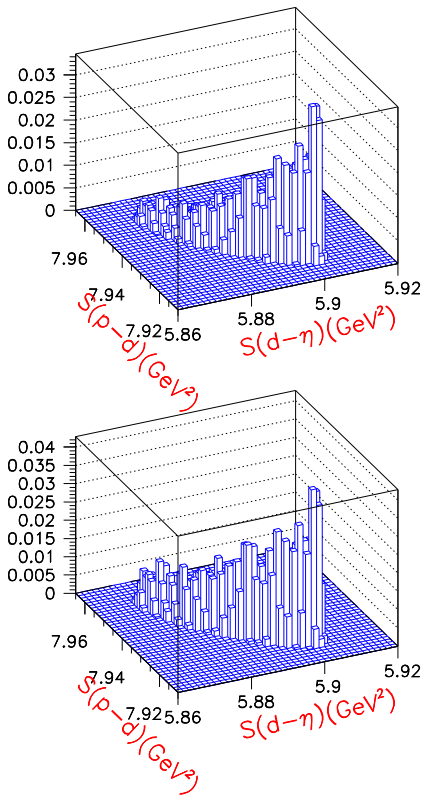

Figure 2: Dalitz plot at the excess energy of 7 MeV for $dp \to pd\eta$ for Monte Carlo events taking into account the p–d and p–η FSI (upper plot) and including in addition the d–η FSI (lower plot). The number of generated and accepted events is 60000 and 6710, respectively.

The enhancement factors were used as weights in Monte Carlo simulation of the $dp \to pd\eta$ measurements performed under the assumption of a uniform phase space distribution of the reaction products. Fig. 2 shows the Dalitz plots for the Monte Carlo events taking into account the p–d and p–η FSI (upper plot) and including also the d–η FSI (lower plot). For small values of the d–η invariant mass squared ($S(d\text{–}\eta)$) the rate is increased roughly by a factor of two when switching on the d–η FSI. From this one can conclude, that the effect of d–η FSI should be visible in the experimental Dalitz plots. For a quantitative interpretation of this effect a possibly realistic model of the three body p–d–η FSI is needed.

3 Feasibility of the dp $\rightarrow$ ^{3}Heη and dp $\rightarrow$ ^{3}Heπ^0 measurements

The detection efficiency for the $dp \rightarrow {}^3He\,\eta$ reaction, with ^3He registered in coincidence in S1 and S3, is higher than 50 % for excess energies in the range up to 10 MeV (see fig. 3). With a proper setting of the experimental trigger this reaction can be measured parallel to the $dp \rightarrow pd\eta$ reaction. Determination of the energy dependence of the $dp \rightarrow {}^3He\,\eta$ cross section can be useful for checking the absolute normalization of the $dp \rightarrow pd\eta$ cross sections and for the beam energy calibration.

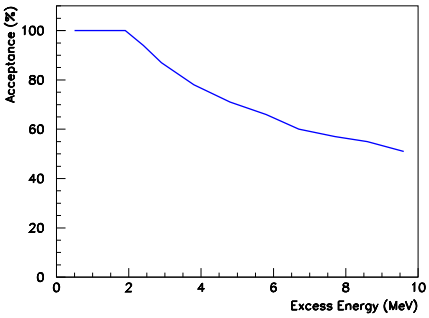

Figure 3: Acceptance of the COSY–11 detection system for a measurement of the outgoing ^3He from the reaction $dp \rightarrow {}^3He\,\eta$.

Another reaction which is considered as a candidate for "parasitic" measurements is $dp \rightarrow {}^3He\,\pi^0$. Measurement of the π^0 production below the η production threshold is very interesting since it can indicate a formation of an η–^3He bound state which decays into a π^0–^3He pair. The result of Monte Carlo simulation of the COSY–11 angular acceptance for $dp \rightarrow {}^3He\,\pi^0$ with the beam momentum set at the $dp \rightarrow pd\eta$ threshold is shown in fig. 4. For pions emitted in the forward direction the acceptance is of about 20 %. Taking from literature the value of $\frac{d\sigma}{d\Omega}(dp \rightarrow {}^3He\,\pi^0)$ at $\Theta_\pi = 0°$ as equal to about 20 nb/sr [5] and assuming the luminosity of $3 \cdot 10^{30}\,\mathrm{cm}^{-2}\,\mathrm{s}^{-1}$ one comes to the counting rate in the angular range $0.95 < \Theta_\pi = 0° < 1.0$ of about 400 events/day. For a more complete check of the feasibility of this measurement one should still determine the missing mass resolution and estimate the possible background.

4 Summary

Monte Carlo simulation of the $dp \rightarrow pd\eta$ measurements at COSY–11 indicates, that FSI(η–d) should give a measurable signal in the Dalitz plot.

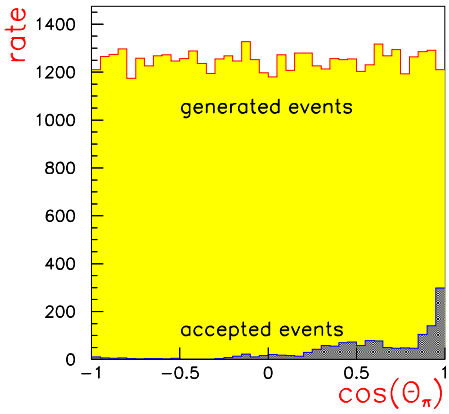

Figure 4: Angular acceptance in the CM system for a measurement of the outgoing ^3He from the reaction $dp \to {}^3He\,\pi^0$ at the beam momentum of 3.142 GeV/c.

One needs a theoretical model to establish this signal. The $dp \to {}^3He\,\eta$ reaction can be measured with a high acceptance in a parasitic mode. It can be used to check the normalization of the cross sections and the beam energy calibration. Acceptance for $dp \to {}^3He\,\pi^0$ at $\Theta_\pi = 0°$ is of about 20 %. Enhanced π^0 production below the η threshold can be an indication of an η–^3He bound state.

References

[1] H.O. Meyer, J.A. Niskanen, Phys. Rev. **C 47** (1993) 2474.

[2] M. Batinić et al., Phys. Scripta **58** (1998) 15.

[3] A.M. Green, S. Wycech, Phys. Rev. **C 55** (1997) 2167.

[4] H. Calén et al., Phys. Rev. Lett. **80** (1998) 2069.

[5] C. Kerbould et al., Phys. Lett. **B 181** (1986) 28.

ISI and FSI in NN → NNX reactions close to threshold [1]

F. Kleefeld [2]

Centro de Física das Interacções Fundamentais, Instituto Superior Técnico, Lisboa, Portugal

Abstract: The present status of the theoretical description of Initial (ISI) and Final State Interactions (FSI) in nucleon induced exclusive meson production processes close to threshold is reviewed. Shortcomings are addressed and new perspectives given.

1 Motivation

It is quite surprising, that the discussion of the theoretical description of ISI and FSI in nuclear and particle collision/production processes is gaining again increasing attention, even though people thought, this issue has been well understood due to an established formalism going back to outstanding scientists such as e.g. K. Brueckner, G. Chew, E. Hart, K.M. Watson, A.B. Migdal, E. Fermi, G. Gamov and A. Sommerfeld entering nearly all standard text books of Scattering Theory, e.g. [1, 2]. The existing formalism for the treatment of ISI and FSI is based on the idea, that T-matrix elements of many processes (in the Distorted Wave Born Approximation (DWBA)) are well described as overlap integrals of initial and final state wavefunctions multiplied by some interaction potential. This idea works quite successfully for (mainly nonrelativistic) textbook examples, in which excitation energies are small compared to the masses of the particles involved, i.e. for the description of electromagnetic transitions in atoms (excitation energies $\sim 1\,\mathrm{eV}$) or $\beta^{\pm}$-decays/transitions of atomic nuclei (excitation energies $\sim 10^2 \ldots 10^3\,\mathrm{keV}$). In these processes the initial/final states hardly go off-shell due to the transition interaction, or at least for a very short time. In reaction processes like $NN \to NNX$ (with X being a mesonic system) close to the particle production threshold the situation is quite different. The excitation energy of the NN system in such a process is of the order of the

[1] Invited talk

[2] URL: http://cfif.ist.utl.pt/~kleefeld/

mass of X. In the case of η-production this yields already about half of the nucleon mass, for heavier mesons the excitation energy is in the range of the nucleon mass. At high excitation energies it is a difficult task for the outgoing NNX system to rearrange the three-momenta and bring the 3 outgoing particles to their mass-shells. In the case of an incoming or outgoing pp system the infinite range of the Coulomb force even prevents the initial or final state particles, respectively, to go to their mass shell within a finite time. The production of "light" π-mesons seems to be quite exceptional. Yet even there one can see already various new aspects being important for the description of ISI and FSI of processes under consideration. The issue of this presentation is not the discussion of various experimental signals for mainly FSI in $NN \to NNX$ shown e.g. in [3, 4, 5] (and references therein). It is an introductory review of present theoretical formalisms and new theoretical developments treating ISI/FSI to enable researchers involved to find to a (still outstanding) *quantitative* covariant theoretical formulation to describe ISI/FSI and a better quantitative analysis of experimental data.

2 Invariants and notation in NN $\to$ NNX

In the following I will introduce quantities used in the theoretical description of the reaction $NN \to NNX$. For convenience I use the metric $(+,-,-,-)$, denote the outgoing meson X by ϕ, the incoming/outgoing particles by 1, 2, 1′, 2′ and 3′, i.e. $N(1)N(2) \to N(1')N(2')\phi(3')$, and the respective four-momenta by p_1, p_2, $p_{1'}$, $p_{2'}$ and $p_{3'} = k_\phi$. Five independent Lorentz invariants s, s_1, s_2, t_1, t_2 and one dependent invariant s_3 are introduced by $s := (p_1 + p_2)^2$, $s_1 := (p_{1'} + p_{2'})^2$, $s_2 := (p_{2'} + p_{3'})^2$, $t_1 := (p_1 - p_{1'})^2$, $t_2 := (p_2 - p_{3'})^2$ and $s_3 := (p_{3'} + p_{1'})^2 = \mathrm{m}_{1'}^2 + \mathrm{m}_{2'}^2 + \mathrm{m}_\phi^2 - s_1 - s_2$. For a discussion of the 3-body phasespace I refer the reader e.g. to [6, 7, 8]. Using the kinematical triangle function $\lambda(x,y,z) := x^2 + y^2 + z^2 - 2\,(xy + yz + zx)$ and defining $|\vec{k}_\phi|_{cm} := \sqrt{\lambda(s, \mathrm{m}_\phi^2, s_1)/(4\,s)}$ there are various ways to introduce quantities, which carry the same energy information as the CM-energy $\sqrt{s}$, e.g. $\mathrm{Q}_{cm} := \sqrt{s} - \mathrm{m}_{1'} - \mathrm{m}_{2'} - \mathrm{m}_\phi$, $|\vec{p}_1|_{cm} = |\vec{p}_2|_{cm} := \sqrt{\lambda(s, \mathrm{m}_1^2, \mathrm{m}_2^2)/(4\,s)}$, $\kappa_0 := \sqrt{\lambda(s, \mathrm{m}_1^2, \mathrm{m}_2^2)}/(2\,(\mathrm{m}_1 + \mathrm{m}_2))$ and $\eta_\phi := |\vec{k}_\phi|_{cm}^{max}/\mathrm{m}_\phi = \sqrt{\lambda(s, \mathrm{m}_\phi^2, s_1^{min})/(4s\mathrm{m}_\phi^2)}$ with $s_1^{min} = (\mathrm{m}_{1'} + \mathrm{m}_{2'})^2$. Here κ_0 is the Lab-wavenumber of the relative motion of the incoming NN-system. The *excess-energy* Q_{cm} and the dimensionless quantity η_ϕ, which is the maximum possible CM-momentum of the produced meson in units of the meson mass m_ϕ, vanish exactly at threshold. The relative motion of

the outgoing 2-particle subsystems $1'2'$, $1'3'$ and $2'3'$ can be described e.g. in terms of relative Lab-wavenumbers κ_{23}, κ_{31} and $\kappa := \kappa_{12}$:

$$\kappa_{12} := \frac{\sqrt{\lambda(s_1, \mathrm{m}_{1'}^2, \mathrm{m}_{2'}^2)}}{2\,(\mathrm{m}_{1'} + \mathrm{m}_{2'})} \quad \kappa_{23} := \frac{\sqrt{\lambda(s_2, \mathrm{m}_{2'}^2, \mathrm{m}_{\phi}^2)}}{2\,(\mathrm{m}_{2'} + \mathrm{m}_{\phi})} \quad \kappa_{31} := \frac{\sqrt{\lambda(s_3, \mathrm{m}_{1'}^2, \mathrm{m}_{\phi}^2)}}{2\,(\mathrm{m}_{1'} + \mathrm{m}_{\phi})} \tag{1}$$

3 The Watson-Migdal Approach

Historical remark

The present theoretical formalism of treating ISI and FSI goes mainly back to ideas formulated by K. Brueckner, G. Chew and E. Hart (1951) [9], K.M. Watson (1951,1952) [10, 11], A.B. Migdal (1955) [12] and E. Fermi (1955) [13], and has been transported through the literature by now as *Watson-Migdal Approximation* (WMA) or *Distorted Wave Born Approximation* (DWBA). The idea behind this formalism is, that the T-matrix T_{fi} of a particle production/anihilation/scattering process can be "factorized" into bound-state or (elastic) scattering wavefunctions describing the particles in the initial and/or final state, and a short-ranged interaction part $T^{(0)}$, describing the transition from the initial to the final state. The T-matrix in the Watson-Migdal Approach can therefore be factorized in dimensionless *enhancement factors* T_{FSI} and T_{ISI} describing the influence of FSI and ISI, respectively (being 1 for no FSI and ISI, respectively), and a short-ranged T-matrix $T^{(0)}$ describing the production/scattering process without ISI/FSI:

$$T_{fi} \;\simeq\; T_{FSI}\, T^{(0)}\, T_{ISI}\,. \tag{2}$$

In Watson's first extensive approach [11] considering a process $12 \to 1'2'$ the energy dependence of the T-matrix and therefore of the (differential) cross section $d\sigma/d\kappa$ stems mainly from the 2-particle final state wavefunction $\psi_{f,L}$, which is asymptotically related to the wavenumber κ, phaseshifts δ_L and the scattering length a_L (L = orbital angular momentum of the $1'2'$ system) [3]:

$$T_{fi} \propto \psi_{f,L} \sim \frac{e^{i\,\delta_L}\sin\delta_L}{\kappa^{L+1}} = \frac{\kappa^L}{\kappa^{2\,L+1}(\cot\delta_L - i)} \simeq -\,\frac{a_L\,\kappa^L}{1 + i\,a_L\,\kappa^{2\,L+1}}\,. \tag{3}$$

Here I used the *Effective Range Expansion* (ERE) $\kappa^{2\,L+1}\cot\delta_L = -\,a_L^{-1} + O(\kappa^2)$ [15]. As a consequence Watson obtained for the square of the T-matrix

[3] K. Brueckner et al. [9] developed the idea, that T_{FSI} is given by the wavefunctions at the interaction point $r = 0$, i.e. by $\psi_f(0)$. This idea has been later used by R. van Royen and V.F. Weisskopf [14] in the initial state to estimate decay rates Γ by $\Gamma \propto |\psi_i(0)|^2$.

and the differential cross section the following wavenumber dependences:

$$|T_{fi}|^2 \propto \frac{|a_L|^2\kappa^{2L}}{1+|a_L|^2\kappa^{4L+2}} \Rightarrow \frac{d\sigma}{d\kappa} \propto \frac{\sin^2\delta_L}{\kappa^{2L}} \propto \kappa^2|T_{fi}|^2 \propto \frac{|a_L|^2\kappa^{2L+2}}{1+|a_L|^2\kappa^{4L+2}}\,. \quad (4)$$

Watson's arguments have been generalised to processes with 3 particles in the final state. Let's e.g. consider the process $NN \to NN\phi$ close to threshold. Assuming for simplicity that FSI are mainly described by the outgoing distorted NN wavefunction $\psi_{f,L}$, while representing the produced meson ϕ by a spherical wave, which is for the orbital angular momentum ℓ of the meson relative to the NN system just proportional to a spherical Bessel function $j_\ell(q'r) \overset{q'\to 0}{\propto} q'^\ell$ (with $q' := |\vec{k}_\phi|_{cm}$), one could — according to Watson — suggest $T_{fi} \propto q'^\ell\,\psi_{f,L}$. Including the 3-body phasespace one obtains *within a nonrelativistic framework* for the total cross section:

$$\sigma \propto \int_0^{\mathrm{m}_\phi\,\eta_\phi} dq'\, q'^2\,\kappa\,|T_{fi}|^2 \propto \int_0^{\mathrm{m}_\phi\,\eta_\phi} dq'\, q'^{\,2\ell+2}\,\frac{|a_L|^2\,\kappa^{\,2L+1}}{1+|a_L|^2\,\kappa^{\,4L+2}}\,. \quad (5)$$

Using the *threshold* identity $\kappa \overset{threshold}{\longrightarrow} \sqrt{(\mathrm{m}_\phi^2\,\eta_\phi^2 - q'^2)\left(\frac{\mathrm{m}_\phi+2\,\mathrm{m}_N}{4\,m_\phi} + O(q'^2)\right)}$ a Taylor expansion in η_ϕ yields for the cross section close to threshold:

$$\sigma\Big(NN \to [[NN]_L\,\phi]_\ell\Big) \propto \eta_\phi^{2\,(\ell+L)\,+\,4}\,. \quad (6)$$

Derivation of the Onshell-Watson-Migdal Approximation

Now I am going to derive a more sophisticated Watson-Migdal formalism, which yields the traditional Watson-Migdal Approach in a certain limit [4]. The derivation — already fully performed by Watson — has recently been rederived and critically reconsidered by the author in [16, 17, 18], while simultaneously promoted in [19]. Let's consider a system of colliding and produced particles being described by a Hamilton operator $H = K + V = K + W + U$, with K being the kinetic energy operator, W being the particle number nonconserving short range interaction potential and U being the particle number conserving interaction potential of long range. Furthermore I define the long range Hamilton operator $h = K + U$. The respective

[4]The formalism to be presented is essentially equivalent to the so called *two potential scattering formalism* which can be found in various textbooks of quantum scattering theory (see e.g. [2]). Throughout such a formalism the potential consists of a sum of a short- and long-ranged potential.

eigenstates to the operators H, h and K fulfil the following Schrödinger equations:

$$(E-H)|\psi_\alpha^\pm>=\ 0\ ,\quad (E-h)|\chi_\alpha^\pm>=\ 0\ ,\quad (E_n-K)|\varphi_n>=\ 0 \qquad (7)$$

yielding the Lippmann–Schwinger equations ($G_0^\pm(E,K) := (E-K\pm i\varepsilon)^{-1}$):

$$|\psi_\alpha^\pm>=\ |\varphi_\alpha>+\frac{1}{E-H\pm i\varepsilon}V|\varphi_\alpha>=\ |\chi_\alpha^\pm>+\frac{1}{E-H\pm i\varepsilon}W|\chi_\alpha^\pm>$$
$$|\chi_\alpha^\pm>=\ |\varphi_\alpha>+\frac{1}{E-h\pm i\varepsilon}U|\varphi_\alpha>=\ |\varphi_\alpha>+G_0^\pm(E,K)T_{el}^\pm(E,K)|\varphi_\alpha>\ .$$

The S-matrix elements of the considered process are determined by $S_{\beta\alpha} = <\psi_\beta^-|\psi_\alpha^+>$ yielding the T-matrix $T_{\beta\alpha}\ =<\psi_\beta^-|(U+W)|\psi_\alpha^+>$. For $E = E_i = E_f$ the T-matrix can be reformulated in terms of *Watson's Theorem* (see e.g. p. 448, 461 in [2]), i.e.:

$$T_{\beta\alpha}\ =<\chi_\beta^-|U|\varphi_\alpha>+<\chi_\beta^-|W|\psi_\alpha^+>=<\varphi_\beta|U|\chi_\alpha^+>+<\psi_\beta^-|W|\chi_\alpha^+> \qquad (8)$$

As the particle number conserving potential U is positioned in matrix elements of states with different particle number, the respective matrix elements have to vanish. As a result I obtain $T_{\beta\alpha}\ =<\chi_\beta^-|W|\psi_\alpha^+>\ =\ <\psi_\beta^-|W|\chi_\alpha^+>$. In the following step we perform the first approximation widely known as *Watson-Migdal Approximation* (WMA) [5]. The exact asymptotic states $|\psi_\alpha^\pm>$ are approximated by the U-destorted asymptotic states $|\chi_\alpha^\pm>$, i.e. $|\psi_\alpha^\pm>\simeq|\chi_\alpha^\pm>$. As a consequence I obtain an approximated Watson's theorem $T_{\beta\alpha}\simeq<\chi_\beta^-|W|\chi_\alpha^+>$. This approximation is valid to first order in W and to all orders in U. Defining the free propagator $G_0^\pm(E,K) = (E-K\pm i\varepsilon)^{-1}$ and inserting complete sets of free asymptotic states $|\phi_n>$ the T-matrix in the WMA can be separated into a short- and long-ranged part via:

$$T_{\beta\alpha}\ \simeq\ <\varphi_\beta|\Big(1+\sum_n T_{el}^+(E,K)|\varphi_n>G_0^+(E,E_n)<\varphi_n|\Big)\,W$$
$$\Big(1+\sum_m|\varphi_m>G_0^+(E,E_m)<\varphi_m|T_{el}^+(E,K)\Big)|\varphi_\alpha>\ . \qquad (9)$$

[5]This approximation yields a "factorable" T-matrix for a field-theory, which is by construction known to be not factorable. To the knowledge of the author there is no theoretical work to quantify the validity of this approximation. Even the consequences of the approximation to the unitarity of the approximated S-matrix for systems of many coupled channels have to be investigated.

If the incoming/outgoing particles are only shortly/weakly offshell, one may approximate the free propagator $G_0^{\pm}(E,K)$ in the following way [6]:

$$G_0^{\pm}(E,K) = \frac{1}{E-K\pm i\varepsilon} = P\,\frac{1}{E-K} \mp i\pi\delta(E-K) \approx \mp i\pi\delta(E-K)\,. \quad (10)$$

The remaining δ-distribution enforces the incoming or outgoing particles, respectively, to go to their mass shell and to scatter elastically. This is why I say, the remaining principle value part of the propagator contains all the "offshell" information of the scattering/production process, *which is in problems with many coupled channels needed to restore the unitarity of the S-matrix* [7]. Let's see, how the OWMA shows up in a non-relativistic treatment of a simple $12 \to 1'2'$ scattering process, in which both the initial and final state are treated onshell. In order to proceed I identify the free asymptotic states $|\varphi_n>$ with momentum eigenstates $|\vec{\kappa}_i>$ and $|\vec{\kappa}_f>$ in the initial and final state, respectively, while in the intermediate state I insert complete sets of momentum eigenstates $|\vec{q}_i>$ and $|\vec{q}_f>$ with $\int d^3q_i\,|\vec{q}_i><\vec{q}_i| = \int d^3q_f\,|\vec{q}_f><\vec{q}_f| = 1$ resembling the symbolic completeness relation $\sum_n |\varphi_n><\varphi_n| = 1$. Using the nonrelativistic dispersion relation $E = \kappa_f^2/(2\mathrm{m}) = \kappa_i^2/(2\mathrm{m})$ the T-matrixof eq. 9 in the OWMA is given explicitly by:

$$\begin{aligned} T(\vec{\kappa}_f;\vec{\kappa}_i) &\overset{onshell}{\simeq} \\ &\simeq \Big(<\vec{\kappa}_f| - i\,\pi \int d^3q_f <\vec{\kappa}_f|T_{el}^{+}(E,K)|\vec{q}_f> \delta(E-\frac{|\vec{q}_f|^2}{2\,\mathrm{m}}) <\vec{q}_f| \Big)\, W \\ &\quad \Big(|\vec{\kappa}_i> - i\,\pi \int d^3q_i|\vec{q}_i> \delta(E-\frac{|\vec{q}_i|^2}{2\,\mathrm{m}}) <\vec{q}_i|T_{el}^{+}(E,K)|\vec{\kappa}_i> \Big)\,. \end{aligned} \quad (11)$$

[6] This approximation I will call here *Onshell-Watson-Migdal Approximation* (OWMA).

[7] K. Nakayama is surely right, if he states, that offshell effects have not to be observable within a field-theoretical formalism. He claims, that results of the principle value integrals are cutoff dependent and therefore dependent on the renormalisation scheme. To the opinion of the author this is due to the approximations made within the Watson-Migdal Approach. A careful parametrisation of the (unknown) principle value contribution of the propagator restoring field-theoretical constraints like unitarity of the S-matrix etc. will again remove the renormalisation-scheme dependence of the Watson-Migdal Approach. The discussion about observability of "offshell" effects shows, how important and instructive a careful quantitative formulation of the treatment of ISI and FSI is.

Now one can perform a partial wave expansion of the elastic T-matrices in the initial and final state. The result is given in the footnote [8]. It is obviously of the form of eq. 2, i.e. $T_{fi} \simeq T_{FSI}\, T^{(0)}\, T_{ISI}$. It is straightforward to generalise the result to the "offshell case", which contains also information about the principle values in the propagators $G_0^{\pm}(E,K)$. Parametrising the principle value contribution by some unknown function $P(\kappa)$ and denoting $T^{(0)} := < \vec{\kappa}_f, L_f | W | \vec{\kappa}_i, L_i >$ the T-matrix in the WMA can be expressed as follows [9]:

$$\begin{aligned} T(\vec{\kappa}_f, L_f; \vec{\kappa}_i, L_i) &= T_{FSI}(L_f)\; T^{(0)}\; T_{ISI}(L_i) \quad = \\ &= \Big(1 + i\, e^{i\,\delta^f_{L_f}(\kappa_f)}\, \sin\delta^f_{L_f}(\kappa_f)\,(1 - P_f(\kappa_f))\Big)\, T^{(0)} \\ &\quad \Big(1 + i\, e^{i\,\delta^i_{L_i}(\kappa_i)}\, \sin\delta^i_{L_i}(\kappa_i)\,(1 - P_i(\kappa_i))\Big) \\ &= \Big(1 + \frac{1}{2}\,(e^{2\,i\,\delta^f_{L_f}(\kappa_f)} - 1)\,(1 - P_f(\kappa_f))\Big)\, T^{(0)} \\ &\quad \Big(1 + \frac{1}{2}\,(e^{2\,i\,\delta^i_{L_i}(\kappa_i)} - 1)\,(1 - P_i(\kappa_i))\Big) \end{aligned} \tag{13}$$

[8] The axially symmetric partial wave expansions of the elastic T-matrices are given by:

$$\begin{aligned} -(2\,\pi)^2\,\mathrm{m}\; &< \vec{\kappa}_f |\, T^+_{el}(E,K)\, | \vec{q}_f > = \\ &= \frac{1}{\kappa_f} \sum_{L_f=0}^{\infty} (2\,L_f + 1)\, e^{i\,\delta^f_{L_f}(\kappa_f)}\, \sin\delta^f_{L_f}(\kappa_f)\, P_{L_f}(\cos\sphericalangle(\vec{\kappa}_f, \vec{q}_f)) \\ -(2\,\pi)^2\,\mathrm{m}\; &< \vec{q}_i |\, T^+_{el}(E,K)\, | \vec{\kappa}_i > = \\ &= \frac{1}{\kappa_i} \sum_{L_i=0}^{\infty} (2\,L_i + 1)\, e^{i\,\delta^i_{L_i}(\kappa_i)}\, \sin\delta^i_{L_i}(\kappa_i)\, P_{L_i}(\cos\sphericalangle(\vec{q}_i, \vec{\kappa}_i))\,. \end{aligned}$$

Denoting $T(\vec{\kappa}_f; \vec{\kappa}_i) \overset{onshell}{\simeq} \sum_{L_f, L_i} T(\vec{\kappa}_f, L_f; \vec{\kappa}_i, L_i)$ I finally obtain in the OWMA:

$$\begin{aligned} T(\vec{\kappa}_f, L_f; \vec{\kappa}_i, L_i) &= \\ &= \Big(1 + i\, e^{i\,\delta^f_{L_f}(\kappa_f)}\, \sin\delta^f_{L_f}(\kappa_f)\Big) < \vec{\kappa}_f, L_f | W | \vec{\kappa}_i, L_i > \Big(1 + i\, e^{i\,\delta^i_{L_i}(\kappa_i)}\, \sin\delta^i_{L_i}(\kappa_i)\Big) \\ &= \frac{\cot\delta^f_{L_f}(\kappa_f)}{\cot\delta^f_{L_f}(\kappa_f) - i} < \vec{\kappa}_f, L_f | W | \vec{\kappa}_i, L_i > \frac{\cot\delta^i_{L_i}(\kappa_i)}{\cot\delta^i_{L_i}(\kappa_i) - i} \\ &= \frac{\mathrm{Re} f^f_{L_f}(\kappa_f)}{f^f_{L_f}(\kappa_f)} < \vec{\kappa}_f, L_f | W | \vec{\kappa}_i, L_i > \frac{\mathrm{Re} f^i_{L_i}(\kappa_i)}{f^i_{L_i}(\kappa_i)}\,. \end{aligned} \tag{12}$$

Here $f^i_{L_i}(\kappa_i)$ and $f^f_{L_f}(\kappa_f)$ denote the well-known *Jost functions* (see e.g. [2]) of the elastic scattering problems in the initial and final state, respectively.

[9] The offshell parametrisation $P(\kappa)$ is related to the offshell quantity $\mathcal{P}(\kappa)$ introduced in [19] by $P(\kappa) = i\,\mathcal{P}(\kappa)/(a_L\,\kappa^{2\,L+1})$ with $\kappa^{2\,L+1}\,\cot\delta_L(\kappa) = -\,a_L^{-1} + O(\kappa^2)$.

or

$$T(\vec{\kappa}_f, L_f; \vec{\kappa}_i, L_i) \quad = \quad T_{FSI}(L_f) \; T^{(0)} \; T_{ISI}(L_i) \quad =$$

$$= \quad \frac{\cot \delta^f_{L_f}(\kappa_f) \; - i P_f(\kappa_f)}{\cot \delta^f_{L_f}(\kappa_f) \; - i} \, T^{(0)} \, \frac{\cot \delta^i_{L_i}(\kappa_i) \; - i P_i(\kappa_i)}{\cot \delta^i_{L_i}(\kappa_i) \; - i}$$

$$= \frac{\mathrm{Re} f^f_{L_f}(\kappa_f) + i P_f(\kappa_f) \mathrm{Im} f^f_{L_f}(\kappa_f)}{f^f_{L_f}(\kappa_f)} \, T^{(0)} \, \frac{\mathrm{Re} f^i_{L_i}(\kappa_i) + i P_i(\kappa_i) \mathrm{Im} f^i_{L_i}(\kappa_i)}{f^i_{L_i}(\kappa_i)} \quad (14)$$

It is interesting to see 2 ways how to "switch off" ISI or FSI: one could perform the limit $\delta_L \to 0$, or one could set the $P(\kappa) \to 1$. The OWMA is obtained by $P(\kappa) \to 0$. In the limit $P(\kappa) \to -1$ the enhancement factors just reduce to a multiplicative complex phase [10], i.e. $T_{ISI} \to \exp\left(2\, i\, \delta^i_{L_i}(\kappa_i)\right)$ or $T_{FSI} \to \exp\left(2\, i\, \delta^f_{L_f}(\kappa_f)\right)$. It has to be explored in future, in how far the restoration of the unitarity of the S-matrix will set some restrictions on the allowed values of the offshell parametrisation and its limits, and between the offshell parametrisations in the initial and final state [11]. T_{ISI} and T_{FSI} derived above are also valid for complex phaseshifts, i.e. even in the case of inelasticities yielding $|\eta_L| < 1$ for $\eta_L := \exp(2\, i\, \delta_L) = |\eta_L| \, \exp(2\, i \, \mathrm{Re}\, \delta_L)$.

Enhancement factors, 2-potential formalism and unitarity of the S-matrix

To get a better understanding of the properties of enhancement factors I want to "define" them in a very schematic way within the standard 2-potential formalism of Quantum Scattering Theory (see e.g. [2]). For a 1-channel scattering problem with a potential V, which is a sum of a short- and long-ranged potential, i.e. $V = V_S + V_L$, the S-matrix S is given in terms

[10] The careful reader may be reminded of the so called *Fermi-Watson Theorem* (see e.g. [2]) based on the idea of the unitarity of the S-matrix, which claims $T_{fi} = \exp(i\, \mathrm{Re}\, \delta_f)\, |T_{fi}| \, \exp(i\, \mathrm{Re}\, \delta_i)$ and $\mathrm{Im}\, \delta_f = \mathrm{Im}\, \delta_i$.

[11] Among the first few models studying the principle value contribution or offshell effects in ISI and FSI there are the following three to be mentioned: C. Hanhart and K. Nakayama [19] investigate the "half-shell" function related to $P(\kappa)$ within a separable potential model. V. Baru et al. [20, 21] find essential differences between separable potential models and realistic NN potentials. They calculate $P(\kappa)$ in $NN \to NNX$ for a simple rescattering graph. It would be very interesting to see, what will change in their results, if the produced meson is coupling to an excited resonance of the nucleon. Finally I want to refer to the work of B.O. Kerbikov [22]. He compares for the first time in a systematic way the effect of "half-shell" and the Jost functions to enhancement factors.

of the corresponding phaseshifts by $S = \exp(2\,i\,\delta) = \exp(2\,i\,(\delta_S + \delta_L))$, while the T-matrix can be decomposed in the standard manner:

$$T \;=\; \frac{e^{i\,\delta}\sin\delta}{\kappa} \;=\; \underbrace{\frac{e^{i\delta_L}\sin\delta_L}{\kappa}}_{=T_L} + e^{2\,i\delta_L}\,\underbrace{\frac{e^{i\delta_S}\sin\delta_S}{\kappa}}_{=T_S} \;=\; T_L \;+\; e^{2\,i\delta_L}\,T_S\,. \qquad (15)$$

Let's now consider a many-channel scattering problem. Here the unitary S-matrix is determined in terms of "phaseshift matrices" Δ, Δ_S and Δ_L by $S = (S^{-1})^+ = \exp(2i\Delta) = \exp(2i(\Delta_S + \Delta_L))$ such, that $\Delta = \Delta_S + \Delta_L$ is *Hermitian*. The question is now, whether it is possible to define an invertible matrix $T_{FSI} = T_{ISI}^{-1}$ such, that $S = \exp(2i\Delta) = T_{FSI}\,\exp(2i\Delta_S)\,T_{ISI} = (S^{-1})^+$. If Δ_S is Hermitian (yielding of course also the Hermiticity of Δ_L), the unitarity of the S-matrix $S = (S^{-1})^+$ leads to $T_{FSI}^+ = T_{FSI}^{-1}$ and $T_{ISI}^+ = T_{ISI}^{-1}$. Remembering, that due to the Baker-Campell-Hausdorff formula we can shift the argument x of a function f according to $f(x+a) = \exp(a\,\frac{d}{dx})\,f(x)\,\exp(-a\,\frac{\partial}{\partial x})$ by a differential operator $\frac{\partial}{\partial x}$ obeying $[\frac{\partial}{\partial x}\,,\,x] = 1$, we can ask the question, whether there exists a "functional derivative matrix" $\frac{\delta}{\delta\Delta_S}$ such, that $\left[\frac{\delta}{\delta\Delta_S}\,,\,\Delta_S\right] = 1$, yielding a factorization of the S-matrix $S = \exp\Big(2i\,(\Delta_S + \Delta_L)\Big)$ and T-matrix $T = (S-1)/(2i\,\kappa)$, i.e.:

$$\begin{aligned} S \;&=\; \exp\left(\Delta_L\,\frac{\delta}{\delta\Delta_S}\right)\,\exp\Big(2i\,\Delta_S\Big)\,\exp\left(-\,\Delta_L\,\frac{\delta}{\delta\Delta_S}\right) \\ \Rightarrow\; T \;&=\; \underbrace{\exp\left(\Delta_L\,\frac{\delta}{\delta\Delta_S}\right)}_{T_{FSI}}\,T_S\,\underbrace{\exp\left(-\,\Delta_L\,\frac{\delta}{\delta\Delta_S}\right)}_{T_{ISI}}\,. \qquad (16) \end{aligned}$$

It is important to realize that the matrix $\frac{\delta}{\delta\Delta_S}$ has to act like a functional derivative [12]. On the other hand the unitarity condition $T_{FSI}^{-1} = T_{FSI}^+$ enforces $\left\{\frac{\delta}{\delta\Delta_S}\,,\,\Delta_L\right\} = 0$. We can learn from the "naive" considerations presented above three points [13]:

• It is a very difficult — most probably only approximately soluble — task to systematically construct enhancement factors, which fulfil simultaneously

[12] One easily can proof, that there exists *for a finite dimensional matrix* Δ_S no matrix $\mathcal{M}$ such, that the commutator $[\mathcal{M}\,,\,\Delta_S]$ yields the unit matrix.

[13] It is left to future work to investigate the constraints of analyticity properties of 5-particle amplitudes [7] like the amplitude of the process $NN \to NNX$ to enhancement factors. For the discussion of 2- and 3-body unitarity in elastic T- and S-matrices I refer the reader e.g. to [23, 24].

the requirements $\left[\frac{\delta}{\delta\Delta_S}, \Delta_S\right] = 1$ and $\left\{\frac{\delta}{\delta\Delta_S}, \Delta_L\right\} = 0$. The commutator can be fulfilled only on a functional or operator level.
• T_{FSI} and T_{ISI} are related ($T_{FSI} = T_{ISI}^{-1}$) and constrained by unitarity (see also [18, 25]).
• The construction of enhancement factors is strongly based on Δ_S, i.e. *enhancement factors do depend on short-range interactions* [14].

4 Energy expansion and behaviour of the total cross section close to threshold

General idea

The total cross section of $NN \to NN\phi$ is given by (defining $P := p_1 + p_2$, $P' := p_{1'} + p_{2'} + k_\phi$ and the flux factor $\mathcal{F}(s) := 2\sqrt{\lambda(s; \mathrm{m}_1^2, \mathrm{m}_2^2)}$):

$$\begin{aligned} \sigma(s) &= \frac{\mathcal{S}}{\mathcal{F}(s)} \int \frac{d^3p_{1'}}{(2\pi)^3\, 2\,\omega_N(|\vec{p}_{1'}|)} \frac{d^3p_{2'}}{(2\pi)^3\, 2\,\omega_N(|\vec{p}_{2'}|)} \frac{d^3k}{(2\pi)^3\, 2\,\omega_\phi(|\vec{k}_\phi|)} \\ &\cdot\ (2\pi)^4\, \delta^4(P' - P)\ \overline{|T_{fi}|^2}\,. \end{aligned} \tag{17}$$

The symmetry factor $\mathcal{S}$ is $\frac{1}{2!}$ for two identical nucleons in the final state, otherwise 1. $\overline{|T_{fi}|^2}$ denotes e.g. spin averaging, i.e. $\frac{1}{4}\ \sum_{s_1,s_2,s_{1'},s_{2'}}\ |T_{fi}|^2$. As for this reaction $\sigma(s)$ at threshold vanishes exactly [15] it is suitable to perform an energy expansion of the $\sigma(s)$ in a sense of a Taylor expansion in terms of the small energy dependent parameters η_ϕ or Q_{cm}. The argument of the phasespace integration $|T_{fi}|^2 = |T_{FSI}\, T^{(0)}\, T_{ISI}|^2$ can be expressed as a function of the 5 independent Lorentz-invariants s, s_1, s_2, t_1, t_2. As discussed above, close to threshold T_{FSI} will mainly depend on κ_{12}, κ_{23}, κ_{31},

[14] With respect to the last point, I have to admit, that V. Baru et al. [20, 21] are right, if they state [21]: "The absolute magnitude of FSI effects depends on the momentum transfer (or on the mass of the produced meson) and hence is not universal." They deduce from a simple rescattering graph in $NN \to NNX$, that the enhancement factor only for heavy produced mesons seem to be universally factorable. Yet if they state, that "... FSI effects cannot be factorized from the production amplitude ...", they ignore the possibility, that for every short-ranged sub-amplitude in the process $NN \to NNX$ the enhancement factor may be constructed individually in a matrix form discussed. Of course it seems more attractive to treat the process $NN \to NNX$ in a Faddeev formalism rather than factorizing short- and long-ranged interactions. Yet for processes involving more particles (especially with spin) it seems at present beyond the numerical capabilites to avoid a Watson-Migdal formalism.

[15] This is not true for nucleon nucleus collisions, which allow also subthreshold production cross sections due to e.g. the Fermi motion of the nucleons in the nucleus.

i.e. $T_{FSI} \simeq T_{FSI}(s, s_1, s_2)$. T_{ISI} depends mainly on κ_0, i.e. $T_{ISI} \simeq T_{ISI}(s)$. If the propagators in the short-ranged T-matrix $T^{(0)}(s, s_1, s_2, t_1, t_2)$ are not too close to their pole and particles are mainly produced through nucleons or S-wave resonances, it is a good approximation to treat close to threshold the T-matrix as a constant [16], i.e. $T^{(0)} \simeq T^{(0)}(s^{thr}, s_1^{thr}, s_2^{thr}, t_1^{thr}, t_2^{thr})$ with

$$\begin{aligned} & s^{thr} = (\mathrm{m}_{1'} + \mathrm{m}_{2'} + \mathrm{m}_\phi)^2,\ s_1^{thr} = (\mathrm{m}_{1'} + \mathrm{m}_{2'})^2,\ s_2^{thr} = (\mathrm{m}_{2'} + \mathrm{m}_\phi)^2, \\ & t_1^{thr} = \mathrm{m}_1^2 - \mathrm{m}_{1'}(\mathrm{m}_{2'} + \mathrm{m}_\phi),\ t_2^{thr} = \mathrm{m}_2^2 - \mathrm{m}_\phi(\mathrm{m}_{1'} + \mathrm{m}_{2'})\,. \end{aligned} \tag{18}$$

To improve this approximation one can perform a Taylor expansion of $T^{(0)}(s, s_1, s_2, t_1, t_2)$ in the variables $\delta s := s - s^{thr}$, $\delta s_1 := s_1 - s_1^{thr}$, $\delta s_2 := s_2 - s_2^{thr}$, $\delta t_1 := t_1 - t_1^{thr}$, $\delta t_2 := t_2 - t_2^{thr}$, or simply a Taylor expansion in the variable $\delta s := s - s^{thr}$, i.e. [17]:

$$\begin{aligned} & T^{(0)}(s, s_1, s_2, t_1, t_2) \ = \\ & = \sum_{n=0}^{\infty} \frac{(\delta s)^n}{n!} \frac{\partial^n T^{(0)}(s^{thr}, s_1, s_2, t_1, t_2)}{\partial s^{thr\, n}} =: \sum_{n=0}^{\infty} (\delta s)^n\, T_n^{(0)}(s_1, s_2, t_1, t_2)\,. \end{aligned} \tag{19}$$

Instead of performing a Taylor expansion in δS or Q_{cm} it is more suitable to perform a Taylor expansion in the dimensionless variable η_ϕ, which is related to s and Q_{cm} by ($2\,\mu := (\mathrm{m}_{1'} + \mathrm{m}_{2'})/\mathrm{m}_\phi$):

$$\sqrt{\frac{s}{\mathrm{m}_\phi^2}} \ = \ \frac{\mathrm{Q}_{cm}}{\mathrm{m}_\phi} + 1 + 2\,\mu \ = \ \sqrt{\eta_\phi^2 + 1} \ + \ \sqrt{\eta_\phi^2 + (2\,\mu)^2}\,. \tag{20}$$

Pulling all factors depending only on s in front of the phasespace integration and selecting one specific spin-isospin channel one obtains for $\sigma(s)$:

$$\begin{aligned} \sigma(s) \ \simeq \ & \frac{1}{(2\pi)^5} \frac{\mathcal{S}}{\mathcal{F}(s)} |T_{ISI}(s)|^2 \sum_{n=0}^{\infty} (\delta s)^n \ \cdot \\ \cdot \ & \int \frac{d^3 p_{1'}}{2\,\omega_N(|\vec{p}_{1'}|)} \frac{d^3 p_{2'}}{2\,\omega_N(|\vec{p}_{2'}|)} \frac{d^3 k}{2\,\omega_\phi(|\vec{k}_\phi|)}\, \delta^4(P' - P) \ \cdot \\ \cdot \ & |T_{FSI}(s, s_1, s_2)\, T_n^{(0)}(s_1, s_2, t_1, t_2)|^2\,. \end{aligned} \tag{21}$$

[16] This approximation yielding very compact analytical results has been shown to work quite well for the reactions $pN \to pNX$ with $X = \eta, \pi^0$ (for details see e.g. [16, 26]). A corresponding approximation has been later applied to similar reactions by [27].

[17] This kind of a energy expansion ot $T^{(0)}$ is (in terms of the variable η_ϕ) for the first time taken into account by [28]. The problem is, that the Taylor coefficients are derived from onshell meson nucleon scattering data and not from any theoretical meson nucleon potential.

The energy behaviour of $\sigma(s)$ is determined on one hand by the s-dependent function in front of the phasespace integral consisting of the flux factor $\mathcal{F}$, the initial state enhancement factor T_{ISI} and the factor $(\delta s)^n$, on the other hand by the energy dependence of the phasespace integral itself, which is affected strongly by T_{FSI}. In the following I perform the threshold energy expansion of the various factors in terms of the varibable η_ϕ separately. The flux factor behaves very close to threshold like a constant, while the dominant term in the power expansion of δs is the term with $(\delta s)^0$, as all terms with $n > 0$ will be of higher order in η_ϕ.

Treatment of ISI

The energy expansion of $T_{ISI}(s) = 1 + i\,(e^{i\,\delta(\kappa_0)}\,\sin\delta(\kappa_0))(1 - P(\kappa_0))$ is discussed in [17]. I will give here merely the general ideas. Even if many people think, the offshell effects in the initial state are very small, i.e. $P(\kappa_0) \simeq 0$, the relation $T_{FSI} = T_{ISI}^{-1}$ shows, that this is most probably not true. Therefore I perform the Taylor expansion $P(\kappa_0) = P^{(0)} + P^{(2)}\,\eta_\phi^2 + O(\eta_\phi^4)$. As phaseshifts [18] are given in terms of the kinetic Lab-energy $\mathrm{T}_{Lab} = (s - (\mathrm{m}_1 + \mathrm{m}_2)^2)/(2\,\mathrm{m}_2)$ (particle 2 at rest!), one performs the following Taylor expansion of the data around threshold:

$$\begin{aligned}
\delta(\mathrm{T}_{Lab}) &= \delta(\mathrm{T}_{Lab}^{thr}) + \delta\,'(\mathrm{T}_{Lab}^{thr})\,(\mathrm{T}_{Lab} - \mathrm{T}_{Lab}^{thr}) + O((\mathrm{T}_{Lab} - \mathrm{T}_{Lab}^{thr})^2) \\
&= \delta(\mathrm{T}_{Lab}^{thr}) + \delta\,'(\mathrm{T}_{Lab}^{thr})\,\frac{m_\phi^2\,\mu}{m_2}\left(1 + \frac{1}{2\,\mu}\right)^2 \eta_\phi^2 + O(\eta_\phi^4) \\
&= \delta^{(0)} + \delta^{(2)}\,\eta_\phi^2 + O(\eta_\phi^4)\,. \qquad (22)
\end{aligned}$$

$(\mathrm{T}_{Lab}^{thr} = ((\mathrm{m}_{1'} + \mathrm{m}_{2'} + \mathrm{m}_\phi)^2 - (\mathrm{m}_1 + \mathrm{m}_2)^2)/(2\,\mathrm{m}_2)\ )$. Combining all we get:

$$\begin{aligned}
T_{ISI}(s) &= 1 + i\,(e^{i\,\delta^{(0)}}\,\sin\delta^{(0)})(1 - P^{(0)}) + \\
&+\ i\left(e^{2i\,\delta^{(0)}}\,\delta^{(2)}(1 - P^{(0)}) - P^{(2)}\,e^{i\,\delta^{(0)}}\,\sin\delta^{(0)}\right)\eta_\phi^2 + O(\eta_\phi^4)\,. \quad (23)
\end{aligned}$$

The NN phaseshifts at the threshold of $pp \to ppX$ are badly known for mesons heavier than the pion. The accuracy of the determination of high energy phaseshifts limits a quantitative theoretical calculation of $\sigma(s)$. ISI — close to threshold — don't seem to affect the energy dependence of the cross section. Their effect is just a multiplication of the cross section by some number [19] (see also e.g. [30]).

[18] I treat here phaseshifts as complex numbers containing also eventual inelasticities!

[19] Assuming $P(\kappa_0) \simeq 0$ and taking $\delta^{(0)} \approx -60°$ and $\delta^{(2)} \approx 0$ from the VPI-phaseshift analysis [29] one obtaines for $pp \to pp\eta$ close to threshold $|T_{ISI}(s^{thr})| \approx 1/2$, i.e. a reduction of $\sigma(s)$ by a factor of about 1/4.

Treatment of FSI

From considerations presented above I conclude, that in leading order the energy-, i.e. η_ϕ-dependence of $\sigma(s)$ close to threshold is determined by the energy-, i.e. the η_ϕ-dependence of the phasespace integral over an FSI-dependent integrand. I.e. the problem is now to determine the threshold energy- or η_ϕ-dependence of the following FSI-modified phasespace integral:

$$\begin{aligned} R_3^{FSI}(s) \quad &:= \quad \int \frac{d^3p_{1'}}{2\,\omega_{1'}(|\vec{p}_{1'}|)} \frac{d^3p_{2'}}{2\,\omega_{2'}(|\vec{p}_{2'}|)} \frac{d^3k}{2\,\omega_\phi(|\vec{k}_\phi|)}\, \delta^4(P'-P)\ \cdot \\ &\cdot \quad |T_{FSI}(s,s_1,s_2)\, T_n^{(0)}(s_1,s_2,t_1,t_2)|^2 \,. \end{aligned} \tag{24}$$

The phasespace integration can be rewritten into a restricted integration over four Lorentz-invariants s_1, s_2, t_1, t_2, or into a restricted integration over three of these invariants (e.g. s_1, s_2, t_1) and one unrestricted angle, while the fourth of these invariants (e.g. t_2) is expressed in terms of the three and the angle (see e.g. [6]). Remembering, that $|T_n^{(0)}(s_1,s_2,t_1,t_2)|$ close to threshold is nearly constant, I want to investigate now only the threshold energy dependence of the phasespace integral with the integrand f being a function of s_1, s_2 and s only [20], i.e. ($S := s/\mathrm{m}_\phi^2$, $S_1 := s_1/\mathrm{m}_\phi^2$, $S_2 := s_2/\mathrm{m}_\phi^2$):

$$R_3^{FSI}(s) \simeq \int \frac{d^3p_{1'}}{2\omega_{1'}(|\vec{p}_{1'}|)} \frac{d^3p_{2'}}{2\omega_{2'}(|\vec{p}_{2'}|)} \frac{d^3k}{2\omega_\phi(|\vec{k}_\phi|)}\, \delta^4(P'-P)\, f\,(S,S_1,S_2)\ . \tag{25}$$

The case considered most in $NN \to NNX$ close to threshold is the scenario, when T_{FSI} is described as a sum of T-matrices describing the FSI of the 2-particle subsystems $1'2'$, $2'3'$ and $1'3'$ in the final state only, i.e. $T_{FSI}(1'2'3') \simeq T_{FSI}(1'2') + T_{FSI}(2'3') + T_{FSI}(3'1') - 2$. This scenario in the OWMA is equivalent of using only the lowest order terms in the Faddeev expansion of the 3-particle elastic T-matrix in the final state. In an incoherent language [21] with the correct limit for no FSI this would yield $|T_{FSI}(1'2'3')|^2 \simeq |T_{FSI}(1'2')|^2 + |T_{FSI}(2'3')|^2 + |T_{FSI}(3'1')|^2 - 2$. Hence in this case we have $f\,(S,S_1,S_2) \simeq f_{12}(\kappa_{12}) + f_{23}(\kappa_{23}) + f_{31}(\kappa_{31})$, i.e.:

$$\begin{aligned} R_3^{FSI}(s) \quad &\simeq \quad \int \frac{d^3p_{1'}}{2\,\omega_{1'}(|\vec{p}_{1'}|)} \frac{d^3p_{2'}}{2\,\omega_{2'}(|\vec{p}_{2'}|)} \frac{d^3k}{2\,\omega_\phi(|\vec{k}_\phi|)}\, \delta^4(P'-P)\ \cdot \\ &\cdot\, (f_{12}(\kappa_{12}) + f_{23}(\kappa_{23}) + f_{31}(\kappa_{31}))\,. \end{aligned} \tag{26}$$

[20] The investigation of the general case is devoted to future research.

[21] The coherent case for $m_{1'} \neq m_{2'}$ has still to be investigated.

If the functions $f_{ij}(\kappa_{ij})$ can be Taylor expanded, i.e. $f_{ij}(\kappa_{ij}) = \sum_\alpha c_{ij}^{(\alpha)}\,\kappa_{ij}^\alpha$, then the threshold behaviour of $R_3^{FSI}(s)$ is given by [18]:

$$R_3^{FSI}(s) \simeq \sum_\alpha \frac{\pi^2\,\mathrm{m}_\phi^{\alpha+2}}{2^{\,\alpha+1}\,(2\mu)}\,I_\alpha\,\cdot$$
$$\cdot\left(c_{12}^{(\alpha)}+c_{23}^{(\alpha)}\left(\frac{\mathrm{m}_\phi J_+}{\mathrm{m}_{1'}}\right)^{\alpha+4}+c_{31}^{(\alpha)}\left(\frac{\mathrm{m}_\phi J_-}{\mathrm{m}_{2'}}\right)^{\alpha+4}\right)\left(\eta_\phi^{\alpha+4}+O(\eta_\phi^{\alpha+6})\right) \quad (27)$$

using the definitions $\Delta := \sqrt{1-(\mathrm{m}_{1'}-\mathrm{m}_{2'})^2(\mathrm{m}_{1'}+\mathrm{m}_{2'})^{-2}}$ and $I_\alpha := \int_0^1 du\,\sqrt{u\,((1+2\mu)\Delta^2(1-u))^{\alpha+1}}$ and $J_\pm := \frac{1}{2}\,\sqrt{2\pm 2\,\sqrt{1-\Delta^2}+(2\mu)\Delta^2}$. Considering these results it is easy to see [22], that the free 3-body phasespace (i.e. $f(S,S_1,S_2)=1$) is proportional to η_ϕ^4. Finally I want to discuss the more general case of eq. 25, yet for equal masses $\mathrm{m}_{1'}=\mathrm{m}_{2'}=\mathrm{m}_N$, i.e. $\Delta=1$. In this case $R_3^{FSI}(s)$ can be rewritten as [16]:

$$R_3^{FSI}(s) =$$
$$\stackrel{!}{=}\frac{1}{2\sqrt{S}}\,\pi^2\,\mathrm{m}_\phi^2\,\eta_\phi^2\int_0^1 du\,\frac{B}{\sqrt{\eta_\phi^2\,u+1}}\int_0^1 dv\,\frac{1}{2}\,[\,f(\,S\,,\,S_1\,,\,A+B\,v\,)$$
$$+\,f(\,S\,,\,S_1\,,\,A-B\,v\,)\,] \quad (28)$$

with $\sqrt{S}\stackrel{!}{=}\sqrt{\eta_\phi^2+1}+\sqrt{\eta_\phi^2+(2\,\mu)^2}$, $S_1\stackrel{!}{=}S+1-\sqrt{4\,S}\,\sqrt{\eta_\phi^2\,u+1}$, $A := \frac{1}{2}\,[S-S_1+2\,\mu^2+1]$ and $B := \sqrt{S\,\eta_\phi^2\,u\,(S_1-(2\,\mu)^2)/S_1}$. Remembering that S, S_1, A and B are functions of η_ϕ^2 and u, i.e. $S=S(\eta_\phi^2)$, $S_1=S_1(u,\eta_\phi^2)$, $A=A(u,\eta_\phi^2)$ and $B=B(u,\eta_\phi^2)$, it is easy to see, that the integrand can be Taylor expanded in the variable η_ϕ^2. Afterwards one has to calculate analytically/numerically the u-/v-integrals in the Taylor coefficients. Using *Mathematica*® it is no problem handle Taylor expansion and integrations.

The Coulomb problem and how to surround it

Up to now we learned, that we easily can deduce the threshold η_ϕ-dependence of the total cross section by performing a Taylor expansion of $|T_{FSI}\,T^{(0)}|^2$ in the relative wavenumbers, say e.g. κ. This is always possible for well behaved long-ranged potentials, which yield e.g. for the S-wave the

[22] Using $\int_0^1 du\,\sqrt{u\,(1-u)}=\pi/8$ one easily can deduce the expression for the free phasespace, i.e. $R_3(s)=\frac{\pi^3}{16}\,\mathrm{m}_\phi^2\,\Delta\,\frac{\sqrt{1+2\,\mu}}{2\,\mu}\,\eta_\phi^4+O(\eta_\phi^6)$.

standard ERE of the following form (see e.g. p. 466 in [31], [32] or p. 12ff in [33]):

$$\kappa \cot \delta_0(\kappa) = -\frac{1}{a} + \frac{1}{2} r \kappa^2 - P r^3 \kappa^4 + Q r^5 \kappa^6 + \ldots \tag{29}$$

If we keep only the leading two terms in the ERE, i.e. only $\kappa \cot \delta_0(\kappa) = -a^{-1} + r\,\kappa^2/2$ we call this ERE "shape independent". Specific properties of the long- and/or short-ranged potential under consideration can be absorbed in higher order "shape dependent" terms of the expansion. In 1959 M. Cini, S. Fubini, A. Stanghellini (CFS) [34] included the singularity of a One-Pion Exchange (OPE) potential at $\kappa^2 = -\mathrm{m}_\pi^2/4$ to the ERE by (see also [31]):

$$\kappa \cot \delta_0(\kappa) \;=\; -\frac{1}{a} \;+\; \frac{1}{2} r \kappa^2 \;-\; \frac{p\,\kappa^4}{1 + q\,\kappa^2}\,. \tag{30}$$

The absorption of more pathologic singularities like the essential singularity of the one-photon exchange (at $\kappa^2 = 0$) in the Coulomb interaction is performed within a formalism using a "Modified Effective Range Function" (MERF) $K_L^M(\kappa^2) := A_L(\kappa^2) + B_L(\kappa^2)\,\kappa^{2\,L+1} \cot \delta_L(\kappa)$ [35, 36] [23]. The corresponding "Modified Effective Range Expansion (MERE)" is given by:

$$B_L(\kappa^2)\,\kappa^{2\,L+1}\,\cot \delta_L(\kappa) + A_L(\kappa^2) = -\frac{1}{a} + \frac{1}{2} r \kappa^2 + \ldots \tag{31}$$

It is easy to see, how the MERE enters T_{FSI} described e.g. in eq. 14, i.e.:

$$\begin{aligned} T_{FSI} \;&=\; \frac{\kappa^{2\,L+1}(\cot \delta_L(\kappa) - i\,P(\kappa))}{\kappa^{2\,L+1}(\cot \delta_L(\kappa) - i)} \\ &\stackrel{!}{=}\; \frac{-\frac{1}{a} + \frac{r}{2}\kappa^2 - \ldots - A_L(\kappa) - i\,\kappa^{2\,L+1}\,B_L(\kappa)\,P(\kappa)}{-\frac{1}{a} + \frac{r}{2}\kappa^2 - \ldots - A_L(\kappa) - i\,\kappa^{2\,L+1}\,B_L(\kappa)}\,. \end{aligned} \tag{32}$$

So, if $|T_{FSI}|^2$ can be Taylor expanded, we immediately can derive the threshold energy dependence of the total cross section. To handle e.g. the *pp*-FSI in $pp \to pp\pi^0$, we have to use a Coulomb Modified Effective Range Expansion (CMERE) suggested by G. Breit et al. (1936) [37] and extensively investigated e.g. by [36, 38, 39, 40] [24]. For S-wave scattering the CMERE yields $B_0(\kappa) = \mathcal{C}_0^2(\eta) := 2\,\pi\,\eta/(\exp(2\,\pi\,\eta) - 1)$ ("Coulomb penetration factor",

[23] As shown in [35] the functions $A_L(\kappa^2)$ and $B_L(\kappa^2)$ are related to the Jost functions and Jost solutions of the potential problem under consideration.

[24] For the theory of *pp*-scattering see e.g. also [41, 42, 43, 44], p. 49ff in [33], [45, 46]. For the quantum-mechanical Coulomb problem and the ERE see e.g. [47, 48, 49], p. 133ff in [2],[50, 51], p. 323 in [52], p. 285 in [53], p. 54ff in [33], p. 161ff in [54], p. 16 in [55].)

"Gamov factor") and $A_0(\kappa) = 2\,\kappa\,\eta\,H(\eta)$ with the "Sommerfeld parameter" $\eta := \alpha/v_{pp} = \alpha\sqrt{(\kappa^2 + (\mathrm{m}_{1'}\mathrm{m}_{2'}/(\mathrm{m}_{1'} + \mathrm{m}_{2'}))^2)/\kappa^2}$ and $\alpha \simeq 1/137$ [25]. In the 2-potential formalism the total phaseshift $\delta_0(\kappa)$ can be decomposed into a sum of the Coulomb phaseshift $\sigma_0(\kappa)$ $(\exp(2\,i\,\sigma_0) = \Gamma(1+i\,\eta)/\Gamma(1-i\,\eta))$ and the phaseshift $\delta^c(\kappa)$ of the short-ranged potential in the presence of the Coulomb potential, i.e. $\delta_0(\kappa) = \sigma_0(\kappa) + \delta_0^c(\kappa)$. In the CFS-CMERE derived by D.Y. Wong et al. (1964) [38], which is based on a 2-potential formalism, one obtains (see e.g. also p. 468 in [31], p. 1869 in [38], or [43, 46, 56, 57, 58]):

$$\mathcal{C}_0^2(\eta)\,\kappa\cot\delta_0^c(\kappa) + 2\,\kappa\,\eta\,H(\eta) \;=\; -\frac{1}{a^c} + \frac{1}{2}\,r^c\,\kappa^2 - \frac{p^c\,\kappa^4}{1+q^c\,\kappa^2}\,. \tag{33}$$

The construction of an enhancement factor described e.g. in eq.14 is straightforward:

$$\begin{aligned}
T_{FSI} \;&=\; 1 + \frac{1}{2}\left(e^{2i\delta_0(\kappa)} - 1\right)\left(1 - P(\kappa)\right) \;=\\
&= 1 + \frac{1}{2}\left(e^{2i\sigma_0(\kappa)}\,e^{2i\delta_0^c(\kappa)} - 1\right)\left(1 - P(\kappa)\right)\\
&= 1 + \frac{1}{2}\left(e^{2i\sigma_0(\kappa)}\,\frac{\kappa\,(\cot\,\delta_0^c(\kappa) + i)}{\kappa\,(\cot\,\delta_0^c(\kappa) - i)} - 1\right)\left(1 - P(\kappa)\right)\\
&= 1 + \frac{1}{2}\left(e^{2i\sigma_0(\kappa)}\,\frac{-\frac{1}{a^c} + \ldots - 2\kappa\eta H(\eta) + i\kappa\mathcal{C}_0^2(\eta)}{-\frac{1}{a^c} + \ldots - 2\kappa\eta H(\eta) - i\kappa\mathcal{C}_0^2(\eta)} - 1\right)\left(1 - P(\kappa)\right)
\end{aligned} \tag{34}$$

Due to essential singularities appearing in the differentiation of $\sigma_0(\kappa)$ and $\mathcal{C}_0^2(\eta)$ in the limit $\kappa \to 0$ it is for a Coulomb potential not possible to perform a Taylor expansion of $|T_{FSI}|^2$ in the variable κ, in order to determine the energy behaviour of the total cross section close to threshold. Yet the problem can be surrounded in the following way: first one regularizes the Coulomb potential according to $(\mu, \varepsilon > 0)$ $(g := \alpha\,\mathrm{m}_p = \lim_{\kappa\to 0} 2\,\kappa\,\eta)$:

$$\begin{aligned}
U(r) = g\,\frac{e^{-\mu\,r}}{r+\varepsilon} \;&=\; g\int_0^\infty dt\,\theta(t-\mu)\,e^{(\mu-t)\,\varepsilon}\,e^{-tr}\\
&\overset{p.i.}{=}\; g\int_0^\infty dt\,\left[\delta(t-\mu) - \varepsilon\theta(t-\mu)\right]\,e^{(\mu-t)\,\varepsilon}\,\frac{e^{-tr}}{r}\,.
\end{aligned} \tag{35}$$

[25] Note, that $H(\eta) = -\gamma - \ln\eta + \sum_{s=1}^{\infty}\eta^2/(s\,(s^2+\eta^2))$ and $2\,\kappa\,\eta \simeq \alpha\,\mathrm{m}_p = (28.82\,\mathrm{fm})^{-1}$!

As the potential fulfils $|\int_0^\infty dr\, r\, U(r)| < \infty$ and is of Yukawa type, one can determine by the method described in [59] the corresponding Jost solution [26] $f_0(\kappa, r)$ and Jost function $f_0(\kappa) := f_0(\kappa, 0)$. As the potential is analytic at $r = 0$, it is then possible — assuming κ to be real positive — to apply the method in section IV of [36] to determine from $f_0(\kappa, r)$ and $f_0(\kappa)$ a MERF $K_0^M(\kappa^2)$ for the regularized potential by ($f_0'(\kappa, 0) := \lim_{r\to 0} \partial f_0(\kappa, r)/\partial r$):

$$K_0^M(\kappa^2) = \frac{f_0'(\kappa, 0)}{f_0(\kappa, 0)} + \frac{1}{|f_0(\kappa)|^2}\, \kappa \left(\cot \delta_0^M(\kappa) - i \right) = -\frac{1}{a} + \frac{1}{2}\, r\, \kappa^2 + \ldots \quad (37)$$

The regularized enhancement factor is now obviously obtained from eq. 34 by the replacements $e^{2\,i\,\sigma_0(\kappa)} \to f_0^*(\kappa^*)/f_0(\kappa)$, $\mathcal{C}_0^2(\eta) \to 1/|f_0(\kappa)|^2$, $2\kappa\,\eta\, H(\eta) \to f_0'(\kappa, 0)/f_0(\kappa, 0) - i\,\kappa/|f_0(\kappa)|^2$, $\delta_0^c(\kappa) \to \delta_0^M(\kappa)$. The result is:

$$T_{FSI} = 1 + \frac{1}{2} \left(\frac{f_0^*(\kappa)}{f_0(\kappa)} \frac{\left(-\frac{1}{a} + \ldots - \frac{f_0'(\kappa,0)}{f_0(\kappa,0)} + \frac{2\,i\,\kappa}{|f_0(\kappa)|^2} \right)}{\left(-\frac{1}{a} + \ldots - \frac{f_0'(\kappa,0)}{f_0(\kappa,0)} \right)} - 1 \right) \left(1 - P(\kappa) \right) \quad (38)$$

Remember, that $f_0^*(\kappa)/f_0(\kappa) = |f_0(\kappa)|^2/(f_0(\kappa))^2$. Now $|T_{FSI}|^2$ can be Taylor expanded and the threshold energy dependendence of the total cross section be determined. The Coulomb FSI is obtained by $\mu \to +0$ and $\varepsilon \to +0$. Eq. 38 can be also used, to construct enhancement factors from Jost functions obtained for singular potentials by the WKB approach [60].

Effective Range Expansion and astrophysics

One valuable source [61, 62] for sophisticated Coulomb distorted wavefunctions at low energies and CMEREs to be used in *pp* scattering is astrophysics,

[26] The Jost solution $f_0(\kappa, r)$ is obtained to be ($\mathrm{Ei}(-z) := -\int_z^\infty \exp(-t)/t$ for $z > 0$):

$$\begin{aligned} f_0(\kappa, r) &= \\ &= e^{i\,\kappa\, r} \Big\{ 1 + \sum_{n=1}^{\infty} (g\, \exp(\mu\,\varepsilon))^n \int_{n\mu}^{\infty} d\tau_n \frac{\exp(-\tau_n(r+\varepsilon))}{\kappa^2 + (-i\,\kappa + \tau_n)^2} \\ &\qquad \cdot \prod_{\nu=1}^{n-1} \left[\int_{\nu\mu}^{\infty} d\tau_\nu \frac{1}{\kappa^2 + (-i\,\kappa + \tau_\nu)^2} \right] \Big\} \\ &= e^{i\,\kappa\, r} \Big\{ 1 + \sum_{n=1}^{\infty} \left(\frac{g\, \exp(\mu\,\varepsilon)}{2\,\kappa\, i} \right)^n [\mathrm{Ei}(-(r+\varepsilon)\, n\mu) - e^{-2i\kappa(r+\varepsilon)}\, \mathrm{Ei}(-(r+\varepsilon)(n\mu - 2i\kappa))] \\ &\qquad \cdot \prod_{\nu=1}^{n-1} \left[\frac{1}{2} \ln \left(\frac{(\nu\mu)^2}{(\nu\mu)^2 + 4\,\kappa^2} \right) + i \left(\frac{\pi}{2} - \arctan \frac{\nu\mu}{2\,\kappa} \right) \right] \Big\}. \end{aligned} \quad (36)$$

which is due to an interesting correspondence between $NN \to NNX$ close to threshold and the theory of radiative capture processes in astrophysics [27].

5 $|T_{FSI}|$ onshell beyond a threshold expansion

The FSI model of Fäldt and Wilkin

A particularly interesting existing nonrelativistic theoretical model for the description of FSI is the model developed by Fäldt and Wilkin [63, 64, 65, 66]. It does not only predict the leading terms in the η_ϕ-Taylor expansion of the total cross section close to threshold, it gives expressions describing the threshold energy behaviour of the total cross section *to all orders* in η_ϕ. The idea of the model is the following: suppose we know the threshold energy dependence of the differential cross section of a process $N_1 N_2 \to (N_{1'} N_{2'})_{BS}\, \phi$, while $(N_{1'} N_{2'})_{BS}$ denotes the bound state (BS) of two components $N_{1'}$ and $N_{2'}$ with binding energy ε_B. Then we can derive — by analytical continuation of the final state wavefunction — the energy dependence of the total cross section of a process $N_1 N_2 \to (N_{1'} N_{2'})_{SS}\, \phi$ with a scattering state $(N_{1'} N_{2'})_{SS}$ of same quantum numbers as the BS. According to Fäldt and Wilkin the BS-wavefunction and the corresponding SS-wavefunction are related through analytical continuation by $\lim\limits_{\kappa \to i\alpha} \{\sqrt{2\,\alpha\,(\alpha^2+\kappa^2)}\,\psi_{SS}(\kappa, r)\} = -\,\psi_{BS}(r)$ with $\alpha = \sqrt{\mu_{12}\,\varepsilon_B}$ and $\mu_{12}^{-1} = \mathrm{m}_{1'}^{-1} + \mathrm{m}_{2'}^{-1}$. As in a Watson-Migdal picture the T-matrix factorizes into wavefunctions, there is now the hope, that also the T-matrix elements of the two processes are related by [28] [66]

[27] Compare e.g. the reaction $pp \to d\pi^+$ close to threshold and the capture process $pA \to (A+1)\gamma$. In the first process the final state $d\pi^+$ is nearly at rest, while in the second process the initial state pA is nearly at rest. The capture process behaves like time reversed compared to a threshold production process. Both processes have enhancement factors. In $NN \to NNX$ we have T_{FSI}, in the capture process we have the astrophysical S-factor S(E). The T-matrix elements look very similar: for $NN \to NN\pi$ we have $T_{fi} \sim \int dr\, u_f\, j_1(|\vec{k}_\pi|\, r) u_i$ with u_f at $\mathrm{E} \simeq 0$, while in the capture process we have $T_{fi} \sim \int dr\, u_f\, r^\lambda\, u_i$ with u_i at $\mathrm{E} \simeq 0$. The only difference is, that the excitation energy of the meson production process is high, while in the capture process all particles stay nearly onshell.

[28] The approximation made in the approach of G. Fäldt and C. Wilkin is, that one has to match the T-matrix element of a $2 \to 2$ process (described by 2 independent Lorentz-invariants s, t) to a T-matrix element of a $2 \to 3$ process (described by 5 independent Lorentz-invariants s, s_1, s_2, t_1, t_2). This is only possible by imposing some approximative (onshell) constraints to s, s_1, s_2, t_1 and/or t_2.

$(q' := |\vec{k}_\phi|_{cm})$:

$$\frac{|T_{fi}(N_1N_2 \to (N_{1'}N_{2'})_{SS}\,\phi)\,|^2}{(2\pi)^3\,2\,\mathrm{m}_{1'}\,(2\pi)^3\,2\,\mathrm{m}_{2'}} \simeq \frac{|T_{fi}(N_1N_2 \to (N_{1'}N_{2'})_{BS}\,\phi)\,|^2}{2\,\alpha\,(\alpha^2+\kappa^2)\,(2\pi)^3\,2\,\mathrm{m}_{BS}}\,. \quad (39)$$

$d\,\sigma(N_1N_2 \to (N_{1'}N_{2'})_{BS}\,\phi)/d\Omega \propto \frac{q'}{\kappa_0}\,|T_{fi}(N_1N_2 \to (N_{1'}N_{2'})_{BS}\,\phi)|^2 \propto q'^n$ at threshold yields $|T_{fi}(N_1N_2 \to (N_{1'}N_{2'})_{SS}\,\phi)|^2 \propto q'^{n-1}/(2\,\alpha\,(\alpha^2+\kappa^2))$. After performing the phasespace integration one obtains for the total cross section with the SS-system in the final state ($\bar{\mu}^{-1} := (\mathrm{m}_{1'}+\mathrm{m}_{2'})^{-1} + \mathrm{m}_\phi^{-1}$):

$$\sigma(N_1N_2 \to (N_{1'}N_{2'})_{SS}\,\phi) \propto \eta_\phi^n\,P^{(n)}(\eta_\phi\,\zeta_\phi) \quad \text{with} \quad \zeta_\phi := \frac{\mathrm{m}_\phi}{\sqrt{2\,\bar{\mu}\,\varepsilon_B}}\,. \quad (40)$$

Some of the functions $P^{(n)}(\eta_\phi\,\zeta)$ are listed without and/or with Coulomb-corrections in [66]. As mentioned in [18, 66] the cross section $\sigma(pp \to pp\pi^0)$ close to threshold can be well described by $\sigma(pp \to pp\pi^0) \propto \eta_\pi P^{(1)}(\eta_\pi\,\zeta_\pi) = \eta_\pi^4\,\zeta_\pi^3/(4\,(1+\sqrt{1+\eta_\pi^2\zeta_\pi^2})^2)$ indicating a quasi-bound state in the corresponding $\{pn\}_{I=1}$ final state. For the discussion of the relation between the $\{pn\}_{I=0}$ system and the deuteron in the final state see e.g. [66, 67, 68]. The $N\Lambda K$-final state is addressed e.g. in [69].

Onshell Faddeev models

For completeness I want to mention here some works going in the direction of a full Faddeev calculation for $NN \to NNX$. Moalem et al. (1995) [70] developed a semiquantitative formalism for describing T_{FSI} (and T_{ISI}) expanding the elastic 3-body T-matrix in the final state according to a Faddeev expansion up to second order. First solutions of simplistic nonrelativistic Faddeev models using separable interaction kernels can be found for the ηd-system in [71, 72] and for the reaction $pp \to pp\eta$ in [73]. The main result of the works is an investigation of the effective range parameters in the ηN system and the ηNN coupling constant. The models have to be improved to be quantitative and predictive [29].

[29] It e.g. should be remarked, that the complex ηN scattering length can't be investigated without considering also the effective range. For the description of a meson nucleon interaction potential parameters, which reproduce phaseshifts, have to be chosen consistently. Finally separable interaction kernels may introduce spurious states (also quasi-bound states) not existing in the original theory yet seen in the phaseshifts.

6 Relativistic OWMA — the ABSSM

As discussed in Section 3 the Watson-Migdal Approach has been based on the idea, that the energy dependence of the T-matrix close to the reaction threshold is mainly driven by ("factorized") distorted wavefunctions of interacting subsystems in the initial or final state, which are usually determined in nonrelativistic Schrödinger frameworks. With the exception of lightfront approaches the consistent factorization of relativistic wavefunctions — so called n-particle Bethe-Salpeter Amplitudes — of bound and scattering states from the T-matrix has up to now been an open problem[30]. In order to remove this lack of formalism and taking into account the fact, that production processes of heavy mesonic systems close to threshold involve high energy and momentum transfers, the author recently developed the relativistic so called *Asymptotic Bethe Salpeter State Method* (ABSSM) [16, 26, 74], which has been applied [16, 75] as a first test in a simplistic way to the reaction $pp \to p\Lambda K^+$ in the quark-gluon picture [31]. In a second step the ABSSM is now applied to reactions like $NN \to dX$. How is the relativistic deuteron wavefunction factorized within the ABSSM? A composite state vector $|P, B>$ being normalised according to $\ll P', B'|P, B >= (2\pi)^3 2\omega_B(|\vec{P}|)\delta^3(\vec{P}' - \vec{P})\delta_{B'B}$ can be expanded into free Fock states. The overlap of the free n-particle Fock states with $|P, B>$ is then reexpressed in terms of respective n-particle Bethe-Salpeter Amplitudes. For details I refer to [74]. The most dominant term of the composite deuteron state vector is the two nucleon sector, i.e. [32]:

$$
\begin{aligned}
|d^+(P,M)> \;&\simeq \\
\simeq \;& \sum_{s_1,t_1}\sum_{s_2,t_2}\int \frac{d^3\mathrm{p}_1}{(2\pi)^3\,2\,\mathrm{m}_N}\frac{d^3\mathrm{p}_2}{(2\pi)^3\,2\,\mathrm{m}_N}\int d^3x_1\,d^3x_2\,e^{-i\,(\vec{\mathrm{p}}_1\cdot\vec{x}_1+\vec{\mathrm{p}}_2\cdot\vec{x}_2)} \\
& b^+(\vec{\mathrm{p}}_1,s_1,t_1)\,b^+(\vec{\mathrm{p}}_2,s_2,t_2)|0> \;\bar{u}^{(1)}(\vec{\mathrm{p}}_1,s_1,t_1)\,\bar{u}^{(2)}(\vec{\mathrm{p}}_2,s_2,t_2) \\
& \ll 0|\,T\,[\,\psi^{(2)}(x_2)\,\psi^{(1)}(x_1)\,]\,|d^+(P,M)> \Big|_{x_1^0=x_2^0=0}\,. \qquad (41)
\end{aligned}
$$

[30] In decay processes there is the general belief, that due to R. van Royen and V.F. Weisskopf [14] the decay rate is — to a good approximation — proportional to the square of the wavefunction of the decaying system at its origin. Yet this assumes the factorizability of this square of the wavefunction.

[31] It should be mentioned that publication [75] contains apart from a quark-gluon description of $pp \to p\Lambda K^+$ the first theoretical investigation of this reaction in the nucleon-meson picture *taking into account* beside the pseudoscalar meson-exchanges (π, K) the up to now by different authors neglected, yet — as shown in [75] — *important vector-meson exchanges* (ρ, K^*).

[32] Here s_i, t_i denote spin and isospin. Spinors/operators fulfil $\bar{u}(\vec{\mathrm{p}},s,t)\,u(\vec{\mathrm{p}},s',t') = 2\,\mathrm{m}\,\delta_{ss'}\,\delta_{tt'}$, $\{b(\vec{\mathrm{p}},s,t)\,,\,b^+(\vec{\mathrm{p}}',s',t')\} = (2\pi)^3\,2\,\omega(|\vec{\mathrm{p}}|)\,\delta^3(\vec{\mathrm{p}}-\vec{\mathrm{p}}')\,\delta_{ss'}\,\delta_{tt'}$, ...

In this form the composite state vector can be conveniently used for the calculation of T-matrix elements with the help of Wick's Theorem in the standard manner. In phasespace integrations the composite deuteron appears only as one particle with mass m_d. It is beyond the scope of this presentation to discuss all the promising results and relativistic corrections predicted by this new method [33].

7 What can go wrong?

The unitarity violation problem

Naive use of enhancement factors may violate unitarity, especially in many channel problems! T_{FSI} and T_{ISI} are related by unitarity!

The fitting problem

Accurate experimental measurements of the total cross section of $NN \to NNX$ close to threshold are supposed to prove or disprove theoretical descriptions of the meson nucleon dynamics. As it seems, that the energy dependence of total cross sections close to threshold is mainly described by FSI parametrised e.g. by a sophisticated Effective Range Theory taking into account eventual quasi-bound states, the experimental measurement of *total* cross sections constrains essentially one number, i.e. $|T^{(0)}\, T_{ISI}|$. Under the assumption, that we can estimate $|T_{ISI}|$ quantitatively, we can constrain the modulus of the short-ranged T-matrix $|T^{(0)}|$. It is therefore curious to observe, that the majority of present theoretical models for the description of $NN \to NNX$ introduces or keeps one free parameter in their models, which allows them to bring their calculated cross sections into the experimental data. The most distributed method (see e.g. [25, 27, 77], the seventh equation in [25] and the second equation in [19]) of introducing a "fitting parameter" is the following: As people know from the WMA, that T_{FSI} is proportional to the dimensional quantity $\psi_f(r=0) \sim 1/(\kappa(\cot\delta - i))$, they introduce a dimensional constant or function N ("numerator") to obtain a dimensionless enhancement factor T_{FSI} by $T_{FSI} = N/(\kappa(\cot\delta - i)) = N/(-a^{-1} + r\,\kappa^2/2 + \ldots - i\,\kappa)$. This numerator N is either fitted to the data or chosen without much reasoning [34]

[33] A further decisive quantitative test of the ABSSM will be its application to the positronium decay compared to standard Bethe-Salpeter descriptions or the new factorization method based on a dispersion approach presented in [76].

[34] As it has been shown in Section 3, the numerator is given by $N = \kappa\cot\delta - i\,\kappa P(\kappa) = -1/a^{-1} + r\,\kappa^2/2 + \ldots - i\,\kappa\,P(\kappa)$ with $P(\kappa)$ staying undetermined. Even in the OWMA,

to be $-a^{-1}$. It is also possible to transfer the quantitative uncertainty in the description of FSI/ISI to a "fitting parameter" in the short ranged T-matrix $T^{(0)}$. While in the model of V. Bernard et al. [27] $|T^{(0)}|^2$ is just chosen to fit to the data, the "fitting parameter" of the Jülich-model for the threshold production of pions in nucleon nucleon collisions (see [78] and references therein) is the heavy meson nucleon (anti-)nucleon coupling constants (ωNN, σNN) in the so called "pair diagrams", which is tuned to meet the $pp \to pp\pi^0$ total cross section.

The Gell-Mann-Watson-Rosenfeld-Koltun-Reitan et al. problem

The interpretation of the total cross section of $pp \to pp\pi^0$ close to threshold has a peculiar history. The theoretical situation is summarized by H. Machner and J. Haidenbauer (1999) [79] as follows: "From phase space alone the cross section should follow a ... η^4 dependence. However, this is in complete disagreement with data. Taking into account 'minimal effects' from the final NN interaction i.e. using the first term in the ERE [35] ..., leads to an η^2 dependence ....". Then the authors give a widely and by now used expansion of $\sigma(pp \to pp\pi^0)$ close to threshold, which they call "barrier penetration model", i.e.

$$\sigma(pp \to pp\pi^0) \stackrel{?}{=} \beta_{\mathrm{Ss}}\, \eta_\pi^2 + \beta_{\mathrm{Ps}}\, \eta_\pi^6 + \beta_{\mathrm{Pp}}\, \eta_\pi^8 \,. \tag{42}$$

This threshold expansion goes back to a phenomenological discussion of M. Gell-Mann, K.M. Watson (1954) [80] and A.H. Rosenfeld (1954) [81]. Early datapoints for $\eta_\pi \geq 0.5$ listed in [82] seemed to support the η_π^2-behaviour of $\sigma(pp \to pp\pi^0)$ very close to threshold, while the 2 datapoints at $\eta_\pi = 0.660$ and 1.11 [81] indicated $\sigma(pp \to pp\pi^0) \propto \eta_\pi^8$ (see also [13]) showing the onset of Pp-production. This is why theory thankfully acknowledged the theoretical model for $\sigma(pp \to pp\pi^0)$ presented by D.S. Koltun and A. Reitan (KR1966) [83], which resulted in $\sigma(pp \to pp\pi^0) \propto \eta_\pi^2$ close to threshold [36]. Accurate data for $0.13 \leq \eta_\pi \leq 0.56$ published by H.O. Meyer et al. (1990) [85, 86] and A. Bondar et al. (1995) [87] could be — within the errorbars — understood as a final confirmation of the η_π^2-dependence of

i.e. with $P(\kappa) \simeq 0$, there is no reason to neglect in N the term $r\,\kappa^2/2$, while keeping it finite in the denominator. Such a procedure strongly affects the energy dependence of the cross section.

[35] At this point the authors refer to the expression $|T_{FSI}|^2 = 1/(k^2 + [-1/a + r\,k^2/2]^2)$.

[36] It should be mentioned, that 1969 there followed a complementary theoretical approach by M.E. Schillaci et al. [84].

$\sigma(pp \to pp\pi^0)$ close to threshold [37]. Yet latest data (see [88, 89] and references therein) show clearly, that the energy dependence of $\sigma(pp \to pp\pi^0)$ very close to threshold is much steeper than η_π^2. It seems, that phasespace behaviour, i.e. an η_π^4-dependence, is restored for $\eta_\pi < 0.2$, while the "η_π^2-plateau" of $\sigma(pp \to pp\pi^0)/\eta_\pi^2$ in the range $0.2 \leq \eta_\pi \leq 0.5$ is a structure due to a quasi-bound state in the pp-system well described within the formalism of G. Fäldt and C. Wilkin [63, 64, 65, 66] (see also Section 5). It is no surprise, that — according to the introduction of [90] — the most theoretical (standard) models of $pp \to pp\pi^0$ are more or less sophisticated versions of the work of KR1966, who differ mainly in the sophistication of $T^{(0)}$, yet use same FSI and phasespace arguments in order to reproduce the η_π^2-dependence of $\sigma(pp \to pp\pi^0)$ close to threshold. The problem is now, that the calculations of KR1966 and therefore also the — often quoted — original considerations of M. Gell-Mann, K.M. Watson (1954) [80] and A.H. Rosenfeld (1954) [81] contain an explicit mathematical mistake. To make the mistake more transparent, I translate the notation of KR1966 in the language used in this presentation, i.e. I perform the replacements $\mathrm{M} \to \mathrm{m}_p$, $\mu \to \mathrm{m}_\pi$, $\mathrm{p}' \to \kappa$, $\mathrm{E}_p \to \mathrm{T}' := \mathrm{T}_{pp'}^{kin} = \sqrt{s_1} - 2\,\mathrm{m}_p$ and $\mathrm{E}_f \to \mathrm{Q}_{cm}$. Using this notation equations 18 and 19 in KR1966 read:

$$\frac{d\sigma}{d\mathrm{T}'} = \frac{2\pi}{v}\frac{1}{4}\sum |T_b|^2 \frac{d\rho(\mathrm{Q}_{cm})}{d\mathrm{T}'}, \quad \frac{d\rho(\mathrm{Q}_{cm})}{d\mathrm{T}'} = \frac{(2\mathrm{m}_\pi \mathrm{m}_p)^{\frac{3}{2}}}{(2\pi)^4}\sqrt{(\mathrm{Q}_{cm} - \mathrm{T}')\mathrm{T}'} \quad (43)$$

Making according to KR1966 the approximation $|T_b|^2 \simeq |T(0)|^2/(1 + a^2\,\kappa^2)$ and using $\kappa^2 = \mathrm{m}_p\,\mathrm{T}' + O(\mathrm{T}'^2)$ we obtain

$$\begin{aligned} \sigma &\simeq \frac{2\pi}{4v}\sum |T(0)|^2 \int_0^{\mathrm{Q}_{cm}} d\mathrm{T}' \, \frac{1}{1 + a^2\,\mathrm{m}_p\,\mathrm{T}' + O(\mathrm{T}'^2)} \, \frac{d\rho\,(\mathrm{Q}_{cm})}{d\mathrm{T}'} \\ &\propto \mathrm{Q}_{cm}^2 \propto \eta_\pi^4 \,. \end{aligned} \quad (44)$$

This should be compared to equation 21 in KR1966. Koltun and Reitan write: "For $\mathrm{Q}_{cm} \gg \mathrm{m}_p^{-1}\,a^{-2}$ we may approximate eq. 18 and write":

$$\sigma \simeq \frac{2\,\pi}{4\,v}\frac{1}{\mathrm{m}_p\,a^2}\sum |T(0)|^2 \int_0^{\mathrm{Q}_{cm}} d\mathrm{T}' \, \frac{1}{\mathrm{T}'} \, \frac{d\rho\,(\mathrm{Q}_{cm})}{d\mathrm{T}'} \propto \mathrm{Q}_{cm} \propto \eta_\pi^2 \,. \quad (45)$$

i.e. they obtain a total cross section with an η_π^2- and not an η_π^4-dependence. We can see, how the error occurs: although the lower integration limit is

[37] If one has a more careful look to the data, one can see already in these data very close to threshold a deviation of the energy dependence of $\sigma(pp \to pp\pi^0)$ from the "expected" η_π^2-behaviour.

0, they allow the replacement $1 + a^2\,\mathrm{m}_p\,\mathrm{T}' \to a^2\,\mathrm{m}_p\,\mathrm{T}'$, which is equivalent neglecting the $-a^{-1}$ term in the ERE [38]. As easy the error is detectable in KR1966, as hidden it is among various features of $T^{(0)}$ in the publications and computer codes of present theoretical calculations. One either can recover it by trying to reproduce their results or from the statements they make in their publications. Many models mentioned in E. Hernández et al. [91, 92], especially the models of C.J. Horowitz et al. [93], J.A. Niskanen [94, 95], G.A. Miller et al. [77] and the Jülich-model (see [78] and refererences therein), are set up nearly in the same way as KR1966. As all these works seem to reproduce the energy dependence of the direct pion production close to threshold predicted in Koltun and Reitan [83], it seems, that they all use the same approximation as Koltun and Reitan [83] [39]. C. Hanhart states in table 1.2 of his doctoral thesis [96], that $\sigma_{11} \propto \eta^2$ and on page 13 below eq. 1.7, that $\sigma^{(0,\ell)}_{NN\to NN\pi}(\eta) \propto \eta^{2\ell+2}$ — in contrast to my result of eq. 6 —, even after having derived the correct integral of eq. 5. N. Kaiser claimed [97], that the $1/a$ term in the ERE could be neglected, from wich they obtained in [27] a Q_{cm}-dependence of the cross section close to threshold. An alternative explanation for the mysterious threshold energy dependence of modern calculations hidden in computer codes might be another systematic mistake, i.e. the use of a 2-body phasespace instead of a 3-body phasespace. E.g. J.A. Niskanen states in [25], that $\sigma \sim (a^2\,\mathrm{p}_f)/(1+(\mathrm{p}_f\,a)^2)$, where "$\mathrm{p}_f$ in the numerator is the momentum dependence of the phase space". Well, from the arguments given above we know, that the momentum dependence must be p_f^2! Finally I want to mention here a semantic problem in the definition of η_π: in [85] H.O. Meyer et al. state correctly, that η_π is "the largest possible center-of-mass pion momentum (with nucleons at rest relative to each other) divided by the pion mass", which yields $\eta_\pi := \sqrt{\lambda(s, \mathrm{m}_\pi^2, s_1^{min})/(4\,s\,\mathrm{m}_\pi^2)}$. In Horowitz et al. (1994) [93] it is stated, that q' is not κ, but "the pion momentum in the final pp center-of-mass system", which would yield the definition $\eta_\pi^{Horowitz} := \sqrt{\lambda(s, \mathrm{m}_\pi^2, s_1^{min})/(4\,s_1^{min}\,\mathrm{m}_\pi^2)} \stackrel{!}{=} \eta_\pi\,\sqrt{s/(2\,\mathrm{m}_p)^2}$. Even if both quantities vanish at threshold, they increasingly differ at higher energies. $\eta_\pi = 0.557$ yields e.g. $\eta_\pi^{Horowitz} = 0.603$.

[38] Even an infinitesimal value for $1/a$ would yield $\sigma(pp \to pp\pi^0) \propto \eta_\pi^4$ close to threshold!

[39] This is quite surprising, as J. Niskanen states in [94], that H.O. Meyer (see e.g. p. 657 in [86]), G.A. Miller, P.U. Sauer [77] are aware, that the cross section "dependence at threshold is not $\sigma_{tot} = a\,\eta^2\,\ldots$". In their case this seems to be due to the energy dependence of their specific form of $T^{(0)}$ (see e.g. eq. 49) and not due to a corrected phasespace.

The Miller-Sauer problem

The energy dependence of the total cross section for $pp \to pp\pi^0$ derived by G.A. Miller and P.U. Sauer (1991) [77] — the standard calculation for direct meson production — is not reproducable by means discussed in their publication. The fall-off of the total cross section for $\eta_\pi > 0.4$ is much to steep compared to Effective Range or Coulomb Modified Effective Range calculations or for a result obtained by a calculation with wavefunctions as solutions of Schrödinger equations with strong and Coulomb potential. The direct meson production is only possible through FSI and ISI and is therefore a crucial test for a correct description of FSI and ISI.

The problem of wrong application of the two potential formalism

Many people nowadays describe the influence of Coulomb interactions in FSI by the CFS-CMERE [34, 31] listed in eq. 33 and derived from a two potential formalism. I.e. the total S-wave phaseshift $\delta_0(\kappa)$ is given by $\delta_0(\kappa) = \sigma_0(\kappa) + \delta_0^c(\kappa)$, while $\sigma_0(\kappa)$ is the S-wave Coulomb phaseshift. In the construction of T_{FSI} we have — according to the two potential formalism — to use $\delta_0(\kappa)$ and not $\delta_0^c(\kappa)$. Therefore T_{FSI} is given in the OWMA according to eq. 34 by

$$T_{FSI} \simeq \simeq \frac{1}{2}\left(e^{2i\sigma_0(\kappa)} \frac{-\frac{1}{a^c} + \frac{1}{2}\, r^c\, \kappa^2 - \frac{p\,\kappa^4}{1+q\,\kappa^2} - 2\,\kappa\,\eta\, H(\eta) + i\,\kappa\, \mathcal{C}_0^2(\eta)}{-\frac{1}{a^c} + \frac{1}{2}\, r^c\, \kappa^2 - \frac{p\,\kappa^4}{1+q\,\kappa^2} - 2\,\kappa\,\eta\, H(\eta) - i\,\kappa\, \mathcal{C}_0^2(\eta)} + 1 \right). \quad (46)$$

The limit $\sigma_0(\kappa) \to 0$ performed by the majority of experimental and theoretical researchers yields results, which one would get, *if one does not apply the two potential formalism properly*. As discussed above the presence of Coulomb phaseshifts $\sigma_0(\kappa)$ introduces essential singularities in the phase-space integrations, when calculating cross sections, which can only be resolved, if the Coulomb potential is regularized consistently.

The numerator or Moalem et al. problem

Going back to the ideas of K. Brueckner et al. [9], i.e. that $T_{FSI} \propto \psi(r=0)$ or equivalently $T_{FSI} \simeq (N \exp(i\,\delta) \sin\delta)/\kappa = N/(\kappa\,(\cot\delta - i))$, it has been very early clear, that the denominator of enhancement factors is determined by the ERE, i.e. by $\kappa\,(\cot\delta - i) = -a^{-1} + \ldots - i\,\kappa$. The unknown numerator of T_{FSI} has been fixed either by hand, i.e. by setting the dimensional constant N to some suitable value, or — to be free of ambiguities

— T_{FSI} was chosen to be the inverse Jost functionfootnoteThis choice can be found in nearly every textbook of scattering theory (see e.g. [1, 2])., i.e. $T_{FSI} = 1/f_0(\kappa)$. Even if the inverse Jost function yields — apart from the correct denominator of T_{FSI} — a κ-dependent numerator, it can be observed in literature, that many authors approximate the numerator of T_{FSI} (after performing a Taylor expansion in κ) by the term, which is $O(\kappa^0)$, i.e. by a constant, while keeping the full κ-dependence of the denominator (see e.g. [19, 98, 99, 100]) [40].

Among others A. Moalem et al. (1996) [57, 101] and R. Shyam (1999) [58] use within an Effective Range Approach complex scattering length and effective range parameters, Moalem for the ηp system in the final state, Shyam for the $K^+\Lambda$ system in the final state. Both authors use a Coulomb modified CFS formula [31, 34] to describe Coulomb interactions and *both authors observe mysterious "oscillations" of the cross section as a function of energy close to threshold.* How can this be, especially as both use different methods for enhancement factors: Moalem uses $T_{FSI} = N/\kappa(\cot\delta_0(\kappa) - i)$, while Shyam uses the inverse Jost function $T_{FSI} = 1/f_0(\kappa)$. *The problem is, that both authors don't use the correct numerator* [41] *in the enhancement factor*, which is determined by the OWMA, i.e. they must use $T_{FSI} = \kappa\cot\delta_0(\kappa)/(\kappa(\cot\delta_0(\kappa) - i)) = (\mathrm{Re}\, f_0(\kappa))/f_0(\kappa)$, which stabilizes the energy dependence very close to threshold. *Both authors don't apply the two potential formalism correctly* by skipping the Coulomb-phaseshifts and the Rutherford amplitude. On the other hand one can observe, that — due to the different numerators of T_{FSI} — the penetration factor $\mathcal{C}_0^2(\eta)$ enters differently in the "more correct" (above) and wrong (below) expression:

$$\begin{aligned}
\frac{\kappa\cot\delta_0^c(\kappa)}{\kappa\,(\cot\delta_0^c(\kappa) - i)} &\rightarrow \frac{-\frac{1}{a^c} + \frac{1}{2}r^c\,\kappa^2 + \ldots - 2\,\kappa\,\eta\,H(\eta)}{-\frac{1}{a^c} + \frac{1}{2}r^c\,\kappa^2 + \ldots - 2\,\kappa\,\eta\,H(\eta) - i\,\kappa\,\mathcal{C}_0^2(\eta)} \\
\frac{N}{\kappa\,(\cot\delta_0^c(\kappa) - i)} &\rightarrow \frac{N\,\mathcal{C}_0^2(\eta)}{-\frac{1}{a^c} + \frac{1}{2}r^c\,\kappa^2 + \ldots - 2\,\kappa\,\eta\,H(\eta) - i\,\kappa\,\mathcal{C}_0^2(\eta)}\,. \qquad (47)
\end{aligned}$$

The Titov et al. problem

As a side effect of the purpose of their calculation Titov et al. (2000) [102] reconsidered to some extend the Inverse Jost Function Method for the descrip-

[40] It should be noted, that this nontrivial approximation changes the energy dependence of the total cross section at larger energies.

[41] By their choice both authors set the numerator of the enhancement factor to a constant: Moalem replaces $\kappa\cot\delta_0(\kappa)$ by a constant, Shyam performs first the replacement $\mathrm{Re}\, f_0(\kappa) \rightarrow 1$, then he removes the κ^2 term of the ERE in the numerator ending up with an enhancement factor like Moalem, i.e. $T_{FSI} = N'/\kappa(\cot\delta_0(\kappa) - i)$.

tion of ISI and FSI. The problem arising in their work is, that they use for the description of the pp FSI the effective range parameters $a_{pp} = -7.8098\,\mathrm{fm}$ and $r_{pp} = 2.767\,\mathrm{fm}$, even not using a CMERE. In order to describe their inverse Jost function they essentially use a simple nuclear "shape independent" ERE $\kappa \cot \delta(\kappa) = -a^{-1} + r\,\kappa^2/2$. In such a nuclear ERE without Coulomb they should use for the pp system the well known effective range parameters $a_{pp} = -17.1\,\mathrm{fm}$ and $r_{pp} \simeq 2.8\,\mathrm{fm}$ (see e.g. p. 254 in [103], p. 425 in [46], p. 115 in [32]). The relation beween nuclear and Coulomb modified effective range parameters is discussed e.g. in [104] or on p. 39 in [55].

The wavenumber problem

The threshold production of heavy mesons in NN collisions involves high relative energies in the initial state and high energy- and momentum-transfers at the meson-production vertex. In quantitative calculations it is therefore important to define quantities carefully and such, that they are valid also at high energies within a relativistic framework. This is, why it is important to mention, that standard EREs are expansions in the Lab-wavenumber and not in momenta [42].

The phaseshift problem

Phaseshifts are described in the Lab-system! This is not only true for proton nucleus scattering, but also for pp scattering, where the CM-system seems more convenient. If phaseshifts are theoretically determined from a Schrödinger equation (e.g. for the pp-system (p. 419ff in [46]), it makes a large difference at higher energies, whether one uses Lab- or CM-quantities:

$$\left(\frac{1}{r^2}\frac{d}{dr}\left(r^2\frac{d}{dr}\right) + K^2 - \frac{L(L+1)}{r^2} - \frac{\alpha\,\mathrm{m}_p}{r}\right) R^{J,I}_{L,S}(K,r) \quad = \\ = \quad \mathrm{m}_p \sum_{L'S'} V^{J,I}_{LS,L'S'}(\tilde{r})\, R^{J,I}_{L'S'}(K,r)\,. \qquad (48)$$

($\tilde{r}_{cm} = r$, $\tilde{r}_{\mathrm{Lab}} = r/2$). I.e. use Lab-quantities $K = \kappa$ and $\mathrm{T}_{\mathrm{Lab}} = \omega_p(2\kappa) - \mathrm{m}_p \simeq 2\,\kappa^2\,/\,\mathrm{m}_p$ (Final State (FS)) or $K = \kappa_0$ and $\mathrm{T}_{\mathrm{Lab}} = \omega_p(2\kappa_0) - \mathrm{m}_p \simeq$

[42] It is therefore not correct, if on p. R241 in [79] it is stated, that "k is the relative baryon momentum". The authors should have written, that k is the relative wavenumber, which makes of course only at high relative energies a difference! On page R242 in [79] the authors define the Gamov factor by $C(q) = 2\,\pi\,\gamma_q/(\exp(2\,\pi\,\gamma_q) - 1)$ with $\gamma_q = \mu\alpha/q$ and state, that "μ and q are the reduced mass and the relative momentum of the two-body subsystem in which the Coulomb interaction occurs ...". This definition is also not exact at higher energies! They should have defined $\gamma_q = \alpha/v$ with v being the relative Lab-velocity of the two-body subsystem in which the Coulomb interaction occurs.

$2\,\kappa_0^2\,/\,\mathrm{m}_p$ (Initial State (IS)) and *not* the CM-quantities $K = 2\mathrm{m}_p\,\kappa/\sqrt{s_1}$ and $\mathrm{T} = \sqrt{s_1} - 2\mathrm{m}_p$ (FS) or $K = 2\mathrm{m}_p\,\kappa_0/\sqrt{s}$ and $\mathrm{T} = \sqrt{s} - 2\mathrm{m}_p$ (IS)!

The transition operator problem

In traditional threshold production models for direct π^0-production in $pp \to pp\pi^0$ close to threshold people don't use one consistent π^0-production operator. There are e.g.:

$$
\begin{aligned}
T_{fi} &\propto \int_0^\infty dr\, r^2\, (R_{00}^{01}(\kappa,r))^*\, j_0(\kappa_{\pi^0}\, r) \left(\frac{d}{dr} + \frac{2}{r}\right) R_{11}^{01}(\kappa_0, r) \;\to [83,\ 86,\ 95] \\
T_{fi} &\propto \int_0^\infty dr\, r^2\, (R_{00}^{01}(\kappa,r))^*\, j_0(\kappa_{\pi^0}\, r) \left(\frac{d}{dr} + \frac{1}{r}\right) R_{11}^{01}(\kappa_0, r) \;\to [93] \\
T_{fi} &\propto \kappa_{\pi^0} \int_0^\infty dr\, r^2\, (R_{00}^{01}(\kappa,r))^*\, j_1(\kappa_{\pi^0}\, r)\, R_{11}^{01}(\kappa_0, r) \;\to [25]\,. \qquad (49)
\end{aligned}
$$

which are more or less related by a partial integration [43]. For a correct description of FSI we need the correct transition operator.

The data reduction problem

For an FSI reduction of their data experimentalists tend to multiply enhancement factors describing the FSI of possible particle subsystems in the final state. I quote here e.g. J. Smyrski et al. [105], who states: "The $pp\eta$ FSI can be factorized into $pp(f_{pp})$ and $p\eta(f_{p\eta})$ factors and integrated over the available phase-space volume ρ_3: $\sigma(\mathrm{Q}) \sim \int f_{pp}(q_{pp}) \cdot f_{p\eta}(q_{p_1\eta}) \cdot f_{p\eta}(q_{p_2\eta})\, d\rho_3$, ...". *For the moment there is no obvious theoretical reason to choose a product of final state factors rather than a sum or anything else to describe the FSI!* Well, the leading terms of a Faddeev expansion would suggest a coherent square of a sum. It is an important theoretical issue in the future, to give a satisfactory answer to this still open problem.

[43] It is unclear, why various terms appearing during this partial integration should vanish or be neglected. The transition operator describes mainly the FSI in the NN-system, as $j_0(\kappa_{\pi^0}\, r)$ representing the produced π^0-meson is nearly constant close to threshold.

8 Conclusions and outlook

Theoretical aspects

We come to the conclusion, that — in order to be able to relate quantitatively and conclusively theoretical quantities to experimental data — one either has to calculate the process $NN \to NNX$ close to threshold completely, e.g. within a three-body Faddeev approach, or there is a *need* of a quantitative theory to separate and estimate Initial-/Final-State effects. It is unsatisfactory and demanding, that — in spite of the vast related activities of theoreticians during the past about 60 years — *such a theory for estimating Initial-/Final-State effects does not exist yet!* This theory also has to be extended to differential cross sections for processes involving unpolarized and/or polarized particles close to threshold to extract independent information from data. Even being under control in the differential description of elastic scattering of charged particles the application of the theory of Coulomb scattering in initial and final states of particle number changing reactions is — due to the infinite range of the Coulomb interaction and the offshellness of the particles in the interaction zone — a highly nontrivial problem, requiring well defined regularization schemes, especially close to the particle production threshold, at which produced charged particles have a long time to interact. The development of an adequate theoretical — if possible, relativistic — formalism is an outstanding task. In order to handle interference effects and inelasticities a consistent field theoretical treatment of intermediate resonant states is demanded. An adequate formalism for the treatment of Fermionic [16, 106, 107] and Bosonic [108] resonances has been recently proposed. Keeping in mind the high relative energies and momenta of the incoming nucleons and the high momentum transfers involved in production processes of heavy mesons, relativistic formulations for nucleon induced meson production close to threshold are crucial. This includes the consideration of boost effects and e.g. tensor components, negative energy and parity components of the deuteron wavefunction within quantitative calculations. For the consistent relativistic treatment of bound of quasi-bound composite systems in the initial and final state the author refers to the new available formalism called ABSSM [74]. It is a pity to observe, that the majority of theoretical models stays nonrelativistic, especially because most of the traditional models have been developed to describe pion production only. Let's go for solving relativistic Faddeev problems! For the $NN\pi$-system I refer e.g. to [109, 110]. Not everything what is written should be believed!

Experimental aspects

Thanks to experimental facilities like COSY in Jülich, the CELSIUS ring in Uppsala or the IUCF in Bloomington the accuracy of cross section data related to nucleon induced meson production processes close to threshold improved significantly within the last ten years. It is a challenging, yet unexpectedly difficult task for theory to handle the experimental results *quantitatively*. In order to obtain as much independent experimental information as possible to constrain theory it is *highly desirable* to continue with the experimental investigation of differential cross sections, polarization and polarization transfer observables, production of heavy mesonic systems with and without strangeness, processes involving a deuteron beam or target and/or further light and heavy nuclei. For a quantitative estimate of the effect of ISI on nucleon induced meson production reactions close to threshold an experimental determination of NN scattering phaseshifts and inelasticities at high relative energies is crucial. As proposed in [111] it is highly desirable to compare experimentally uncharged and charged reaction channels like e.g. $nn \to nnX$ and $pp \to ppX$ to learn something about the influence of Coulomb effects in the Initial/Final State and the effective range parameters of uncharged strongly interacting particle systems. In the meantime we ask for being patient with slowly theoreticians!

Acknowledgement. F.K. thankfully acknowledges the kind invitation to the COSY-11 collaboration meeting and the long-term interest in and support of the presented work by K. Kilian and M. Dillig. For young physicists like the author it is very hard to develop independent research in an extensive field of established theoretical phenomenology, if there were not people, who believe, that theory should be predictive and quantitatively constrained by experiment. This work dedicated to my friend and experimental collegue P. Moskal has been supported mainly by the Forschungszentrum Jülich under contract No. ER-41154523, COSY FFE-project No. 41324880 and in part by the *Fundação para a Ciência e a Tecnologia* (FCT) of the *Ministério da Ciência e da Tecnologia* of Portugal, under Grant no. PRAXIS XXI/BPD/20186/99.

References

[1] M.L. Goldberger, K.M. Watson, *Collision Theory*, Structure of matter series, Wiley, New York (1964).

[2] C.J. Joachain, *Quantum collision theory*, North Holland, Amsterdam (1975).

[3] R. Bilger et al., Acta Phys. Polon. **B 29** (1998) 2981.

[4] P. Moskal et al., Phys. Lett. **B 482** (2000) 365.

[5] P. Moskal et al., Acta Phys. Polon. **B 31** (2000) 2277.

[6] E. Byckling, K. Kajantie, *Particle kinematics*, Wiley, London, New York (1973).

[7] R.F. Alvarez-Estrada, Nuovo Cim. **A 13** (1973) 1.

[8] H. Pietschmann, *Weak Interactions — Formulae, Results, and Derivations*, Springer, Wien (1983).

[9] K. Brueckner, Phys. Rev. **82** (1951) 598.

[10] K.M. Watson, K. Brueckner, Phys. Rev. **83** (1951) 1.

[11] K.M. Watson, Phys. Rev. **88** (1952) 1163.

[12] A.B. Migdal, Sov. Phys. JETP **1** (1955) 2; Zh. Eksp. Teor. Fiz. **28** (1955) 3.

[13] E. Fermi, Nuovo Cim. Suppl. **Vol. II (S. X) No. 1** (1955) 17.

[14] R. van Royen, V.F. Weisskopf, Nuovo Cim. **50** (1967) 617; Nuovo Cim. **51** (1967) 583.

[15] G.F. Chew, M.L. Goldberger, Phys. Rev. **75** (1949) 1637.

[16] F. Kleefeld, *Exclusive threshold production of π^0-, η- and K^+-mesons in proton-proton collisions*, doctoral thesis, University of Erlangen-Nürnberg (1999).

[17] F. Kleefeld, πN-Newslett. **15** (1999) 250.

[18] F. Kleefeld, Acta Phys. Polon. **B 31** (2000) 2225.

[19] C. Hanhart, K. Nakayama, Phys. Lett. **B 454** (1999) 176.

[20] V. Baru et al., Acta Phys. Polon. **B 31** (2000) 2127.

[21] V. Baru et al., Phys. Atom. Nucl. **64** (2001) 579, Yad. Fiz. **64** (2001) 633.

[22] B.O. Kerbikov, Phys. Atom. Nucl. **64** (2001) 1835, Yad. Fiz. **64** (2001) 1918.

[23] S. Waldenstrøm, Nucl. Phys. **B 77** (1974) 479.

[24] S. Gardner et al., Phys. Lett. **B 508** (2001) 44.

[25] J.A. Niskanen, Phys. Lett. **B 456** (1999) 107.

[26] F. Kleefeld, M. Dillig, 8th Int. Conf. On The Structure Of Baryons (Baryons '98), Bonn, Germany, 22–26 Sep 1998, Proc. ed. by D.W. Menze, B. Metsch, World Scientific, Singapore (1999) 613 and e–Print Archive nucl–th/9811003.

[27] V. Bernard, N. Kaiser, U.-G. Meißner, Eur. Phys. J. **A 4** (1999) 259.

[28] G. Fäldt, C. Wilkin, Phys. Scripta **64** (2001) 427.

[29] Virginia Tech Partial-Wave Analysis Facility (SAID), http://gwdac.phys.gwu.edu/ .

[30] M. Batinic, A. Svarc, T.S.H. Lee, Phys. Scripta **56** (1997) 321.

[31] H.P. Noyes, Ann. Rev. Nucl. Part. Sci. **22** (1972) 465.

[32] G.L. Squires, Prog. Part. Nucl. Phys. **2** (1952) 89.

[33] G.E. Brown, A.D. Jackson, *The nucleon–nucleon interaction*, North–Holland, Amsterdam (1976).

[34] M. Cini, S. Fubini, A. Stanghellini, Phys. Rev. **114** (1959) 1633.

[35] H. van Haeringen, L.P. van Kok, Phys. Rev. **A 26** (1982) 1218.

[36] H. van Haeringen, *Charged particle interactions. Theory and Formulas*, Coulomb Press, Leiden (1985).

[37] G. Breit, E.U. Condon, R.D. Present, Phys. Rev. **50** (1936) 825.

[38] D.Y. Wong, H.P. Noyes, Phys. Rev. **126** (1962) 1866.

[39] H.P. Noyes, Congress Int. de Physique Nucleaire, Paris, Jul 1964, Proc. ed. by P. Gugenberger, Vol. II, Editions du Ctr. Natl. de la Recherche Scientifique, Paris (1964) 172.

[40] G.J.M. Austen, *Effective range formalism and the electromagnetic interaction with applications to proton-proton scattering*, doctoral thesis, Catholic Univ. of Nijmegen, Netherlands (1982).

[41] L. Landau, I. Smorodinskii, J. Exper. Theoret. Phys. **14** (1944) 269.

[42] L. Landau, I. Smorodinskii, *Collected papers of L.D. Landau*, Gordon and Breach, New York (1965) 404 and J. Phys. U.S.S.R. **8** (1944) 154.

[43] G.D. Jackson, J.M. Blatt, Rev. Mod. Phys. **22** (1950) 77.

[44] G. Breit, H.M. Thaxton, L. Eisenbud, Phys. Rev. **55** (1939) 1018.

[45] G.G. Chew, M.L. Goldberger, Phys. Rev. **75** (1949) 37.

[46] R.V. Reid, Jr., Annals Phys. **50** (1968) 411.

[47] F.L. Yost, J.A. Wheeler, G. Breit, Phys. Rev. **49** (1936) 174.

[48] J.R. Taylor, Nuovo Cim. **B 23** (1974) 313.

[49] M.D. Semon, J.R. Taylor, Nuovo Cim. **A 26** (1975) 48.

[50] C. Hofmann et al., Phys. Scripta **48** (1993) 257.

[51] H.A. Bethe, Phys. Rev. **76** (1949) 38.

[52] G. Ebel et al., Nucl. Phys. **B 33** (1971) 317.

[53] O. Dumbrajs et al., Nucl. Phys. **B 216** (1983) 277.

[54] R. Omnès, *Introduction to particle physics*, Wiley, London (1971).

[55] A.N. Diddens, H.Pilkuhn, K. Schlüpmann, *Properties and Production Spectra of Elementary Particles*, ed. by H. Schopper, Landolt-Börnstein, *New Series* **I/6**, Springer, Berlin, Heidelberg (1972).

[56] J.R. Bergervoet et al., Phys. Rev. **C 38** (1988) 15.

[57] A. Moalem et al., Nucl. Phys. **A 600** (1996) 445.

[58] R. Shyam, Phys. Rev. **C 60** (1999) 055213

[59] L. Trlifaj, J. Math. Phys. **21** (1980) 1724.

[60] A. Sofianos et al., Phys. Rev. **A 60** (1999) 337.

[61] D. Baye, E. Brainis, Phys. Rev. **C 61** (2000) 025801.

[62] A. Sattarov et al., Phys. Rev. **C 60** (1999) 035801.

[63] G. Fäldt, C. Wilkin, Phys. Lett. **B 382** (1996) 209.

[64] G. Fäldt, C. Wilkin, Nucl. Phys. **A 604** (1996) 441.

[65] G. Fäldt, C. Wilkin, e–Print Archive: quant–ph/9610032.

[66] G. Fäldt, C. Wilkin, Phys. Rev. **C 56** (1997) 2067.

[67] Y.N. Uzikov, C. Wilkin, Phys. Lett. **B 511** (2001) 191.

[68] V. Abaev et al., Phys. Lett. **B 521** (2001) 158.

[69] A. Sibirtsev, W. Cassing, e–Print Archive: nucl–th/9802025.

[70] A. Moalem, L. Razdolskaya, E. Gedalin, e–Print Archive: hep–ph/9505264.

[71] H. Garcilazo, M.T. Peña, Phys. Rev. **C 61** (2000) 064010.

[72] S. Wycech, A.M. Green, Phys. Rev. **C 64** (2001) 045206.

[73] M.T. Peña, H. Garcilazo, D.O. Riska, Nucl. Phys. **A 683** (2001) 322.

[74] F. Kleefeld, Nucl. Phys. **A 689** (2001) 471.

[75] F. Kleefeld, M. Dillig, F. Pilotto, Acta Phys. Polon. **B 27** (1996) 2867.

[76] J. Pestieau, C. Smith, S. Trine, e–Print Archive: hep–ph/0105034.

[77] G.A. Miller, P.U. Sauer, Phys. Rev. **C 44** (1991) 1725.

[78] J. Haidenbauer et al., Acta Phys. Polon. **B 31** (2000) 2321.

[79] H. Machner, J. Haidenbauer, J. Phys. **G 25** (1999) R231.

[80] M. Gell-Mann, K.M. Watson, Ann. Rev. Nucl. Part. Sci. **4** (1954) 219.

[81] A.H. Rosenfeld, Phys. Rev. **96** (1954) 139.

[82] R.A. Stallwood et al., Phys. Rev. **109** (1958) 1716.

[83] D.S. Koltun, A. Reitan, Phys. Rev. **141** (1966) 1413.

[84] M.E. Schillaci, R.R. Silbar, J.E. Young, Phys. Rev. **179** (1969) 1539.

[85] H.O. Meyer et al., Phys. Rev. Lett. **65** (1990) 2846.

[86] H.O. Meyer et al., Nucl. Phys. **A 539** (1992) 633.

[87] A. Bondar et al., Phys. Lett. **B 356** (1995) 8.

[88] J. Złomańczuk et al., Phys. Lett. **B 436** (1998) 251.

[89] T. Johansson, Nucl. Phys. **A 663** (2000) 85.

[90] W.W. Daehnick et al., e–Print Archive: nucl–ex/0108021.

[91] E. Hernández, E. Oset, Phys. Lett. **B 350** (1995) 158.

[92] E. Hernández, E. Oset, Phys. Rev. **C 60** (1999) 025204.

[93] C.J. Horowitz, H.O. Meyer, D.K. Griegel, Phys. Rev. **C 49** (1994) 1337.

[94] J.A. Niskanen, Phys. Lett. **B 289** (1992) 227.

[95] J.A. Niskanen, Phys. Rev. **C 53** (1996) 526.

[96] C. Hanhart, *Pion-production in proton-proton collisions*, doctoral thesis, University of Bonn (1998), Berichte des Forschungszentrums Jülich **Jül-3476**.

[97] N. Kaiser, private communication in 8th Int. Symp. On Meson-Nucleon Physics And The Structure Of The Nucleon (MENU 1999), 16-20 Aug 1999, Zuoz, Switzerland.

[98] A. Sibirtsev, W. Cassing, Eur. Phys. J. **A 2** (1998) 333.

[99] A. Sibirtsev, Acta Phys. Polon. **B 29** (1998) 3123.

[100] A. Sibirtsev, W.Cassing, e–Print Archive: nucl–th/9904046.

[101] A. Moalem et al., πN-Newslett. **10** (1995) 170.

[102] A.I. Titov et al., Eur. Phys. J. **A 7** (2000) 543.

[103] M.M. Nagels et al., Nucl. Phys. **B 147** (1979) 189.

[104] L. Heller, P. Signell, N.R. Yoder, Phys. Rev. Lett. **13** (1964) 577.

[105] J. Smyrski et al., Phys. Lett. **B 474** (2000) 182.

[106] F. Kleefeld, Acta Phys. Polon. **B 30** (1999) 981.

[107] F. Kleefeld, 14th Int. Seminar On High Energy Physics Problems: Relativistic Nuclear Physics and Quantum Chromodynamics (ISHEPP 98), 17-22 Aug 1998, Dubna, Russia, Proc. ed. by A.M. Baldin, V.V.Burov, JINR, Dubna (2000) Vol. I 69 and e–Print Archive nucl–th/9811032.

[108] F. Kleefeld, E. van Beveren, G. Rupp, Nucl. Phys. **A 694** (2001) 470.

[109] A.N. Kvinikhidze, B. Blankleider, Phys. Rev. **C 59** (1999) 1263.

[110] D.R. Phillips, I.R. Afnan, Annals Phys. **247** (1996) 19.

[111] P. Moskal et al., Phys. Lett. **B 517** (2001) 295.

Present knowledge about the pp $\rightarrow$ ppη reaction

Saša Ceci[1] and Alfred Švarc

Ruđer Bošković Institute, Zagreb, Croatia

Abstract: To check the applicability of the Zagreb-UCLA-ANL meson-nucleon T matrices, we have calculated the total cross section for the $pp \rightarrow pp\eta$ process up to 4.5 GeV kinetic energy. Since there is no successful treatment of the initial and the final state interaction, comparing with experimental data possesses large uncertainties. Hence, we have aligned our result with published theoretical results of relevant models, calculated in the simplest approximations.

1 Introduction

Zagreb-UCLA-ANL meson nucleon partial wave analysisčiteBat95 opened the possibility to predict a number of middle energy data. Important result of the PWA is the eta nucleon elastic T matrix. All recent data from the two-body meson nucleon processes [2] have been used as the input to the PWA. We want to decrease the error of T matrices, but an enormous enlargement of the experimental data is required to give significant raise of the precision of result. Moreover, this would not help some channels, like elastic ηN. There is no way to experimentally measure this process. The three-body processes can serve us to lower the error of the two-body T matrices. The idea is to take two-body T matrices from existing PWA's and apply them to three-body processes.

The most convenient process for that purpose is the $pp \rightarrow pp\eta$. It is the isospin 1/2 process, what enables us to test the half of the amplitudes at a time. Well known is high energy PWA for the initial pp pair [3], as well as the low energy parameters for the final two protons, and the $p\eta$čiteBat95,Wyc97 subsystem. We believe that the dominant contribution to the production process comes through meson-exchange [5], and decay of nucleon resonances.

[1] Invited talk given by S. Ceci

1.1 Zagreb-UCLA-ANL PWA

Zagreb PWA is a unitary multi-channel multi-resonance pion-nucleon partial wave analysis *à la* Cutkosky [6]. Inputs to the our PWA are: pion nucleon elastic scattering T matrices, differential and total cross sections of pion-nucleon eta-producing cross section. Result is a 3×3 matrix in channel indexes.

Positions, widths and branching ratios for dominant partial waves are obtained. Branching ratios make definite predictions for the η production. Mesons in meson-nucleon channels covered with this PWA are π, η and π^2 (in $\pi^2 N$ all other channels are included — $\pi\pi N, \pi N^*, \rho N, \omega N, \ldots$ — it is an effective channel, needed for unitarity of the model).

2 Eta production model

We have used this relation to calculate the cross section:

$$\frac{d^5\sigma}{dq\, d\Omega_\eta\, d\Omega_1} = \frac{1}{\sqrt{(P_b\, P_t)^2 - \mathrm{m}_p^4}} \frac{1}{(2\pi)^5} \frac{(2\mathrm{m}_p)^4 \mathrm{p}_1^2 \mathrm{p}_\eta^2}{8\mathrm{E}_\eta \mid \mathrm{E}_2\, \mathrm{p}_1 - \mathrm{E}_1\, \widehat{\mathbf{p}}_1 \cdot \mathbf{p}_2 \mid} \frac{1}{4} \sum_{spins} \mid \mathcal{M} \mid^2$$

where P_b and P_t are four vector momenta of target and beam protons, $\widehat{\mathbf{p}}_1$ is the unit three-vector momentum of the first of two final protons. Rest of parameters are clear from figure 1.

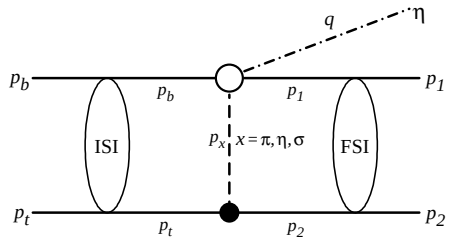

Figure 1: This is how we see the η production. We believe that resonance production dominates. Here σ designates the third, effective, channel meson.

The transition amplitude M is given by:

$$\sum_{x=\pi,\eta,\ldots} \Big\{ \overline{u}(\mathrm{p}_1, s_1)(A_x + \not{q} B_x) u(\mathrm{p}_b, s_b) \frac{i}{\mathrm{p}_x^2 - \mathrm{m}_x^2} \overline{u}(\mathrm{p}_2, s_2) F_{xNN}(\mathrm{p}_x^2) u(\mathrm{p}_t, s_t) \\ -1 \leftrightarrow 2\} - \{b \leftrightarrow t\}$$

where A_x and B_x are invariant amplitudes calculated via summation of partial wave amplitudes [2] given in our PWA [1], and $\overline{u}$ and u are normalized

Dirac spinors [7]. Coupling constants, cut-off masses and form factors are from the Bonn model [5]:

$$F_{xNN}\left(\mathrm{p}_x^2\right) = g_{xNN}\,\frac{\Lambda_x^2 - \mathrm{m}_x^2}{\Lambda_x^2 - \mathrm{p}_x^2} \tag{1}$$

3 Initial and final state problem

Two initial particles, on their way to a final state, undergo radical changes. Their energy is reduced at least by the mass of the η meson. Their angular momentum state also changes, due to the negative parity of the produced η. Two protons may create a quasi-stable S-wave state in the final state, likewise η and any of two protons.

There is no successful model, yet, to include effects of initial and final state interaction. This is the reason we have chosen, in checking of our two body T matrices, to use a different approach. Normally, theoretical results are compared to the experimental data. We have decided to compare our theoretical prediction of the process with other theoretical models, under the same conditions.

Nevertheless, much of the theorists' effort has been put into the understanding of the initial and final state interaction, so we must mention at least some. We have included the realistic initial state interaction factor [8] — almost constant lowering of cross section by 70 %. After we have included the *pp* final state interaction, the theoretical curve has described experimental data very well. The problem of this model is that there is no way to estimate ISI and FSI at higher energies (higher than 45 MeV in the excess energy). Earlier models had not considered ISI effects [9, 10] at all. Later on, there have been works from Gedalin et al. [11] and Santra et al. [12]. The former group has not used initial state interaction and has given a recipe for FSI, claiming that there is no strong FSI at excess energies higher than 15 MeV, while the latter have used the distorted wave Born approximation with lowering of the cross section by 50 %. The latest, and hopefully the most promising, is the work from Hanhart et al. [13]. They predict that near threshold initial state interaction lowers the cross section by 80 %. There has been shown that the choice of the production model could not be separated from the treatment of the initial and final state interaction of two protons. The experimental situation is ahead of the theoretical. It looks like ηN final state interaction is very important in this process [14], what might be in agreement with our value of the S-wave η – nucleon scattering length. But the statement is not proven beyond the reasonable doubt.

4 Other theoretical models

We have calculated the cross sections within our model with parameters and treatment resembling the original model as much as possible. We give the ratio to published cross sections, at energies where they reasonably well describe the experimental results in figure 2. Parameters and some specific features of models are in table 1.

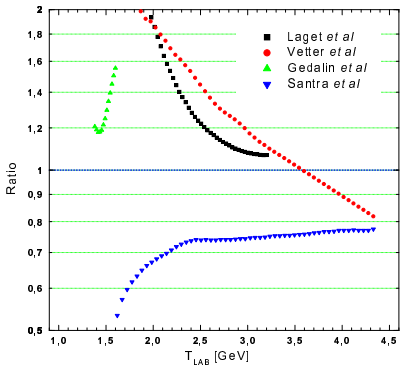

Figure 2: Ratio between published and our cross sections. We compare results where original curves stand close to experimental values. We consider ratios differing not more then 50 % from one as a good result.

Parameter	Laget [9]	Vetter [10]	Gedalin [11]	Santra [12]
$g^2_{\pi NN}/4\pi$	14.5	14.5	14.6	14.97
Λ_π [GeV]	1.2	1.0	1.3	1.2
$g^2_{\eta NN}/4\pi$	...	...	3.0	0.6
Λ_η [GeV]	...	...	1.5	1.5
$g^2_{\rho NN}/4\pi$	0.81	0.178	0.95	0.5
Λ_ρ [GeV]	2.15	1.566	1.3	2.0
Comments	Bonn	$F_x(\mathrm{p}_x^2) = \frac{\Lambda_x^2}{\Lambda_x^2 - \mathrm{p}_x^2}$	Bonn	$F_\rho(\mathrm{p}_\rho^2) = \frac{\Lambda_\rho^2 - \mathrm{m}_\rho^2}{\Lambda_\rho^2 - \mathrm{p}_\rho^2}$
	...	$g = g^0 e^{-\beta\sqrt{s - 4\mathrm{m}_p^2}}$	...	...
	DWBA $\approx$ 10 %	No ISI nor FSI	No FSI Q > 15 MeV	DWBA $\approx$ 50 %

Table 1: Parameters of the considered models. For further details on each model, one should take a look in original articles.

5 Conclusion

Resemblance of our mimicking the other models exists, so we are encouraged to take further steps in the development of pion-nucleon T matrices (increase

the number of channels). The high energy behavior of calculated total cross sections is in an acceptable agreement in most of the models. This enables us to calculate the high or, at least, middle energy cross section. At those energies, there must not be significant final state interaction to take care. If we obtain agreement and eliminate the differences between our and other models at higher energies and fix the model, then we can return to near threshold, and try to understand what is going on there. In order to do it, we would kindly appreciate some more intermediate and higher energy data for $pp \to pp\eta$ from the experimental community.

References

[1] M.Batinić et al., Phys. Rev. **C 81** (1995) 2310; Phys. Scripta **58** (1998) 15.

[2] G. Höhler, *Elastic and Charge Exchange Scattering of Elementary Particles*, ed. by H. Schopper, Landolt-Börnstein, *New Series* **I/9 2b**, Springer, Berlin (1983).

[3] Virginia Tech Partial-Wave Analysis Facility (SAID), http://gwdac.phys.gwu.edu/ .

[4] A.M. Green, S.Wycech, Phys. Rev. **C 55** (1997) 2167.

[5] R. Machleidt, Adv. Nucl. Phys. **19** (1989) 189.

[6] R.E. Cutkosky et al., Phys. Rev. **D 20** (1979) 2839.

[7] J.D. Bjorken, S.D. Drell, *Relativistic Quantum Mechanics*, Int. series in pure and applied physics, MacGraw Hill, New York (1964).

[8] M. Batinić, A. Švarc, T.S.H. Lee, Phys. Scripta **56** (1997) 321.

[9] J.M. Laget, F. Wellers, J.F. Lecolley, Phys. Lett. **B 257** (1991) 254.

[10] T. Vetter, A. Engel, T. Biró, U. Mosel, Phys. Lett. **B 263** (1991) 153.

[11] E. Gedalin, A. Moalem, L. Razdolskaja, Nucl. Phys. **A 634** (1998) 368.

[12] A.B. Santra, B.K. Jain, Nucl. Phys. **A 634** (1998) 309.

[13] C. Hanhart, K. Nakayama, Phys. Lett. **B 454** (1999) 176.

[14] P. Moskal et al., Phys. Lett. **B 482** (2000) 356.

The Faddeev Equations and Three Nucleon Forces[1]
- Introductory lecture -

R. Skibiński[a], W. Glöckle[b], J. Golak[a], H. Kamada[b], J. Kuroś-Żołnierczuk[a], A. Nogga[b], H. Witała[a]

[a] *Institute of Physics, Jagellonian University, Cracow, Poland*

[b] *Institut für Theoretische Physik II, Ruhr–Universität Bochum, Germany*

Abstract: After a short introduction into the Faddeev equations we present our recent theoretical results on binding energies, nucleon-deuteron (Nd) elastic scattering and deuteron break-up obtained with the modern, realistic nucleon-nucleon (NN) interactions. Existing discrepancies to data point to possible effects of the three nucleon forces (3NF). Indeed, an inclusion of 3NF's improves a description of some of the existing data, while other ones also show that 3NF's are still not sufficiently well understood. The knowledge of $3N$ bound and continuum states is also important for understanding other processes, like electromagnetic ones. As an example of such processes we show a new result for ^3He photodisintegration.

1 Introduction

Since the very beginning of nuclear physics people try to establish the form of the nuclear Hamiltonian. Nowadays one can construct such a Hamiltonian from different NN interactions, like CD Bonn [1], AV18 [2] or the family of Nijmegen potentials [3]. All those interactions are inspired by meson theory and are tuned to the NN data in an energy range up to 350 MeV. The results of $3N$ scattering calculations, using those potentials can be found in [4]. Despite the fact that the binding energies of the $3N$ bound states (^3H and ^3He) predicted by modern NN potentials are not in agreement with experimental values (see the first part of table 1), the description of the experimental data for the $3N$ scattering observables is generally quite good and the results are stable against the exchange of interaction. However, despite the overall good agreement, there is still some room for improvement and a natural way to look for effects, which could be responsible for this discrepancy, is to introduce a 3NF. There exist nowadays a few different 3NF's (a brief review was done in [5]), but unfortunately, the form of the

[1] Invited talk

3NF is still not established and it is the aim of our work to shed light on this form. We present the results of calculations of a large number of observables in [6, 7] using different 3NF's [8, 9]. We find that for some observables an inclusion of 3NF's improves the description of the data (like for elastic cross sections), whereas for others the modern 3NF's do not give a proper description.

In the next section we briefly present our theoretical formalism and show the idea of the Faddeev equations. In section 3 we present some results for binding energies, observables for Nd scattering and an example for ^3He photodisintegration.

2 The Faddeev equations

A heuristic approach and an exact derivation of the Faddeev equations can be found in [4, 10]. Here we restrict ourselves to a short description of the physical content of these equations. One can see (Fig. 1) the idea of the Faddeev equations on an example of a break-up process, where in the initial state two nucleons build the deuteron (the half-moon on the right side of each graph) and the third one is the free particle. After scattering all three nucleons are free (the left side of each graph). The transition operator $U_{0,3}$, where 0 and 3 label the final and the initial channel, respectively, can be build from mutual interactions between different nucleons. For example the first graph on the right-hand side of the first line is the case when nucleons 2 and 3 interact. The black dot depicts the 3NF. The first step to the Faddeev equations is to divide all possible graphs on the right-hand side into four groups (partial transition operators) according to the last interaction on the left. Looking at fig. 2 one easily reads off the equation for such an operator acting onto a suitable channel function

$$U_{0i}^{j}\Phi_i = V_j\Phi_i\bar{\delta}_{ij} + V_jG_0\sum_{k=0,3} U_{0i}^{k}\Phi_i \quad i=1,3; j=1,4\,, \tag{1}$$

where Φ_i is the i-th channel wave function (where the i-th nucleon is a free particle), V_j is an interaction between nucleons i and k $(i,k \neq j)$ and V_4 stands for a 3NF, G_0 is a free propagator of three particles and $\bar{\delta}_{ij} = 1-\delta_{ij}$. Introducing a two-body t-operator t_i connected to an interaction V_i by

$$t_i = V_i + V_iG_0V_i + V_iG_0V_iG_0V_i + \ldots\,, \tag{2}$$

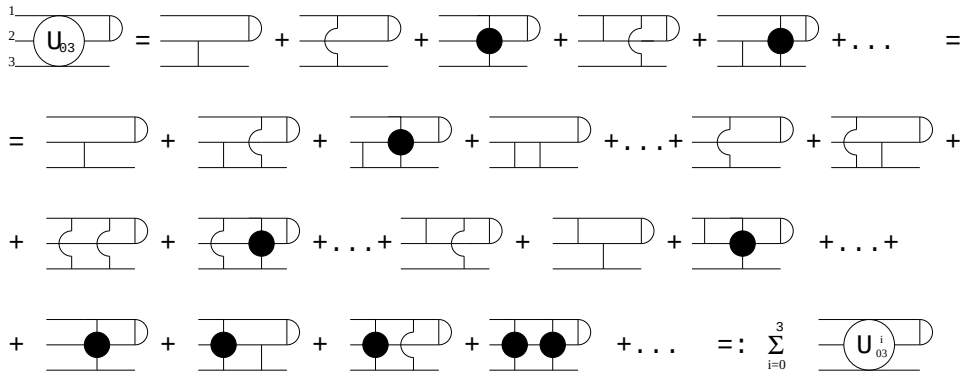

Figure 1:

one gets, after some algebra, the set of four coupled equations, which is known as a set of Faddeev equations:

$$U_{0i}^{j}\Phi_i = \bar{\delta}_{ij} t_j \Phi_i + t_j G_0 \sum_{m=0,3;m\neq l} U_{0i}^{m}\Phi_i \quad i=1,3; j=1,4\,. \tag{3}$$

For identical particles, one can introduce the permutation operator P, which is the sum of cyclical and anti-cyclical permutations of three particles, and we finish with one equation for a new transition operator T (connected to the previous one U_{0i}^{j}), which should be solved numerically:

$$\begin{aligned} T\Phi_i &= t_i P\Phi_i + (1+t_i G_0)V_4^1(1+P)\Phi_i + \\ &\quad t_i P G_0 T\Phi_i + (1+t_i G_0)V_4^1(1+P)G_0 T\Phi_i\,, \end{aligned} \tag{4}$$

where V_4^1 is that part of the 3NF, which is symmetrical under the exchange of the nucleons 2 and 3, and the channel function Φ_i is a product of a deuteron wave function and a momentum eigenstate of the projectile nucleon. The knowledge of the transition operator T allows one to calculate different observables for Nd elastic scattering and the break-up process [11]. For the technical details on solving eq. 4 see ref. [4].

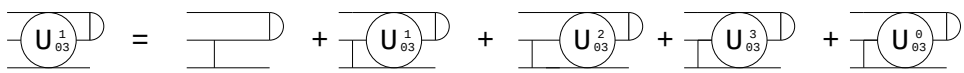

Figure 2:

Table 1: The binding energies.

Potential	^{3}H	^{3}He	^{4}He
CD Bonn	-8.012	-7.272	-26.26
AV18	-7.623	-6.924	-24.28
CD Bonn + TM	-8.464	-7.734	-29.15
AV18 + Urbana IX	-8.426	-7.756	-28.84
Exp.	-8.48	-7.72	-28.30

3 A short review of the 3N systems results

Some results for binding energies are presented in table 1. In all cases realistic NN forces lead to a clear underbinding, which for ^3He and ^3H amounts to $\approx 0.5 - 0.9$ MeV, and for ^4He to about $2 - 4$ MeV. By inclusion of a 3NF, adjusted to the $3N$ binding energy, one can drastically improve the description of ^4He, which is now only a little overbound.

Valuable information on a 3NF's structure can also be obtained from the Nd elastic scattering observables. From a rich set of such observables [7] we present here in fig. 3 the differential cross section $d\sigma/d\Omega$, the vector $A_y(N)$ and tensor T_{22} analyzing powers and finally the spin transfer coefficient $K_{yy}^{y'}$. In all these cases we present our results for the four energies: 3, 65, 135 and 190 MeV. In all the above mentioned figures always two bands appear. The lighter one covers the predictions of NN-interaction only (AV18, CD-Bonn, NijmI, II and 93), the darker one covers the predictions of the same NN-interactions combined with the TM 3NF and individually adjusted to the ^3H binding energy. Finally, the most modern 3NF was taken into account, which is the dashed curve for CD Bonn + TM' 3NF [12] (it is a modified TM force more consistent with chiral symmetry). The solid curve stands for AV18 + Urbana IX [8]. The predictions for the differential cross sections are more or less similar for the different potentials and agree very well with the data, except in the region of the minimum where NN-interactions only underestimate the data. The inclusion of each of the 3NF's, especially for the higher energies, improves the description of the data. A strong discrepancy for low angles and the lowest energy is due to the Coulomb force, which is not included into our calculations [13].

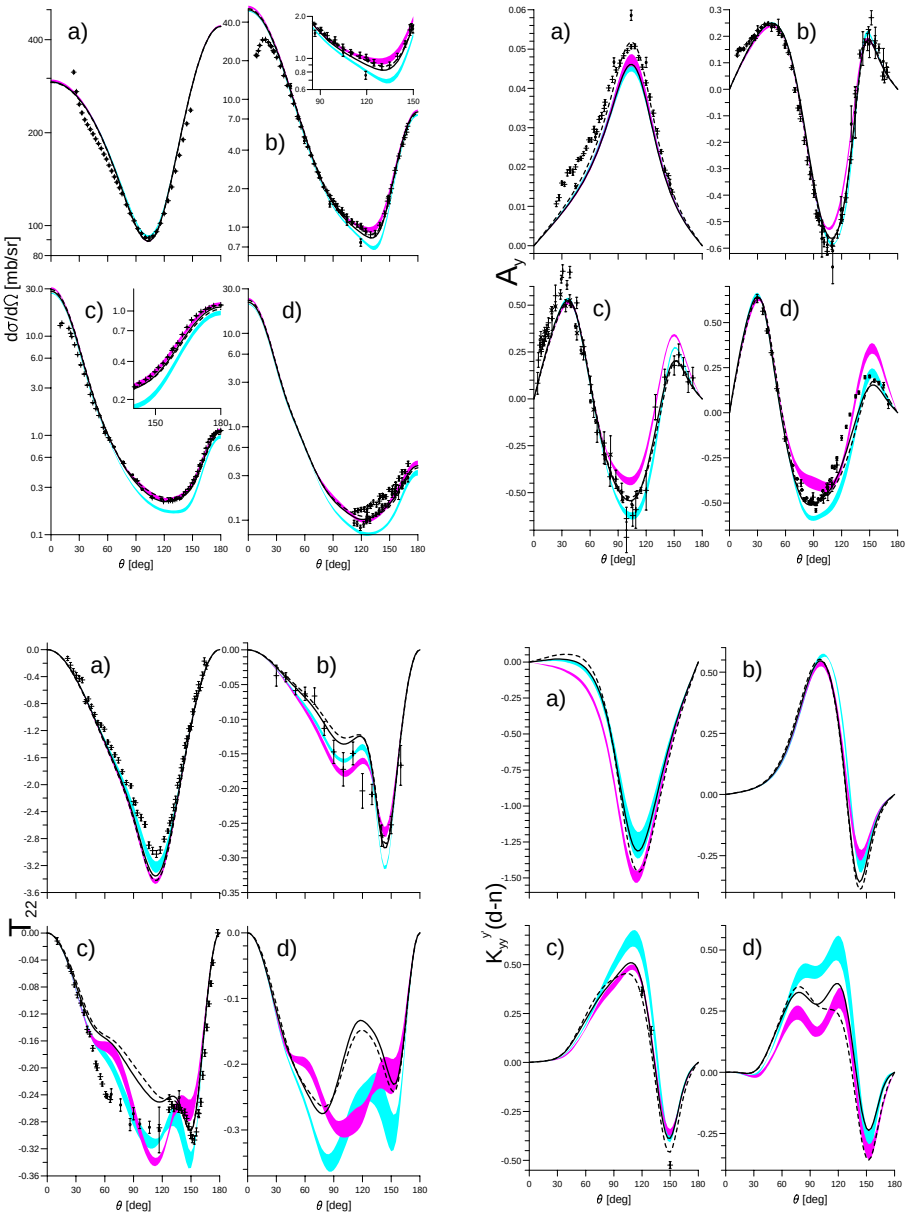

Figure 3: The differential cross section $d\sigma/d\Omega$, vector A_y and tensor T_{22} analyzing powers and spin transfer coefficient $K_{yy}^{y'}$, for Nd elastic scattering at energies a) 3 MeV, b) 65 MeV, c) 135 MeV d) 190 MeV. For a description of bands and curves see text, for references to experimental data see ref. [7].

The situation for the spin observables is less clear. For the nucleon analyzing power A_y at low energy there is a puzzle, which points to the necessity of improving the modern 3NF's. For T_{22} the situation is, especially for higher energies, more complicated. For E = 135 MeV the predictions for the CD-Bonn + TM' and the AV18 + Urbana IX lie close to each other, but they disagree with the other calculations and, what is more disturbing, with the experimental points. For the energy E = 190 MeV all the above mentioned predictions are quite different, and because of that data are very much needed to nail down the spin structure of 3NF's. Also the predictions on the spin transfer coefficient $K_{yy}^{y'}$ for high energies show a dependence on the 3NF's used. Two of three experimental points for E = 135 MeV agree very well with the calculations, but there is a discrepancy for one point close to $\Theta = 150°$. Unfortunately, for E = 190 MeV, where there is a big spread between the different 3NFs predictions, there are no experimental data.

Also for the Nd break-up very interesting kinematic configurations were found, in which effects of the 3NF could possibly be observed. Examples for the five-fold differential cross section and vector and tensor analyzing powers are presented in figs. 4,5. For E = 65 MeV effects of the 3NF's are nearly 30 % and the modern 3NF's describe the data quite well. The last example shows that for certain spin observables one can find kinematic situations, where the differences between different predictions are huge; even the sign of A_y can change.

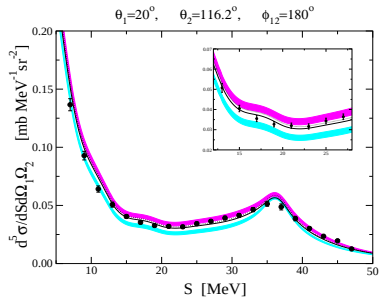

Figure 4: The differential cross section for Nd break-up at neutron energy E = 65 MeV. Data are from [12].

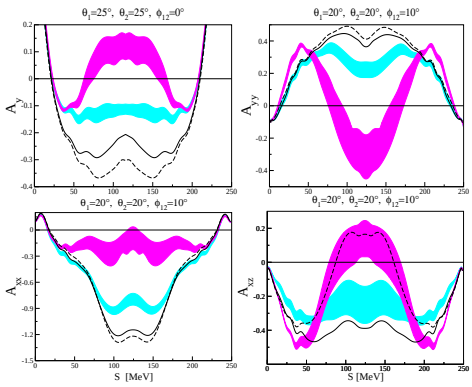

Figure 5: The vector and tensor pd break-up analyzing powers at proton lab energy E = 200 MeV.

The knowledge of the $3N$ bound and continuum states allows to look for 3NF's effects in other processes. Fig. 6 is an example of the differential

cross section for ^3He photodisintegration and again the difference between predictions with and without 3NF is clearly visible.

4 Summary

The Faddeev equations are a powerful tool for investigating the three-nucleon system. The numerically exact solutions of the three-nucleon problem, which are based on realistic NN and $3N$ interactions, allow to investigate the nuclear Hamiltonian. As a result of such investigations one can see, that the structure of 3NF's is still not well understood. A precise and rich set of data is badly needed to establish the final form of 3NF's. We show some examples of observables and kinematics in which effects of current 3NF's are strongly noticeable. Also the electromagnetic processes could give interesting information on the nuclear Hamiltonian.

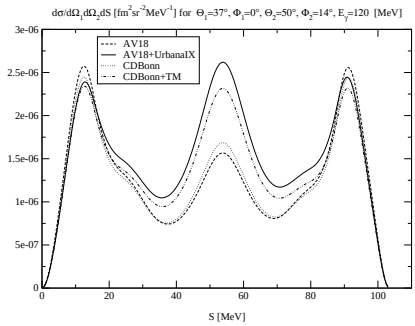

Figure 6: The differential cross section for ^3He photodisintegration for $E_\gamma = 120\,\mathrm{MeV}$.

Acknowledgement. This work was supported by the Deutsche Forschungsgemeinschaft and by the Polish Committee for Scientific Research under Grant No. 2P03B02818. The numerical calculations have been performed on the Cray T90 and T3E of the NIC in Jülich, Germany.

References

[1] R. Machleidt, Phys. Rev. **C 63** (2001) 024001 and references therein.

[2] R.B. Wiringa, V.G.J. Stoks, R. Schiavilla, Phys. Rev. **C 51** (1995) 38.

[3] V.G.J. Stoks, R.A.M. Klomp, C.P.F. Terheggen, J.J. de Swart, Phys. Rev. **C 49** (1994) 2950.

[4] W. Glöckle, H. Witała, D. Hüber, H. Kamada, J. Golak, Phys. Rep. **274** (1996) 107.

[5] D. Hüber, J.L. Friar, A. Nogga, H. Witała, U. van Kolck, Few Body Syst. **30** (2001) 95.

[6] A. Nogga, H. Kamada, W. Glöckle, Phys. Rev. Lett. **85** (2000) 944.

[7] H. Witała et al., Phys. Rev. **C 63** (2001) 024007.

[8] B.S. Pudliner, V.R. Pandharipande, J. Carlson, S.C. Pieper, R.B. Wiringa, Phys. Rev. **C 56** (1997) 1720.

[9] S.A. Coon, P.C. McNamee, Nucl. Phys. **A 317** (1979) 242; S.A. Coon, W. Glöckle, Phys. Rev. **C 23** (1981) 1970.

[10] W. Glöckle, *The Quantum Mechanical Few-Body Problem*, Texts and monographs in physics, Springer, Berlin (1983).

[11] D. Hüber, H. Kamada, H. Witała, W. Glöckle, Acta Phys. Polon. **B 28** (1997) 167.

[12] J.L. Friar, D. Hüber, U. van Kolck, Phys. Rev. **C 59** (1999) 53.

[13] A.Kievsky et al., Nucl. Phys. **A 607** (1996) 402; Phys. Rev. **C 64** (2001) 024002.

The Dalitz Plot as a Tool in Particle Physics

D. Grzonka and K. Kilian

Institut für Kernphysik, Forschungszentrum Jülich, Germany

Abstract: Some basic kinematical relations and Dalitz plot observables are given and the Dalitz plot as a descriptive tool to extract physics information from event distributions is discussed.

1 Introduction

In reactions with a two–body exit channel the important observables to extract the physics are the energy dependent total cross section σ (Q) and the differential cross section $d\sigma/d\cos\Theta^*$ depending on the angular correlation (Θ^*) between entrance and exit directions in the CM system. Observables are always of the type: number of events per some phase space interval and per number of beam particles. The cross section shows resonance masses M_R and widths Γ_R. The angular distribution $d\sigma/d\cos\Theta^*$ depends on the square of the wave function and thus contains information on the spin/parity J^P content of the reaction. For a three body exit channel there are much more distributions possible and one has to choose the best ones to extract physics information.

The Dalitz plot is the best way to show all observables in a three–body reaction $1+2 \rightarrow i+j+k$ which depend on exit coordinates alone. The three particles $i+j+k$ form three two–body subsystems $(i+j)$, $(j+k)$ and $(k+i)$ which we can consider as quasiparticles. The quantum numbers and resonance parameters of these quasiparticles m_{ij}, Γ_{ij}, and J^P_{ij} can be seen in the event distribution in the Dalitz plot. The Dalitz plot does not show any correlations with coordinates of the entrance.

2 Basic kinematics

For any reaction like $1+2 \rightarrow i+j$ in any system the conservation of energy and momentum holds. Both together are simply written for a two particle reaction in four–vector notation: $\wp_1 + \wp_2 = \wp_i + \wp_j$ with $\wp_i = (\mathrm{E}_i, \vec{\mathrm{p}}_i)$, where

$E_i^2 = m_i^2 + \vec{p}_i^{\,2}$. In different frames of reference the Lorentz transformation conserves one quantity, namely the total available energy in CM $M_{12} = \sqrt{s} = M_{ij}$ (also called effective mass or the length of the four–vector) where $s = (\wp_i + \wp_j)^2$. In figure 1 a graphical presentation of the two–body kinematics is given which follows from these conservation laws.

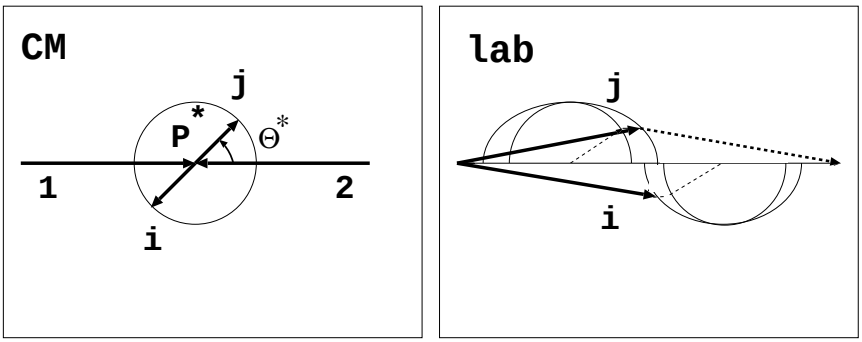

Figure 1: Two–body kinematics in the center of mass and laboratory system.

An important quantity for the determination of CM quantities from lab quantities is the CM momentum (in the exit channel). From the relations above the CM momenta as a function of s and the masses (m_1 and m_2) or (m_i and m_k) are given by:

$$|p_k^*| = |p_l^*| = \sqrt{[(s^2 - 2s(m_k^2 + m_l^2) + (m_k^2 - m_l^2)^2]/(4s)}. \qquad (1)$$

With a target m_2 at rest the scattering angle in the center of mass system $\cos\Theta^*$ is given by

$$\cos\Theta_{1i}^* = \frac{\vec{p}_1 \cdot \vec{p}_i^*}{|\vec{p}_1| \cdot |\vec{p}_i^*|} = \frac{(\vec{p}_i + \vec{p}_j) \cdot \vec{p}_i^*}{|\vec{p}_i + \vec{p}_j| \cdot |\vec{p}_i^*|} \qquad (2)$$

Information about the physics is given in the angular distribution of reaction events shown over $\cos\Theta_{1i}^*$. The contribution of different partial waves to the cross section as well as the J^P of possible resonances in the ij–system are visible in this angular distribution. The mass and width of resonances in the ij–system can be extracted from the excitation function.

A three particle exit channel $1 + 2 \to i + j + k$ contains three two–body subsystems (ij), (jk), and (ki). They are treated as two–body systems. If (jk) is the subsystem then the partial waves in the (jk)–subsystem (quasi-particle) can be extracted in complete analogy to the two–body case shown

above. Now the emission angle of j in the $(j+k)$ CM system is denoted by **, where $\vec{p}_j^{**} + \vec{p}_k^{**} = 0$ relative to the "beam direction" which is now along $\left(\vec{p}_j^{*} + \vec{p}_k^{*}\right)$ in the three–body CM system. The reference axis for angular distributions is now not at all the beam axis $(\vec{p}_1)$ but the negative direction of i or the direction of the (jk)–subsystem in the three–body CM system, respectively $(\vec{p}_j^{*} + \vec{p}_k^{*} = -\vec{p}_i^{*})$. One has to be careful in selecting the correct directional correlations. While for example the absolute CM momentum in the (jk)–system is a Lorentz invariant quantity, the CM $\cos\Theta_{ij}^{**}$ is not equal to $\cos\Theta = ((\vec{p}_j + \vec{p}_k) \cdot \vec{p}_j^{*}) \,/\, (|\vec{p}_j + \vec{p}_k| \cdot |\vec{p}_j^{*}|)$ created with the lab momenta $\vec{p}_j$ and $\vec{p}_k$. With this choice there is no collinear reaction partner to M_{ij}. Such an angular distribution would be nonsense. For a three–body reaction one gets only in the three–body CM system the correct collinear reaction partner, namely m_i with its four vector $(E_i^{*}, \vec{p}_i^{*})$.

In the three–body system the counting sequence ijk is important. It defines a certain helicity and going to ikj changes some signs of $\cos\Theta^{*}$.

3 Dalitz plot coordinates

For a three–body exit channel like $1 + 2 \rightarrow i + j + k$ the invariant total energy squared s is given by:

$$\begin{aligned} s = (\wp_1 + \wp_2)^2 &= (\wp_i + \wp_j + \wp_k)^2 \\ &= \wp_i^2 + \wp_j^2 + \wp_k^2 + 2\wp_i\wp_j + 2\wp_j\wp_k + 2\wp_k\wp_i \\ &= (\wp_i + \wp_j)^2 + (\wp_j + \wp_k)^2 + (\wp_k + \wp_i)^2 - \wp_i^2 - \wp_j^2 - \wp_k^2 \end{aligned}$$

which results in:

$$s + m_i^2 + m_j^2 + m_k^2 = M_{ij}^2 + M_{jk}^2 + M_{ki}^2 \tag{3}$$

with the invariant squared masses $M_{mn}^2 = (\wp_m + \wp_n)^2$. These invariant squared masses M_{mn}^2 are mostly used as the coordinates of the Dalitz plot. In a geometrical representation the Dalitz plot is a plane in the 3–dimensional $(M_{ij}^2, M_{jk}^2, M_{ki}^2)$ space which is orthogonal to the space diagonal (its direction is $\sqrt{1/3}(1,1,1)$). Each point in the Dalitz plot is given in a vector representation by a scalar product with the space diagonal $(1,1,1)(M_{ij}^2, M_{jk}^2, M_{ki}^2)$. For a constant s two of the three coordinates are sufficient for an unambiguous presentation of the Dalitz plot observables (eq. 3).

Alternative to the invariant squared masses the total energies of the particles can be written at the Dalitz plot axes. Using the four–vector

relations in the overall CM system:

$$\wp^*_{jk} = (\wp^*_j + \wp^*_k) = (\wp^*_{entrance} - \wp^*_i) \ ; \ \mathrm{M}^2_{jk} = [(\sqrt{s}, \vec{0}) - (\mathrm{E}^*_i, \vec{\mathrm{p}}^*_i)]^2$$

we find a linear relation between M^2_{jk} and E^*_i given by:

$$\mathrm{M}^2_{jk} = s + \mathrm{m}^2_i - 2\sqrt{s}\mathrm{E}^*_i$$

(and cyclic exchange).

4 Physics in the Dalitz plot

The Dalitz plot allows in a very instructive way to extract physics from the event distribution.

The cross section for a certain reaction can be decomposed in a phase space factor and a reaction matrix element. The phase space element $d\rho$ is given by:

$$d\rho = d\mathrm{E}_i \, d\mathrm{E}_j = \frac{1}{4s} \, d\mathrm{M}^2_{ij} \, d\mathrm{M}^2_{ki} \tag{4}$$

These are surface elements of the Dalitz plot. For a pure S–wave reaction with an isotropic emission of the reaction products these phase space elements have a constant occupation density (same number of events per surface). The integration over the phase space elements is just the available total phase space, i.e. the surface of the Dalitz plot. The projection of the Dalitz plot (surface between its boundary curve) onto the M^2_{ij} or E^*_k axes gives the shape of the mass/energy spectra as expected if only phase space behaviour exists (eq. 2). At low energies the Dalitz plot surface is proportional to the square Q^2 of the excess energy $\mathrm{Q} = \sqrt{s} - \mathrm{m}_i - \mathrm{m}_j - \mathrm{m}_k$. Each point in the Dalitz plot is connected with the 3 two–body subsystems and their internal relative momenta. The physics, for example final state interactions and resonance effects depend on the CM momenta in the two–body subsystems. Therefore each point in the Dalitz plot gets in the simplest picture weight factors g_{nm} from each of the three subsystems, and the cross section represented as an integral over the phase space is modified by these weight factors.

$$\sigma \sim \int d\rho \, g_{ij}(\mathrm{p}^{**}_{ij}) \, g_{jk}(\mathrm{p}^{**}_{jk}) \, g_{ki}(\mathrm{p}^{**}_{ki}) \tag{5}$$

A special feature of the invariant squared mass (or E^*_n) spectra is the linear correlation with the cosine of the relevant angle in the considered

subsystem. For a fixed invariant squared mass like M_{ij}^2 the distribution of events on the line in the Dalitz plot corresponds to the $\cos\theta_j^*$ of particle j in the (jk)–subsystem relative to the direction of the (jk)–system. The situation is illustrated in figure 2.

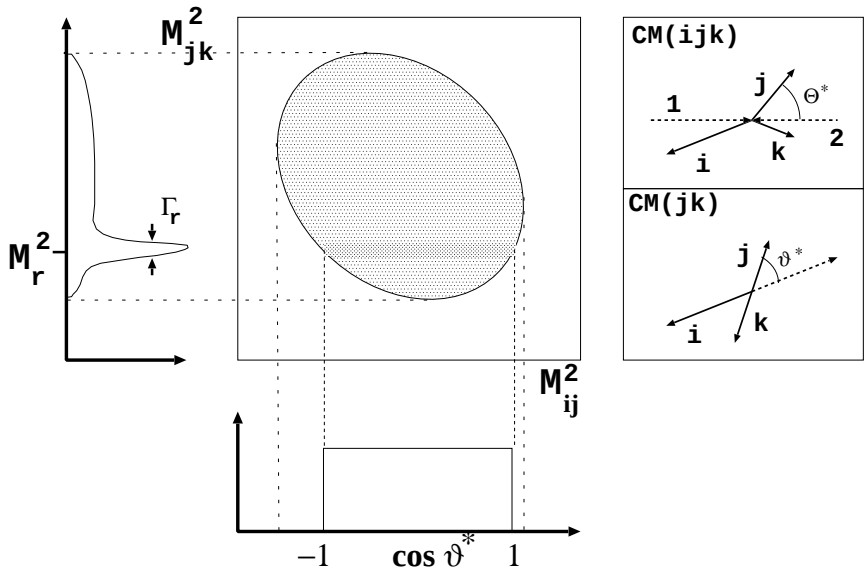

Figure 2: Dalitz plot for a three–body exit channel i, j, k with a resonance in the (jk)–subsystem and the influence of the typical decay angular distribution over the events in the slice of events around $M_{jk}^2 = M_R^2$.

A resonance in the (jk)–system is observed on the M_{jk}^2 axis as an enhancement of events in the Dalitz plot for a fixed mass, and on the M_{ij}^2 axis directly the $\cos\theta_j^*$ distribution in the (jk) CM system is given from which the resonance spin can be derived. In general a resonance can be present in the different subsystems which complicates the situation. The observed angular distribution in one M_{ij}^2 slice can be (strongly) distorted by effects in the other subsystems. Crossing resonances for example can only be disentangled by a Dalitz plot analysis and not in projected M_{ij}^2 spectra alone. Helpful are Dalitz plots at different s values. They change in size and the crossing effects shift and can be disentangled.

The three–body exit observables for a reaction are an incoherent sum over Dalitz plots for different J^P entrance values. In principle these different Dalitz plots for each J^P entrance value may be separable (e.g. by using

polarized beams and targets in the entrance). Within the differential distributions for a given J^P entrance interference terms will show up between various amplitude contributions of m_{ij} subsystems and between amplitudes of m_{jk} and m_{ki} subsystems. Therefore the Dalitz plot occupation can have a very complex structure but within an appropriate analysis the individual components can be extracted as was shown by the Crystal Barrel collaboration at LEAR. Details on the partial wave analysis can be found for instance in [1, 2, 3].

References

[1] B. Pick et al., Technical report, University of Bonn (1997).

[2] S.U. Chung et al., Annalen Phys. **4** (1995) 404.

[3] C. Amsler, J.C. Bizot, Comput. Phys. Commun. **30** (1983) 21.

The final state interactions of η and η' [1]

Sławomir Wycech

Sołtan Institute for Nuclear Studies, Warsaw, Poland

Abstract: The K-matrix used to describe the coupled πN, ηN, γN, $\pi\pi N$ systems favours large $0.7 - 1.05\,\mathrm{fm}$ ηN scattering lengths. The large ηN elastic amplitudes generate quasi-virtual states with two nucleon ηd and ηpp systems. Quasi-bound states are likely in heavier nuclei. To some extent, these states may be detected via final state interactions of the η meson.

1 The K-matrix for ηN interactions

One can check the ηN interaction models with the η-few-nucleon physics. In these systems an interesting spectroscopy of quasi-bound and virtual states exists. Several related topics are discussed in this note.

At low energies the ηN interactions are dominated by the $N^*(1540)$ resonance. It is also established that due to this resonance the ηN channel is coupled to the πN, γN, $\pi\pi N$ channels. Such systems are conveniently described by a multi-channel real reaction matrix K. To account for the N^* dominance one parameterises this matrix as

$$K_{i,j} = \frac{g_i g_j}{\mathrm{E}_0 - \mathrm{E}} + B_{i,j}\,. \tag{1}$$

The first term represents an N^* of energy E_0 coupled to the four channels i by coupling constants g_i. In addition, a background matrix $B_{i,j}$ is necessary to describe the data. It affects essentially the ηN elastic scattering and the physical origin of $B_{\eta\eta}$ is not understood. The K matrix may be fitted to the data and a solution for the elastic ηN amplitude may be obtained. One result is shown in fig. 1 [1].

The ηN scattering length, i.e. the amplitude at threshold is $a_{\eta N} = 0.75(4) + i\,0.27(3)\,\mathrm{fm}$. Similar results are obtained by other methods [2], but the actual numbers for $a_{\eta N}$ and $B_{\eta\eta}$ are not well settled. At low ηN energies the elastic scattering matrix is given by

$$T_{\eta N} = \frac{a_{\eta N}}{1 - i\mathrm{q}_{\eta N} a_{\eta N}}\,, \tag{2}$$

[1] Invited talk

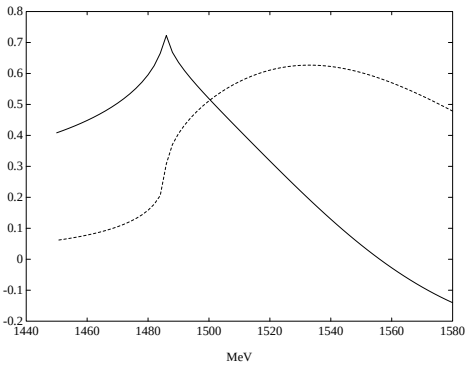

Figure 1: The elastic ηN scattering amplitude (in fm units) vs. the CM energy. The real part (continous line) displays a cusp at the threshold and a zero close to $N^*(1540)$. The imaginary part (dashed line) follows the resonance. Close to threshold the resonant shape is deformed due to the strong energy dependence of the elastic width.

where $\mathrm{q}_{\eta N}$ is the momentum in CM system. $\mathrm{Re}\, a_{\eta N}$ is positive and sizable. It reflects an attraction in this system which may generate a virtual ηN state. Properties of this virtual state are determined by the singularity in $T_{\eta N}$ at a complex value of $\mathrm{q}_{\eta N}$. One finds it as the position of zero in the denominator in eq. 2. It occurs at $\mathrm{q}_s = 1/i\, a_{\eta N}$ and is located in the third quadrant of the complex q plane. If couplings to the γ, π channels are swiched off, then $\mathrm{Im}\, a_{\eta N} = 0$ and q_s settles on the negative imaginary axis. Such a case presents a direct analog to the well known virtual pp state. The existence of a virtual ηN state is signaled by the cusp in fig. 1. Since $\mathrm{Re}\, a_{\eta N}$ is not very large, q_s is rather far away from the threshold and this interpratation may be strongly model dependent. On the other hand, in the $\eta-$deuteron system a virtual ηd state may be quite close to the threshold. The cusp in the ηd elastic amplitude may be very large. Unfortunately, the ηd scattering is not feasible and one has to study similar effects in final state interactions of η mesons.

A large negative $\mathrm{Re}\, a_{\eta N}$ would be a signal of a bound state - an analog to the deuteron in the np system. It would give a singularity in the second quadrant of the complex q plane. Such a situation is not materialised in the ηN channel but, possibly, it exists in the $\eta\, {}^4He$ system.

The effect of virtual states is visualised in fig. 2. The scattering length a in a two-body system is plotted as a function of the strength of the interaction potential. On the right side the potential is repulsive and a is negative. Let us reduce the strength of the potential and go over to the attraction in the left side. The length becomes positive, and at a critical potential well depth it explodes up to infinity. At this critical point, eq. 2 produces $\mathrm{q}_s = 0$, i.e. a bound state of zero binding energy. A further increase of the well depth changes a to negative values, again. The situation to the right of

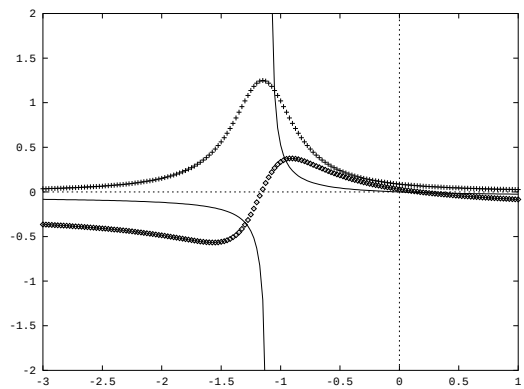

Figure 2: A typical dependence of the scattering length a (y-axis) on the depth of a potential well (x-axis). Continous line – single channel – no absorption. When a strong absorptive potential is added: $\mathrm{Re}\, a$ – squares, $\mathrm{Im}\, a$ – crosses.

the critical point (but close to it) is called a *virtual* state. The situation on the left describes a *bound* state. Dramatic changes follow when an inelastic channel is open in the system. In fig. 2 this is described by a complex potential which makes the scattering lengths complex. The bound states become quasi-bound. Close to the onset of such a state the $\mathrm{Re}\, a$ crosses zero instead of infinity and $\mathrm{Im}\, a$ displays a maximum. The realistic situation in the ηN and $\eta - \mathrm{few} - N$ systems is located in between the two cases shown in fig. 2.

The elastic scattering data at low energies are $\sigma = 4\pi|a|^2$. One cannot find the sign of a from these, and the distinction between bound states, virtual states and the repulsion is not possible. However, the sign of a may be detected in the final state interactions (FSI).

2 The FSI in the ηd and ηpp systems

The ηN interaction, due to the $N^*(1540)$, is attractive. This mechanism by itself cannot produce bound states, unless it is supplemented by a large B which apparently is not the case. A quasibound state may exist already in the ηd system. However, calculations [3] yield the scattering length $A_{\eta d} = 2.5 + i\, 2.8\,\mathrm{fm}$ corresponding to the virtual ηd state. With $\mathrm{Re}\, a_{\eta N}$ as large as 1 fm one enters a critical region of $\mathrm{Re}\, A_{\eta d} \approx 0$ which signals the ηd system close to binding. A genuine quasi-bound state is formed with $\mathrm{Re}\, a_{\eta N} > 1.2\,\mathrm{fm}$. That is beyond the limits allowed by two body data [1]. Now, the experimental $np \to \eta d$ data indicate a moderate cusp at the threshold [4]. It is shown in fig. 3 and compared with the calculations. The latter are done to check the ηN scattering lengths. The values of $\mathrm{Re}\, a_{\eta N}$ in the $0.6 - 0.8\,\mathrm{fm}$ range are allowed and that excludes the existence of an ηd quasi-bound state.

There is a simple structure in the amplitudes shown in fig. 3. For a given

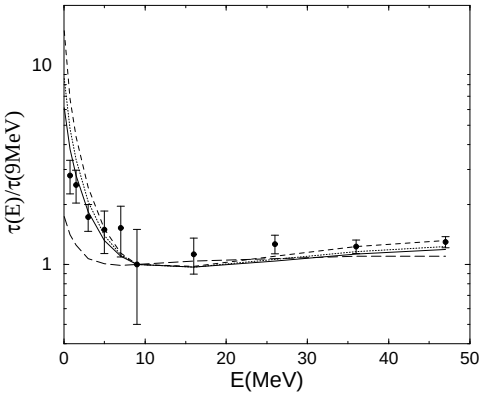

Figure 3: The reduced cross section $\tau = \sigma(pn \to \eta d)/\mathrm{p}_\eta(\mathrm{E})$ from ref. [4] arbitrarily normalised. Theoretical equivalent is calculated for $\mathrm{Re}\, a_{\eta N} =$ 0.75 fm (solid line), 0.87 fm (dotted line), 1.05 fm (dashed line) and 0.21 fm (long-dashed line) from [3].

final state momentum q, the transition amplitude $A(\mathrm{q})$ is roughly given by an integral

$$A(\mathrm{q}) = \int d\mathrm{r}\, [\frac{sin(\mathrm{qr})}{\mathrm{qr}} + T_{\eta d} \frac{exp(i\mathrm{qr})}{\mathrm{r}} v(\mathrm{r})] F_{form}(\mathrm{r}). \tag{3}$$

Here, $F_{form}(\mathrm{r})$ is a source factor responsible for the formation of the final η meson and deuteron. Three body calculations for $A(\mathrm{q})$ have been undertaken [3, 5]. The structure of F_{form} is discussed in ref. [3], it is not well known but it seems weakly dependent on q. The parametrisation 3 is always possible but calculations indicate that the separation of $A(\mathrm{q})$ into formation and FSI is an approximation. The term in brackets consists of the noninteractive wave $sin(\mathrm{qr})$ and the scattered wave $exp(i\mathrm{qr})/\mathrm{r}$. The latter enters with the final state ηd elastic scattering amplitude $T_{\eta d}$ and a function $v(\mathrm{r})$ which describes the ηd interactions at very short distances while $v(\infty) = 1$. Integral 3 may be presented as

$$A(\mathrm{q}) = A_0(\mathrm{q})\, [1 + \frac{T_{\eta d}}{\mathrm{R}}]\,. \tag{4}$$

where $A_0(\mathrm{q})$ involves essentially the noninteractive final wave. By dimensional reasons $T_{\eta d}$ is scaled by a radius R which arises from 1/r in the scattered final wave. A good guess for R is the deuteron radius, but a good calculation in the three body case is rather involved. Eq. 4 indicates three features seen already in fig. 3. The enhancement at threshold is due to the large $A_{\eta d}$. However, the effect is weaker than the elastic scattering cusp due to the large deuteron radius. At about 10 MeV a weak minimum is indicated by the data. This is due to phases of $T_{\eta d}$ and R. With a better experimental precision this minimum might be of some informative value.

Finally, at much higher energies the FSI is of no significance and the process tests directly the η formation mechanism.

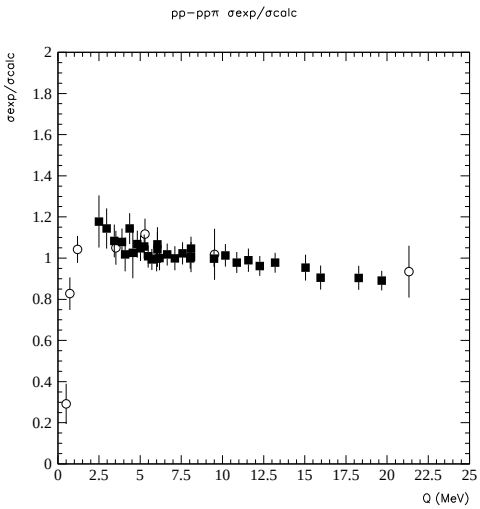

Figure 4: The experimental [7] pion production cross section scaled by the calculated σ_{model} and plotted against the excess energy.

There exist no full calculations of the *meson* FSI in the $pp \to pp\eta(\eta', \pi^0)$ reactions. In order to *indicate* the magnitude of these effects we calculate the ratio $\sigma_{exp}(\mathrm{Q})/\sigma_{model}(\mathrm{Q})$ with a simple meson exchange model for the meson production [6]. This model does include the final pp interactions. For pions this ratio is shown in fig. 4. Essentially, it is a straight line with a weak slope that is almost model independent. Effects of the mesonic FSI are not visible apart from a weak enhancement at the π^+ threshold. The two points at low energies reflect uncertainties in Q. These could be pushed up to line with some 0.5 MeV error brackets in the Q values. The situation differs in the η production case shown in fig. 5. The enhancement close to threshold is due to a strong η attraction in the final state. Again it signals a kind of virtual state in the three body system. In terms of eq. 4, such a state is built upon the pp virtual state which is a deuteron-like object of about 5 fm radius. In the η case the calculated enhancement does depend on the η formation model and a more refined analysis is required. Finally, in fig. 6 we give a similar estimate for the η' production. The lowest two points are puzzling. In contrast to the η case these indicate a destructive interference at low energies. As discussed in the context of fig. 2 it may reflect either the repulsion of η' or the existence of an $\eta' pp$ quasi-bound state. Further studies might be exciting.

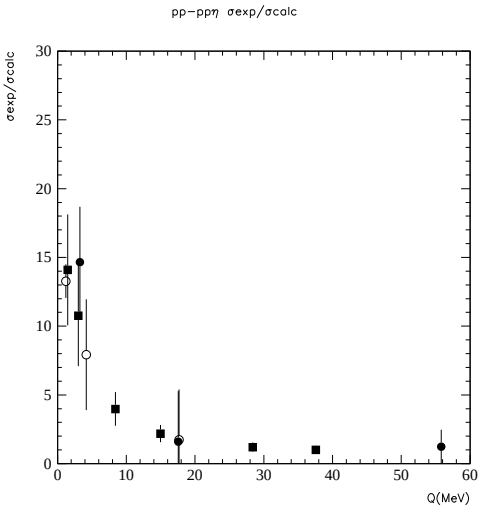

Figure 5: The experimental [8] η production cross section scaled by a calculated one, plotted against the excess energy.

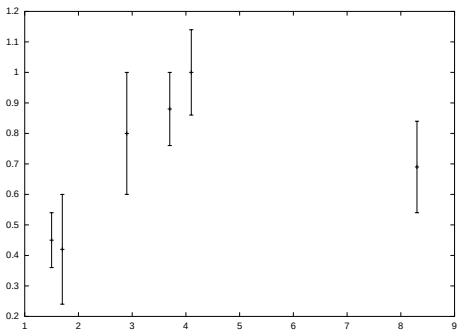

Figure 6: The experimental [9] η' production cross section scaled by a calculated one, plotted against the excess energy.

Partial support from KBN grant 5P 03B 04521 is acknowledged.

References

[1] A.M. Green, S. Wycech, Phys. Rev. **C 55** (1997) 2167R; Phys. Rev. **C 60** (1999) 036208.

[2] M. Batinic et al., Phys. Rev. **C 51** (1995) 2310.

[3] S. Wycech, A.M. Green, Nucl. Phys. **A 663** (2000) 529; Phys. Rev. **C 64** (2001) 045206; A.M. Green, J.A. Niskanen, S. Wycech, Phys. Rev. **C 54** (1996) 1970; A. Deloff, Phys. Rev. **C 61** (2000) 024004.

[4] H. Calén et al., Phys. Rev. Lett. **80** (1998) 2069; Phys. Rev. Lett. **79** (1997) 2642.

[5] A. Fix, H. Arenhövel, Phys. Lett. **B 492** (2000) 32; H. Garcilazo, M.T. Pena, Phys. Rev. **C 63** (2001) 021001; V.Yu. Grishina et al., Phys. Lett. **B 475** (2000) 9; N.V. Shevchenko et al., Eur. Phys. J. **A 9** (2000) 143.

[6] S. Wycech, Acta Phys. Polon. **B 27** (1996) 2981.

[7] H.O. Meyer et al., Phys. Rev. Lett. **65** (1990) 2846; Nucl. Phys. **A 539** (1992) 633; A. Bondar et al., Phys. Lett. **B 356** (1995) 8.

[8] A.M. Bergdolt et al., Phys. Rev. **D 48** (1993) 2969; E. Chiavassa et al., Phys. Lett. **B 322** (1994) 270; H. Calén et al., Phys. Lett. **B 366** (1996) 39.

[9] P. Moskal et al., Phys. Lett. **B 474** (2000) 416; F. Hibou et al., Phys. Lett. **B 438** (1998) 41.

First measurement of the analysing power in the reaction $\vec{p}p \to pp\eta$

P. Winter

Institut für Kernphysik, Forschungszentrum Jülich, Germany

Abstract: In order to determine the influence of higher partial waves in η meson-production, polarization observables provide the optimum tool. Therefore, the reaction $\vec{p}p \to pp\eta$ at an excess energy Q = 40 MeV has been measured at the COSY-11 facility in January 2001. The analysis will determine the analysing power A_y and thus new information for a further theoretical description of the mechanism for η meson production in nucleon-nucleon scattering.

1 Brief theoretical overview

In the following, we describe a spin-$\frac{1}{2}$ particle with the 2-component spinor $\chi = (p_\uparrow,\ p_\downarrow)^T$. The density matrix ρ is defined by [1]:

$$\rho := \chi \cdot \chi^\dagger = \begin{pmatrix} |p_\uparrow|^2 & p_\uparrow p_\downarrow^* \\ p_\uparrow^* p_\downarrow & |p_\downarrow|^2 \end{pmatrix}$$

With this definition, we easily find that the expectation value for every quantum mechanical operator Ω can be expressed by:

$$\langle \Omega \rangle := \chi^\dagger \Omega \chi = \mathrm{Tr}(\rho\Omega)$$

As ρ is a Hermitian operator ($\rho = \rho^\dagger$) it can be shown[1] that for spin-$\frac{1}{2}$:

$$\rho = \frac{1}{2}(\sigma_0 + \sum_{i=1}^{3} P_i\, \sigma_i),$$

[1] Therefore write $\rho = \sum_{\mu=0}^{3} a_\mu \sigma_\mu$ and take into account that $\mathrm{Tr}(\sigma_\mu \sigma_\nu) = 2\delta_{\mu\nu}$. Here, σ_0 denotes the unit matrix $\mathbb{1}_2$ and σ_i the Pauli matrices. In general, greek indices cover the range from 0 to 3, latin from 1 to 3.

with the polarization $P_i := \langle \sigma_i \rangle$.
In scattering theory [2] it is shown that the cross section for a reaction with spin-$\frac{1}{2}$ particles is given by:

$$W(i \to f) = \frac{k_f}{k_i} \, \mathrm{Tr}(\rho_f) \tag{1}$$

The final density matrix ρ_f is related to the initial one:

$$\rho_f = \chi_f \cdot \chi_f^\dagger = \mathcal{M} \, \rho_i \, \mathcal{M}^\dagger \tag{2}$$

Here, $\mathcal{M}$ denotes the transition matrix, which converts an initial spin state into a final spin state:

$$\chi_f \;=\; \mathcal{M}(\vec{k}_i, \vec{k}_f) \, \chi_i$$

The initial density matrix ρ_i for $\vec{p}p \to pp\eta$ is given by:

$$\rho_i = \underbrace{\frac{1}{2}(\sigma_0 + \sum_{i=1}^{3} P_i \, \sigma_i)}_{\vec{p}} \otimes \underbrace{\frac{1}{2} \, \sigma_0}_{p} \tag{3}$$

Combining equations 1, 2 and 3 gives the differential cross section for reactions of spin-$\frac{1}{2}$ with a polarized projectile and an unpolarized target:

$$W = W_0 \cdot (1 + \sum_{i=1}^{3} P_i \, A_i),$$

where W_0 denotes the cross section without polarization, and the analysing power A_i is given by:

$$A_i = \frac{\mathrm{Tr}(\mathcal{M} \, \sigma_i \, \mathcal{M}^\dagger)}{\mathrm{Tr}(\mathcal{M} \, \mathcal{M}^\dagger)}$$

Because of the parity invariance of strong interaction, we find $A_x = A_z = 0$ and therefore

$$W = W_0 \cdot (1 + A_y \cdot P_y)$$

This formula is independent of the particular choice of the coordinate system. Therefore, it is possible to choose the following system (see fig. 1) matching the experimental situation[2]:

$$\hat{z} = \frac{\vec{\mathrm{p}}_{beam}}{|\vec{\mathrm{p}}_{beam}|}, \quad \hat{y} = \frac{\vec{P}}{|\vec{P}|} \quad \text{und} \quad \hat{x} = \frac{\vec{y} \times \vec{z}}{|\vec{y} \times \vec{z}|}$$

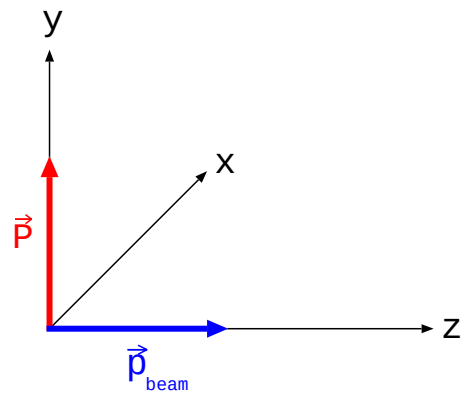

Figure 1: Fixing of the coordinate system with the z-axis along the beam momentum and the y-axis along the beam polarization.

The experimentally measured counting rate n is with the given luminosity $\mathcal{L}$ connected to the cross section via $n = \frac{1}{\mathcal{L}} \cdot W$. If one further defines $n_{\uparrow}(n_{\downarrow})$ as the reaction rate for beam polarization up (down) it is possible to connect the analysing power to the left-right-asymmetry:

$$\begin{aligned} \varepsilon &:= \frac{n_{\uparrow} - n_{\downarrow}}{n_{\uparrow} + n_{\downarrow}} \\ &= {}^{3} \frac{A_y \cdot (P_{y,\uparrow} + P_{y,\downarrow})}{2 + A_y \cdot (P_{y,\uparrow} - P_{y,\downarrow})} \end{aligned} \tag{4}$$

A measurement of this left-right asymmetry ε therefore enables to determine the analysing power A_y.

2 Experimental setup

The reaction $\vec{p}p \to pp\eta$ was measured with a beam momentum of $\vec{\mathrm{p}}_{beam} = 2.096\,\mathrm{GeV/c}$ for 10 days in January 2001. This corresponds to an excess energy $\mathrm{Q} = 40\,\mathrm{MeV}$.

The measurement was performed at the COSY-11 facility [3, 4] (see fig. 2) where the four-momenta of the two outgoing protons are reconstructed via drift chambers (D1 and D2) and a time-of-flight measurement with two

[2]Here, $\vec{P}$ denotes the experimental COSY beam polarization.
[3]Here, the same luminosity for both polarizations was assumed.

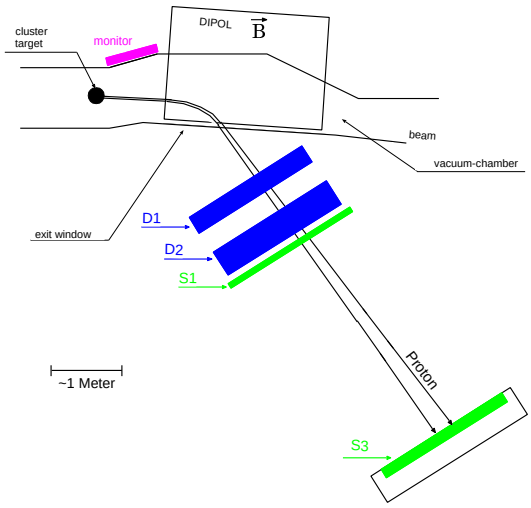

Figure 2: Experimental setup of the COSY-11 detector.

scintillation detectors (S1 and S3). The undetected uncharged meson is reconstructed via the missing mass technique.
During the beamtime, the reaction was measured for spin up and down alternately in flat top cycles of 10 minutes. The polarization will be determined either via the measurement of the proton-proton elastic scattering in the up and down luminosity detectors or from the data taken at the same time by the EDDA collaboration.

3 Status of the analysis

3.1 Proton-proton elastic scattering

The events from proton-proton elastic scattering will be used both to determine the polarization and to calibrate the relative position of the drift chambers.
Events originating from proton-proton elastic scattering were reconstructed both in Monte Carlo simulations and real data from hits in the S1 scintillator and the monitor detector (see fig. 2). Furthermore, after a time calibration of these detector components, a cut on the invariant mass is used to separate protons from pions (see fig. 3).

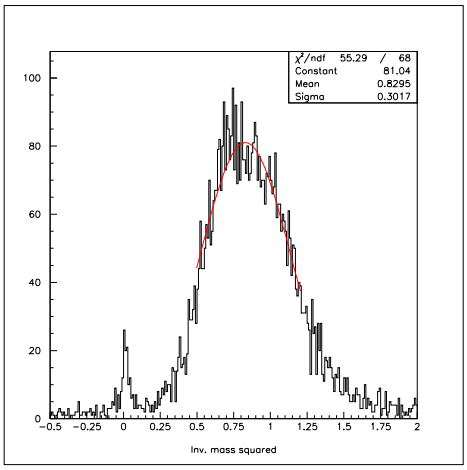

Figure 3: Reconstruction of the invariant mass for possible elastic events in real data. The proton peak can be easily separated from the pion peak by a cut on the mass. The slight deviation of the proton mass from its literature value results from a wrong time offset in the reconstruction which was corrected later.

3.2 Target position

For events with two reconstructed proton tracks, a clear η peak is seen in the missing mass spectrum (see fig. 4,top).
By determing the resolution of this η-peak for several target positions, the target location will be reconstructed [5].

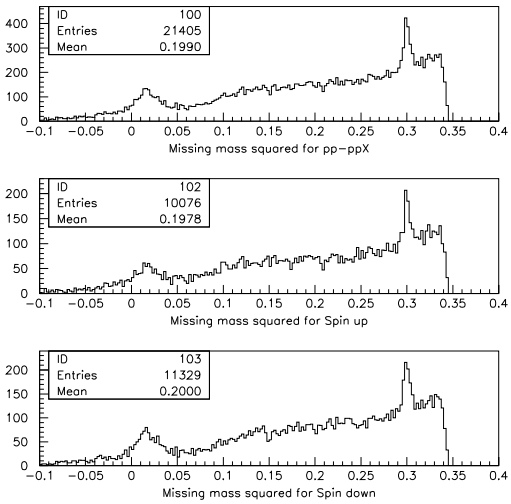

Figure 4: Missing mass spectra for events with two reconstructed protons (data). Besides the background, predominantly from multi-pion production, the η and π^0 peaks are clearly visible. In the upper figure, all events are shown, the other two are separated for spin up and down.

3.3 Further analysis

After completing the calibration of the two drift chambers, the target position and the relative angle and location of the drift chambers will be reconstructed as mentioned above. Then, the left-right asymmetry will be determined for several angle intervals. With the knowledge of the polarization, the analysing power A_y will be calculated with equation 4.

References

[1] D. Fick, *Einführung in die Kernphysik mit polarisierten Teilchen*, BI–Hochschulskripten, Bibliographisches Institut, Mannheim (1971).

[2] M.L. Goldberger, K.M. Watson, *Collision theory*, Structure of Matter Series, Wiley, New York (1964).

[3] W. Oelert et al., *Threshold Meson Production at the Internal COSY-Beam in the Range of Scalar Mesons Involving Strangeness*, COSY Proposal No. 11, 1988.

[4] S. Brauksiepe et al., Nucl. Instr. & Meth. **A 376** (1996) 397.

[5] P. Moskal et al., Nucl. Instr. & Meth. **A 466** (2001) 448.

Pseudoscalar and Vector Meson Production in NN Collisions [1]

K. Nakayama[a,b]

[a] *Department of Physics and Astronomy, University of Georgia, Athens, USA*

[b] *Institut für Kernphysik, Forschungszentrum Jülich, Germany*

Abstract: Heavy meson production in nucleon-nucleon collisions is discussed within a meson exchange model of hadronic interactions, paying special attention to the basic dynamics that determine the behavior of the cross sections near the threshold energy. The $pp \to pp\phi$ reaction is discussed as an example of the production of vector mesons in NN collisions. For the pseudoscalar meson production, results for the η production in both the pp and pn collisions are presented.

1 Introduction

With the advent of particle accelerators in the few GeV energy region, heavy meson production in hadronic collisions has attracted increasing attention in the past few years. In particular, heavy meson production in nucleon-nucleon (NN) collisions is of special interest because it allows to investigate in a simple system the short range hadron dynamics for which, so far, we have a very limited knowledge. Due to the large momentum transfer between the initial and final states, these reactions necessarily probe the dynamics at short distances. In this context, apart from the intrinsic interest associated with the particular meson produced, the production of pseudoscalar and vector mesons can be used as a tool to probe the short distance dynamics systematically. Table 1 illustrates this point: it shows the momentum transfer and the corresponding distance probed by producing mesons of different masses at the respective threshold energy. At threshold, the momentum transfer is given by $\mathrm{q} = (\mathrm{m}_N\,\mathrm{m}_M + \mathrm{m}_M^2/4)^{1/2}$, where m_N and m_M denote the nucleon and meson mass, respectively. As one can see, the distance probed in these reactions ranges from 0.53 fm for pion production to 0.18 fm for ϕ meson production.

The theory of heavy meson production is still in its early stage of development. As we have seen above, heavy meson production reactions can

[1] Invited lecture

Table 1: Momentum transfer q and the corresponding distance r probed by the $NN \to NNM$ reaction at the threshold energy for different particles M produced.

particle	mass (MeV)	q (fm^{-1})	r (fm)
γ	0	0.0	∞
π	140	1.9	0.53
η	550	3.9	0.26
ρ, ω	780	4.8	0.21
η'	960	5.4	0.19
ϕ	1020	5.6	0.18

probe quite short distances - down to less than 0.2 fm. These short distances correspond to the region of confinement where the relevant degrees of freedom are the constituent quarks and gluon flux tubes. Thus, the appropriate approach to describe these short range dynamics might be the constituent quark models rather than the hadronic models. However, such an approach still remains to be developed. On the other hand, the transition region from the hadronic to constituent quark degrees of freedom does not have a well-defined boundary and, consequently, it is of special interest to see how far down in distance one can "push" the hadronic models.

In principle, effective field theories can be used to describe near-threshold particle production processes in terms of hadronic degrees of freedom. However, although such an approach (Chiral Perturbation Theory) might be appropriate for describing the production of pions [1] in spite of the relatively large expansion parameter, $\mathrm{Q} = \sqrt{\mathrm{m}_\pi/\mathrm{m}_N} \sim 1/3$, for the description of heavy meson production there is, *a priori*, no obviously preferred approach. The majority of existing calculations of heavy meson production in NN collisions are based on meson exchange models of strong interactions [2, 3, 4, 5, 6, 7, 8, 9, 10, 11] with a few exceptions [12]. The price one pays for insisting on such models is that their predictions become more and more sensitive to the short range part of the model, usually parametrized in terms of the form factors at the hadronic vertices involved. The success of such models should be measured in terms of their capability to correlate as many independent processes as possible in a consistent manner. We mention that although the approach used in ref. [11] is based on meson exchange models, it differs from conventional meson exchange models in a number of aspects, such as the absence of the form factors at the hadronic vertices, etc.

2 Meson Exchange Models

As mentioned in the previous section, the majority of the existing calculations of meson production in NN collisions are based on conventional meson exchange models. Even within such models, the description of these reactions is not a simple task in principle, for the final state is a three-body state and, consequently, one needs to solve the three-body Faddeev equation. Of course, a complete three-body calculation of this reaction is at present not available [13]. How can one then start to describe these reactions? In order to gain some insight to this question, let us examine some of the features exhibited by the production cross sections near threshold. In reactions like NN bremsstrahlung, where a (massless) photon is produced, the measured cross section varies with the inverse of the photon energy ω_γ near threshold. This feature of the cross section is expressed by the so-called soft-photon theorem [14] which gives

$$\sigma = \frac{A}{\omega_\gamma} + B\,, \tag{1}$$

where A and B are constants containing only the on-shell information of the NN interaction (or, in other words, the asymptotic behavior of the NN wave function). This result is not surprising at all if we recall from table 1 that, close to threshold, the photon production reaction in NN collisions probes only the asymptotic behavior of the NN wave function. Eq. 1 is, therefore, regarded as a model-independent result and, as such, it should be reproduced by any model describing the NN bremsstrahlung reaction.

For production of heavy mesons, we do not have a model independent result like the low energy theorem for NN bremsstrahlung. However, as early as 1952, Watson [15] showed that in heavy particle production reactions in which strongly (attractively) interacting particles are present, the energy dependence of the cross sections should be dictated by the energy dependence of the interaction between those strongly interacting particles and the available phase space. In particular, for meson production in NN collisions, the energy dependence of the total cross section should be given by the energy dependence of the on-shell NN final state interaction (FSI), $T(\mathrm{p}', \mathrm{p}')$, plus the phase space

$$\begin{aligned} \sigma(\mathrm{E}) &\propto \int d\rho(\mathrm{E}, \mathrm{p}')|T(\mathrm{p}', \mathrm{p}')|^2 \\ &\propto \int d\rho(\mathrm{E}, \mathrm{p}') \left(\frac{\sin(\delta(\mathrm{p}'))}{\mathrm{p}'}\right)^2 , \end{aligned} \tag{2}$$

where the integration is over the available phase space, $\rho(\mathrm{E}, \mathrm{p}')$, with p' denoting the relative momentum of the two interacting nucleons in the final state. $\delta(\mathrm{p}')$ denotes the corresponding NN phase shift. Watson's result is based on the observation that the massive particle production is a short range process and, as such, the primary production amplitude of such a particle should have a weak energy dependence. Note that the production cross section $\sigma(\mathrm{E})$ cannot be expressed in a model-independent way, for its absolute value depends on the short range part of the interaction. We shall elaborate more on Watson's result later. For the moment, we mention that all the recently measured meson production cross sections in NN collisions near threshold follow the energy dependence given by eq. 2 with the exception of η meson production, where one sees a relatively small deviation at energies close to threshold. This deviation is commonly attributed to the ηN FSI.

The above consideration indicates that any model of heavy meson production reaction in NN collisions should have built in the feature given by Watson's result, eq. 2. As we shall show in the following, this can be achieved within a Distorted Wave Born Approximation. Here we follow a diagrammatic approach to derive the total amplitude. We start by considering the meson-nucleon (MN) and NN interactions as the building blocks for constructing the total amplitude describing the $NN \to NNM$ reaction. We then consider all possible combinations of these building blocks in a topologically distinct way, with two nucleons in the initial state and two nucleons plus a meson in the final state. In this process of constructing the total amplitude, care must be taken in order to avoid diagrams that lead to double counting. Specifically, these are the diagrams that lead to the mass and vertex renormalizations, since we choose to use the physical masses and coupling constants. The resulting amplitude constructed in this way is displayed in fig. 1. The ellipsis indicates those diagrams that are more involved numerically (including, in particular, the MN FSI, which otherwise would be generated by solving the three-body Faddeev equation). So far there are very few attempts to account for them [6, 16]. Therefore, neglecting those diagrams, the total amplitude is given by the diagrams displayed explicitly in fig. 1 and reads

$$M = (1 + T_f^{(-)\dagger} G_f^{(-)*})\, J\, (1 + G_i^{(+)} T_i^{(+)})\,, \tag{3}$$

where $T_{(i,f)}$ denotes the NN T-matrix interaction in the initial(i)/final(f) state and, $G_{(i,f)}$, the corresponding two nucleon propagator. The superscript $\pm$ in $T_{(i,f)}$ as well as in $G_{(i,f)}$ indicates the boundary condition ($(-)$ for

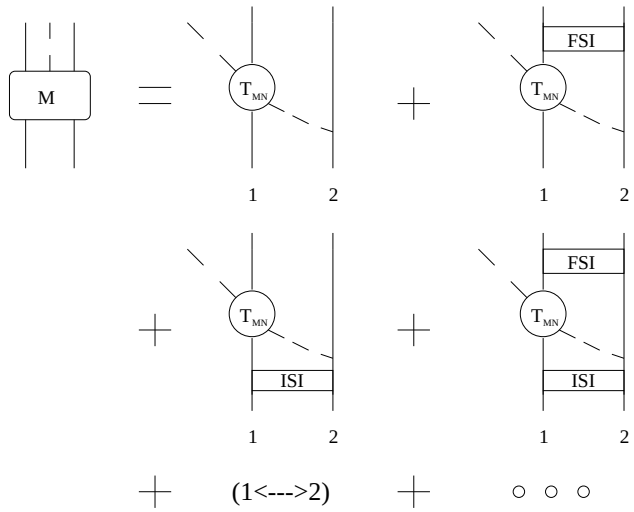

Figure 1: Meson production amplitude obtained in a diagrammatic approach to the $NN \to NNM$ reaction considering the MN and NN T-matrices as the basic building blocks. T_{MN} stands for the MN T-matrix. FSI and ISI stand for the final and initial state NN T-matrices, respectively. The first diagram on the r.h.s. is referred to as the production current J which enters in other diagrams as can be noted.

incoming and (+) for outgoing waves). The production current is denoted by J, which is nothing other than the MN T-matrix, T_{MN}, with one of the meson legs attached to a nucleon (first diagram on the r.h.s. in fig. 1). Eq. 3 is the basic formula on which the large majority of existing calculations are based.

We now wish to exhibit the essential features of the meson production reaction contained in eq. 3. In particular, we would like to make close contact between the amplitude M and Watson's result given by eq. 2. To this end, we use the relation

$$G_\alpha^{(\pm)} = \mathcal{P}\left(\frac{1}{\mathrm{E}_\alpha - \mathrm{E(k)}}\right) \mp i\pi\delta(\mathrm{E}_\alpha - \mathrm{E(k)})\,, \tag{4}$$

where $\alpha = i, f$, to express M as

$$\begin{aligned} M &= \left\{1 - i\kappa_f T_f(\mathrm{p}', \mathrm{p}')[1 + i\frac{1}{a\mathrm{p}'}\mathcal{P}_f(\mathrm{E}, \mathrm{p}')]\right\} J(\mathrm{E}, \mathrm{p}') \\ &\times \left\{1 - i\kappa_i T_i(\mathrm{p}, \mathrm{p})[1 + i\frac{1}{a\mathrm{p}}\mathcal{P}_i(\mathrm{E}, \mathrm{p}')]\right\}\,, \end{aligned} \tag{5}$$

where $T_i(\mathrm{p},\mathrm{p})$ denotes the on-shell NN T-matrix with the relative momentum p of the interacting two nucleons in the initial state i and $T_f(\mathrm{p}',\mathrm{p}')$ denotes the on-shell NN T-matrix with the relative momentum p' of the interacting two nucleons in the final state f. Here the superscript (+) of $T_{(i,f)}$ has been omitted. $\kappa_i \equiv \pi \mathrm{p}\varepsilon(\mathrm{p})/2$ and $\kappa_f \equiv \pi \mathrm{p}'\varepsilon(\mathrm{p}')/2$ are the phase space densities of the two nucleons in the initial and final states, respectively. $\varepsilon(\mathrm{q}) \equiv \sqrt{\mathrm{q}^2 + \mathrm{m}_N^2}$ and a is a constant (scattering length) introduced for convenience. Note that in the above equation, only those arguments of the quantities relevant to the discussion related to Watson's result are explicitly displayed. $\mathrm{E} \equiv \mathrm{E}_i$. The function $\mathcal{P}_i$ is given by

$$\mathcal{P}_i(\mathrm{E},\mathrm{p}') = \left(\frac{a\mathrm{p}}{\kappa_i}\right)\mathcal{P}\int_0^\infty d\mathrm{k}\mathrm{k}^2 \frac{f_i(\mathrm{E},\mathrm{k})}{\mathrm{E}_i - \mathrm{E}(\mathrm{k})}, \tag{6a}$$

$$f_i(\mathrm{E},\mathrm{k}) \equiv \frac{T_i(\mathrm{p},\mathrm{k})J(\mathrm{E},\mathrm{k})}{T_i(\mathrm{p},\mathrm{p})J(\mathrm{E},\mathrm{p}')} = \frac{K_i(\mathrm{p},\mathrm{k})J(\mathrm{E},\mathrm{k})}{K_i(\mathrm{p},\mathrm{p})J(\mathrm{E},\mathrm{p}')}. \tag{6b}$$

Similarly,

$$\mathcal{P}_f(\mathrm{E},\mathrm{p}') = \left(\frac{a\mathrm{p}'}{\kappa_f}\right)\mathcal{P}\int_0^\infty d\mathrm{k}\mathrm{k}^2 \frac{f_f(\mathrm{E},\mathrm{k})}{\mathrm{E}_f - \mathrm{E}(\mathrm{k})}, \tag{7a}$$

$$f_f(\mathrm{E},\mathrm{k}) \equiv \frac{T_f(\mathrm{p}',\mathrm{k})A(\mathrm{E},\mathrm{k})}{T_f(\mathrm{p}',\mathrm{p}')A(\mathrm{E},\mathrm{p}')} = \frac{K_f(\mathrm{p}',\mathrm{k})A(\mathrm{E},\mathrm{k})}{K_f(\mathrm{p}',\mathrm{p}')A(\mathrm{E},\mathrm{p}')}, \tag{7b}$$

with $K_{(i,f)}$ denoting the NN K-matrix and $A \equiv (1+G_iT_i)J$. The functions $\mathcal{P}_{(i,f)}(\mathrm{E},\mathrm{p}')$ summarize all the off-shell effects of the NN interaction and production current. As such, it is an unmeasurable and model-dependent quantity. For production of heavy mesons near threshold, the off-shell NN interaction required in $\mathcal{P}_f(\mathrm{E},\mathrm{p}')$ is at very low energy. In calculations based on conventional meson exchange models this function is very large and cannot be neglected. In contrast, the function $(1/a\mathrm{p})\mathcal{P}_i(\mathrm{E},\mathrm{p}')$ is relatively small. This is because for heavy meson production the energy of the two nucleons in the initial state has to be large enough to produce the meson in the final state. For example, for η meson production, the incident energy of the beam nucleon corresponding to the threshold energy is about 1.25 GeV. At such high energies, the on-shell NN interaction has a rather weak energy dependence. Note that the inverse scattering theory tells us that, for a local and energy-independent NN potential, the off-shell behavior of the NN amplitude is completely determined if one knows the corresponding on-shell amplitude in the entire energy domain. At least in the case of meson exchange models, the weak energy dependence of the on-shell NN interaction implies

also a flat off-shell behavior and leads to a small value of $(1/a\mathrm{p})\mathcal{P}_i(\mathrm{E},\mathrm{p}')$. Therefore, at least for the discussion of the essential features of the cross section near threshold, the function $(1/a\mathrm{p})\mathcal{P}_i(\mathrm{E},\mathrm{p}')$ may be neglected.

Using then the relation between the on-shell T-matrix and the phase shift $\delta(\mathrm{q})$ and inelasticity $\eta(\mathrm{q})$

$$\kappa(\mathrm{q})T(\mathrm{q},\mathrm{q}) = \frac{i}{2}\left(\eta(\mathrm{q})e^{2i\delta(\mathrm{q})} - 1\right) , \tag{8}$$

together with the effective range expansion for the FSI,

$$\mathrm{p}'\cot(\delta(\mathrm{p}')) = -\frac{1}{a} + \frac{1}{2}\Lambda^2 \sum_{n=0}^{\infty} r_n \left(\frac{\mathrm{p}'^2}{\Lambda^2}\right)^{n+1} , \tag{9}$$

eq. 5 can be reduced to

$$\begin{aligned} M &\cong \left\{-e^{i\delta_f(\mathrm{p}')}\left(\frac{\sin(\delta_f(\mathrm{p}'))}{a\mathrm{p}'}\right)[1+\mathcal{P}_f(\mathrm{E},\mathrm{p}') - ...]\right\} J(\mathrm{E},\mathrm{p}') \\ &\times \left\{\frac{1}{2}\left(\eta_i(\mathrm{p})e^{i2\delta_i(\mathrm{p})}+1\right)\right\} , \end{aligned} \tag{10}$$

where the inelasticity in the final NN state is set to unity, $\eta_f(\mathrm{p}') = 1$. The above equation is the desired result. It exhibits the essential features of the meson production reaction in NN collisions. First, it shows that the relevant energy dependence of the total amplitude near threshold is indeed determined by the strong energy dependence of the on-shell NN FSI, proportional to $\sin(\delta_f(\mathrm{p}'))/a\mathrm{p}'$. This, when combined with the phase space factor, determines the energy dependence of the cross section as given by eq. 2. Note that for heavy meson production the production current $J(\mathrm{E},\mathrm{p}')$, as well as $\mathcal{P}_f(\mathrm{E},\mathrm{p}')$, should be weakly energy-dependent, for they summarize all the short range dynamics of the reaction. Thus, none of the terms in eq. 10, apart from the on-shell NN FSI, should introduce any significant energy dependence near threshold; they just amount to a constant. Therefore, the total cross section data near threshold determine just this constant. Second, the major effect of the NN initial state interaction (ISI) (the term in the last curly brackets) is to reduce the cross section by a factor of

$$\begin{aligned} \lambda &= \left|\frac{1}{2}\left(\eta_i(\mathrm{p})e^{i2\delta_i(\mathrm{p})}+1\right)\right|^2 \\ &= \eta_i(\mathrm{p})\cos^2(\delta_i(\mathrm{p})) + \frac{1}{4}[1-\eta_i(\mathrm{p})]^2 \le \frac{1}{4}[1+\eta_i(\mathrm{p})]^2 . \end{aligned} \tag{11}$$

As mentioned before, the majority of the existing calculations of meson production in NN collisions are based on eq. 3. The differences among them reside in how the production current J is modeled, as well as in the different treatments of both the NN FSI and ISI. Let's first concentrate on the NN interactions. It is clear that the description of meson production processes in NN collisions based on eq. 3 requires the half-off-shell NN ISI and FSI. This has been exhibited explicitly in eq. 5 through the functions $\mathcal{P}_{(i,f)}$ given by eqs. 6,7. Although the on-shell NN interaction can be determined from the NN elastic scattering experiments, the off-shell behavior of it can only be provided by a given model of the NN interaction. For energies below pion threshold, there exist a number of accurate meson exchange models [17, 18, 19] which can provide the half-off-shell extension of the NN interaction. As previously noted, these so-called realistic NN interactions, based on meson exchange models, yield a rather large value for the function $\mathcal{P}_f(\mathrm{E}, \mathrm{p}')$ that, consequently, cannot be neglected. In this connection, for production of heavy mesons, the predicted total cross sections can easily differ by a factor of two or more due to the different off-shell behavior of these realistic NN FSIs. This indicates that a consistent treatment of the NN FSI and the production current J is required. Maintaining the consistency between the NN FSI and the production current, however, is not a trivial task. While in models where the underlying meson exchange structure is known this consistency can, in principle, be maintained, in the case of purely phenomenological models, such as the parametrized version of the Paris NN interaction [18], such a consistency is impossible to achieve - even in principle. In the excess energy region below $\mathrm{Q} \cong 100\,\mathrm{MeV}$ however, the introduced difference in the predicted total cross section due to off-shell differences of these realistic NN interactions is practically a constant. It should also be mentioned that the procedure of just evaluating J in the on-shell tree level approximation and simply multiplying it by the on-shell NN FSI,as has been done by many authors (see references quoted in [20]), is not acceptable for obtaining quantitative predictions. As it can be seen from eq. 10, the strength of the amplitude M depends on the function $\mathcal{P}_f(\mathrm{E}, \mathrm{p}')$. Using just the on-shell T-matrix as the FSI instead of the full half-off-shell T-matrix means setting the function $\mathcal{P}_f(\mathrm{E}, \mathrm{p}')$ to zero. Such a procedure simply lacks a consistent regularization scheme between the NN interaction and the production current J [20].

One of the major limitations in the current models of heavy meson productions in NN collisions is the lack of a reliable model for the NN ISI. As mentioned before, the energy of the two interacting nucleons in the initial state must be large enough to produce a meson. For example, for the η

meson this means nucleon incident energies of at least 1.25 GeV. For heavier mesons, like η' and ϕ, the corresponding threshold incident energy is well above 2 GeV, where no reliable model exists to provide the half-off-shell NN T-matrix that is required in the evaluation of the function $\mathcal{P}_i(\mathrm{E}, \mathrm{p}')$ in eq. 6. Note that, although this quantity is expected to be small and may be neglected for estimates of cross sections, for more quantitative predictions it should be taken into account. In particular, predictions of spin observables are expected to be sensitive to this function. The situation with the NN ISI is even worse in the case of heavy meson production in pn collisions. There, we lack even the on-shell NN interaction. While for total isospin $T = 1$ states rather reliable phase shift analyses exist up to 3 GeV incident energy, for $T = 0$ states the reliability is limited to 1.3 GeV [21, 22]. This situation imposes a severe limit in all existing models of production of mesons heavier than the η meson in pn collisions.

There are basically three different approaches in literature in modeling the production current J based on meson exchange models. One is a microscopic model of $MN \to M'N'$ reactions whose data are reproduced by the model [4, 10]. The off-shell behavior of the MN T-matrices that are required in the construction of J is then provided by the model. Another approach is a "pseudo" empirical model in which the production current is constructed using the on-shell amplitudes of the $MN \to M'N'$ as well as $\gamma N \to M'N'$ reactions extracted directly from the available data [3, 9]. In the latter reaction the VMD is used to convert its on-shell amplitude to an $MN \to M'N'$ amplitude ($M = \rho, \omega$). The off-shell behavior of the corresponding amplitudes necessary to construct J is then an assumption in this approach. The third approach is to split the MN T-matrix into the pole (T^P) and non-pole (T^{NP}) parts and consider the non-pole part in the Born approximation only in order to construct the production current J [6, 7]. As has been shown elsewhere [23], the MN T-matrix can be split into the pole and non-pole parts according to

$$T = T^P + T^{NP}\,, \tag{12}$$

where

$$T^P = \sum_B f^\dagger_{MNB}\, g_B\, f_{MNB}\,, \tag{13}$$

with f_{MNB} and g_B denoting the physical meson-nucleon-baryon (MNB) vertex and baryon propagator, respectively. The summation runs over the relevant baryons B. The non-pole part of the T-matrix is given by

$$T^{NP} = V^{NP} + V^{NP}\, G\, T^{NP}\,, \tag{14}$$

where $V^{NP} \equiv V - V^P$, with V^P denoting the pole part of the MN potential V. V^P is given by the equation analogous to eq. 13 with the renormalized vertices and propagators replaced by the corresponding bare vertices and propagators. This third approach then leads to a production current which is obtained by approximating the full MN T-matrix as $T \cong T^P + V^{NP}$.

3 Our Model

In our model of $NN \to NNM$, the reaction amplitude M is calculated using eq. 3. It is based on a relativistic meson exchange model of hadronic interactions. The results we shall show in the next section are obtained by using the NN interaction developed by the Bonn group [17]. This interaction is obtained by solving a three dimensionally reduced (Blankenbecler-Sugar) version of the Bethe-Salpeter equation. The loop integrals in eq. 3 are calculated consistently with the three dimensional reduction used in constructing the NN interaction, i.e., the two-nucleon propagators $G_{(i,f)}$ are taken to be the Blankenbecler-Sugar propagator. The production current J is modeled according to the third approach discussed in the previous section. It consists of the nucleonic, resonance and mesonic currents as displayed diagrammatically in fig. 2. Note that they are all Feynman diagrams and, as such, they include both the positive- and negative-energy propagation of the intermediate particles. All the parameters of our model for the production current (coupling constants and form factors) are confined to the hadronic vertices Γ_{MNB}, $\bar{\Gamma}_{MNB}$ and Γ_{MMM} indicated in fig. 2 ($B = N, N^*$). Below, we discuss briefly these parameters for each vertex. For more details, see refs. [7, 24].

$\bar{\Gamma}_{MNB}$: At the meson production vertex $\bar{\Gamma}_{MNN}$, the coupling constant is taken consistently with that used in the construction of the NN interaction. In addition, this vertex contains an extra form factor ($F_N(\mathrm{p}^2)$) to account for the off-shellness of the intermediate nucleon, which is far off-shell if a heavy meson is produced. It is given by

$$F_N(\mathrm{p}^2) = \frac{\Lambda_N^4}{\Lambda_N^4 + (\mathrm{p}^2 - \mathrm{m}_N^2)^2}\,, \tag{15}$$

with $\Lambda_N = 1.2\,\mathrm{GeV}$. p and m_N stand for the four-momentum and mass of the intermediate nucleon, respectively.

The coupling constant in the vertex $\bar{\Gamma}_{MNN^*}$ is extracted from the measured decay width of the resonance into a meson and a nucleon,

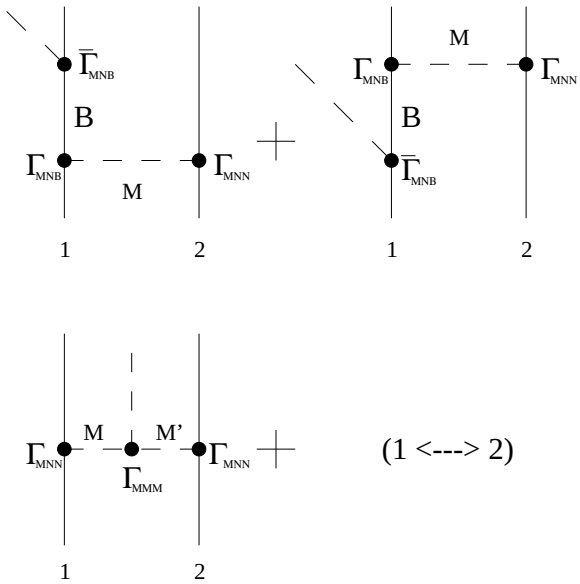

Figure 2: Model for the meson production current J. The upper two diagrams are called nucleonic or resonance current depending on the intermediate baryon B being a nucleon (N) or a nucleon resonance (N^*). The lower diagram is the mesonic current. $M, M' = \pi, \eta, \rho, \omega, \sigma, a_0$.

$N^* \to M + N$, whenever available [25]. For the vertex involving a vector meson, the coupling constant can be extracted from the measured radiative decay using the VMD. The sign of the coupling constant is chosen in accordance with the relevant photo-production reaction analysis [26, 27]. $\bar{\Gamma}_{MNN^*}$ is also multiplied by the form factor given by eq. 15, with m_N replaced by m_{N^*}.

Γ_{MNB}: The vertex Γ_{MNN} is taken consistently with that used in the construction of the NN interaction. For Γ_{MNN} involving the off-shell nucleon that produces the meson, it is also multiplied by the form factor $F_N(\mathrm{p}^2)$ given by eq. 15. The vertex Γ_{MNN^*} is the same as $\bar{\Gamma}_{MNN^*}$, except that it contains an extra form factor due to the off-shell meson which is taken to be the same as that of the corresponding vertex Γ_{MNN}.

Γ_{MMM}: The coupling constants in the three-meson vertices (Γ_{MMM}) are extracted from both the strong and radiative (measured) decay widths [25] in combination with SU(3) symmetry, plus the OZI rule [28].

The latter relates the basic SU(3) octet and singlet coupling constants. Γ_{MMM} includes the form factor

$$F_M(\mathrm{q}^2, \mathrm{q}'^2) = \left(\frac{\Lambda_M^2 - \mathrm{m}_M^2}{\Lambda_M^2 - \mathrm{q}^2}\right)\left(\frac{\Lambda_{M'}^2 - x\mathrm{m}_{M'}^2}{\Lambda_{M'}^2 - \mathrm{q}'^2}\right), \tag{16}$$

with $\Lambda_M = \Lambda_{M'} = 1.45\,\mathrm{GeV}$. q and q′ denote the four momenta of the two mesons with masses m_M and $\mathrm{m}_{M'}$, respectively, that fuse to produce the third meson. The parameter $x(= 0, 1)$ ensures the proper normalization according to the normalization point $\mathrm{q}'^2 = 0, \mathrm{m}_{M'}^2$ at which the corresponding coupling constant is extracted.

There is a number of features in the model described above which are perhaps worth mentioning here. This model is suited for a systematic analysis of the production of different mesons within the same model due to the simplicity of modeling the production current. Also, the model is especially suited for studying the role of different reaction mechanisms that produce a meson. The consistency between the NN interaction and the production current can be easily maintained when one knows the underlying meson exchange structure of the NN interaction used (note that the way the parameters of our model are fixed ensures the consistency between the NN interaction and the production current). As mentioned before, this is critical if one wishes to achieve quantitative predictions, especially for production of heavy mesons.

4 Some selected results

In this section we shall present some selected results on the vector and pseudoscalar meson productions based on the model described in the previous section. As an example of vector meson production, we consider ϕ meson production in pp collisions. For the pseudoscalar meson production, we discuss the results for η production in both the pp and pn collisions.

4.1 pp → ppϕ

The study of this reaction is of particular importance in connection with the questions related to the amount of hidden strangeness in the nucleon [29, 30]. In the context of ϕ meson production processes one expects [30] that a large amount of hidden strangeness in the nucleon would manifest itself in reaction cross sections that significantly exceed the values estimated from the

OZI rule [28]. This phenomenological rule states that reactions involving disconnected quark lines are forbidden. In the naive quark model the nucleon has no $\bar{s}s$ content, whereas the ϕ meson is an ideally mixed pure $\bar{s}s$ state. Thus, in this case, the OZI rule implies vanishing ϕNN coupling and, accordingly, a negligibly small production of ϕ mesons from nucleons by non-strange hadronic probes. In practice there is a slight deviation from ideal mixing of the vector mesons, which means that the ϕ meson has a small $\bar{u}u + \bar{d}d$ component. Thus, even if the OZI rule is strictly enforced, there is a non-zero coupling of the ϕ to the nucleon, although the coupling is very small. Its value can be used to calculate lower limits for corresponding cross sections. For example, under kinematic conditions chosen to cancel out phase space effects, one expects cross section ratios of reactions involving the production of a ϕ and an ω meson, respectively, to be

$$R = \frac{\sigma(A + B \to \phi X)}{\sigma(A + B \to \omega X)} \approx \tan^2(\alpha_V)\,, \tag{17}$$

where A, B and X are systems that do not contain strange quarks. $\alpha_V \equiv \theta_V - \theta_{V(ideal)}$ is the deviation from the ideal $\omega - \phi$ mixing angle. This result arises from simply equating the cross section ratio to the square of the ratio of the relevant coupling constants at the ϕ and ω production vertices. According to the OZI rule plus SU(3) symmetry, these couplings are proportional to $\sin(\alpha_V)$ and $\cos(\alpha_V)$, respectively. With the value $\alpha_V \cong 3.7°$ [25] one gets a rather small ratio of $R = 4.2 \times 10^{-3}$. The data presented by the DISTO collaboration [31, 32] in pp collisions indicate that this ratio, after correcting for phase space effects, is about eight times larger than the above OZI estimate.

In principle, the ϕ meson production cross section can be used for a direct determination of the ϕNN coupling strength. Any appreciable ϕNN coupling in excess of the value given by the OZI rule ($g_{\phi NN} \cong -(0.60 \pm 0.15)$) [7] could be interpreted as evidence for hidden strangeness in the nucleon. Of course, there is also an alternative picture: one in which the coupling of the ϕ meson to the nucleon does not occur via possible $\bar{s}s$ components in the nucleon, but via intermediate states with strangeness. Specifically, this means that the ϕ meson couples to the nucleon via virtual ΛK, ΣK, etc. states. Corresponding model calculations [33, 34] have shown, however, that such processes give rise to (effective) ϕNN coupling constants comparable to the OZI values and therefore should not play a role in drawing conclusions concerning hidden strangeness in the nucleon.

Details of our calculation may be found in ref. [7]. The work of ref. [7] is a combined analysis of the ω and ϕ meson production in pp collisions in order

to reduce the number of free parameters in the model. Here we only report on the essential results. For the production current J we consider only the nucleonic and mesonic currents. The latter consists of $v\rho\pi$ exchange current ($v = \omega, \phi$). Other mesonic currents have been investigated in a systematic way and found to be very small. The nucleon resonance current is not considered because, presently, there is no established resonance that decays into a vector meson and a nucleon (see ref. [35] in this connection). It is found that the ϕ meson is produced significantly from the $\phi\rho\pi$ exchange current in pp collisions. This means that one must be able to disentangle this current from the nucleonic current (where the ϕ meson is emitted directly from the nucleon) if one wishes to extract the ϕNN coupling strength from this reaction. As pointed out in ref. [5], this can be done by looking at the angular distribution of the emitted meson. Because the mesonic current contribution yields an isotropic angular distribution, whereas the nucleonic current contribution exhibits a $\cos^2(\theta)$ dependence, the two currents can be disentangled uniquely from the angular distribution data. Fig. 3 illustrates this point for the $pp \to pp\omega$ reaction at a proton beam energy of 2.2 GeV. The upper panel illustrates the situation when the nucleonic current (dashed curve) is smaller than the mesonic current (dash-dotted curve) resulting in a nearly flat angular distribution (solid curve). Note that the interference between the two currents is destructive, which is a direct consequence of the signs of the relevant coupling constants determined in our model as discussed in the previous section. The lower panel shows the situation when the nucleonic current is larger than the mesonic current. Here the angular distribution exhibits a pronounced angular dependence. In both scenarios the total cross sections have been kept to be about the same.

The earlier data of the ϕ meson angular distribution by the DISTO collaboration [31] at a proton beam energy of 2.85 GeV are shown in fig. 4 together with our result. The absolute normalization of these data has been determined as described in ref. [7]. Although the data have large uncertainties, the observed angular distribution is rather flat. Note that the angular distribution should be symmetric about $\theta = 90°$, due to the identity of the two protons. The solid curve is one of our calculations fitted to the data. The dash-dotted and dashed curves are the corresponding mesonic and nucleonic current contributions, respectively. As one can see, the data require a very small contribution from the nucleonic current. The value of the ϕNN coupling constant thus extracted is in the range $g_{\phi NN} \approx -(0.2-0.9)$. More data for both the ϕ and ω meson at low excess energies are necessary in order to determine better the parameters of the model, and thus reduce the uncertainties in the extracted value of $g_{\phi NN}$. In this connection,

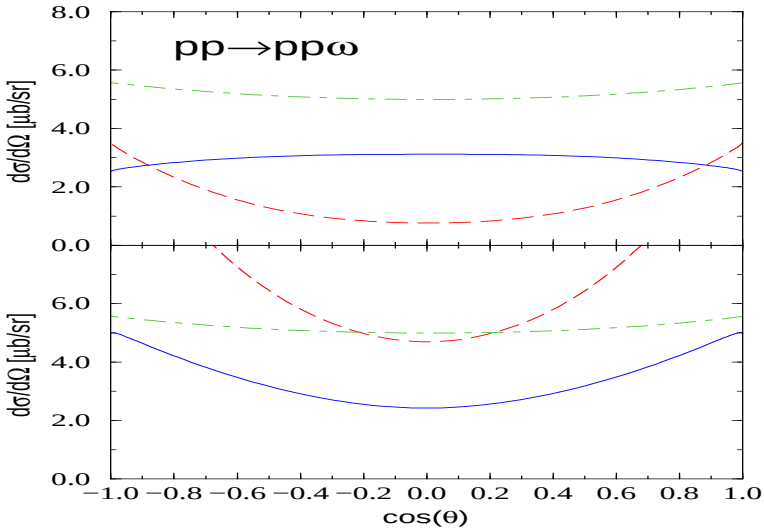

Figure 3: Angular distribution of the emitted ω meson in the CM frame of the total system for two possible scenarios at a proton incident energy of 2.2 GeV. The upper panel corresponds to the case when the nucleonic current is smaller than the mesonic current. The lower panel corresponds to the case when the nucleonic current is larger than the mesonic current. The dashed curves represent the nucleonic current contribution while the dash-dotted curves represent the mesonic current contribution. The solid curves correspond to the total contribution.

current experimental efforts at COSY (see contributions by M. Wolke, G. Schepers/D. Grzonka and A. Khoukaz at this meeting) are of particular interest. In any case, the value extracted here is compatible with the OZI value of $g_{\phi NN} \cong -(0.60 \pm 0.15)$. More recent data with an improved data analysis from the DISTO collaboration [32] exhibit a nearly isotropic angular distribution, corroborating a very small nucleonic current contribution.

Fig. 5 shows the predicted ratio $R_{\phi/\omega} = \sigma_{pp\to pp\phi}/\sigma_{pp\to pp\omega}$ of the total cross section as a function of excess energy. For low excess energies, the predicted ratio is about 4 to 7 times that of the OZI estimate. At higher energies, the enhancement over the OZI estimate decreases to a factor of 3 or so. What then is the origin of this enhancement over the OZI estimate as predicted by our model? One source of the enhancement is in the mesonic current. As discussed in detail in ref. [7], the violation of the OZI rule at the $\phi\rho\pi$ vertex had to be introduced in order to achieve a simultaneous and consistent description of the then available data on the reactions $pp \to pp\omega$

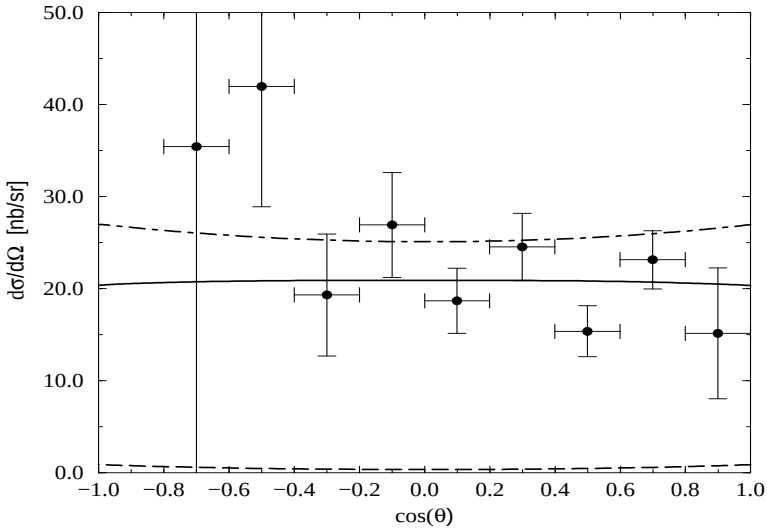

Figure 4: Angular distribution of the emitted ϕ meson in the CM frame of the total system at a proton incident energy of 2.85 GeV. The dashed curve corresponds to the nucleonic current contribution while the dash-dotted curve to the mesonic current contribution. The solid curve corresponds to the total contribution. The data are from ref. [31]. The absolute normalization of the data has been determined as described in ref. [7].

and $pp \to pp\phi$. This explicit OZI violation in terms of the $\phi\rho\pi$ and $\omega\rho\pi$ coupling constants used suggests an enhancement of around 3 in the cross section ratio. With regard to the nucleonic current, the employed ωNN and ϕNN coupling constants lead to results that exceed the OZI value only in one case: namely for the parameter set with $g_{\phi NN} = -0.9$ [7]. The corresponding enhancement factor for the cross section ratio amounts to about 2. It is then evident from the above consideration that the cross section ratios resulting from the model calculation differ significantly from those values implied by the employed coupling constants. Obviously, dynamical effects such as interferences, etc., play a rather important role here and can lead to fairly large deviations from the OZI prediction within a conventional picture, i.e., without introducing any "exotic" mechanisms. Consequently, one should be very cautious in drawing direct conclusions regarding the strangeness content in the nucleon from such cross section ratios. The behavior of the cross section ratio as the excess energy approaches zero is due to the finite width of the ω, which prevents the ω meson production cross

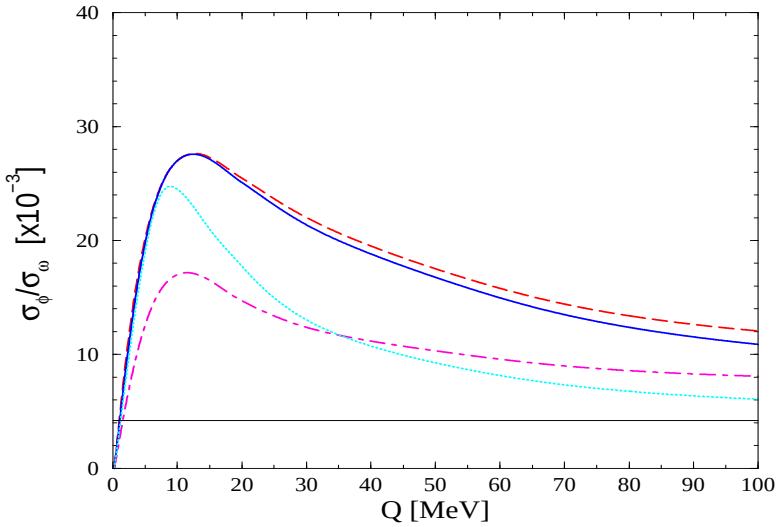

Figure 5: Total cross section ratio $R_{\phi/\omega} = \sigma_{pp\to pp\phi}/\sigma_{pp\to pp\omega}$ as a function of excess energy. Different curves correspond to the possible sets of parameters as determined in ref. [7]. The horizontal line corresponds to the OZI prediction.

section from decreasing rapidly, as it does in the case of ϕ meson.

Evidently, the enhancement of a factor of 3 or so over the OZI estimate at higher excess energies in fig. 5 is much smaller than the enhancement over the OZI prediction of about a factor 10 found by the DISTO collaboration [31] at an excess energy Q $\approx$ 80 MeV in ϕ meson production. However, it is important to realize that their measurement was done at a fixed incident beam energy of 2.85 GeV, and therefore the corresponding excess energy of the produced ω is already 319 MeV. Though corrections for the differences in the available phase space were obviously applied when extracting the above result, there are other effects that may influence the ratio, such as the energy dependence of the production amplitude, the onset of higher partial waves, etc., that cannot be corrected for easily. It is therefore possible that the actual deviation in the value of $R_{\phi/\omega}$ from the OZI prediction is also smaller. Thus, it would be interesting to perform a measurement of the cross section ratio at the same (or at least similar) excess energies. From the theoretical side, the newer data on ϕ production by the DISTO collaboration [32] and, especially, the new data on ω production from COSY [36] (see also the contribution by A. Khoukaz at this meeting), should already impose much more stringent constraints on the parameters of our model and help address

better the problem of OZI violation and related issues in NN collisions. In fact, these new data seem to indicate that we overpredict the ω meson production cross section above Q $\sim$ 30 MeV. This has a direct implication on the cross section ratio $R_{\phi/\omega}$ at higher excess energies as discussed above.

4.2 NN $\rightarrow$ NNη

We now turn to the production of pseudoscalar mesons. Here we confine our discussion to the production of η meson in NN collisions. The production of this meson near the threshold energy is of special interest, since the existing data are by far the most accurate and complete among those for heavy meson production and, consequently, they offer a possibility to investigate this reaction in much more detail than any of the other heavy meson production reactions. In addition to the total cross sections for the $pp \rightarrow pp\eta$ reaction [37, 38, 39, 40, 41], we have data for $pn \rightarrow pn\eta$ [42] and $pn \rightarrow d\eta$ [41, 43]. The differential cross section data for the $pp \rightarrow pp\eta$ reaction [44] are available as well. Consequently, there is a large number of theoretical investigations on these reactions. The production of η mesons in NN collisions is thought to occur predominantly through the excitation (and de-excitation) of the $S_{11}(1535)$ resonance, to which the η meson couples strongly. However, the excitation mechanism of this resonance is currently an open issue. For example, Batinić et al. [4] (see also the contribution by S. Ceci to this meeting) have found both the π and η exchange as the dominant excitation mechanism. However, they have considered only the $pp \rightarrow pp\eta$ reaction. Gedalin et al. [6] and Fäldt and Wilkin [9] have considered both the $pp \rightarrow pp\eta$ and $pn \rightarrow pn\eta$ reactions. In the analysis of ref. [9] the $pn \rightarrow d\eta$ reaction was also included. These authors [6, 9] find the ρ exchange to be the dominant excitation mechanism of the $S_{11}(1535)$ resonance. In particular, it has been claimed [9] that ρ meson exchange is important for explaining the observed shape of the angular distribution in the $pp \rightarrow pp\eta$ reaction. We mention that, in contrast to the dominant resonance current contribution found in refs. [4, 6, 9], in a recent calculation of the $pp \rightarrow pp\eta$ reaction by Peña et al. [8] it is found that the dominant contribution arises not from the $S_{11}(1535)$ resonance current, but from what they refer to as the short range amplitude. In our language this corresponds to the shorter range part of the nucleonic current. Here we shall report on yet another possible scenario that reproduces both the $pp \rightarrow pp\eta$ and $pn \rightarrow pn\eta$ reactions and discuss a possibility to disentangle these reaction mechanisms.

Although here we shall confine ourselves to the problem just mentioned, the description of η meson production in NN collisions presents other inter-

esting aspects. For example, the η meson interacts much more strongly with the nucleon than do mesons like the pion so that not only the NN FSI, but also the ηN FSI is likely to play an important role, thereby offering an excellent opportunity to learn about the ηN interaction at low energies. In fact, the near-threshold energy dependence of the observed total cross section for η meson production differs from that of pion and η' production, which follow the energy dependence given simply by the available phase-space together with the NN FSI. The enhancement of the measured cross section at small excess energies in η production compared to those in π and η' production is generally attributed to the strong attractive ηN FSI. In addition to all these issues, the theoretical understanding of η meson production in NN collisions near threshold in free space is also required for investigating the dynamics of the $S_{11}(1535)$ resonance in the nuclear medium, possible existence of ηNN bound states, and the possibility of using η to reveal the properties of high-density nuclear matter created in relativistic heavy-ion collisions.

Our model for the η production current includes the nucleonic, mesonic and resonance currents. The mesonic current consists of the $\eta\rho\rho$, $\eta\omega\omega$, and $\eta a_0\pi$ exchange contributions. The resonance current consists of the $S_{11}(1535)$, $P_{11}(1440)$, and $D_{13}(1520)$ resonances excited via π, η, ρ and ω exchange. For the NN FSI, we use the Bonn interaction [17]. For the NN ISI, we consider only the on-shell interaction obtained from ref. [21]. The details of the calculation will be reported elsewhere [45]. The results for the total cross section as a function of excess energy are shown in fig. 6. The upper panel shows the results for pp collisions while the lower panel those for pn collisions. The dashed curves are the nucleonic current contribution; the dash-dotted curves correspond to the mesonic current and the dotted curves to the resonance current. The solid curves are the total contribution. As one can see, the total cross sections are dominated by the resonance current, and more specifically by the strong $S_{11}(1535)$ resonance (see fig. 7). Our nucleonic current contributions (dashed curves) are much smaller than the resonance current contributions. This is in contradiction to the findings of ref. [8]; there, instead of the resonance current, the short range amplitude (shorter range part of the nucleonic current) gives a large contribution to the $pp \to pp\eta$ cross section. For small excess energies, our calculation underpredicts the data. As mentioned above, this is usually attributed to the ηN FSI, which is not accounted for in the present model. Note that the results for $pn \to pn\eta$ with excess energy $Q > 50\,\mathrm{MeV}$, corresponding to incident beam energy larger than $1.3\,\mathrm{GeV}$, should be interpreted with caution, as no reliable NN phase shift analyses for $T = 0$ states exist at present for

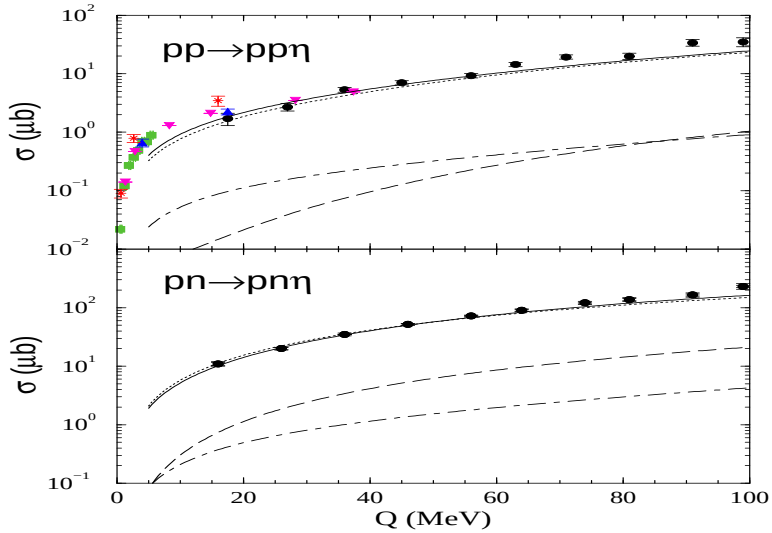

Figure 6: Total cross sections for the $pp \to pp\eta$ (upper panel) and $pn \to pn\eta$ (lower panel) reactions as a function of excess energy. The dashed curves correspond to the nucleonic current contribution while the dash-dotted curves to the mesonic current contribution; the dotted curves represent the resonance current contribution. The solid curves are the total contribution. The data are from refs. [37, 38, 39, 40, 41, 42].

energies above 1.3 GeV [22].

In fig. 7 the $S_{11}(1535)$ resonance contribution to the total cross sections is shown (solid curves), together with the contributions from the individual meson exchange excitation mechanisms. The dashed curves correspond to the π exchange, while the dash-dotted curves correspond to the η exchange contribution. The dotted curve is due to ρ exchange. Although the ω exchange is included in the calculation, its contribution is not shown here separately because it is much smaller than the ρ exchange contribution. As can be seen, the dominant contribution is due to the π exchange followed by η exchange. The ρ exchange is very small. Several observations are in order here:

1) The major reason for the small ρ exchange contribution, in contrast to the result of refs. [6, 9], is that in our model we have not allowed the vector (γ^μ) coupling in the ρNN^* vertex for spin-1/2 resonances. Note that for an odd-parity spin-1/2 resonance, there is an overall extra γ^5 factor. Unlike the case of the ρNN vertex, the presence of this coupling in the ρNN^* vertex leads to a violation of gauge invariance,

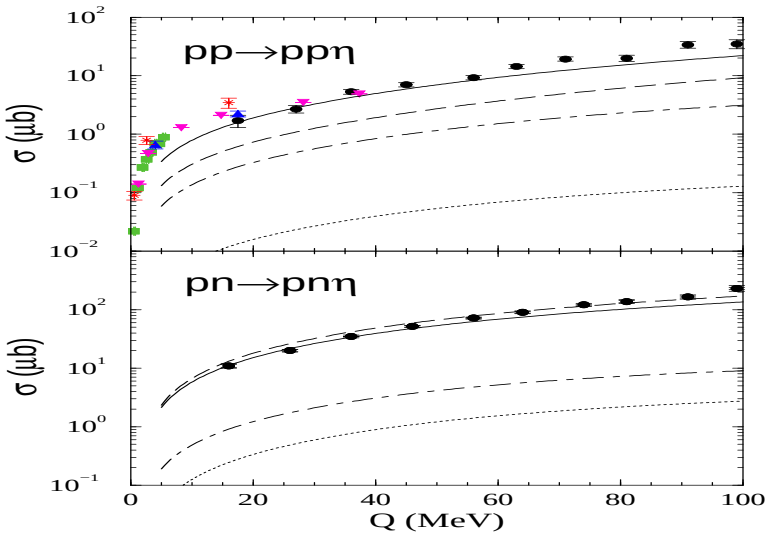

Figure 7: Same as fig. 6, except that it shows the $S_{11}(1535)$ resonance contribution only. The dashed curves correspond to the π exchange contribution while the dash-dotted curves to the η exchange contribution; the dotted curves represent the ρ exchange contribution. The solid curves show the total contribution.

which is especially relevant when used in connection with the VMD. As mentioned in the previous section, the ρNN^* coupling constant in our model is extracted from the radiative decay, $N^* \to \gamma + N$, using the VMD. The simplest way of satisfying the gauge invariance constraint is to omit the γ^μ coupling from the ρNN^* vertex, which we have done in the present work. Note that the tensor ($\sigma^{\mu\nu}$) coupling is free of this problem. A direct consequence of omitting the vector coupling in the ρNN^* vertex is a very small ρ exchange contribution to the cross section as shown in fig. 7. Note that in ref. [6] the $\rho NS(1535)$ vertex is given by the $\gamma^5\gamma^\mu$ coupling. An alternative to avoid the gauge invariance problem while keeping the γ^μ term is to use a vertex of the form $\Gamma^\pm[\gamma^\mu \mathrm{q}^2 - (\mathrm{m}_{N^*} \mp \mathrm{m}_N)\mathrm{q}^\mu]$ [46], where $\Gamma^- \equiv \gamma^5$ and $\Gamma^+ \equiv 1$. In fact, Peña et al. [8] have used a modified version of this vertex in conjunction with the coupling constant determined from a quark model [46]. They found a non-negligible contribution of the ρ exchange to the excitation of $S_{11}(1535)$ in $pp \to pp\eta$. Relevant experimental information should decide whether the vector coupling is required or not in the ρNN^* vertex.

2) The η exchange contribution is relatively large in the present calculation. In fact, in the case of $pp \to pp\eta$ its contribution to the cross section is about half of that due to the π exchange. The ηNN coupling strength is subject to a rather large uncertainty; the value of this coupling constant ranges from $g_{NN\eta} \sim 2.7$ to $g_{NN\eta} \sim 6.4$ [26]. The relatively large contribution of η here results from using the ηNN coupling constant of $g_{\eta NN} = 6.14$, as used in the construction of the Bonn NN interaction [17]. This value is close to the upper limit. However, the η meson exchange in the Bonn potential [17] might just be an exchange of a $(J^P, T) = (0^-, 0)$ quantum number and not of a genuine η meson. Consequently, the contribution from η exchange is subject to this uncertainty in the coupling constant. Anyway, in the present calculation for $pp \to pp\eta$, the η exchange interferes constructively with the dominant π exchange contribution, yielding the total contribution as shown by the solid line in fig. 7. For $pn \to pn\eta$, the η exchange interferes constructively with the π exchange in the $T = 1$ channel (as in the case of $pp \to pp\eta$), but destructively in the $T = 0$ channel due to the isospin factor -3 in the π exchange amplitude.

3) The correct description of both $pp \to pp\eta$ and $pn \to pn\eta$ reactions depends not only on different isospin factors involved for isoscalar and isovector mesons exchanged but, also on a delicate interplay between the NN FSI and ISI in each partial wave involved. While the NN FSI enhances the total cross section, the NN ISI has an opposite effect (see discussion in section 2). In this connection, we mention that in ref. [9] the reduction factor due to the NN ISI is estimated to be about $(0.77)^2 = 0.59$ due to the $^3P_0$ state and $(0.73)^2 = 0.53$ due to $^1P_1$. In our calculation, however, the corresponding reduction factors are about 0.19 and 0.27 near the threshold energy. This large discrepancy between the results of ref. [9] and ours is due to the fact that, whereas our reduction factor is given by eq. 11, the reduction factor in ref. [9] is given by $\lambda \equiv \eta_L^2 = (e^{-Im(\delta_L)})^2$. We argue that the latter formula is inappropriate to estimate the effect of the NN ISI for it does exhibit a pathological feature: namely, when the absorption is maximum ($\eta_L = 0$), this formula yields $\lambda = 0$, implying the total absence of the NN elastic channel and thus not allowing the production reaction to occur. However, scattering theory tells us that when the absorption cross section is maximum, the corresponding elastic cross section does not vanish, but is 1/4 of the absorption cross section. Note that this feature is present in eq. 11. Furthermore, the authors of ref. [9] apparently

have identified incorrectly the inelasticity η_L with $\cos^2(\rho)$, where ρ is one of the two parameters (the other is the phase shift) given in ref. [21]. The phase shift parametrization given in ref. [21] differs from the standard Stapp parametrization as given by eq. 8. It is obvious that with a more appropriate estimate of the reduction factor λ as given by eq. 11 the result of ref. [9] would underpredict considerably the cross section data.

Fig. 8 shows the predicted angular distribution of η in $pp \to pp\eta$ at an excess energy of Q = 37 MeV together with the data of ref. [44]. Again,

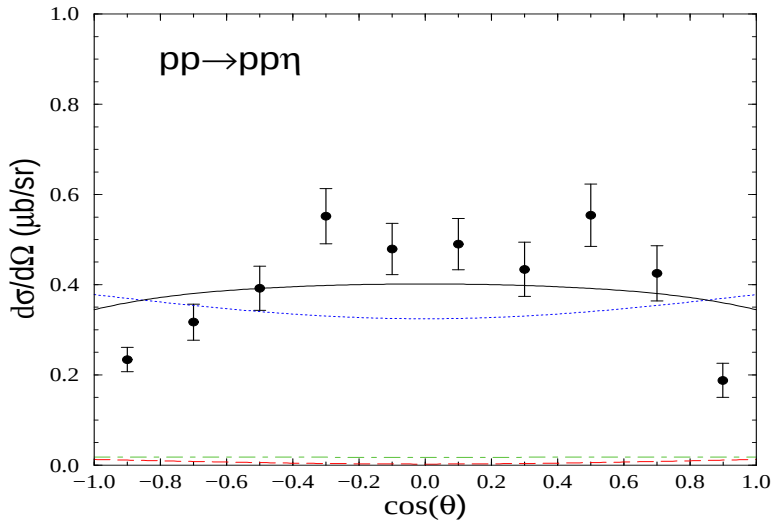

Figure 8: Angular distribution of the emitted η meson in the CM frame of the total system at an excess energy of Q = 37 MeV. The dashed curve corresponds to the nucleonic current contribution while the dash-dotted curve to the mesonic current contribution; the dotted curves represent the resonance current contribution. The solid curve shows the total contribution. The data are from ref. [44].

the resonance contribution (dotted curve) dominates the cross section. As pointed out in ref. [9], the shape of the angular distribution of the latter contribution bends upwards at the forward and backward angles due to the π exchange dominance in the $S_{11}(1535)$ resonance contribution. However, due to an interference with the nucleonic (dashed) and mesonic (dash-dotted) currents, the shape of the resulting angular distribution (solid curve) is inverted with respect to that of the resonance current contribution alone. As one can see, although the overall magnitude is rather well reproduced, the

rather strong angular dependence exhibited by the data is not reproduced by our model. At this point one might argue that the excitation mechanism of the $S_{11}(1535)$ resonance as given by the present model is not correct and that, indeed, the ρ meson exchange should give the dominant contribution, as has been claimed in ref. [9]. However, judging the level of agreements between the predictions of ref. [9] and ours with the data, one cannot discard the dominance of π and η exchange in favor of the ρ exchange mechanism for exciting the $S_{11}(1535)$ resonance. In this connection, we mention that the new data from COSY which will become available soon show a flat angular distribution [47].

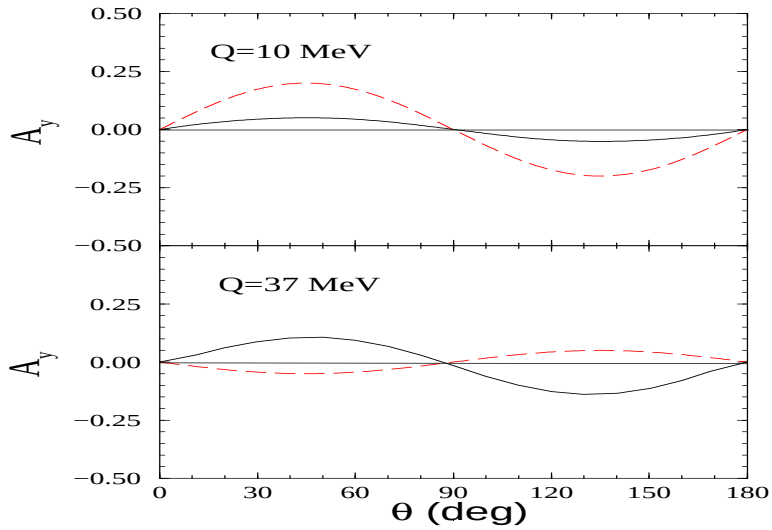

Figure 9: Analyzing power for the reaction $pp \to pp\eta$ as a function of emission-angle of η in the CM frame of the total system at an excess energy of Q = 10 MeV (upper panel) and Q = 37 MeV (lower panel). The dashed curve corresponds to the case of ρ exchange dominance according to ref. [9]. The solid curve corresponds to the present model calculation.

From the above considerations, we conclude that, at present, the excitation mechanism of the $S_{11}(1535)$ resonance in NN collisions is still an open question. Indeed, we have just offered a scenario other than the ρ exchange mechanism that reproduces the available data equally well. It is therefore of special interest to seek a way to disentangle these possible scenarios. In this connection, spin observables may potentially help to resolve this issue. According to ref. [9], the ρ exchange contribution is expected to lead to an

analyzing power given by

$$A_y = A_y^{max} \sin(2\theta) \tag{18}$$

in $pp \to pp\eta$, where A_y^{max} is positive for low excess energies, peaking at $Q \approx 10\,\mathrm{MeV}$ and becoming negative for excess energies $Q > 35\,\mathrm{MeV}$. The results (dashed curves) at $Q = 10\,\mathrm{MeV}$ (upper panel) and $Q = 37\,\mathrm{MeV}$ (lower panel) are shown in fig. 9. The corresponding predictions of the present model are also shown (solid curves). The different features exhibited by the two scenarios for the excitation mechanism of the $S_{11}(1535)$ is evident. In this connection, the COSY-11 effort to measure the analyzing power in $\vec{p}p \to pp\eta$ (see the contribution by P. Winter in this meeting) is of great importance. We emphasize that these different results should be interpreted with caution. The reason for this is that, as mentioned before, the present model accounts for the NN ISI only in the on-shell approximation. While this may be a reasonable approximation for calculating cross sections, it may introduce rather large uncertainties in the calculated spin observables.

5 Summary

The production of heavy mesons in NN collisions has been discussed within the meson exchange model of hadronic interactions, paying special attention to the basic dynamics that determine the behavior of the cross sections near the threshold energy. Differences in the existing meson exchange models as well as their limitations have been also discussed. Heavy meson production processes necessarily probe the short range dynamics, a domain where we have very limited knowledge so far. In this regime even the relevant reaction mechanisms are largely unknown. The theory of heavy meson production in NN collisions is still in its early stage of development. Successful description of these processes in terms of purely hadronic degrees of freedom calls for correlation of as many independent data as possible in a consistent way. The $pp \to pp\phi$ reaction has been discussed as an example of the production of vector mesons in NN collisions. As for the pseudoscalar meson production, results for the η production in both the pp and pn collisions were presented. From these examples, it is clear that not only the $pp \to ppM$, but also the $pn \to pnM$ and $pn \to dM$ reactions should be investigated. Also more exclusive observables than the total cross section such as the spin observables should be studied.

Acknowledgement. I would like to take this opportunity to thank the organizers of this symposium for inviting me to present this lecture. I also thank H. Arellano, J. Durso, J. Haidenbauer, C. Hanhart, H. Lee, J. Speth, and A. Szczurek who have collaborated in our study of heavy meson production reactions at one stage or another. I thank J. Durso, J. Haidenbauer and C. Hanhart for a careful reading of this manuscript.

References

[1] C. Hanhart, U. van Kolck, G.A. Miller, Phys. Rev. Lett. **85** (2000) 2905 and references therein.

[2] M.P. Rekalo, J. Arvieux, E. Tomasi-Gustafsson, Phys. Rev. **C 55** (1997) 2630; A.B. Santra, B.K. Jain, Nucl. Phys. **A 634** (1998) 309; E. Gedalin, A. Moalem, L. Razdolskaja, Nucl. Phys. **A 650** (1999) 471; K. Nakayama, J. Haidenbauer, J. Speth, Phys. Rev. **C 63** (2000) 015201; A.I. Titov, B. Kämpfer, B.L. Reznik, Eur. Phys. J. **A 7** (2000) 543; V.Yu. Grishina et al., Phys. Lett. **B 475** (2000) 9.

[3] A. Sibirtsev, W. Cassing, Eur. Phys. J. **A 2** (1998) 333.

[4] M. Batinić, A. Svarc, T.-S.H. Lee, Phys. Scripta **56** (1997) 321.

[5] K. Nakayama et al., Phys. Rev. **C 57** (1998) 1580.

[6] E. Gedalin, A. Moalem, L. Razdolskaja, Nucl. Phys. **A 634** (1998) 368.

[7] K. Nakayama et al., Phys. Rev. **C 60** (1999) 055209.

[8] M.T. Peña, H. Garcilazo, D.O. Riska, Nucl. Phys. **A 683** (2001) 322.

[9] G. Fäldt, C. Wilkin, Phys. Scripta **64** (2001) 427.

[10] V. Baru et al., in preparation.

[11] V. Bernard, N. Kaiser, U.-G. Meißner, Eur. Phys. J. **A 4** (1999) 259; N. Kaiser, Phys. Rev. **C 60** (1999) 057001.

[12] S. Ahlig et al., Phys. Rev. **D 64** (2001) 014004.

[13] S. Wycech, A.M. Green, NuclPhys. **A 663** (2000) 529; A. Fix, H. Arenhövel, e–Print Archive nucl–th/0104032 and references therein.

[14] F.E. Low, Phys. Rev. **110** (1958) 974.

[15] K. Watson, Phys. Rev. **88** (1952) 1163. For a recent discussion, see ref. [20].

[16] A. Moalem, L. Razdolskaja, E. Gedalin, e–Print Archive hep–ph/ 9505264.

[17] R. Machleidt, Adv. Nucl. Phys. **19** (1989) 189.

[18] M. Lacombe, B. Loiseau, J.M. Richard, R. Vinh Mau, J. Côté, P. Pirès, R. de Tourreil, Phys. Rev. **C 21** (1980) 861.

[19] T. Rijken, V.G.J. Stoks, Phys. Rev. **C 59** (1999) 21.

[20] C. Hanhart, K. Nakayama, Phys. Lett. **B 454** (1999) 176.

[21] Virginia Tech Partial-Wave Analysis Facility (SAID), http://gwdac.phys.gwu.edu/.

[22] I. Strakovsky, private communication.

[23] B.C. Pearce, I.R. Afnan, Phys. Rev. **C 34** (1986) 991.

[24] K. Nakayama et al., Phys. Rev. **C 61** (1999) 024001.

[25] C. Caso et al., *The Review of Particle Physics*, Eur. Phys. J. **C 3** (1998) 1.

[26] M. Benmerrouche, N.C. Mukhopadhyay, Phys. Rev. **D 51** (1995) 3237.

[27] J.F. Zhang, N. Mukhopadhyay, M. Benmerrouche, Phys. Rev. **C 52** (1995) 1134; H. Garcilazo, E. Moya de Guerra, Nucl. Phys. **A 562** (1993) 521; A.Yu. Korchin, O. Scholten, R.G.E. Timmermans, Phys. Lett. **B 438** (1998) 1.

[28] S. Okubo, Phys. Lett. **5** (1963) 165; G. Zweig, Report CERN–TH–412 (1964); J. Iizuka, Prog. Theor. Phys. Suppl. **37–38** (1966) 21.

[29] J.F. Donoghue, C.R. Nappi, Phys. Lett. **B 168** (1986) 105; J. Gasser, H. Leutwyler, M.E. Sainio, Phys. Lett. **B 253** (1991) 252; J. Ashman et al., Phys. Lett. **B 206** (1988) 364.

[30] J. Ellis, E. Gabathuler, M. Karliner, Phys. Lett. **B217** (1989) 173; E.M. Henley, G. Krein, A.G. Williams, Phys. Lett. **B 281** (1992) 178.

[31] F. Balestra et al., Phys. Rev. Lett. **81** (1998) 4572.

[32] F. Balestra et al., Phys. Rev. **C 63** (2001) 024004.

[33] P. Geiger, N. Isgur, Phys. Rev. **D 55** (1997) 299.

[34] U.-G. Meißner, V. Mull, J. Speth, J.W. Van Orden, Phys. Lett. **B 408** (1997) 381.

[35] S. Capstick, W. Roberts, Phys. Rev. **D 49** (1994) 4570; Q. Zhao, Z. Li, C. Bennhold, Phys. Lett. **B 436** (1998) 42, Phys. Rev. **C 58** (1998) 2393; Y. Oh, A. Titov, T.-S.H. Lee, Workshop On the Physics Of Excited Nucleons (NSTAR 2001), 7-10 Mar 2001, Mainz, Germany, e–Print Archive nucl–th/0104046.

[36] K. Brinkmann, private communication; S. Abd El–Samad et al., Phys. Lett. **B 522** (2001) 16.

[37] E. Chiavassa et al., Phys. Lett. **B 322** (1994) 270.

[38] F. Hibou et al., Phys. Lett. **B 438** (1998) 41.

[39] H. Calén et al., Phys. Lett. **B 366** (1996) 39.

[40] J. Smyrski et al., Phys. Lett. **B 474** (2000) 182.

[41] H. Calén et al., Phys. Rev. Lett. **79** (1997) 2642.

[42] H. Calén et al., Phys. Rev. **C 58** (1998) 2667.

[43] H. Calén et al., Phys. Rev. Lett. **80** (1998) 2069.

[44] H. Calén et al., Phys. Lett. **B 458** (1999) 190.

[45] K. Nakayama, T.-S.H. Lee, J. Speth, in preparation.

[46] D.O. Riska, G.E. Brown, Nucl. Phys. **A 679** (2001) 577.

[47] K. Kilian, private communication.

Time Reversal Symmetry Violation
Search Examples[1]

Stanisław Kistryn

Institute of Physics, Jagellonian University, Kraków, Poland

Abstract: Areas of intensive research on effects which would signal breaking of the Time Reversal Symmetry (TRS) are discussed, with an emphasis put on presenting recent and complete review articles. Limitations on physics beyond the Standard Model, implied by the experimental results of such precise studies are briefly presented, with a focus on the electroweak interaction sector. Two examples of running experiments, aimed at determination of the magnitude or establishing upper limits of triple spin-momentum correlations forbidden by TRS are presented in some details.

Time Reversal Symmetry $\mathcal{T}$ is one of the discrete symmetries of the physical systems, which validity has to be checked experimentally [1]. Since the combined $\mathcal{CPT}$ symmetry holds in any gauge quantum field theory (as a consequence of locality and Lorentz invariance), there is a certain equivalence of expressing the properties of the system under $\mathcal{T}$ or $\mathcal{CP}$ transformation.

The Standard Model (SM) of electroweak and colour interactions takes into account the well known breaking of each, parity $\mathcal{P}$ and charge conjugation $\mathcal{C}$ symmetries. In fact, the whole vector–axial vector (V-A) structure of the SM of the electroweak interaction is based on the maximal parity violation in this sector. In contrast, the Time Reversal Violation (TRV) incorporated in the SM is small and grounded on essentially only one class of experimentally found effects, manifesting themselves by mixing of neutral kaons. It was indeed this experimental evidence of the $\mathcal{CP}$ nonconservation which lead to proposing the third quark family, necessary for incorporating TRV into the SM — here, instead of numerous references, I advertise the whole collection of papers [2], selected and commented by Wolfenstein. Another beautiful discussion of several experimental and theoretical aspects of $\mathcal{CP}$ violation has been edited by Jarlskog [3].

Except the above mentioned evidence from the micro-world, another indication that $\mathcal{T}$ is not conserved comes from the observation of the asymmetry of matter over antimatter in the Universe. The fact that the Universe

[1] Invited talk

is devoid of antimatter lead to suggesting some kind of $\mathcal{CP}$-violating effects over 40 years ago [4]. Nevertheless this aspect of baryogenesis still remains a puzzle - the TRV mechanism build into the SM is by far too small to account for the cosmological effects. That calls for extensions of the SM [5] and brings up a question if and where other evidences of TRV can be found.

Experimental searches for TRV effects can be considered as hunting for physics beyond the SM. They are usually directed at investigating the electroweak interaction, probing possible contents of exotic couplings [6, 7], i.e. admixtures of scalar, pseudoscalar, tensor terms or phase different from π in the known vector–axial vector structure. However, also the so-called strong $\mathcal{CP}$ problem (see e.g. [8]) is probed experimentally, providing insight into the structure of the QCD Lagrangian. In any case the experiments are very demanding and complicated, usually aimed at measuring zero effects, from which upper limits on the TRV effects and further on the SM extensions (see e.g. [2, Section 3] and [9] for some discussion of $\mathcal{CP}$ violation models) can be extracted.

The present-day searches for TRV effects can be divided into a few groups, depending on the investigated systems and on the chosen observables. Below a very brief listing of only most important experiments is given, the more detailed discussion and references to the original papers can be found in [6, 7, 10, 11]:

- Decays of neutral mesons
  $\longmapsto$ K^0, B^0 (in B_d effects are expected to be large, in B_s – even maximal),
- Correlations between nuclear spin polarization and γ-polarization
  $\longmapsto$ 2 γs from polarized nuclei, e.g. ^{180}Hf, ^{182}W, ^{192}Pt, ^{169}Tm,
  $\longmapsto$ γ-polarization from polarized nuclei, e.g. ^{57}Fe, ^{191}Ir, ^{131}Xe,
  $\longmapsto$ β-γ correlations, e.g. ^{56}Fe, ^{106}Pd, ^{36}Cl,
- Spin-momentum correlations in β-decay of nuclei and in decays of strange particles
  $\longmapsto$ $\mathcal{P}$-even, e.g. $\vec{n}$, $^{19}\vec{N}e$,K^+, K^0, $\vec{\Sigma}^0$,
  $\longmapsto$ $\mathcal{P}$-odd, e.g. ^{60}Co, $^{19}\vec{N}e$, $\vec{\Lambda}^0$, $\vec{\mu}^+$, $^{8}\vec{L}i$,
- Neutron, atomic and molecular electric dipole moments (EDM)
  $\longmapsto$ n, ^{199}Hg, ^{129}Xe, TlF,
- Symmetry of reaction yields (detailed balance)
  $\longmapsto$ transmission of $\vec{n}$ through polarized or aligned targets, e.g. ^{165}Ho, ^{139}La.

Let us consider shortly the EDM measurements, in particular the EDM of the neutron. The reason for distinguishing that particular observable

is its power for verification of various hypothesis of the SM extensions (as noted previously, this observable probes the strong $\mathcal{T}$-violating mechanism rather than the electroweak sector). A non-zero value of the EDM would signal unambiguously TRV and therefore a need to include in the SM a new physics. From the mid-fifties, when the first neutron EDM measurement has been performed, the experimental accuracy has improved by several orders of magnitude (see [12, 13, 14] and [2, 8] for extensive reviews of theories, descriptions of current experiments and prospects in the neutron EDM research). This achievement allowed to rule out over 20 different theories of the SM generalization. Nowadays the experiments on the neutron EDM, performed with ultra-cold neutrons stored in appropriate traps, reach the accuracy of $10^{-26}\,\mathrm{e}\cdot\mathrm{cm}$, what corresponds to testing the SM extensions based on multiple Higgs doublets, Supersymmetry or left-right symmetric models. The new generation of experiments is planned, in which the limit should be shifted by another two orders of magnitude down. It should be, however, noted that the predictions of the SM itself (of the order of $10^{-32}\,\mathrm{e}\cdot\mathrm{cm}$), are by far out of reach for the experimental verification.

In the electroweak sector of the SM the most precise experiments have been performed by means of exploring the β-decay of particles and nuclei. In systems without strangeness the investigations are usually concentrated on observables connected with triple vector products of momenta and spins of the parent and daughter particles. Below follows a short presentation of two such projects, carried out at the Paul Scherrer Institute in Switzerland, in which the author and the Polish group are strongly involved.

The simplest testing ground is obviously the pure leptonic system, where no strong interaction interference can take place. An example of such a process is the decay of polarized, positive muons: $\mu^+ \to e^+ + \nu_e + \overline{\nu}_\mu$. In the experiment one uses polarized muons and determines components of the emitted positron polarization, which are perpendicular to its (also measured) momentum vector. The component P_{T_1} lying in the plane spanned by the positron momentum and the muon polarization is allowed in the SM, while the component P_{T_2}, perpendicular to both the positron momentum vector and the muon spin direction, is forbidden by the TRS. By measuring both transverse polarization components as a function of the electron energy one is able to determine certain so-called muon decay parameters [6] and by allowing additional exotic (e.g. right-handed scalar) interaction - to set limits on its possible admixture to the standard V-A interaction. The current experiment is an upgrade of the former undertaking [15], which delivered results of P_{T_1} and P_{T_2} consistent with zero at the accuracy of few times 10^{-2}. By several improvements in the detection system [16] one aims at achieving

an accuracy of $3 \cdot 10^{-3}$. The analysis of the first data taking series confirmed that the aim is reachable and the final result should be published within one year. The experimental accuracy translates, within the framework of a general analysis, onto about an order of magnitude smaller error of the muon decay parameters η, η'', α'/A and β'/A, while if allowing only one exotic coupling, the right-handed scalar coupling g^S_{RR}, its magnitude will be limited to below 0.01. In a similar investigation [17], aimed at determination of the longitudinal positron polarization, another set of muon decay parameters will be inspected, allowing to set limits also on possible tensor interaction admixture.

Considering the semileptonic systems, only the free neutron decay is a field, where the strong interaction effects can be separated exactly [7] (the Fermi and Gamow-Teller transition matrix elements are known). In light nuclei the nuclear structure effects must be taken into account, what is no longer model independent. However, also in such systems valuable results have been achieved, for instance in our experiment with polarized ^8Li [18], from which the best currently available limit on the scalar coupling has been determined. Therefore we have started an experiment to measure the so-called R-correlation amplitude in the free, polarized neutron decay, $\vec{n} \rightarrow p + e^- + \overline{\nu}_e$. This, never before measured parameter, gives a strength of a triple product of the neutron spin $\vec{J}$, the electron momentum vector $\vec{p}$ and its polarization $\vec{\sigma}$, $\vec{J} \cdot (\vec{p} \times \vec{\sigma})$ or, in other words, describes the positron polarization perpendicular to both, its momentum vector and the parent neutron spin. The amplitude R must vanish if $\mathcal{T}$ symmetry holds. An experimental accuracy of below 0.01 will significantly improve limits on the scalar and tensor interaction contributions in the electroweak sector [19]. In the experiment the beam of cold neutrons, polarized in the specially equipped supermirror guide [20], is passing through a helium-filled decay chamber volume. The electrons emitted in neutron decays are observed by a specially designed detection system [21] and their polarization is analyzed by means of Mott scattering off a gold foil. Details of the experiment can be found elsewhere [19, 22], as well as very promising results of the first tests. The experiment will possibly open a way for a whole series of measurements on the free, highly polarized and very intense cold neutron beam.

The above considerations can be summarized as follows. The investigations of Time Reversal Violation probe our current understanding of the physics of both micro- and macro-world. They are a very promising route to discover physics beyond the Standard Model or to set very stringent limits on its possible manifestations. Their importance is widely recognized - the plans for large installations (e.g. LHC, ESS) include many projects de-

voted to TRV quests [23]. Experimentally they pose a challenge in reaching enormous sensitivities, requiring brilliant solutions of complicated technical problems.

References

[1] N.F. Ramsey, Phys. Rev. **109** (1958) 225.

[2] Collection of papers concerning CP violation edited by L. Wolfenstein, *CP Violation*, Current Physics - Sources and Comments, vol. **5**, North-Holland, Amsterdam (1989).

[3] Collection of papers on CP violation edited by C. Jarlskog, *CP Violation*, Adv. Ser. Direct. High Energ. Phys. **3**, World Scientific, Singapore (1989).

[4] A.D. Sakharov, JETP Lett. **5** (1967) 24.

[5] M. Trodden, Rev. Mod. Phys. **71** (1999) 1463.

[6] W. Fetscher, H.-J. Gerber in *Precision Tests of the Standard Electroweak Model*, ed. by P. Langacker, Adv. Ser. Direct. High Energ. Phys. **14**, World Scientific, Singapore (1995) 657.

[7] J. Deutsch, P. Quin in *Precision Tests of the Standard Electroweak Model*, ed. by P. Langacker, Adv. Ser. Direct. High Energ. Phys. **14**, World Scientific, Singapore (1995) 706.

[8] I.B. Khriplovich, S.K. Lamoreaux, *CP Violation Without Strangeness: Electric Dipole Moments of Particles, Atoms and Molecules*, Springer (1996).

[9] P. Herczeg in *Precision Tests of the Standard Electroweak Model*, ed. by P. Langacker, Adv. Ser. Direct. High Energ. Phys. **14**, World Scientific, Singapore (1995) 786.

[10] K. Boehm in *Symmetries and Fundamental Interactions in Nuclei*, ed. by W.C. Haxton, E.M. Henley, World Scientific, Singapore (1995) 67.

[11] P. Herczeg in *Symmetries and Fundamental Interactions in Nuclei*, ed. by W.C. Haxton, E.M. Henley, World Scientific, Singapore (1995) 89.

[12] N.F. Ramsey, Ann. Rev. Nucl. Part. Sci. **40** (1990) 1.

[13] J.M. Pendlebury, Ann. Rev. Nucl. Part. Sci. **43** (1993) 687.

[14] R. Golub, S.K. Lamoreaux, Phys. Rep. **237** (1994) 1.

[15] H. Burkard et al., Phys. Lett. **B 160** (1985) 343.

[16] I.C. Barnett et al., Nucl. Instr. & Meth. **A 455** (2000) 329.

[17] P. Knowles et al., Phys. Rev. Lett. **82** (1999) 57.

[18] J. Sromicki et al., Phys. Rev. **C 53** (1996) 932.

[19] J. Sromicki, Nucl. Instr. & Meth. **A 440** (2000) 609.

[20] K. Bodek et al., Neutron News **11** (2000) 29.

[21] K. Bodek et al., Nucl. Instr. & Meth. **A 461** (2001) 282.

[22] M. Beck et al., Proposal for an Experiment at PSI (2001).

[23] H. Abele et al. in *ESS–SAC/ENSA Workshop on Scientific Trends in Condensed Matter Research and Instrumentation Opportunities at ESS*, Engelberg, Switzerland, 3-5 May 2001, Proc. ed. by D. Richter, ESS/SAC/Report/1/01, Forschungszentrum Jülich (2001) 119.

Electron-Positron Pair Spectroscopy with HADES at GSI [1]

P. Salabura for the HADES collaboration

M. Smoluchowski Institute of Physics, Jagellonian University, Kraków, Poland

Abstract: The High Acceptance DiElectron Spectrometer HADES is presently set up at GSI, Darmstadt, for the systematic study of medium modifications of hadron properties. Short lived hadrons will be produced in nuclear matter from normal up to medium baryon densities utilizing pion, proton and heavy ion induced reactions. Electron pair spectroscopy will be used to measure resonance widths and effective masses of vector mesons as well as transition formfactors of neutral mesons and baryon resonances in the low mass region $\mathrm{M} \leq 1\,\mathrm{GeV/c^2}$. The spectrometer is designed for an invariant mass resolution $\Delta\mathrm{M}_{inv}/\mathrm{M}_{inv} \simeq 1\,\%\,(\sigma)$, a large signal to background ratio, and a large acceptance $\Omega_{pair} \simeq 40\,\%$.

1 Introduction

The investigation of the basic properties of hadrons embedded in a surrounding of strongly interacting matter has increasingly become of interest. Experimental verification of possible changes of these properties will shed additional light on our understanding of non perturbative quantum chromodynamics (QCD) and one of its fundamental symmetries: chiral symmetry valid in the limit of the massless quarks. In the QCD chiral models the constituent masses of quarks are dynamically generated by a coupling of almost massless bare quarks to the sea of $q\bar{q}$ pairs appearing, due to a non-trivial character of the QCD vacuum, with a large expectation value of $(-230 \pm 25)^3\,\mathrm{MeV}^3$ (see for example [1, 2].) This phenomenon leads to the spontaneous breakdown of the chiral symmetry and appearance of Goldstone bosons which can for 2 quark flavors be identified with pions. Hadron mass modifications are discussed in this context as a key observable for the chiral symmetry restoration when temperature and (or) density of nuclear matter is increased [3]. Various theoretical approaches (see [2, 4, 5] and references therein) predict that the hadron spectral functions are significantly

[1] Invited talk

modified inside medium even below transition to the quark-gluon plasma phase where chiral symmetry should be completely restored.

In this framework a special role of the light vector mesons ρ, ω and also ϕ and dilepton spectroscopy should be stressed. ρ and ω mesons are made of u- and d-quarks of very small bare mass and are relevant hadrons to discuss chiral symmetry restoration. The ϕ meson contains $s\bar{s}$ pair and can give interesting information about strangeness in nuclear matter. Due to the same quantum numbers they can convert into massive photons which in turn materialize into dilepton pairs with small but considerable branching ratios ($\sim 10^{-4}$). Their life times range from $\tau = 1.3\,\mathrm{fm/c}\,(\rho)$ and $\tau = 24\,\mathrm{fm/c}\,(\omega)$ to $\tau = 44\,\mathrm{fm/c}\,(\phi)$ and therefore are an ideal tool for in-medium dilepton spectroscopy. Dileptons are of special interest here, since as an electromagnetic radiation they escape the reaction volume without final state interactions and therefore provide direct information about decaying hadron properties.

In earthbound laboratories hot and dense nuclear matter can be provided in nuclear collisions, however with finite space-time volume only. For the low energy $1 - 2\,\mathrm{AGeV}$ heavy ion collisions accessible at GSI, baryon densities of $3 - 4$ times larger than in normal nuclear matter and temperatures in the order of 60 MeV can be achieved in a fireball with a mean life time of $\tau \sim 10\,\mathrm{fm/c}$ [6]. At higher beam energies available at SPS, RHIC and in near future at LHC, nuclear matter dominated by meson gas and low or vanishing baryon densities but at much higher temperatures is investigated. Therefore experiments at GSI provide an important piece of information complementary to that obtained at higher energies.

The new **H**igh **A**cceptance **D**i-**E**lectron **S**pectrometer HADES at GSI (Darmstadt, Germany) aims at precision measurements [7] of e^+e^- pair production in elementary and heavy ion induced reactions with unprecedented invariant mass resolution, event statistics, and signal to background discrimination.

2 Selected aspects of e^+e^- pair spectroscopy in the GSI energy regime

In central heavy ion collisions of $1 - 2\,\mathrm{AGeV}$ incident energy a hadronic fireball is formed, with a temperature and baryon density ranging up to $\mathrm{T} = 50 - 90\,\mathrm{MeV}$ and 3 times normal nuclear matter density, respectively. The formation of the reaction volume lasts for as long as $10\,\mathrm{fm/c}$ and expands with comparatively moderate changes in temperature and density [8].

The light and short lived vector mesons ρ and ω are produced in multi-step processes below the threshold for creation in direct nucleon-nucleon collisions and thus are strongly related to the high density region of the collision zone [9]. Their production depends crucially on the hadronic composition of the fireball, its time evolution, electromagnetic form factors and cross sections for production near the thresholds. In fact, many of these parameters are unknown and need to be studied in details. This issue is addressed in the HADES physics program by the dedicated studies of elementary dielectron sources in proton-proton and pion-proton reactions. In particular a role of baryonic resonances in the meson production and also in its later propagation through nuclear matter should be considered as it has been pointed out by several authors [2, 4, 10, 11]. For example a strong ρN coupling in the $D_{13}(1520)$ has been proposed [12] as an alternative mechanism to the Brown-Rho scenario of the dropping ρ mass [13] in the explanation of the spectacular dielectron excess in the invariant mass spectra measured in $S + Au$ and $Pb + Au$ collisions by the CERES collaboration at SPS [14]. A direct experimental test of the $N^*N\rho$ and also $N^*N\omega$ vertices could be performed in pion induced reactions as described below.

2.1 e^+e^- pairs from heavy ion reactions

Dielectron (e^+e^-) invariant mass spectra have already been measured for proton-proton, light and heavy ion reactions at the $1-2$ AGeV energy range by the DLS collaboration at the BEVELAC [15, 16]. Within the given experimental error bars the extracted e^+e^- production rates in proton-proton reactions could be well reproduced by the theoretical calculations including various hadronic sources: pn bremsstrahlung, π^0, η, ω, Δ Dalitz decays, and two-body vector meson decays [17]. For the heavier collision systems $Ca + Ca$ and $C + C$ a remarkable excess of the dielectron yield in the low mass range $200\,\mathrm{MeV/c^2} < \mathrm{M}_{inv} < 600\,\mathrm{MeV/c^2}$ as compared to the theoretical calculations using BUU transport [18] can be visible in fig. 1.

In the calculation in addition to a cocktail of free hadronic sources a medium modified ρ meson spectral function of [2] has been used. Nevertheless, an enhancement of about a factor 3 remains below the ρ/ω pole. Also calculations implementing explicitly a dropping of the ρ mass according to the Brown-Rho scaling fail to describe the experimental data [19]. In spite of this a new series of measurements with a better mass resolution and statistics are seriously needed to solve the "DLS puzzle".

The HADES spectrometer should provide such a data in the nearest future. The expected yield of e^+e^- pairs has been studied by detailed Monte

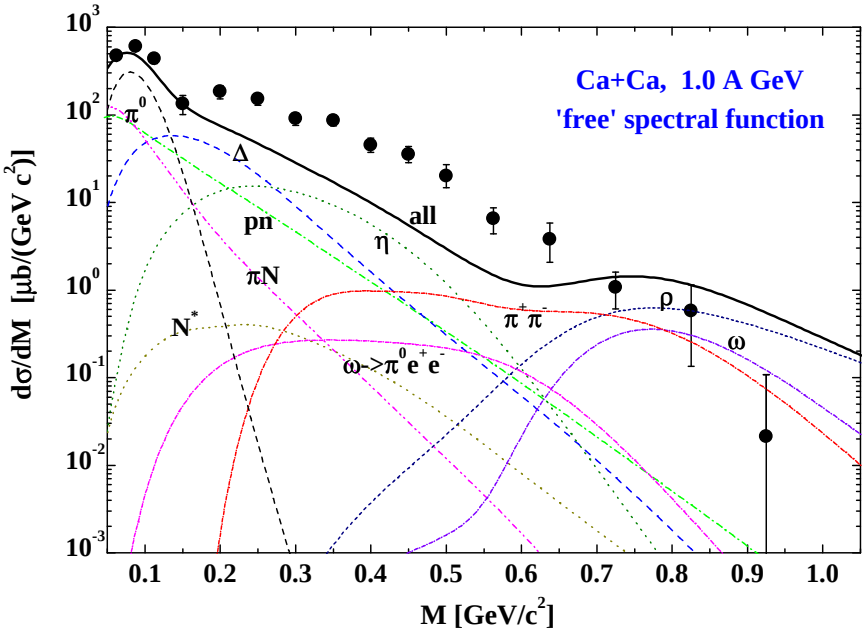

Figure 1: Differential cross sections (full circles) for dilepton production as a function of invariant mass measured by the DLS collaboration. The sum (full line) of contributing sources has been calculated with BUU-transport code using spectral functions in vacuum.

Carlo simulations (Fig. 3) for heavy collision systems ranging from a light $C+C$ to heaviest $Au+Au$ [20, 21]. We present here simulation results for the most difficult case of central $Au+Au$ collisions at 1 AGeV where almost 200 charged hadrons are detected in the HADES detector per one event. The low dielectron invariant mass range ($100\,\mathrm{MeV/c^2} < \mathrm{M}_{inv} < 600\,\mathrm{MeV/c^2}$) is dominated by contributions from pn bremsstrahlung, π^0, η and less pronounced Δ Dalitz decays. In the upper mass range ($600\,\mathrm{MeV/c^2} < \mathrm{M}_{inv} < 1\,\mathrm{GeV/c^2}$) only two-body ρ/ω decays are expected with little contributions from ω Dalitz and ϕ decays. The good suppression of combinatorial background from multiple external pair production ($\pi^0 \to \gamma\gamma \to \gamma e^+e^-$) and the high mass resolution of $\Delta\mathrm{M/M} \sim 1\,\%$ will allow to detect any significant mass shift or a resonance broadening (not included in the simulations). The large and flat acceptance gives access to systematic investigations of a pair yield as a function of transverse momentum and rapidity necessary for comparisons with various theoretical models.

2.2 e^+e^- pairs from proton and pion induced reactions

Individual components of the heavy ion induced e^+e^- cocktail can be studied in elementary πp or pp reactions taking into account well-defined production thresholds and adjusting respectively the projectile energy. Additional advantage of such studies is electron background from secondary sources which can be kept at minimum. In fact some of these sources are poorly known. For example the electromagnetic from factor of the nucleon in the time-like region at four-momentum transfer $q^2 < (1\,\mathrm{GeV})^2$ is not known at all although it is of large importance for the description of pn bremsstrahlung and Δ Dalitz decay. Data with smaller error bars are badly needed for the understanding of the ω Dalitz decay process where the simple Vector Dominance Model fails to describe available experimental data points [22]. The η Dalitz decay is an important dielectron source at the intermediate mass region where the excess in the DLS data has been observed. Also for this meson data with better precision than available from the measurements published so far [23, 24] are needed. These data can be obtained with the HADES detector using proton and pion beams at GSI [9]. As an example the η Dalitz decay can be studied in pp collisions ($pp \to pN^*(1535) \to pp\eta \to ppe^+e^-(\gamma)$) at energies around the η production threshold. With both protons and electrons identified and measured beam energy the reconstruction of the Dalitz decay is kinematically complete without requiring an additional photon detector for γ detection.

As it has already been mentioned above, the production and propagation of vector mesons in the nuclear matter is strongly affected by their coupling to baryonic resonances. Since they can be produced directly in elementary $\pi^\pm N$ collisions, measurements of dielectron production rates in these reactions are of fundamental interest.

Exclusive e^+e^- production in $\pi^-p \to \rho(\omega)n$ reactions can be used to probe the coupling of off-shell ρ/ω mesons to the $S_{11}(1535)$ and $D_{13}(1520)$ resonances at energies close to or below the production threshold ($\sqrt{s} = 1.72\,\mathrm{GeV}$). As it has been demonstrated by [25] amplitudes of an intermediate ω and ρ meson contribute coherently to the pair production cross section and a ρ/ω interference term may cause pronounced structures in the respective excitation function. The e^+e^- pair production cross section in this reaction can be measured with HADES by selecting neutrons by a proper missing mass cut for events where only e^+e^- are detected and a projectile is tracked with a momentum resolution of 0.5 % allowing for a precise $\sqrt{s}$ determination.

Studies of dielectron production in π^-p and π^-n reactions are also im-

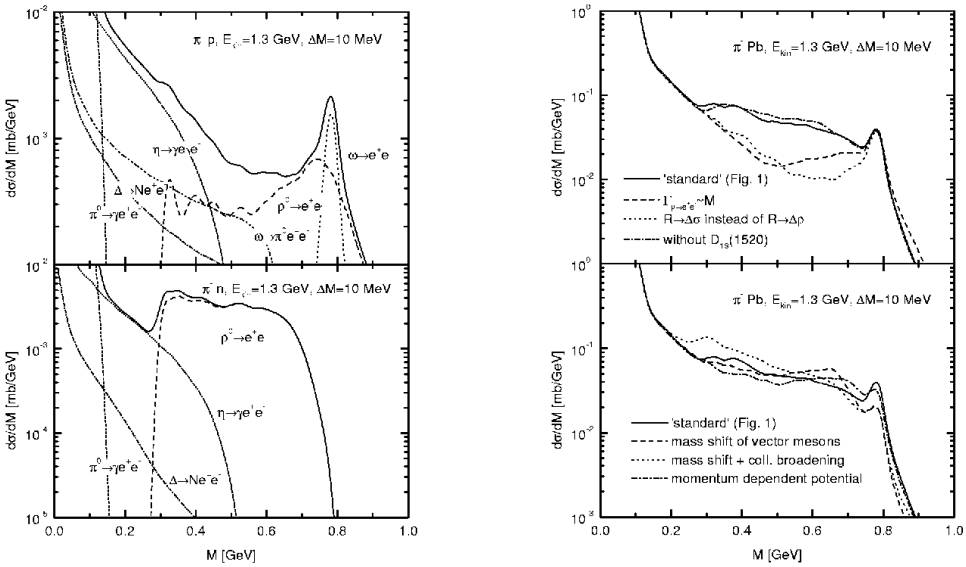

Figure 2: Dielectron invariant mass distribution from pion induced reactions at a beam kinetic energy of $E_{kin} = 1.3\,\mathrm{GeV}$.*Left panel:* $\pi^- p$ (upper part) and $\pi^- n$ (lower part) reactions. Various dielectron channels are shown separately. *Right panel:* $\pi^- Pb$ reaction. Results of various model assumptions concerning ρ meson production and propagation are shown separately (see text and ref. [28]). The lower part shows the influence of 'dropping masses' and collisional broadening for vector mesons.

portant for other reasons. It has been predicted that precursor phenomena for chiral symmetry restoration, shifts of vector meson masses, should occur already at normal nuclear matter density [26]. It opens a possibility to study the vector meson mass inside nuclei via recoilless production of ω mesons in a $\pi^- Pb$ reaction with the HADES spectrometer [27]. This requires, however, a detailed knowledge of the elementary processes responsible for dielectron production in $\pi^- N$ reactions. It has even been suggested [28] that at an optimum pion beam energy of 1.3 GeV for such studies the contribution from $\pi^- n$ collisions (which are subthreshold for ω production) is so large that expected medium modifications of the ω meson can be obscured (see fig. 2 right). This is due to the effect presented in fig. 2 (left), where for the $\pi^- n$ reaction a significant enhancement in the intermediate mass region is visible as compared to the $\pi^- p$ case. The main reason for this effect comes from excitation of baryonic resonances, in particular $D_{35}(1950)$ and $F_{37}(1950)$ with isospin component $I_3 = 3/2$, decaying strongly into the $\Delta^{++}\rho$ channel.

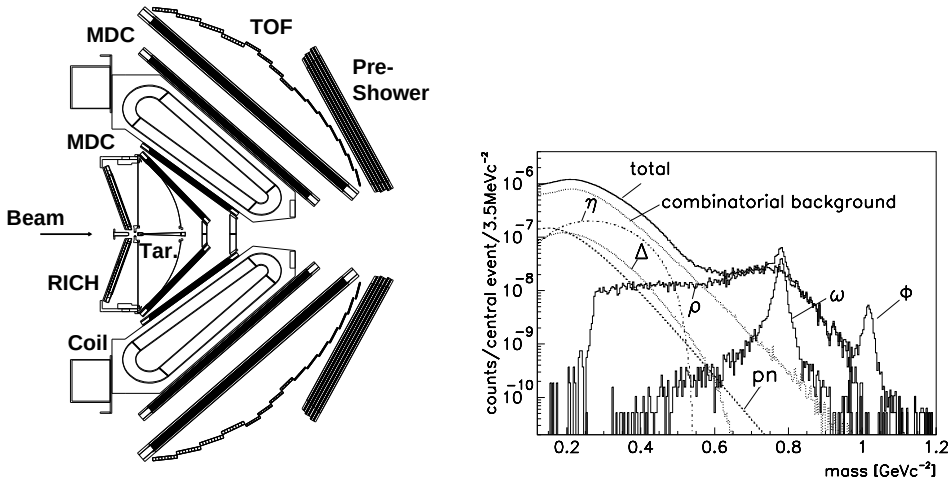

Figure 3: The new e^+e^- spectrometer HADES. *Left panel:* Azimuthal cross section of the HADES setup. The RICH consists of a gaseous radiator, carbon fiber mirror and the tilted UV detector segments. The target is positioned in the center of the radiator. Two sets of mini-drift chambers (MDCs) in front and behind the magnetic field produced by superconducting coils measure the trajectory. A time of flight wall (TOF) is accompanied at polar angles $< 45°$ by a PreShower detector for second electron identification. *Right panel:* Simulated e^+e^- invariant mass distributions for central $Au + Au$ collisions. Dalitz decay of η and Δ and pn bremsstrahlung are the main contributing sources below 0.5 GeV/c^2. Above 0.5 GeV/c^2 dielectrons from ρ, ω and ϕ mesons dominate the spectrum.

It has to be noted that a similar effect of enhanced low mass ρ contribution can be achieved by exchanging the mass dependence of the electromagnetic decay width of the Vector Dominance Model from $\sim$ M^{-3} to $\sim$ M (solid and dashed line in fig. 2 right). As it has been pointed in [28], the amplitude of this particular reaction channel is uncertain and experimental data are strongly needed. This can again be provided by the HADES spectrometer in the dedicated experiment studying dielectron production in the π^+p and π^-p reactions.

3 The Spectrometer Setup

The HADES experiment is designed to cope with the high-multiplicity environment of heavy ion collisions and the small branching ratios for the dielectron production channels. The key features are a large acceptance $\Omega_{pair} \simeq 40\%$ combined with a high resolution for invariant mass recon-

struction $\Delta M_{inv}/M_{inv} \simeq 1\,\%\,(\sigma)$ and a signal to background ratio > 1 for invariant masses up to $M \simeq 1\,GeV/c^2$. The instrument (see left panel in fig. 3) is azimuthally segmented into 6 sectors and covers polar angles $18° \leq \theta \leq 85°$. Four planes of 6 trapezoidal Multi-wire Drift Chambers (MDC) [29] together with a superconducting toroid form a magnetic spectrometer for charged particle momentum measurement. A hadron blind RICH counter with a gaseous decafluorobutan (C_4F_{10}) radiator around the target is used for electron identification. Rings of Čerenkov photons with nearly constant diameter are detected in an MWPC type photon detector with CsI pad cathode [30]. A set of electromagnetic PreShower detectors covering polar angles up to 45° and a Time-of-Flight (TOF) wall with 648 scintillators provide additional lepton identification and a multiplicity signal to trigger on central collisions. The Time-of-Flight (TOF) wall has a time resolution $100\,ps \leq \sigma_{tof} \leq 150\,ps$ [31] and allows to discriminate electrons from pions up to 0.5 GeV/c and from protons up to 2 GeV/c. The low effective radiation length $\rho d/X_0 \simeq 10^{-2}$ of the inner detectors keeps multiple scattering and combinatorial background from external pair production low.

The data acquisition is based on a switched ATM network [32] with a sustained transfer rate of 14 Mbyte/s and uses a three level trigger system [33] to reduce the primary data rate of 4 Gbyte/s from all 73,000 detector channels to a maximum of about 4 Mbyte/s. While the first level trigger selects central collisions, e^+e^- pair candidates are selected at the second level by position matching of ring centers found with hardware image processing in the RICH [34] and hits in the TOF and PreShower detectors. The third level suppresses background by an online tracking analysis with drift chamber hits.

The installation of the spectrometer is nearly completed, with the exception of the outer drift chambers, where the first sector is presently installed. Several subsystems have been successfully tested in commissioning runs with beam intensities up to $10^7\,s^{-1}$. As an example, the electron identification capability of the RICH is illustrated in fig. 4. In a preliminary analysis of $2 \cdot 10^5$ central $Ar + Ti$ collisions at $E = 1.75\,AGeV$ about 2500 candidates for Čerenkov rings were found, in reasonable agreement with simulation results. The corresponding electrons and positrons come mostly from external pair conversion of γs in the target and the radiator gas. In almost all events the ring candidates (left panel of fig. 4) were not obscured by electronic noise or signals from charged particle background. The yield of ring centers declines homogeneously with increasing polar angle and is in good agreement with simulation results. The time-of-flight spectra in the right panel of fig. 4 demonstrate the achieved suppression of pions and pro-

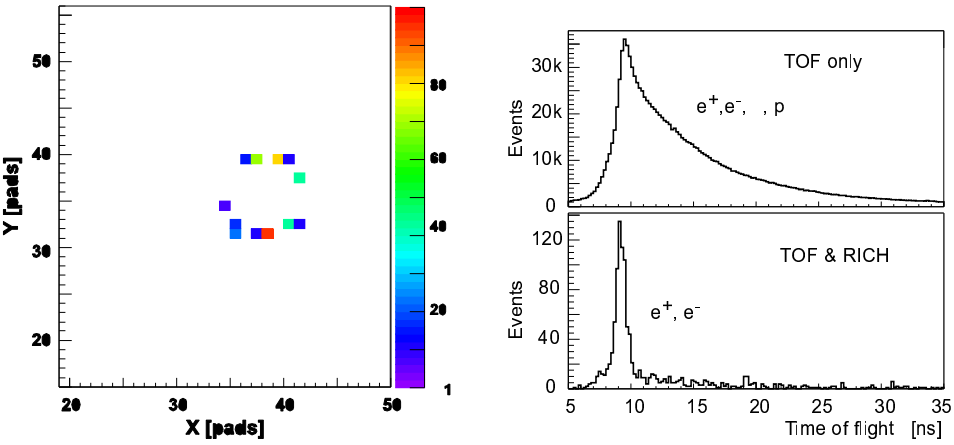

Figure 4: Hadron suppression with the RICH in $Ar + Ti$ collisions at E = 1.75 AGeV. *Left panel:* Ring image of a single $e^{\pm}$ from external pair conversion in the target or radiator gas with a coincidence track signal in the drift chamber. *Right panel:* Time of flight distribution for all particles (*upper*) and for electrons (*lower*) with rings found in the RICH. Note the suppression in yield.

tons when electron identification with RICH is switched on. Fig 5 presents momentum analysis and particle identification using the combined analysis of RICH, PreShower/TOF detectors and tracking system. The lower panel of fig 5 shows the electron signal when lepton identification in RICH and PreShower is required.

4 Conclusions and Outlook

HADES is a high rate, high acceptance apparatus for electron pair spectroscopy with $< 1\,\%$ invariant mass resolution and a fast and selective multi level trigger scheme. The spectrometer is meanwhile ready for first runs and results obtained in commissioning runs demonstrate the efficient and redundant lepton identification.

The physics program is broad and includes the study of lepton pair emission in relativistic heavy ion collisions, dielectron production in elementary reactions and experiments aimed at studying the structure of hadrons. Particular attention will be paid to the decay properties of vector mesons with respect to mass shifts and resonance broadening. The shape of the invariant mass spectrum will give access to electromagnetic transition form factors of neutral mesons. The long-range aim is to understand the dynamical prop-

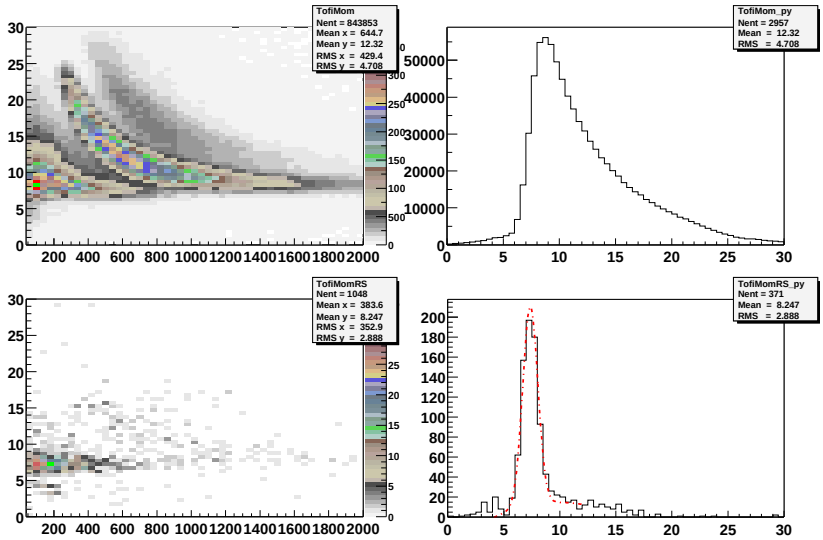

Figure 5: Momentum analysis and particle identification with the RICH, PreShower/TOF detectors and tracking system in $Ar + Ti$ collisions at E = 1.75 AGeV. *Lower panel:* Electron signal from lepton identification in RICH and PreShower detectors. Note the suppression in yield.

erties of hot and compressed hadronic matter, an environment in which partial restoration of chiral symmetry is expected to show up. The experimental program of HADES will focus first on pp collisions and light heavy ion systems to verify the yield enhancements found in earlier measurements. Dedicated investigations of the ω meson decay are foreseen utilizing both pion and heavy ion induced reactions.

References

[1] F. Klingl, N. Kaiser, and W. Weise, Z. Phys. **A 356** (1996) 193.

[2] R. Rapp, J. Wambach, Adv. Nucl. Phys. **25** (2000) 1.

[3] G.E. Brown, M. Rho, Phys. Rev. Lett. **66** (1991) 2720.

[4] W. Cassing, E.L. Bratkovskaya, Phys. Rep. **308** (1999) 65.

[5] C.M. Ko, V. Koch, and G.Q. Li, Ann. Rev. Nucl. Part. Sci. **47** (1997) 505.

[6] W. Ehehalt et al., Phys. Rev. **C 47** (1993) 2467.

[7] P. Salabura et al., Nucl. Phys. **B 44** (1995) 701c.

[8] B. Friman, W. Nörenberg, and V.D. Toneev, Eur. Phys. J. **A 3** (1998) 165.

[9] V. Metag, Acta Phys. Polon. **B 27** (1996) 3175.

[10] W. Peters, M. Post, H. Lenske, S. Leupold, U. Mosel, Nucl. Phys. **A 632** (1998) 109.

[11] B. Friman, H. Pirner, Nucl. Phys. **A 617** (1997) 496.

[12] R. Rapp, G. Chanfray, J. Wambach, Nucl. Phys. **A 617** (1997) 472.

[13] G.Q. Li, C.M. Ko, G.E. Brown, Phys. Rev. Lett. **75** (1995) 4007.

[14] A. Drees, Nucl. Phys. **A 630** (1998) 449c.

[15] R.J. Porter et al., Phys. Rev. Lett. **79** (1997) 1229.

[16] W.K. Wilson et al., Phys. Rev. **C 57** (1998) 1865.

[17] E.L. Bratkovskaya et al., Nucl. Phys. **A 653** (1999) 301.

[18] E.L. Bratkovskaya et al., Nucl. Phys. **A 634** (1998) 168.

[19] C. Ernst et al., Phys. Rev. **C 58** (1998) 447.

[20] H. Neumann et al., Acta Phys. Slov. **44** (1994) 195.

[21] R. Schicker et al., Nucl. Instr. & Meth. **A 380** (1996) 586.

[22] L.G. Landsberg, Phys. Rep. **226** (1985) 301.

[23] M.R. Jane et al., Phys. Lett. **B 59** (1975) 103.

[24] G. Agakishiev et al., Eur. Phys. J. **C 4** (1998) 231.

[25] M. Soyeur, M. Lutz, B. Friman, 28th Int. Workshop On Gross Properties Of Nuclei And Nuclear Excitation: Hadrons in Dense Matter (Hirschegg 2000), Hirschegg, Austria, 16-22 Jan 2000, Proc. ed. by M. Buballa et al., Darmstadt, GSI (2000) 170 and e–Print Archive nucl–th/0003013.

[26] S Klimt et al., Phys. Lett. **B 249** (1990) 386.

[27] W. Schön et al., Acta Phys. Polon. **B 27** (1996) 2959.

[28] M. Effenberger et al., Phys. Rev. **C 60** (1999) 027601.

[29] C. Garabatos et al., Nucl. Instr. & Meth. **A 412** (1998) 38.

[30] K. Zeitelhack et al., Nucl. Instr. & Meth. **A 433** (1999) 201.

[31] C. Agodi et al., IEEE Trans. Nucl. Sci. **45** (1998) 665.

[32] M. Münch, 37th Int. Winter Meeting On Nuclear Physics, Bormio, Italy, 25-29 Jan 1999, Proc. ed. by I. Iori, Ricerca Scientifica ed Educazione Permanente Supplemento No. **114** (1999) 509.

[33] M. Petri, 36th Int. Winter Meeting On Nuclear Physics, Bormio, Italy, 26-31 Jan 1998, Proc. ed. by I. Iori (1998) 622.

[34] J. Lehnert et al., Nucl. Instr & Meth. **A 433** (1999) 268.

The Measurement of pp $\rightarrow$ ppω at COSY-11

D. Grzonka, G. Schepers [1]

Institut für Kernphysik, Forschungszentrum Jülich, Germany

Abstract: Dedicated measurements for the production of ω mesons at COSY-11 have been performed for excess energies of 25, 50 and 107 MeV. Besides the production cross section the coverage of the whole Θ_{CM}-angular range will allow the extraction of angular distributions for the ω production. Both, the cross sections and angular distributions will give valuable information for the study of the ω production mechanism. Furthermore the data are analyzed with regard to the visibility of effects from $\rho - \omega$ mixing.

1 Introduction

The COSY data of ω-production in proton proton collisions fill the gap between the data far above threshold [1] and the recent measurement at SATURNE [2] very close to threshold. First data in this area have been published recently by the TOF collaboration [3].

Theoretical analyses of ω production in proton-proton collisions have been performed within different models which mainly base on meson exchange. Nakayama et al. [4] studied the ω production within a meson exchange model with the two basic production mechanisms, the nucleonic and mesonic currents. It turns out that the angular distribution provides a unique and clear signature for the magnitude of the two production mechanisms. Therefore within this model the data will allow to determine the relative contributions of nucleonic and mesonic exchange currents. The data will of course also yield information needed for an extraction of the $NN\omega$ coupling constant and will in general increase the accuracy of meson exchange model descriptions.

Referring to the topic of $\rho - \omega$ mixing it is a question if the mixing results in a detectable effect in the pp induced ω production. Such a clear signature as in the pion production data [5] will not occur but a certain deviation due

[1] talk given by G. Schepers

to the $\rho - \omega$ mixing is expected in the missing mass distribution of the data. Depending on the strength of the mixing which is given by the pion data, a shift in the peak position and an enhancement at the high energy part of the ω distribution is expected.

2 Vector meson production at COSY-11

The measurement of the vector meson production in the reaction $pp \to pp\omega$ is performed via the missing mass technique. The two protons in the exit channel can be detected in the standard COSY-11 setup [6], allowing the determination of the four-momentum components of positively charged ejectiles from which a calculation of the four–momentum components of the neutral meson is possible. The acceptance of the COSY-11 detection system is rather low at higher excess energies needed for these analyses (from 1.80 % down to 0.14 % for Q-values of 25 to 107 MeV), but due to the large exit window the whole Θ_{CM}-angular range is covered. A disadvantage of the missing mass technique, especially in the detection of mesons with a width of a few MeV or more, is the unavoidable background from e.g. multi pion production.

3 Discussion of the data

For all the three data sets the selection of the events for the $pp \to ppX$ reaction and for the elastics which serves for the determination of luminosity is close to the end. Yet it is still a challenge to extract the correct number of produced omega mesons from the missing mass distribution. As an example the missing mass distribution for the most critical data set at Q = 25 MeV is given in fig. 1. First of all the measured peak (solid line) is not located at the mass of the ω. The reason could be a wrong beam momentum but a check of the reconstructed peaks of η from $pp \to pp\eta$ and Λ from $pp \to pK^+\Lambda$ exclude this possibility. The most interesting explanation for this behaviour could be an effect of the $\rho - \omega$-mixing. This mixing would, comparable to the pion production data [5], also effect the missing mass distribution in the pp-induced ω production. A more trivial effect could be the pp final state interaction which results in an enhancement in the phase space distribution for small relative momenta of the two exit protons. The different effects are studied presently with Monte Carlo simulations. The ω is produced as a Breit-Wigner shaped resonance with the mass and width given by the particle data booklet. As background channels $pp \to pp\pi\pi$, $pp \to pp3\pi$ and

$pp \to pp\rho$ are considered.

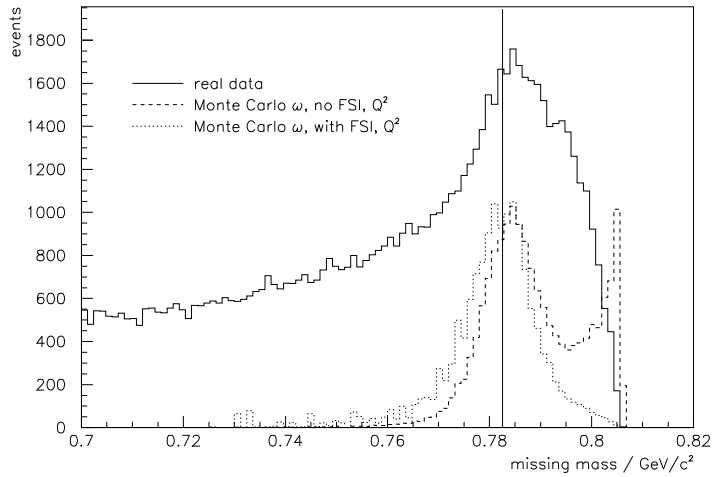

Figure 1: Shift in the missing mass of the ω-production. The solid line shows the data, the dashed the simulation with only phase space weights, the dotted the influence of the FSI and the Q^2-dependence of the phase space.

In the event generation S-wave phase space distributions without any final state interaction are used. The events are passed through the COSY-11 detection system used for the ω measurement and are analyzed in the same way the real data are analyzed. The pp FSI is introduced by a weight factor calculated for each event as a function of the pp relative momentum. Furthermore a second weight factor considers the dependence on the square of the excess energy ("Q^2-dependence") to the missing mass distribution for a wide resonance. The Q^2-dependence represents the increasing phase space for higher Q-values. With this method it is possible to see the effects of the two contributions (FSI and Q^2 dependence) and to study variations in the pp FSI without generating each time new Monte Carlo event samples. Both mechanisms lead to a shift of the peak position, FSI to higher energies and Q^2-dependence to lower energies. The combined effect results in the right order of magnitude in the peak shift as it is seen in the real data.

A first try to describe the measured data with Monte Carlo distributions is given in fig. 2. The statistics of the Monte Carlo data is still much too low, but it demonstrates that a good description of the measured missing mass

distribution is achievable. The upper plots show the measured spectrum (solid line) in different missing mass ranges with the sum of Monte Carlo data including the channels $\pi^+\pi^-$, ρ and ω (dashed line) and the lower plots show the missing mass distribution in the individual channels.

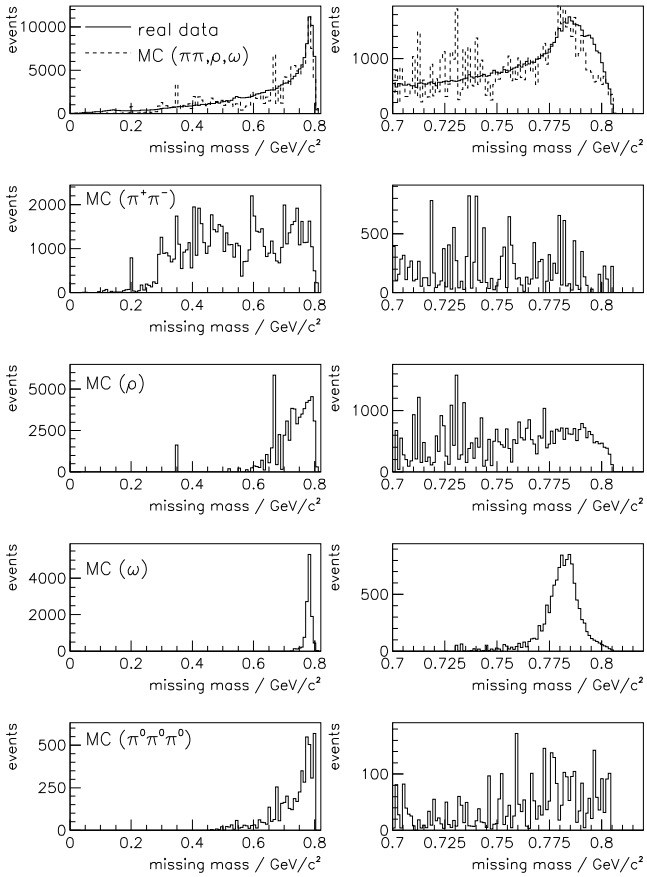

Figure 2: Fit to the experimental distribution with Monte Carlo data including the dominant background channels.

The experimental missing mass distribution is well described within the statistical errors except a part at the high energy side which could be attributed to the three-pion channels. It seems that the data can be described

by adjusting the amplitudes of the considered background channels without need for extra effects like $\rho - \omega$ mixing. This does not mean that $\rho - \omega$ mixing is not present but that the effect is too low to be clearly visible in our data.

Since the FSI is a function of the pp relative momentum a two-dimensional distribution of the missing mass as a function of the pp relative momentum should allow a closer look to the FSI effects. On the left side of fig. 3 the distribution for the measured data is shown.

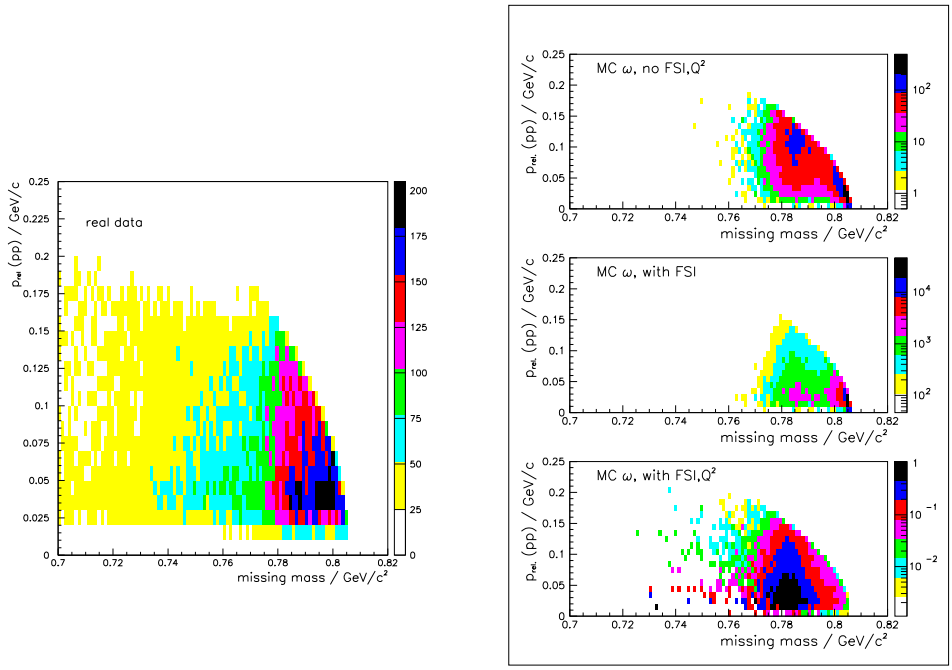

Figure 3: Relative momentum in the pp system versus the missing mass. On the left side the distribution is shown for the real data and on the right side for Monte Carlo data with a pure Breit Wigner ω resonance. The effects of pp FSI and Q^2-dependence are separately shown.

If the peak shift is induced by FSI effects the peak position should move from the nominal position at high pp relative momenta to higher energies with lower pp relative momenta. Before drawing conclusions from the plot, which doesn't show a clear picture, the distribution has to be compared to Monte Carlo data with pure ω events which is given on the right side of fig. 3. Without FSI and Q^2-dependence (upper plot on the right side

in fig. 2) the efficiency of the COSY-11 detection system results in a more complex structure of the ω "peak" than it is expected. Including the weight factors the distribution is strongly modified. For a correct interpretation of the measured data a careful comparison with Monte Carlo data is necessary where such two-dimensional distributions will be very helpful.

Concerning the data at higher excess energies the determination of the background is a bit simplified because the ω peak is located far away from the kinematical limit where the missing mass distribution has a smoother Q-value dependence. Here the extraction of the angular distribution is the bigger problem. From physics the angular distribution has to be symmetric around 90 degrees, but instead a strong asymmetry is observed which can be caused by several unknown dependencies due to the limited acceptance.

4 Outlook

For the selection of the correct ω-events the knowledge of the background is crucial especially for the data at a Q-value of 25 MeV. Monte Carlo data with higher statistics including the dominant background channels will be used to describe the distribution of the real data where the consideration of the correct FSI is very important. Within these studies also the sensitivity to deviations from pure S-wave phase space distributions will be checked.

Furthermore using Monte Carlo data the possible sources for an asymmetry of the angular distribution will be studied in order to extract a reliable angular distribution for the ω-emission angle.

References

[1] V. Flaminio at al., *Compilation of cross sections*, CERN-HERA report 84-01 (1984); F. Balestra et al., Phys. Rev. **C 63** (2000) 024004.

[2] F. Hibou et al., Phys. Rev. Lett. **83** (1999) 492.

[3] S. Abd El–Samad et al., Phys. Lett. **B 522** (2001) 16.

[4] K. Nakayama et al., Phys. Rev. **C 57** (1998) 1580; Phys. Rev. **C 60** (1999) 055209; e–Print Archive: nucl–th/0108032 (2001).

[5] L.M. Barkov et al., Nucl. Phys. **B 256** (1985) 365; D. Benaksas et al., Phys. Lett. **B 39** (1972) 289.

[6] S. Brauksiepe et al., Nucl. Instr. & Meth. **A 376** (1996) 397.

Production of ω- and η'-Mesons in pp Collisions at Higher Excess Energies

A. Khoukaz, C. Quentmeier, R. Santo

Institut für Kernphysik, Westfälische Wilhelms-Universität, Münster, Germany

Abstract: The production of ω- and η'-mesons in proton-proton collisions is studied at the COSY-11 facility at beam momenta of p_{beam} = 3.292 GeV/c, 3.311 GeV/c and 3.356 GeV/c. Preliminary angular distributions of the η'-mesons in the overall center of mass system are compatible with an isotropic emission and the excitation function can be described by three body phase space calculations modified by the proton-proton final state interaction. Clear signals of the ω-meson production are seen at all three beam momenta. The evaluation of the data is in progress.

1 The reaction pp $\rightarrow$ ppη'

Data on the η' meson production in the reaction channel $pp \rightarrow ppX$, one of the main research topics [1, 2, 3] of COSY-11, have been taken at incident proton beam momenta of p_{beam} = 3.292, 3.311 and 3.356 GeV/c, corresponding to excess energies of Q = 26.5, 32.5 and 46.6 MeV [4]. The event selection was performed by accepting events with two identified protons. The four-momentum determination of positively charged ejectiles yields a full event reconstruction for the reaction type $pp \rightarrow ppX$ and the X-particle system can be identified using the missing mass method. Therefore, kinematical distributions of all reaction ejectiles can be studied. In fig. 1 η' angular distributions in the overall center of mass system are shown for Q = 32.5 and 46.6 MeV. The quoted error bars include statistical and systematical errors. Within the errors the presented distributions are compatible with an isotropic emission, which is consistent with the result from the DISTO collaboration at an excess energy of Q = 144 MeV [5]. However, both distributions expose indications of higher partial waves, i.e. D-waves.

The new preliminary COSY-11 total cross sections at Q = 26.5, 32.5 and 46.6 MeV are presented in fig. 2 together with other available data [1, 2, 5, 6] and are compared with model calculations. The dotted line indicates a fit

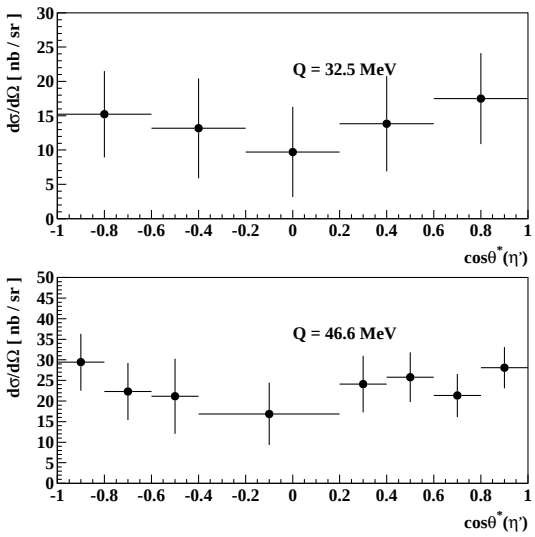

Figure 1: Preliminary angular distribution of the emitted η' meson in the center of mass system at Q = 32.5 and 46.6 MeV.

to the data resulting from pure S-wave three body phase space calculations modified by the proton-proton final state interaction (FSI) and Coulomb effects which describes the whole set of existent data even up to an excess energy of Q = 144 MeV. Obviously, one can conclude that the excitation function can be described without any further contributions from higher partial waves and in particular without strong effects of an η'-proton interaction. The formerly discussed possibility of a repulsive η'-proton interaction [7, 8] seems to be of minor importance. This observation is in agreement with the result that the η'-proton scattering length is small and similar to the one of the π^0-proton system [3].

Recently, the η' meson production has been investigated within a relativistic meson-exchange model, including effects of the *pp* initial state interaction as well as of the *pp* final state interaction [9]. Fig. 2 displays two results with different combinations of the diagrams discussed in [9] (solid and dashed curves), which lead to an appropriate description of the cross section data. While the lower (solid) curve represents a calculation only on basis of the nucleonic and the mesonic currents, the remaining (dash-dotted) curve shows a result on a calculation including also contributions of the nucleonic resonance current. Obviously, these calculations agree well with the data up to excess energies of Q = 50 MeV. However, the best agreement is

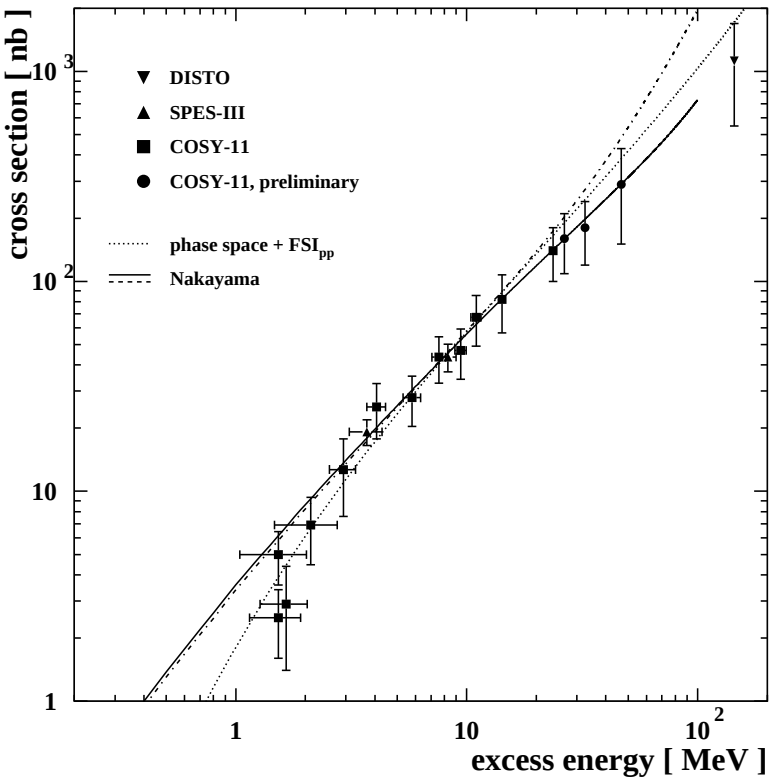

Figure 2: Near threshold total cross sections for the reaction channel $pp \to pp\eta'$. The lines indicate results of different models and are explained in the text. The data are taken from [2, 4, 5, 6, 8]. The three highest COSY-11 data are still preliminary.

obtained with only a small contribution of the nucleonic resonance current (solid curve).

2 The reaction pp → ppω

Studies on the ω meson production in the proton-proton scattering provide valuable information on the properties of this vector meson and relevant production processes in the elementary nucleon-nucleon interaction. Recent calculations on the $pp \to pp\omega$ reaction [10] demonstrate a significant influence of different production mechanisms on the angular disribution of the emitted ω mesons. Data for the reaction channel $pp \to ppX$ taken at beam momenta of 3.292, 3.311 and 3.356 GeV/c were analyzed with respect

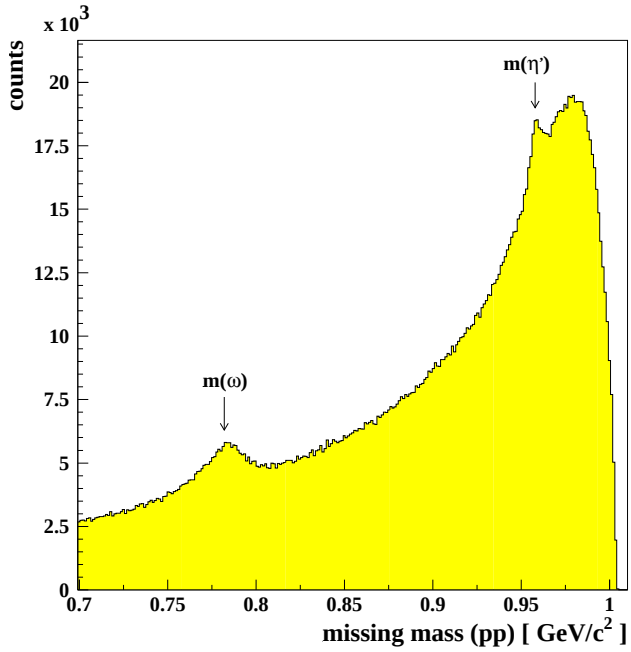

Figure 3: Missing mass of the proton-proton system at a beam momentum of $p_{beam} = 3.356\,\mathrm{GeV/c}$.

to the ω meson production [4]. The excess energies covered by these data are Q = 202.3, 208.3 and 222.5 MeV. The event selection was performed by accepting events with two identified protons. Similarly to the η' meson production the four-momentum determination of positively charged ejectiles yields a full event reconstruction for the reaction type $pp \to ppX$, and the X-particle system can be identified using the missing mass method (Fig. 3). Therefore, kinematical distributions of all reaction ejectiles can be studied in detail.
The evaluation of differential and total cross sections is in process.

References

[1] P. Moskal et al., Phys. Rev. Lett. **80** (1998) 3202.

[2] P. Moskal et al., Phys. Lett. **B 474** (2000) 416.

[3] P. Moskal et al., Phys. Lett. **B 482** (2000) 356.

[4] C. Quentmeier, doctoral thesis, Westfälische Wilhelms-Universität Münster, Germany (2001).

[5] F. Balestra et al., Phys. Lett. **B 491** (2000) 29.

[6] F. Hibou et al., Phys. Lett. **B 438** (1998) 41.

[7] V. Baru et al., Eur. Phys. J. **A 6** (1999) 445.

[8] P. Moskal et al., Acta Phys. Polon. **B 29** (1998) 3091.

[9] K. Nakayama et al., Phys. Rev. **C 61** (2000) 024001.

[10] K. Nakayama et al., Phys. Rev. **C 57** (1998) 1580.

Stochastic Beam Cooling [1]
- An Introduction -

H. Stockhorst

Institut für Kernphysik, Forschungszentrum Jülich, Germany

1 Introduction

At COSY the stochastic cooling system operates in the entire momentum range from about 1.5 GeV/c up to 3.4 GeV/c. It is possible to cool the beam simultaneously in all three phase space planes, i.e. in the horizontal, vertical and longitudinal plane. Opposite to electron cooling, stochastic cooling can be applied in all three planes independently. I.e., cooling in each plane can be adjusted separately, or cooling in only one plane is possible.

Also in this written version of my talk I will dispense with the underlying mathematical formalism of stochastic cooling, so that only necessary equations are given and most details are explained in a heuristic way. Also, no details of the necessary electronic components as well as pickup and kicker devices, which finally determine the performance of the cooling system, are discussed. Only cooling of unbunched (rf-cavity off) beams is discussed and I use the horizontal cooling as an example. Vertical cooling is the same, just change both words. So I speak about transverse cooling or betatron cooling. Longitudinal cooling is a little bit more complicated because the momentum distribution changes during cooling. But it can be shown that a similar cooling equation for the variance of the momentum distribution applies as given below. In all cases stochastic cooling of protons is assumed.

At the end references are given where the reader can find detailed derivations and discussions. The references show also where I borrowed knowledge and pictures for this talk.

2 Transverse Phase Space

Figure 1 sketches the horizontal plane of an accelerator in which a reference particle moves on a circle (closed orbit or design orbit) determined by the bending magnets. Due to the quadrupoles in the ring, any particle that

[1] Invited talk

starts with an offset (error) x with respect to the closed orbit will execute betatron oscillations around the closed orbit.

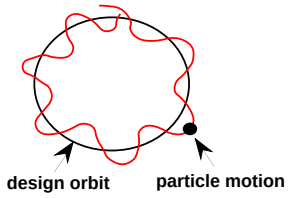

Figure 1:

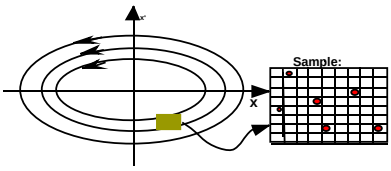

Figure 2:

As indicated, this motion is not closed so that the number of betatron oscillations per revolution, called tune Q, is not an integer or a half integer.

As the figure suggests the betatron motion of a particle rotating in the ring with angular frequency Ω can be approximately described by a simple oscillator equation

$$x'' + Q\Omega x = 0$$

in which the tune Q is

$$Q = ||Q|| + Q_f$$

with integer part $||Q||$ and fractional part Q_f $(0 \leq Q_f \leq 1)$. Typical values at COSY in the horizontal or vertical plane are in the range $Q = 3.55$ to 3.65.

Solutions of the harmonic oscillator equation can be represented in phase space (x',x) where (Figure 2) each individual particle will circulate around the origin on an ellipse. In this phase space the whole beam is distributed (e.g. Gaussian) and the area that encloses all (or some fraction) is called phase space area.

Albeit the particle number distributed in phase space may be large it is a finite number. If then a small area of phase space is magnified one sees a lot of particles (a sample) but also a lot of empty space between them due to the finite particle number (Figure 2).

The idea of beam cooling is now:

Rearrange the phase space so that the empty space is moved from the center of the distribution to the edges. That is, the distance between particles is reduced so that the particles come closer to the origin and at the same time the particle density is increased.

3 Stochastic Cooling of Betatron Motion

The basic setup for horizontal stochastic cooling is sketched in figure 3. At some location in the ring a pickup is installed with which the mean position of particles is measured. Further downstream the beam a kicker is located, which receives the amplified pickup signals. This device applies an angle kick to the particle that is proportional to the position error.

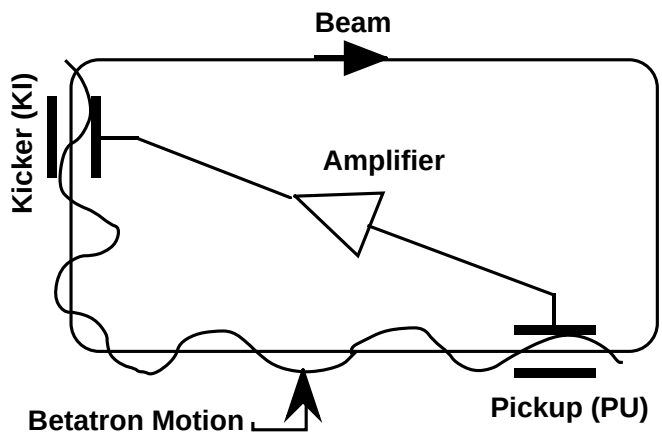

Figure 3:

To see how cooling works, suppose we could measure the position of only one particle that undergoes betatron oscillations as shown. Three different situations at the pickup are depicted in the next figure 4. If the position error is at maximum at the pickup (case 1) then, 90 degrees downstream, this error is converted in the corresponding maximum angle. If we place there the kicker it will apply a kick with negative maximum angle and the particle would stay on the close orbit with zero angle **and** zero position error, i.e. the particle has been cooled! If, as in case 2, the position is not at maximum there is still a correction at the kicker, but the betatron oscillation is only partly damped. In case 3 the position error is zero at the pickup and the particle suffers no deflection at the kicker (zero angle). But, since the number of betatron oscillations around the ring is neither an integer nor a half integer, a situation like case 1 or 2 will occur after some turns and the particle will be cooled. By this all particles will be cooled, i.e. the betatron oscillations are damped over many turns.

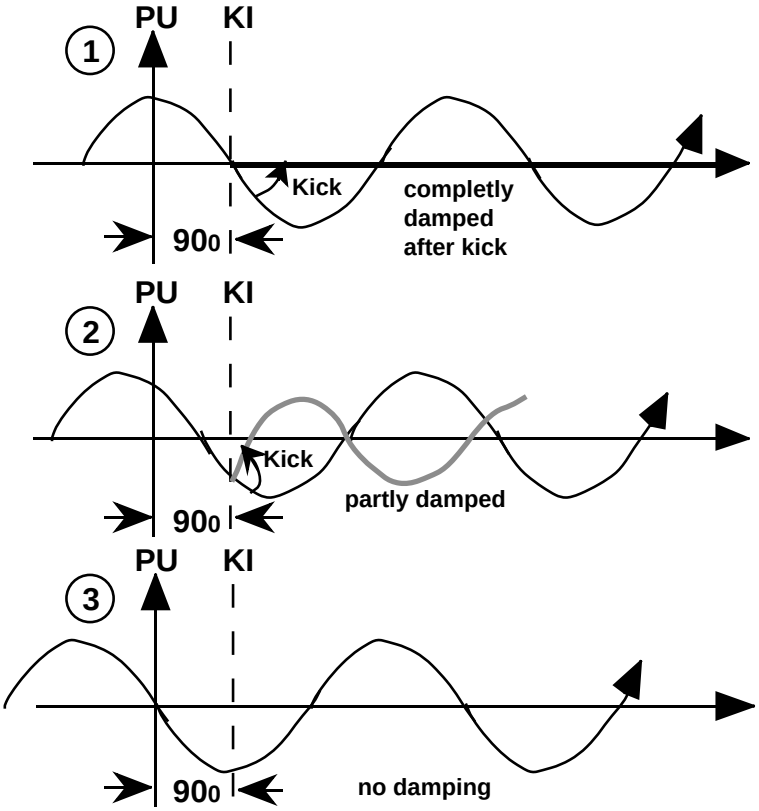

Figure 4:

Note, in all cases we implicitly assumed the necessary condition that the particle signal arrives at the kicker at the same time with the particle. Otherwise the particle would see no or at least only an incorrect correction. Thus (at least) two conditions are necessary for good betatron cooling:

- *Phase advance from pickup to kicker must be an odd multiple of 90 degrees.*

- *The particle must arrive at the kicker simultaneously with the signal. Hence, the position of the kicker can not be arbitrarily chosen. E.g., if the particles are very fast the distance between pickup and kicker should not be too small.*

3.1 Finite Bandwidth of the Cooling System

So far we assumed that the pickup and kicker as well as the electronics are able to resolve a single particle. In reality this is not the case because the frequency bandwidth of any electronic device including pickups and kickers is limited. Certainly, it is possible to build the components with a bandwidth up to around ten GHz (COSY: $W = 2\,\mathrm{GHz}$). But this is not sufficient to resolve a single particle. A single particle at the pickup produces a short (delta-function-like) pulse. Due to the cooling chain this pulse is broadened having now a duration T_S which according to signal processing theory is given by the relation

$$T_s = \frac{1}{2W}. \tag{1}$$

In other words, the cooling system samples the beam with a finite resolution T_S. In a uniform beam (unbunched beam) of revolution period T there are then

$$l_s = \frac{T}{T_s} = 2WT$$

equally spaced samples. The particle number in each sample is

$$N_s = \frac{N}{l_s} = \frac{N}{2WT}. \tag{2}$$

So in large rings, where the revolution period T becomes small, the sample size becomes large for a large number of beam particles. Consequently, as we will see, a large sample size leads to a small cooling rate. Increasing the bandwidth decreases the sample size.
Example: $N = 10^{10}$, $T = 1\,\mu\mathrm{s}$, $W = 2\,\mathrm{GHz}$, $T_s = 250\,\mathrm{ps}$, $l_s = 4000$ and $N_s = 2.5 \cdot 10^6$

3.2 Cooling Equation

The finite bandwidth means that a particle passing the kicker not only receives its own correcting kick but also experiences kicks due to all other particles that pass the pickup during the sampling time T_s. If the particle receives a correction Δx which is proportional to its own position error x, $\Delta x = \lambda \cdot x$, the error will change from x to x_C:

$$x_C = x - \underbrace{\lambda x}_{\textit{coherent, cooling term}} - \underbrace{\lambda \sum_{others} x_i}_{\textit{incoherent term, heating}} \tag{3}$$

where "others" denotes all particles in the sample except the particle considered. The correction of the particle due to its own error (coherent term) is thus disturbed by the other sample members (incoherent term, heating) having in general errors $x_i \neq x$. The last expression can be rewritten as

$$x_C = x - (\lambda N_s)\frac{1}{N_s}\sum_{i=1}^{N_s} x_i = x - g < x >_s \tag{4}$$

to include the "test" particle in the sum. On the right hand side of eq. 4 the "gain" $g = \lambda N_s$ has been introduced and $< x >_s$ is the sample average. From eq. 4 we conclude:

- Every particle in the sample receives a correction that is proportional to the sample average error.

Assume a beam with N particles which is centered, $< x >= 0$, and has the variance x^2_{rms} before cooling. Since $N_s \ll N$, the sample averages are in general not all zero. Instead they will fluctuate around zero. Averaging over all samples recovers the beam distribution with zero mean and variance as before cooling. Now, if the "gain" g in eq. 4 is equal to one, every sample is kicked on the axis, so that after one turn the sample averages are all zero. Averaging again over all samples gives the cooled beam with a reduced variance. This is demonstrated in an example given below.

To find the cooling equation for the horizontal (or vertical) beam variance x^2_{rms} the change Δx^2 in the squared error x^2, $\Delta x^2 = x_c^2 - x^2$ is considered. From eq. 4 it follows that taking the sample average of squared error and then averaging over all samples:

$$\Delta x^2_{rms} = -\frac{1}{N_s}(2g - g^2)x^2_{rms}. \tag{5}$$

This expression gives the *change in the beam variance per turn* during cooling.
The *cooling rate for the transverse beam variance* is then:

$$\frac{1}{\tau_{x^2}} = -\frac{1}{T}\frac{\Delta x^2_{rms}}{x^2_{rms}} = \frac{1}{N_s T}(2g - g^2)$$

or, using the sample size from eq. 2 we have the *cooling rate*

$$\frac{1}{\tau_{x^2}} = -\frac{2W}{N}(2g - g^2) \tag{6}$$

in which the bandwidth of the cooling system and the total particle number appear. This relation shows:

- *the cooling rate has its maximum for the optimum gain $g = 1$.*
- *the cooling rate increases with increasing bandwidth W*
- *stochastic cooling becomes a hard job with increasing particle numbers*
- *the gain must be greater then zero and less then 2.*

Lets make an example for sampling and cooling shown on the following table:

The "beam" can take on the three values $x = -1, 0, 1$ with equal probability. The "beam" is then centered with $< x >= (-1 + 0 + 1)/3 = 0$ and $< x^2 >= (-1^2 + 0^2 + 1^2)/3 = 2/3$. Take all samples of size $N_s = 2$, i.e. take all pairs out of $-1, 0, 1$. These 9 samples are listed in the left column of the table before correction. For all samples the sample average and sample variance, $< x^2 >_s$, are listed. Now apply to each sample member the correction $x \to x - < x >_s$ $(g = 1)$. The resulting sequence is labeled "After Correction". Now all sample averages are zero. Averaging over all nine sample averages and all nine sample variances shows that the variance is reduced from 2/3 to 1/3 "within one turn" corresponding to a relative change –1/2 according to eq. 5 with size $N_s = 2$.

Before Correction:				After Correction:			
Sequence:		Sample average $< x >_s$	variance $< x^2 >_s$	Sequence:		Sample average	variance
-1	-1	-1	1	0	0	0	0
-1	0	-1/2	1/2	-1/2	1/2	0	1/4
-1	1	0	1	-1	1	0	1
0	-1	-1/2	1/2	1/2	-1/2	0	1/4
0	0	0	0	0	0	0	0
0	1	1/2	1/2	-1/2	1/2	0	1/4
1	-1	0	1	1	-1	0	1
1	0	1/2	1/2	1/2	-1/2	0	1/4
1	1	1	1	0	0	0	0
mean:		**0**		mean:		**0**	
variance:			**2/3**	variance:			**1/3**
		average over 9 samples					

Now cooling will stop since all sample averages are zero so that in the next turn the correction would be zero. <u>However this is not true in practice</u>.

There is always **mixing**, i.e. the sample members will change due to the finite momentum spread in the beam. This results in a spread ΔT (see appendix A) in revolution time T of the particles. Consequently, the sample changes on its way from pickup to kicker, which is bad (bad mixing) and also from kicker to pickup, which is good (wanted mixing). So the kicker should be as close as possible to the pickup so that the sample which is to be corrected does not change. In practice one has to accept compromises, e.g. due to space constraints, as is the case for COSY.

In the example above one can simulate mixing by shifting above the gray column by one entry. The sample average is then again unequal to zero. Doing the same exercise one sees that the variance decreases from 1/3 to 1/6 in the second turn.

Equation 6 assumes a perfect mixing condition, i.e. after each turn a re-randomization takes place. A more realistic formula includes mixing from pickup to kicker as well as from kicker to pickup.

The resulting cooling equation is

$$\frac{1}{\tau_{x^2}} = -\frac{1}{x_{rms}^2}\frac{dx_{rms}^2}{dt} = \frac{2W}{N}\left\{2g(1-\frac{1}{\tilde{M}^2}) - g^2(M + U(x_{rms}^2))\right\} \quad (7)$$

- The mixing factor M that enters in the heating term graphically gives the number of turns a particle needs to migrate by one sample length. Optimum: $M = 1$. $M > 1$ means heating because a particle stays together with its "noisy" neighbours longer then one turn.

- The factor $1 - \frac{1}{\tilde{M}^2}$ takes into account the bad (unwanted) mixing from pickup to kicker. This factor should be close to one. Otherwise the correction (coherent term) becomes worse.

- In COSY the path lengths from pickup to kicker and from kicker to pickup are the same (see the arrangement of pickup and kicker below) to achieve cooling in the whole momentum range from 1.5 GeV/c to 3.4 GeV/c. Therefore, $M = \tilde{M}$ and the mixing factor M must be greater then one.

- The mixing factor is determined by the lattice optics (see appendix A): In COSY $M \approx 8$ so that the unwanted mixing can be neglected.

- Any electronic system contains noise. This noise will also drive the kicker and heats the beam. The larger the beam signal (particle number times pickup sensitivity times beam variance) is the less important noise is. Thus the quantity U which is the noise to signal ratio enters

the heating term. The value of U becomes small for large particle numbers.

To solve the differential equation 7 for the beam variance as a function of time one has to take into account that the noise to signal ratio U depends on the beam variance, $U \propto x_{rms}^{-2}(\infty)$. U increases during cooling, i.e. the heating term increases during cooling, so that cooling slows down. For constant gain g cooling will stop if both terms in the curly brackets of eq. 7 are equal: An equilibrium variance is reached. The solution of eq. 7 then gives an exponential decrease in the beam variance

$$x_{rms}^2(t) = \left\{x_{rms}^2(0) - x_{rms}^2(\infty)\right\} e^{\frac{-t}{\tau}} + x_{rms}^2(\infty) \tag{8}$$

with the *cooling* rate

$$\frac{1}{\tau} = \frac{2W}{N}\left\{2g - g^2 M\right\} \tag{9}$$

and the *equilibrium variance*

$$x_{rms}^2(\infty) \propto \underbrace{kT}_{\textit{thermal noise}} \frac{1}{ZN}\frac{g^2}{2g - g^2 M} \tag{10}$$

with the pickup sensitivity Z and particle number N. From eq. 9 follows that the gain must lie in the range $0 < g < 2/M$. The maximum cooling rate is achieved with the optimum gain $g = 1/M$.
Good cooling conditions:

- Cool the pickup structures (30 K at COSY) especially for small proton numbers and use low noise amplifiers to reduce the equilibrium variance.

- Increase the pickup sensitivity Z by moving the pickup electrodes close to the beam. This is done at COSY: At injection when the beam variance is large the electrodes are set to a distance so that no particle losses occur. At flat top when the variance is smaller (due to adiabatic shrinking) the electrodes are moved as close as possible to the beam. In machines where the initial beam variance is very large (e.g. the former AA at CERN) it is also helpful to reduce the distance of the electrode bars continuously during cooling.

- Adjust the gain to get the fastest cooling rate. It may also be helpful to reduce the gain during cooling.

4 Present Cooling System at COSY

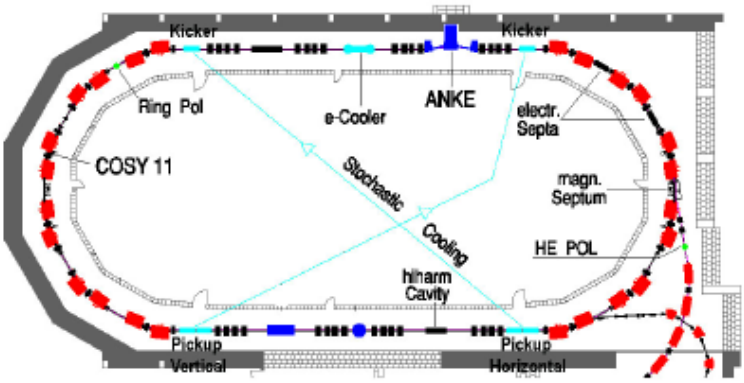

Figure 5:

- Freqeuncy range $(1-3)$ GHz, i.e. $W = 2$ GHz, divided into two bands:
  - band I: $(1-1.8)$ GHz
  - bandII: $(1.8-3)$ GHz
- Cooling: in all planes (horizontal, vertical and longitudinal) independently possible.
- Pickup:
  - Tank length: 4 m
  - 112 "single" loop pairs, mounted on electrode bars, are combined to give the beam signal.
  - the electrodes are cooled down to 30 K.
  - the electrode bars can be moved by 60 mm.
- Kicker:
  - Tank length: 2 m
  - 56 "single" loop pairs
  - the electrode bars can be moved by 60 mm.
- Total rf power: 1 kW
- Position of pickups and kickers: The diagonal signal paths were chosen due to space constraints and to realize cooling in the large momentum range with only two systems (cost!).

- System

vertical cooling	Band I + Band II
horizontal cooling	Band II only
longitudinal cooling (filter method)	Band I only

5 Results

In June 1997 the first vertical cooling experiments were carried out. Vertical beam profiles of a beam with $N = 2 \cdot 10^9$ protons at a momentum p = 2.6 GeV/c were measured with the EDDA detector. Only the cooling band I (1 − 1.8) GHz was used and the system was not optimized at that time. From the vertical beam variance σ^2 at the EDDA location with beta function $\beta = 4\,\mathrm{m}$ the beam emittance $\varepsilon = 6\,\sigma^2/\beta$ was calculated and is plotted versus time in figure 6.

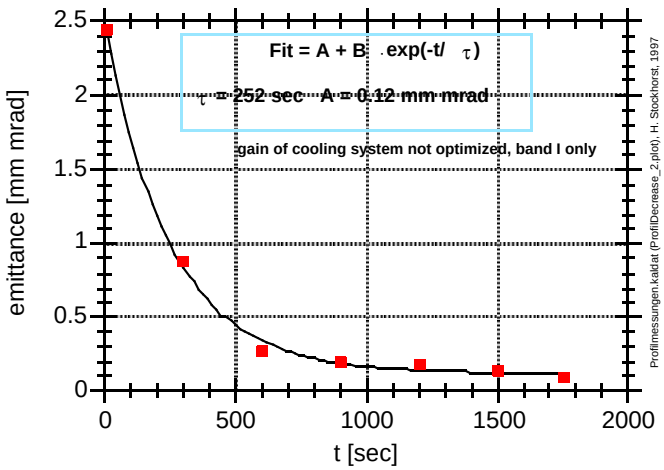

Figure 6:

The figure shows the exponential decrease in emittance according to eq. 8. The initial emittance is reduced by about a factor of 20. However the measured cooling rate 1/(252 s) is far away from the optimum cooling rate expected from eq. 9 in the range $1/\tau \approx 1/(20\,\mathrm{s}) - 1/(40\,\mathrm{s})$. Meanwhile the gain and the phase of the cooling system can be adjusted so that the cooling rates come close (within a factor of two to three) to the expected cooling rates (without internal targets). Figure 7 shows the benefit from stochastic

cooling in all three phase space planes for the COSY-11 experiment.

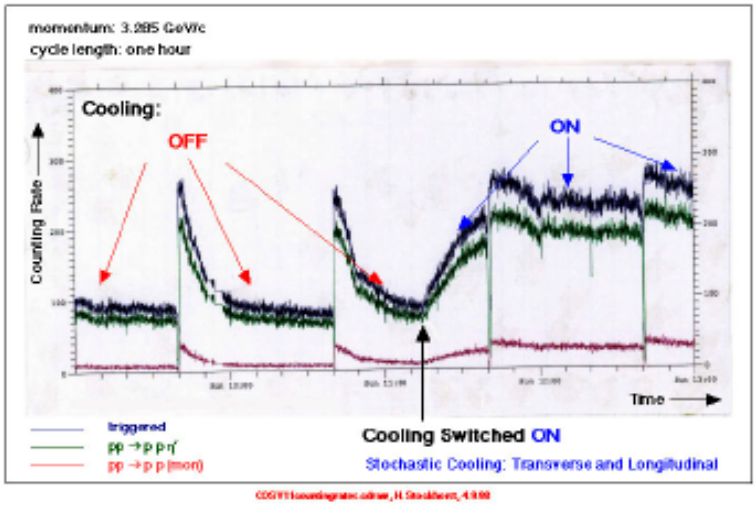

Figure 7:

References

Stochastic cooling was invented by S. van der Meer (CERN, Nobel prize 1984). He published his idea in the CERN-note CERN/ISR-PO/72-31 in the year 1972. Since then hardware studies started and first stochastic cooling was observed at CERN in 1975. In the following years the cooling hardware could be significantly improved. L. Thorndahl (CERN) invented the filter method for longitudinal cooling. Also the cooling theory including signal processing was further developed. A very detailed discussion of stochastic cooling and its application to increase beam quality and intensity at different laboratories (CERN, FERMILAB, GSI (cooling of heavy ions)) together with a lot of additional references as well as an historical review can be found in:

D. Möhl, *Stochastic Cooling*, CERN ACCELERATOR SCHOOL, CERN 87-03 (1987) 453.

D. Möhl, *Stochastic Cooling for Beginners*, CERN ACCELERATOR SCHOOL, CERN 84-15 (1984) 97.

Appendix A

Transition Energy Suppose a particle of momentum p_0 circulates in a ring with mean radius R_0, determined by the magnetic dipole field B. If v_0 is the particle velocity then the revolution frequency is

$$f_0 = \frac{v_0}{R_0}$$

If the mean velocity is close to the speed of light <u>only</u> the radius R_0 will increase when the momentum is slightly increased by $\Delta\mathrm{p}$ at <u>fixed</u> magnetic field B. In this case the revolution frequency will decrease with increasing momentum! On the other hand, at low velocities, both velocity and radius will increase when the momentum is increased by $\Delta\mathrm{p}$. However the relative velocity change is greater than the relative radius change so that the revolution frequency will increase.

- Thus there is an intermediate energy, called transition energy, at which a change in momentum does not alter the frequency. In other words, if we have a momentum distribution at transition then particles with different momenta will all circulate with the same revolution frequency.

Formally this can be written as

$$\frac{\Delta f_0}{f_0} = \left\{ \frac{1}{\gamma^2} - \frac{1}{\gamma_{tr}^2} \right\} \frac{\Delta \mathrm{p}_0}{\mathrm{p}_0} = \eta \frac{\Delta \mathrm{p}_0}{\mathrm{p}_0} \tag{11}$$

where $\gamma^2 = \left\{1 - (v_0/c)^2\right\}^{-1}$ and the kinematic factor at transition energy is labeled with "tr". The value of transition energy of γ_{tr} depends on the optics of the COSY ring. In the standard lattice of COSY $\gamma_{tr} \approx 2$. However during acceleration focusing is continuously changed to shift the transition energy upwords in order to avoid beam instabilities at transition (see COSY News No. 9 (2000)).

- Relation 11 shows that the momentum spread of the beam can be determined if the frequency spread and the "frequency slip factor" η are measured.

The spread in revolution frequency corresponds to a spread in revolution times $\Delta T_0/T_0 = -\Delta f_0/f_0$.
Thus in order to have good mixing from kicker to pickup one must stay away from transition energy. At COSY-11 energies $\eta \approx -0.1$.

Track reconstruction in the hexagonal drift chamber

C. Kolf

Institut für Kernphysik, Forschungszentrum Jülich, Germany

Abstract: Based on studies on the drift behaviour of electrons in hexagonal cells, distance-to-drifttime relations (calibrations) for the COSY-11 hexagonal drift chamber were developed. A first version for track recognition and track reconstruction in the chamber is available.

1 GARFIELD simulations

With the simulation programme GARFIELD [1], several studies on the drift behaviour for hexagonal cells of the new COSY-11 hexagonal drift chamber [2] were performed. Figure 1 (left side) shows an isochrone plot, i.e. lines with equal drifttime, with the P10 gas mixture used in the current setup.

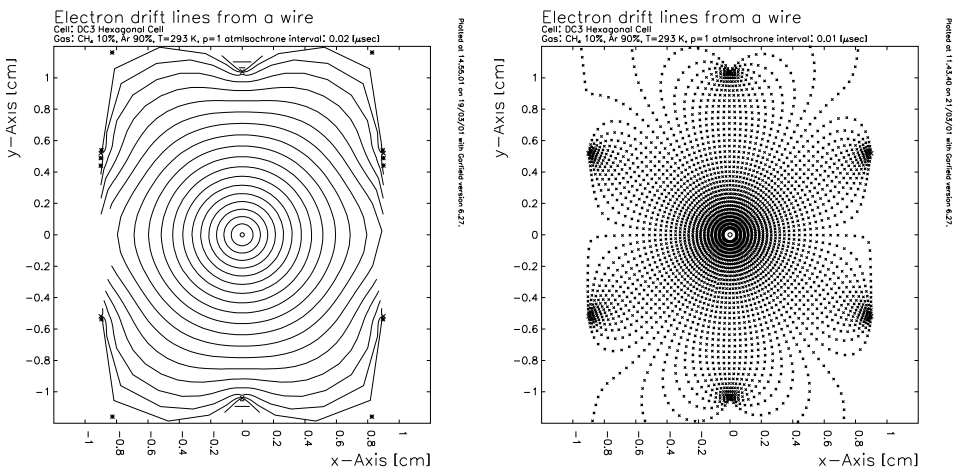

Figure 1: *left:* isochrone plot (interval: 20 ns), *right:* digitized isochrones

It turns out that the isochrones are not radially symmetric, which means that the distance-to-drifttime relation $r(t)$ depends on the track angle of the particle crossing the chamber.

After digitization of the isochrones (see right side of figure 1), angle-dependant 'lookup-tables' were created (see also figure 5), thus allowing a calibration $r(t, \alpha)$, where α denotes the track angle.

Another result of the GARFIELD studies is that the position of neighbouring detection planes does not affect the distance-to-drifttime relation. Figure 2 shows that the calibrated distance in one cell differs by less than $50\,\mu$m for the cases of an identical neighbouring plane and an adjacent plane shifted by half a cell width, respectively.

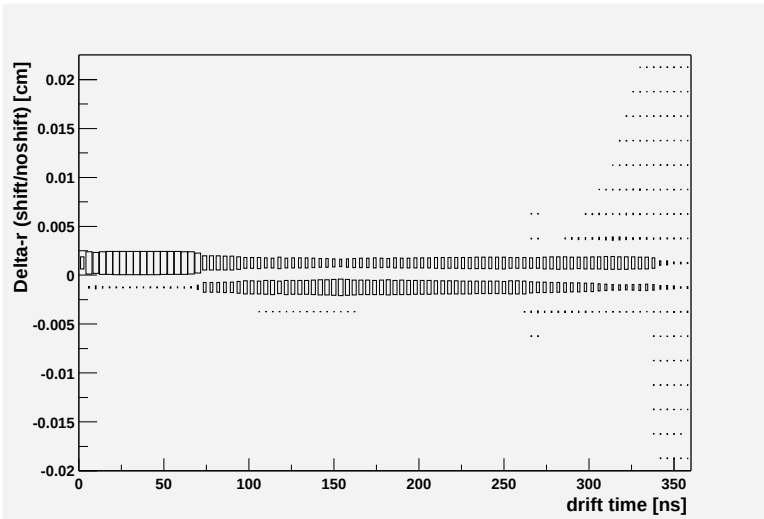

Figure 2: Difference in $r(t)$ for an identical neighbouring plane and a plane shifted by half a cell width.

2 Reconstruction

The reconstruction in the hexagonal drift chamber consists mainly of the steps described in the next subsections:

2.1 DSC level Data Monitoring

The first part of the reconstruction program reads the COSY-11 detector-subdector-channel (DSC) data, with which one can control the drifttime spectra and optimize them with respect to operating voltage and discriminator threshold. Another part performs an "event display" and is useful to detect inefficiencies in the chamber and to show the topology of an event (multiplicity, number of fired adjacent cells, ...), see figure 3.

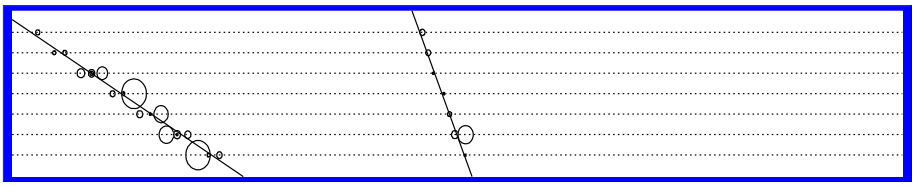

Figure 3: Event display with reconstructed tracks.

2.2 Track recognition

The track recognition combines every hit in the first and last (7th) plane of the chamber to a possible track candidate. The number of hits in a corridor of 2 cm width around this candidate are counted and those with less than 5 hits in the corridor are rejected for the following reconstruction code. Thus one reduces the number of track candidates roughly by a factor of 2 to 3, without losing real physical tracks.

2.3 Fit straight line

If one neglects the influence of a magnetic field at the position of the drift chamber (the maximum field strength is less than 15 mT), the track model is just a straight line. Starting with the line between a hit in the first and last plane, a χ^2 value is calculated as the sum of the distances between the assumed line and the drift circle calculated with the drifttime-to-distance relation $r(t, \alpha)$. Minimization of the χ^2 yields the track parameters (slope and position) after 3 or 4 iterations.

2.4 χ^2 Determination

The smallest χ^2 values are taken as the results of the reconstruction. First reconstructed tracks in the event display seem to be reasonable, figure 3

shows a typical two-track event recorded in the COSY-11 data taking period of March/April 2001.

2.5 Calibration Improvement by iterative procedure

The difference between measured and fitted distances of the tracks from the sense wire for each time t_i corresponding to the TDC channel i is calculated for each track angle α:

$$\Delta r(\alpha, t_i) = \langle r^{exp}(\alpha, t_i) \rangle - r(\alpha, t_i) \qquad \alpha = \text{const.}$$

The distance-to-drifttime relation of the first step is corrected:

$$r'(\alpha, t_i) = r(\alpha, t_i) + \Delta r(\alpha, t_i)$$

and the track reconstruction is performed again with the new $r'(\alpha, t_i)$. First results show that there is still an underlying structure in the plots of the difference Δr (see figure 4).

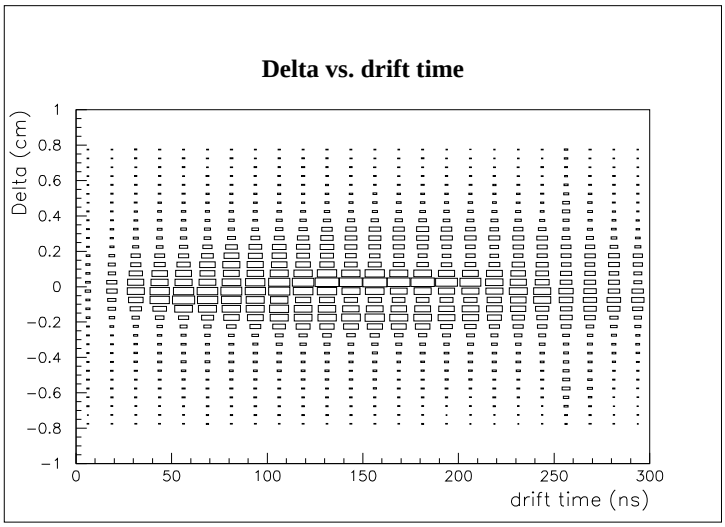

Figure 4: Difference between measured and fitted distances versus drifttime.

Further investigations on these Δr plots show a strong dependance on the starting calibration. The different starting calibrations used in the analysis (see figure 5) are calculated by means of GARFIELD simulations and with

the 'uniform irradiation method' [3] (labelled 'integrated drifttime spectrum' in figure 5).

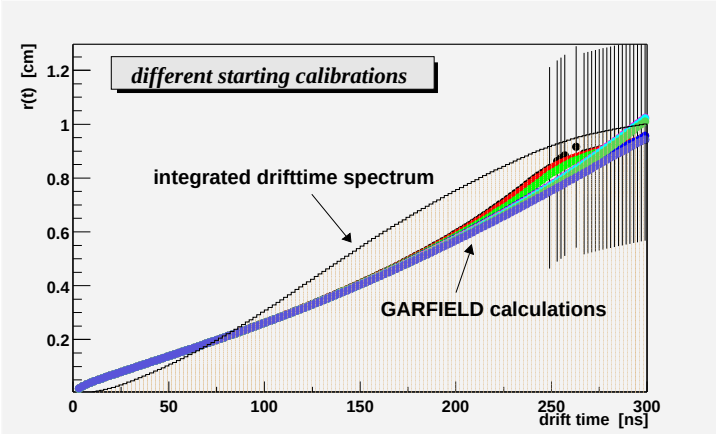

Figure 5: Different starting calibrations used for the reconstruction.

To apply the iterative procedure, further investigations on the calibrations are needed, also taking effects of the COSY dipole's stray field into account. Furthermore, the so far 2-dimensional reconstruction has to be extended into 3 dimensions by means of the information of the inclined wires.

References

[1] R. Veenhof, *GARFIELD, Simulation of gaseous detectors, Version 7.04*, CERN, Geneva (2001).

[2] J. Smyrski, Annual Report 1998, IKP, Forschungszentrum Jülich, **Jül-3640** (1999) 41.

[3] A. Breskin et. al., Nucl. Instr. & Meth. **119** (1974) 9.

Reduction of pion background by means of Čerenkov detector; can we measure the $pp \to n\Sigma^+K^+$ reaction?

M. Siemaszko

Institute of Physics, University of Silesia, Katowice, Poland

Abstract: A description is given of the new threshold Čerenkov detector for the COSY-11 facility. Possible role and operation of this detector for the purpose of reduction of pion background for the reaction $pp \to n\Sigma^+K^+$ in the threshold region is briefly discussed.

1 Introduction

The strong suppression of Σ^0 production compared to Λ production at the same excess energies observed experimentally in the reactions $pp \to p\Sigma^0K^+$ and $pp \to p\Lambda K^+$ near threshold [1] has been recently studied theoretically [2]. It is shown in [2] that this suppression can be explained by a destructive interference between π and K exchange in the reaction $pp \to p\Sigma^0K^+$. The authors discuss also the consequences of application of their model to the reaction $pp \to n\Sigma^+K^+$. Unfortunately the only existing experimental data for this reaction were taken at high excess energies (five experimental points were measured in the Q range from 350 to 1200 MeV [3]). Therefore, as it was also pointed out in [2], it would be interesting to measure this reaction at threshold energies and estimate for example the experimental cross section ratios $\sigma_{pp\to n\Sigma^+K^+}$ / $\sigma_{pp\to p\Sigma^0K^+}$ in that energy region. In section 3 we discuss briefly some experimental difficulties which one can expect for this particular reaction at threshold energies.

2 Čerenkov detector: design, construction and principles of operation

Design of the Čerenkov detector consisting of a radiator, eight scintillation detectors, a degrader and support has been performed at the Institute

of Physics, University of Silesia in Katowice (Poland). The radiator was constructed in the mechanical workshop at the University of Silesia. Scintillation counters, degrader and support were supplied by IKP Jülich. In July 2000 the Čerenkov detector has been installed at the COSY-11 experimental setup [4]. It has been placed behind the existing S1 scintillation detector (see schematic view in fig. 1).

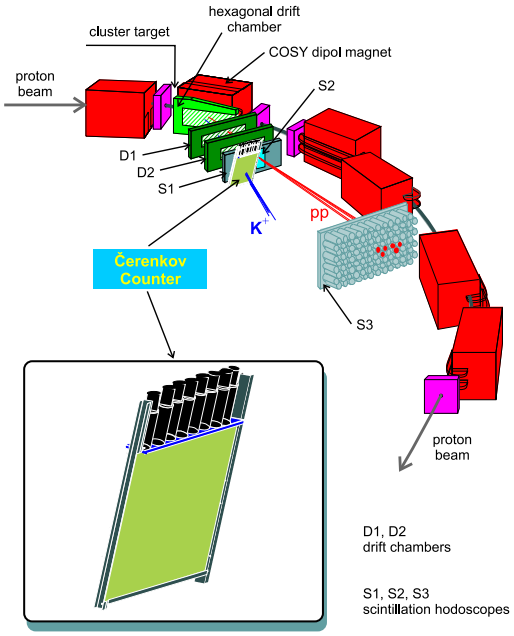

Figure 1: Schematic view of the COSY-11 detection setup with the new Čerenkov detector.

The radiator of the Čerenkov detector has a rectangular shape of dimensions $85 \times 85 \times 5\,\mathrm{cm}^3$ (HWD). Inner parts of two squared walls (front and back sides) made of 2.5 mm thick iron-plates (type H17) form the reflecting layers. Additionally, three rectangular ribbons of the same material are glued to the aluminum frame of the radiator (left, right and bottom sides). As a medium in which Čerenkov radiation arises pure water has been used. In the upper part of the radiator there are eight photomultipliers supplied with cylindrical plastic light guides (95 mm length, 40 mm diameter) which serve as a readout. During some test measurements we tried also a wavelength shifter (Polyphenyl 2) which added to the water improves matching of the Čerenkov light with spectral sensitivity of the scintillation counter photocathode.

The radiator, with the scintillation counters attached, can be inclined with respect to the direction of incoming particles. This feature allows to optimize conditions of reflection of the Čerenkov light inside the radiator. For a particular reaction an optimal inclination angle can be chosen by performing a simulaion of propagation of the Čerenkov light inside the radiator. Fig. 2 shows the new Čerenkov detector in the COSY ring.

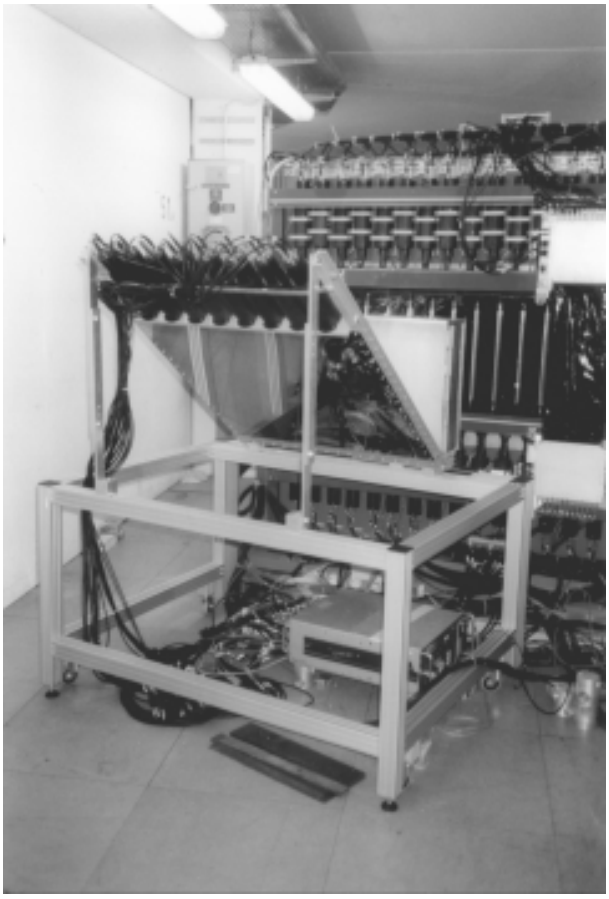

Figure 2: The place of the Čerenkov detector in COSY.

The Čerenkov detector works in a threshold regime, i.e. no Čerenkov radiation is produced until the particle velocity exceeds $\beta_t = 1/n$ (since $n = 1.33$ for water one has $\beta_t = 0.75$). This, for example, allows to distinguish between two particles, provided the velocity of one of them is below the Čerenkov threshold velocity. In our case we would like to distinguish kaons and pions. However, for a particular proton beam momentum, the maximum

β value of the outgoing K^+ can exceed β_t for water. Therefore in front of the radiator there is a lead degrader of which thickness and shape can be easily adjusted for particular reaction conditions.

The Čerenkov detector has been used for the first time during measurements of the reactions $pp \to pK^+\Lambda$ and $pp \to pK^+\Sigma^0$ close to their thresholds in July 2000. In this experiment $\Lambda(\Sigma^0)$-production at equivalent excess energies in the range from 14 MeV to 60 MeV has been measured. Application of the new Čerenkov detector allowed a significant reduction of the pion background [5]. In addition, during March/April 2001 beam time, various tests of functioning of the Čerenkov detector were carried out. These data are currently analyzed.

3 The reaction $pp \to n\Sigma^+K^+$

The threshold momentum for this reaction is $p_{thr} = 2560.5$ MeV/c. In the exit channel one has two short lived charged particles ($\tau_{\Sigma^+} = 0.80 \times 10^{-10}$ s and $\tau_{K^+} = 1.24 \times 10^{-8}$ s). This feature causes certain experimental problems concerning particle identification. Assuming that one has an effective neutron detector, the main difficulty is to identify shortly living K^+ by the time of flight method. Positively charged kaons do not reach the S3 detector ($c\tau = 3.7$ m for K^+). Therefore one has to measure time of flight of K^+ between an additional scintillation detector placed close to the exit window in the vacuum chamber (start signal) and the S1 detector (stop signal). Then the Σ^+ hyperon can be identified by the missing mass method. Since in that type of reaction we are able to register only a fraction of outgoing K^+ and one knows that concurrent multi-pion production reactions occur, one has to take into account an elimination of pion background. This would be possible by application of the threshold Čerenkov detector.

Applying the EVD program package we have performed several simulations for the reaction $pp \to pK^+\Sigma^0$. This program version takes into account the new Čerenkov detector. As an example we show the results of calculations for two proton beam momenta, namely $p_{beam} = 2.602$ GeV/c and $p_{beam} = 2.740$ GeV/c, corresponding to excess energies of 14 MeV and 60 MeV, respectively. Fig. 3 shows the calculated histograms representing the number of K^+ and π^+ hits in the Čerenkov detector as a function of their velocities (in units of β) for these two excess energies. One clearly sees that for both cases, in order to fully discriminate kaons, one has to apply a degrader of which thickness and preferable shape should be estimated for given proton beam momenta.

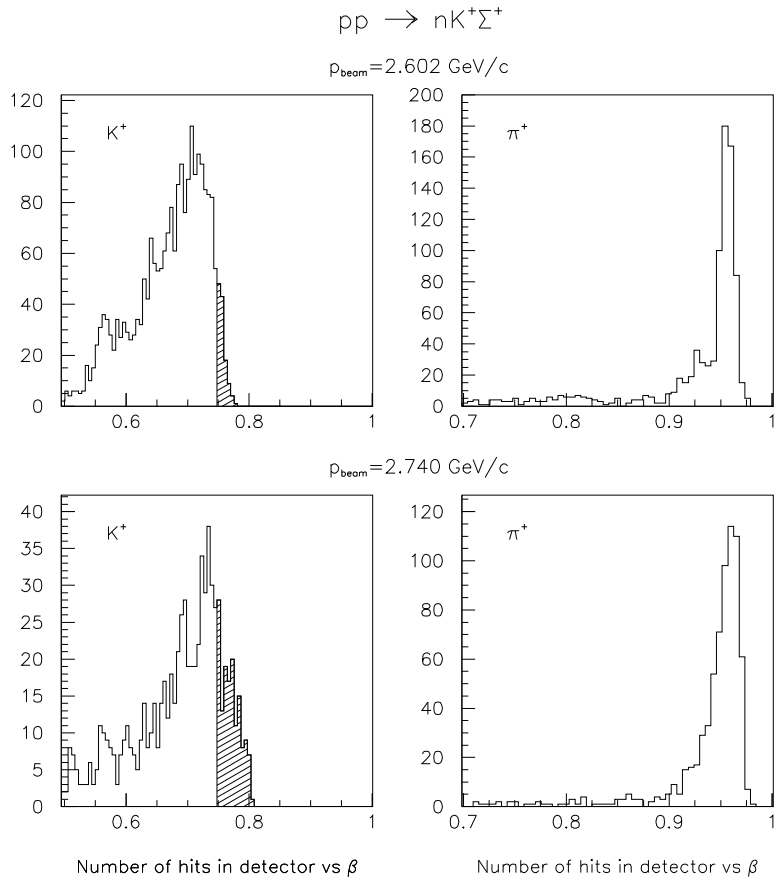

Figure 3: Simulated histograms showing the number of K^+ and π^+ hits in the Čerenkov detector as a function of their velocities. Calculations were done for two different proton beam momenta. Hatched areas correspond to kaon events for which β exceeds β_t.

4 Conclusions

To summarize, we have described the design, construction and principles of operation of the new Čerenkov detector for the COSY-11 facility. Its applicability has been demonstrated during measurements of the reactions $pp \to pK^+\Lambda$ and $pp \to pK^+\Sigma^0$ near threshold [5]. Therefore, we can also expect similar results for the reaction $pp \to nK^+\Sigma^+$, provided one has functioning neutron detector [6] and additional start detector (installation of such detector has been completed recently). Further tests of the Čerenkov detector based on the data collected during March/April 2001 beam time

are in progress.

References

[1] S. Sewerin et al., Phys. Rev. Lett. **83** (1999) 682.

[2] A.M. Gasparian et al., Phys. Lett. **B 430** (2000) 273.

[3] V. Flaminio at al., *Compilation of cross sections*, CERN-HERA report 84-01 (1984).

[4] S. Brauksiepe et al., Nucl. Instr. & Meth. **A 376** (1996) 397.

[5] P. Kowina, contribution to these proceedings.

[6] P. Moskal, contribution to these proceedings.

Energy dependence of the $\Lambda/\ \Sigma^0$ cross section ratio

Piotr Kowina[a,b]

[a] *Institute of Physics, University of Silesia, Katowice, Poland*
[b] *Institut für Kernphysik, Forschungszentrum Jülich, Germany*

Abstract: The first part of the talk presents the latest results of the analysis of the near threshold Λ and Σ^0 production via $pp \to pK^+\Lambda/\Sigma^0$ at COSY–11. The second part describes effects of using the Čerenkov counter for the reduction of the pion background.

1 New results of the analysis of Λ and Σ^0 production

Measurements of the near threshold Λ and Σ^0 production via the reactions $pp \to pK^+\Lambda/\Sigma^0$ at COSY-11 [1] showed a strong discrepancy compared to high energy data [2]. Close to threshold at excess energies $Q \leq 13\,\mathrm{MeV}$ the Λ/Σ^0 cross section ratio has been determined to be 28^{+6}_{-9} which exceeds the value at high excess energies ($Q \geq 150\,\mathrm{MeV}$) of about 2.5 by an order of magnitude.

To explain this behaviour different theoretical investigations have started. Calculations within a meson exchange model taking into account pion and kaon exchange [3] reproduce the measured ratio by a destructive interference of π and K exchange amplitudes. Within a factor of 2 also other models manage to describe the data by including heavier exchange mesons and/or nucleon resonances [4, 5].

Since the theoretical predictions were described in [6], this contribution rather concentrates on the experimental results.

In two runs during December 1999 and July 2000 the energy dependence of the Λ/Σ^0 cross section ratio was investigated at COSY-11.

The measurement of the reaction channels $pp \to pK^+\Lambda$ and $pp \to pK^+\Sigma^0$ were performed at the internal COSY-11 cluster target using the standard missing mass technique. The fours-momentum vectors of the final state proton and K^+-meson were measured with the COSY-11 detection system from which a missing mass distribution has been extracted.

Preliminary results were already published in the last IKP Annual Report [7]. In the further analysis several aspects were improved. For instance a more precise calibration of the scintillator hodoscopes, gave better resolution of the calculated invariant mass. Also a better calibration of the drift chambers reduced inaccuracy of the momentum determination. This results in a better identification of the K^+ in the exit channel. All these improvements allow to reduce the background, and extract the results with a smaller statistical error.

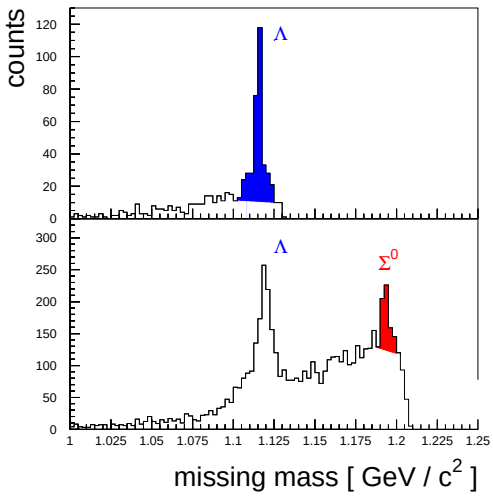

Figure 1: Missing mass distributions resulting from events with an identified proton and a K^+ for beam momenta of 2.386 GeV/c and 2.614 GeV/c corresponding to an excess energy of 16 MeV for Λ (upper part) and Σ^0 (lower part) production, respectively.

In fig. 1 the missing mass spectra for the threshold production of Λ and Σ^0 hyperons are given, both at an excess energy of 16 MeV. The peaks of the produced hyperons are clearly seen. Still — especially at the higher beam momentum — there is a rather large background. Attempts to reduce the background with using Čerenkov counter will be described later on. Results of our new analysis for the excitation function for the production ratio of the two hyperons at the same excess energy are given together with former results in fig. 2. New data points (marked as diamonds) for excess energies $Q = 14, 16, 20$ MeV lead to the same points in comparision to the results of the former analysis. Anyhow the error bars are slightly smaller.

An excess energy range up to 60 MeV is covered by the data which suggest a strong decrease of the ratio in the excess energy range between 10 and 20 MeV.

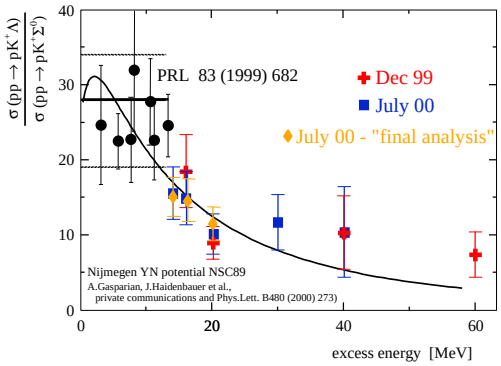

Figure 2: Cross section ratio of Λ/Σ^0 production as a function of the excess energy. Data have been taken during two beam times in December 1999 and July 2000. To increase the statistics at 16, 20 and 40 MeV data have been taken at both beam times.

2 Reduction of the pion background using the Čerenkov counter

As it was mentioned in the previous section hyperon signals are measured above a relatively large background. This seems to be mainly due to a misidentification of pions as kaons in the exit channel. In fig. 3 the invariant mass squared of the second particle is given (first particle was identified as a proton). One can easily find, that a kaon peak (on linear scale on y-axis) indicated by the arrow is almost not seen in a tail of the pion peak. So our aim was to reduce the pion signal. For this purpose a Čerenkov counter has been built [8], and has been used for the first time during measurements of the reactions $pp \to pK^+\Lambda$ and $pp \to pK^+\Sigma^0$ in July 2000.

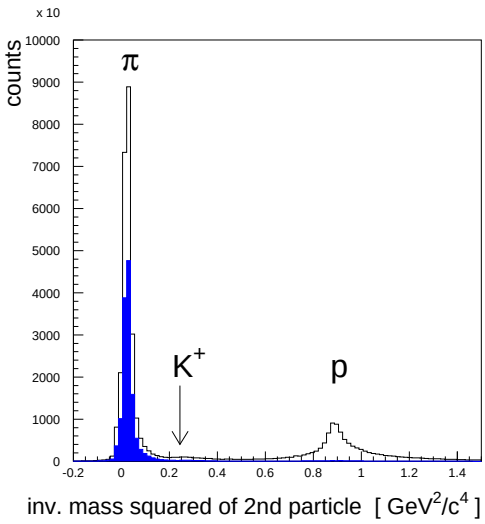

Figure 3: Invariant mass squared of the second particle for the events without and with (dashed area) the usage of a signal by the Čerenkov counter. The arrow depicts the area where a kaon enhancement is expected.

Particles which were detected by the Čerenkov counter are indicated in fig. 3 as a dashed area. Using the Čerenkov detector as a veto results in a reduction of the pion signal by a factor of three.

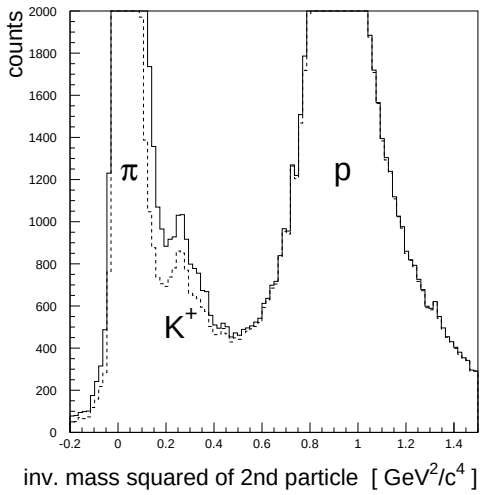

Figure 4: Reduction of the pion background under the kaon signal with the use of veto by Čerenkov counter (dashed line).

Changing the scale a clear K^+ enhancement is seen in fig. 4. The effect of using the Čerenkov counter is indicated by the dashed line. In the kaon range the reduction of the pion background is in the order of 20 %. However, the integrated number of kaons above the pion tail remains unchanged, i.e. the kaon yield is not reduced.

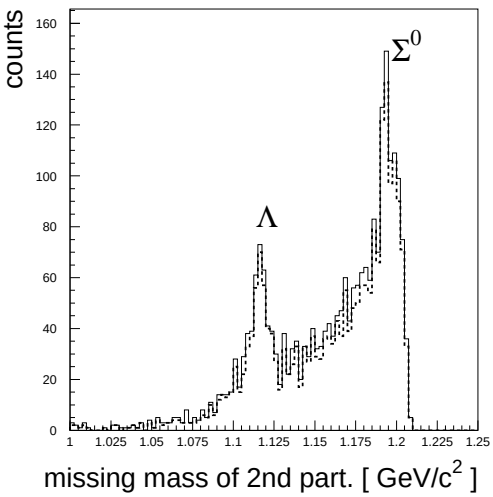

Figure 5: Reduction of the background in the missing mass spectrum using Čerenkov counter. Only those events were taken, for which the second particle was passing through the area covered by the Čerenkov counter.

In result, the background under the Σ^0 signal observed in the missing

mass spectrum (Fig. 5) is reduced by only 8 %. This seems to be a hint that the background might have another origin than misidentification of particles. This could be other reaction channels like $pp \to pK^+\Lambda\gamma$. Those possibilities will be checked in the further analysis using Monte Carlo simulations.

The relatively small efficiency of the Čerenkov detector can be explained by the low quality of the surface of the mirror walls. Also one can expect improvements in the program code used in the offline analysis. Tests described in [8] performed in March 2001 should also give a clue what one can do to increase the quality of the discrimination of particles.

References

[1] S. Sewerin, G. Schepers et al., Phys. Rev. Lett. **83** (1999) 682.

[2] V. Flaminio at al., *Compilation of cross sections*, CERN-HERA report 84-01 (1984).

[3] A. Gasparian et al., Phys. Lett. **B 480** (2000) 273.

[4] A. Sibirtsev et al., e–Print Archive: nucl–th/0004022.

[5] R. Shyam, G. Penner, U. Mosel, Phys. Rev. **C 63** (2001) 022202.

[6] A. Gasparian, contribution to these proceedings.

[7] P. Kowina, D. Grzonka, Annual Report 2000, IKP, Forschungszentrum Jülich, **Jül-3852** (2001) 45.

[8] M. Siemaszko, contribution to these proceedings.

Theoretical explanations for the energy dependence of the Λ/Σ^0 cross section ratio? [1]

A. Gasparyan[a,b], J. Haidenbauer[a], C. Hanhart[a], L. Kondratyuk[b]

[a] *Institut für Kernphysik, Forschungszentrum Jülich, Germany*

[b] *Institute of Theoretical and Experimental Physics, Moscow, Russia*

Abstract: A model calculation for the reactions $pp \to p\Lambda K^+$ and $pp \to N\Sigma K$ near their thresholds is presented. It is argued that the experimentally observed strong suppression of Σ^0 production compared to Λ production at the same excess energy could be due to a destructive interference between the π and K exchange contributions in the reaction $pp \to p\Sigma^0 K^+$. Predictions for $pp \to p\Sigma^+ K^0$ and $pp \to n\Sigma^+ K^+$ are given. It is shown that in order to explain the energy dependence of the Λ/Σ^0 cross section ratio a more detailed dynamics should be included.

1 Introduction

Recently the total cross sections for the reactions $pp \to p\Lambda K^+$ and $pp \to p\Sigma^0 K^+$ were measured for the first time near their thresholds, and specifically at the same excess energies [1, 2]. It was found that the cross section for the Σ^0 production is about a factor of 30 smaller than the one for the Λ production [2]. This is rather surprising because data at higher energies [3] indicate that the cross section for Λ production exceeds the one for Σ^0 production only by a factor of around 2.5.

We want to report on an exploratory investigation of the origin of this strong suppression of the near-threshold Σ^0 production [4]. Specifically we want to examine a possible explanation that was suggested in ref. [2], namely effects from the strong ΣN final state interaction (FSI) leading to a $\Sigma N \to \Lambda N$ conversion. Evidence suggesting this conversion hypothesis can be readily found in the literature. E.g., the predictions of modern meson-theoretical models of the hyperon-nucleon YN interaction for the ΛN cross section show a large cusp structure at the ΣN threshold, which arises from the strong coupling between the ΛN and ΣN channels in those models [5]. Inclusive measurements of K^+ production in the reaction $pp \to K^+ X$ at 2.3 GeV show a significant enhancement near the ΣN threshold [6]. Finally, data on the reaction $K^- d \to \pi^- \Lambda p$ show a sharp peak at an effective mass of

[1] Invited talk

$m_{\Lambda p} \approx 2130\,\mathrm{MeV/c^2}$, i.e. at the ΣN threshold [7]. Thus, it is obvious that there is a strong enhancement of the Λ counting rate in those reactions. However, it is much less clear whether this enhancement is indeed due to produced "real" Σ's being converted into Λ's in the FSI so that the number of experimentally observed Σ's in any exclusive measurement will be greatly reduced.

2 The model

We assume that the strangeness production process is governed by the π- and K-exchange mechanisms as depicted in fig. 1. In order to have a solid basis for our study of the final-state effects we employ a microscopic YN interaction model from the Jülich [5] group. The Jülich YN model is derived in the meson-exchange picture and has been constructed according to the same guidelines as those used in the Bonn NN potential [8]. The model is given in momentum space and contains the full nonlocal structure resulting from the relativistic meson exchange framework. The parameters at the NN vertices (coupling constants and cutoff masses in the form factors) are taken from the Bonn potential. The coupling constants at the strange vertices are determined from $SU(6)$ symmetry relations. The only free parameters in this model are the cut-off masses of the form factors at the strange vertices - which are determined by a fit to the empirical hyperon-nucleon data. The model describes existing ΛN and ΣN observables reasonably well as can be seen in ref. [5].

We treat the associated strangeness production in the standard distorted wave Born approximation. Thus, the production amplitude M is obtained from the formal equation

$$M \;=\; A \;+\; AG_0T_{YN}\;, \tag{1}$$

where A is the elementary production process (π- and/or K-exchange, fig. 1), T_{YN} the interaction in the final state, and G_0 the free YN propagator. Note that the second term on the right-hand side involves, in fact, a sum over the (coupled) ΛN and ΣN states.

The vertex parameters (coupling constants, form factors) appearing at the πNN and KNY vertices in the production diagrams in fig. 1 are taken over from the Jülich YN interaction. The elementary amplitudes T_{KN} and $T_{\pi N\to KY}$ can be taken from microscopic models of KN scattering [9] and of the reaction $\pi N \to K\Lambda, K\Sigma$ [10] that were developed by our group. However, since in the present more exploratory study we would like to focus

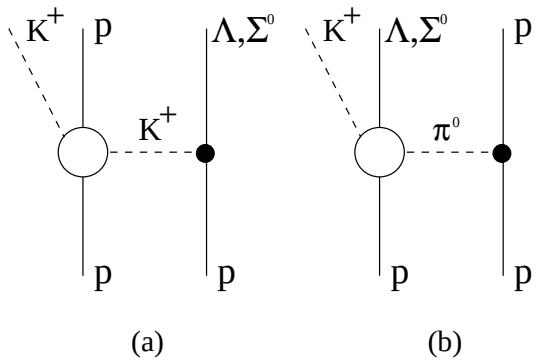

Figure 1: Mechanisms for the reactions $pp \to p\Lambda K^+, p\Sigma^0 K^+$ considered in the present investigation: (a) kaon exchange; (b) pion exchange.

mainly on the FSI effects we will restrict ourselves to a simplified treatment of the production amplitude. Thus, instead of the full (off-shell) KN and $\pi N \to KY$ transition amplitudes we use the scattering length and on-shell threshold amplitudes of those reactions. The off-shell extrapolation of the amplitudes is done by multiplying those quantities with the same form factor that is used at the vertex where the exchanged meson is emitted. Furthermore we take into account only S-waves.

Since we will concentrate on energies very close to the thresholds we consider only the lowest partial waves in the outgoing channels; the Λp and $\Sigma^0 p$ system can be in a $^1S_0$ or in a $^3S_1$ state and the K^+ is assumed to be in an S-wave relative to the YN state. Angular momentum and parity conservation then tells us that the initial pp system has to be in the $^3P_0$ or in the $^3P_1$ state. Note that the $^3S_1$ partial wave couples to the $^3D_1$ and this coupling is taken into account in our calculations.

We do not take into account the initial state interaction (ISI) between the protons. Based on a recent examination of the influence of the ISI for the reaction $pp \to pp\eta$ by Batinić et al. [11] we expect that the neglection of the ISI should result in an overestimation of the cross sections by a factor 2 to 3 in our calculation. But since the thresholds for the Λ and Σ^0 production are relatively close together (at $T_{lab} = 1582\,\mathrm{MeV}$ and at $T_{lab} = 1796\,\mathrm{MeV}$) and, moreover, the energy dependence of the NN interaction is relatively weak in this energy region we expect that the ISI effects are very similar for the two strangeness production channels and therefore should roughly drop out when ratios of the cross sections are taken. Thus, we believe that our model calculation allows a quite reliable estimation of $\sigma_\Lambda/\sigma_{\Sigma^0}$. The same is also true for a comparison of the relative magnitude of the pion- and kaon-exchange contributions.

3 The results

Let us first discuss the K-exchange. The cross section ratio based on the Born diagram alone (term A in eq. 1) is 16, cf. table 1. Including the YN FSI, i.e. possible conversion effects $\Sigma N \to \Lambda N$, leads to a strong enhancement of the cross section in the Λ channel but only to a moderate enhancement in the Σ^0 channel. As a consequence, the resulting cross section ratio becomes significantly larger than the value obtained from the Born term and, in fact, exceeds the experimental value. In case of pion exchange the Born diagram yields a cross section ratio of 0.9. Adding the FSI increases the cross section ratio somewhat, but it remains far below the experiment.

Thus, it's clear that, in principle, K-exchange alone could explain the cross section ratio - especially after inclusion of FSI effects. However, we also see from table 1 that π-exchange is possibly the dominant production mechanism for the Σ^0 channel and therefore it cannot be neglected. Indeed, the two production mechanisms play quite different roles in the two reactions under consideration. K-exchange yields by far the dominant contribution for $pp \to p\Lambda K^+$. The influence from π-exchange is very small. In case of the reaction $pp \to p\Sigma^0 K^+$, however, π- and K-exchange give rise to contributions of comparable magnitude. This feature becomes very important when we now add the two contributions coherently and consider different choices for the relative sign between the π- and K-exchange amplitudes.

Table 1: Total cross section of the reactions $pp \to p\Lambda K^+$ (σ_Λ) and $pp \to p\Sigma^0 K^+$ (σ_{Σ^0}) at the excess energies Q = 13.2 MeV (σ_Λ) and Q = 13.0 MeV (σ_{Σ^0}).

diagrams	$\sigma_{pp\to p\Lambda K^+}$ [nb]	$\sigma_{pp\to p\Sigma^0 K^+}$ [nb]	$\frac{\sigma_{pp\to p\Lambda K^+}}{\sigma_{pp\to p\Sigma^0 K^+}}$
K (Born)	739	46	16
K (FSI)	2426	57	43
π (Born)	71	77	0.9
π (FSI)	113	105	1.1
"$K+\pi$" (FSI)	2471	251	9.9
"$K-\pi$" (FSI)	2607	73	36
experiment	505 ± 33	20.1 ± 3.0	25 ± 6

In one case (indicated by "$K+\pi$" in table 1) the π- and K-exchange contributions add up constructively for $pp \to p\Sigma^0 K^+$ and the resulting total cross section is significantly larger than the individual results. For the other

choice (indicated by "$K - \pi$") we get a destructive interference between the amplitudes yielding a total cross section that is much smaller. Consequently, in the latter case the cross section ratio is much larger and, as a matter of facts, in rough agreement with the experiment (cf. table 1) - suggesting a destructive interference between the π- and K-exchange contributions as a possible explanation for the observed suppression of near-threshold Σ^0 production.

It is now interesting to look also at corresponding results for other Σ production channels. E.g., for the reaction $pp \to n\Sigma^+K^+$ the predicted cross sections at the excess energy of 13 MeV are 86 ("$K + \pi$") and 229 nb ("$K - \pi$"), respectively. Thus, the interference pattern is just the opposite as for $pp \to p\Sigma^0K^+$, cf. table 1. For the "$K - \pi$" case favoured by the experimental $\sigma_\Lambda/\sigma_{\Sigma^0}$ ratio our calculation yields a cross section for $pp \to n\Sigma^+K^+$ that is about 3 times larger then the one for $pp \to p\Sigma^0K^+$. Such a ratio is in fair agreement with data and model calculations at higher energies, see, e.g. ref. [12]. The other choice, "$K + \pi$", leads to a $\sigma_{pp\to n\Sigma^+K^+}$ that is a factor of about 3 smaller than $\sigma_{pp\to p\Sigma^0K^+}$ - a result which is rather difficult to reconcile with the present knowledge about these reactions at higher energies. These features are displayed graphically in fig. 2 as a function of the excess energy. Note that all curves are multiplied by a common reduction factor of 0.3 [4] to compensate for ISI effects [11].

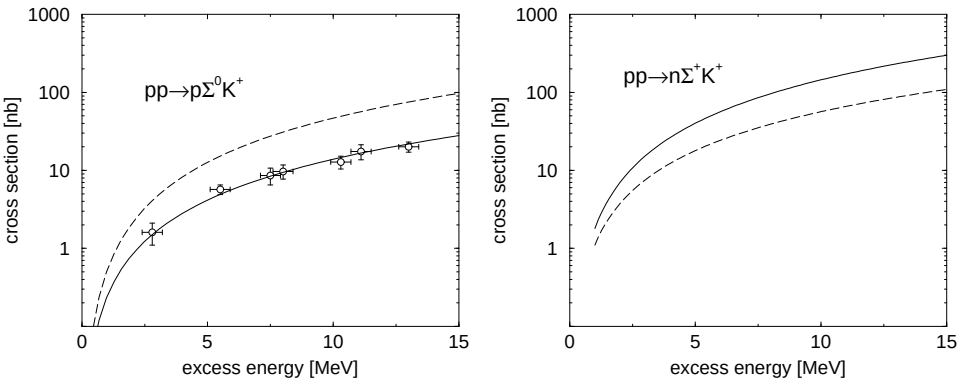

Figure 2: Total cross sections for the reactions $pp \to p\Sigma^0K^+$ and $pp \to n\Sigma^+K^+$. The solid curve corresponds to the choice "$K-\pi$" and the dashed curve to "$K+\pi$", cf. text. All curves are normalized by a factor of 0.3. The experimental data are from ref. [2].

For the reaction $pp \to p\Sigma^+K^0$ the predicted cross sections at the excess energy of 13 MeV are 725 ("$K + \pi$") and 423 nb ("$K - \pi$"), respectively.

Thus, in this case the interference pattern is the same as for $pp \to p\Sigma^0 K^+$. Furthermore, for either choice ("$K \pm \pi$") the cross section for $pp \to p\Sigma^+ K^0$ is about 3.3 times larger than the one for $pp \to p\Sigma^0 K^+$. Note that the experimental evidence at higher energies suggests a ratio of around 1 for those channels.

Very recently new preliminary data from the COSY-11 collaboration for the Λ/Σ^0 cross section ratio became available in the excess energy region $20 - 60\,\mathrm{MeV}$ [13]. Our model fails to describe the energy dependence of the ratio (Fig. 3). The bump at about 30 MeV that shows up when we use the Jülich model A is a consequence of the spurious bound state in the $^1S_0$ partial wave present in this model. This bump disappears when calculating with the new Jülich model [14], which is free of such an artefact, but the ratio remains roughly a constant. That means, most likely, that our assumptions on the weak energy dependence of the elementary amplitudes and S-wave final state dominance is no longer valid at energies higher than 20 MeV. Therefore, we believe that more detailed dynamics should be included in the production mechanism before conclusions can be drawn. This work is in progress now.

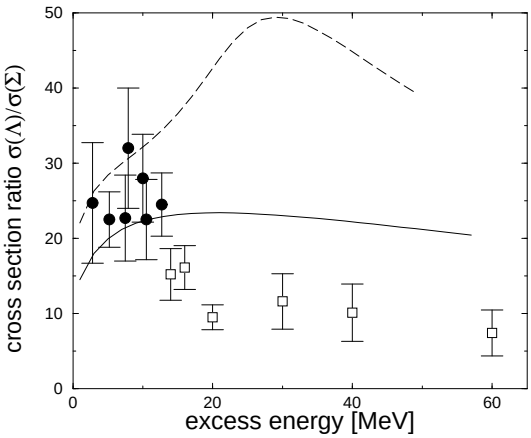

Figure 3: Energy dependence of the Λ/Σ^0 cross sections ratio $pp \to p\Sigma^0 K^+$ and $pp \to n\Sigma^+ K^+$. Theoretical curves are are calculated using Jülich model A (dashed line) and new Jülich model [14] (solid line). The experimental data are from ref. [13].

References

[1] J.T. Balewski et al., Phys. Lett. **B 420** (1998) 211.

[2] S. Sewerin et al., Phys. Rev. Lett. **83** (1999) 682.

[3] V. Flaminio at al., *Compilation of cross sections*, CERN-HERA report 84-01 (1984).

[4] A.M. Gasparian et al., Phys. Lett. **B 480** (2000) 273.

[5] B. Holzenkamp et al., Nucl. Phys. **A 500** (1989) 485.

[6] R. Siebert et al., Nucl. Phys. **A 567** (1994) 819.

[7] D. Cline, R. Laumann, and J. Mapp, Phys. Rev. Lett. **20** (1968) 1452; T.H. Tan, Phys. Rev. Lett. **23** (1969) 395.

[8] R. Machleidt, K. Holinde and Ch. Elster, Phys. Rep. **1499** (1989) 1.

[9] M. Hoffmann et al., Nucl. Phys. **A 593** (1995) 341.

[10] M. Hoffmann, Jülich report, No. 3238 (1996).

[11] M. Batinić et al., Phys. Scripta **56** (1997) 321.

[12] J.M. Laget, Phys. Lett. **B 259** (1991) 24.

[13] P. Kowina, COSY NEWS No.10 (2001), in print.

[14] J. Haidenbauer, in preparation.

Investigation on the cross section of the overlapping scalar resonances $f_0(980)$ and $a_0(980)$ produced in proton-proton collisions in the range of the reaction threshold

P. Moskal[a,b], W. Oelert[b]

[a] *Institute of Physics, Jagellonian University, Kraków, Poland*

[b] *Institut für Kernphysik, Forschungszentrum Jülich, Germany*

Abstract: Utilizing a missing mass technique we investigate the $pp \to ppX$ reaction scanning beam energies in the range permitting to create a mass close to that of the $f_0(980)$ and $a_0(980)$ scalar resonances, but still below the K^+K^- threshold where they decay dominantly into $\pi\pi$ and $\pi\eta$ mesons, respectively. Prior to the data analysis we introduce a notion of the close to threshold total cross section for broad resonances. This is estimated to be about 400 nb at excess energy of Q = 5 MeV.

A study of the $1\,\mathrm{GeV/c^2}$ mass range is motivated by the continuing discussion on the nature of the scalar resonances $f_0(980)$ and $a_0(980)$, which have been interpreted as exotic four quark states [1], conventional $q\bar{q}$ [2, 3] or molecular like $K\bar{K}$ bound states [4, 5].

Within the framework of the Jülich meson exchange model for $\pi - \pi$ [6] and $\pi - \eta$ scattering the $K\bar{K}$ interaction dominated by vector meson exchange gives rise to a $K\bar{K}$ bound state identified with the $f_0(980)$ in the isoscalar sector, while the isovector $a_0(980)$ is concluded to be a dynamically generated threshold effect [7, 8]. Both shape and absolute scale of $\pi\pi \to K\bar{K}$ transitions turn out to depend crucially on the strength of the $K\bar{K}$ interaction, which, in turn is prerequisite of a $K\bar{K}$ bound state interpretation of the $f_0(980)$. Similar effects might be expected for the elementary kaon-antikaon production in proton-proton scattering. However, no microscopic calculations are presently available.

Although the $K\bar{K}$ decay mode of $f_0(980)$ and $a_0(980)$ is rather weak in comparison to the dominant $\pi\pi$ and $\pi\eta$ decay channels [9], even a new theoretical analysis based on the chiral approach can not account for the $f_0(980)$ and $a_0(980)$ if the $K\bar{K}$ channel is not introduced additionally to the $\pi\pi$ and $\pi\eta$ interaction [10]. An analysis of the $\pi\pi$ and $K\bar{K}$ interaction [11]

showed that f_0 corresponds to poles on three Riemann-sheets, and appears physically as an object with a decay width of about 400 MeV and a narrow peak width of about 50 MeV. The same parameters of the f_0 were found by utilizing a unitarized quark model, according to which f_0 was interpreted as a $q\bar{q}$ state with a large admixture of $K\bar{K}$ virtual state [12]. The origin of the scalar resonances was also thouroughly studied by means of a coupled channel analysis considering $\pi\pi$, $K\bar{K}$ and $\sigma\sigma$ meson-meson scattering [13, 14]. Decreasing gradually the interchannel coupling constants it was inferred that for some solutions at the limit of the fully uncoupled case the f_0 corresponds to the $K\bar{K}$ bound state [14, 15].

In the high energy experiments, the f_0 meson is observed as a resonance in the system of two pions produced in the variety of hadro-production reactions [16, 17, 18, 19] or in the hadronic decays of heavier mesons [20, 21, 22] or the Z^0 boson [23, 24] created in the e^+e^- collisions. These experiments study the invariant masses of the created neutral (($\pi^0\pi^0$) [16, 18, 22] and charged ($\pi^+\pi^-$) [17, 19, 20, 21, 23]) pion pairs. Similarly, charged [25, 26] and neutral [27] a_0 mesons were observed as a clear signal in an invariant mass spectrum of the $\eta\pi$ system.

Complementary to these approaches, studied the interaction of $\pi\pi$, $K\bar{K}$, and $\pi\eta$ meson pairs, we investigate the possible manifestation of the mesons f_0 and/or a_0 as a doorway state leading to meson production in proton-proton collisions, namely $pp \to ppf_0(a_0) \to ppMesons$. By measuring the missing mass of the pp-system we study the $f_0 - a_0$ system as a genuine particle produced directly at the reaction place.

We report here the first experimental investigation, which concerns the close to threshold production of the broad resonances in the 1 GeV/c^2 mass range. Moreover, we have studied the f_0 and a_0 mass range below the $K\bar{K}$ threshold, where they can decay into non-strange mesons only.

It is obvious that for the excitation of a broad resonance the phrase "close to threshold" is not well defined and implies here that the beam momentum is such that masses just in the range of the resonance can be excited. It is worth to note, that recently first measurements of the f_0 meson production relatively close to its threshold but still above the $K\bar{K}$ threshold were performed by observing ϕ meson decays into the $f_0\gamma$ channel [21, 22], where ϕ is only about 40 MeV/c^2 heavier than f_0.

In a recent publication [28] we presented data on the close-to-threshold K^+K^- production following the proton-proton interaction at the excess energy of Q = 17 MeV. The obtained distribution of the missing mass to the pp-system is shown in figure 1 and demonstrates that the non-resonant K^+K^- production (shaded area) is hardly distinguishable from the resonant

$pp \to ppf_0(980) \to ppK^+K^-$ reaction sequence (dashed line) [29]. Since the statistics of the data was not sufficient to favour one of the two processes, the cross section was extracted for both and resulted in nearly identical values of: $\sigma_{non-resonant} = 1.80 \pm 0.27^{+0.28}_{-0.35}$ nb and $\sigma_{resonant} = 1.84 \pm 0.29^{+0.25}_{-0.33}$ nb including statistical and systematical errors, respectively. The issue whether there is a chance to distinguish between $K\bar{K}$ pairs originating from the decay of genuine f_0/a_0 resonance and those produced by strong $\pi\pi - K\bar{K}$ correlation is at present under investigation [8].

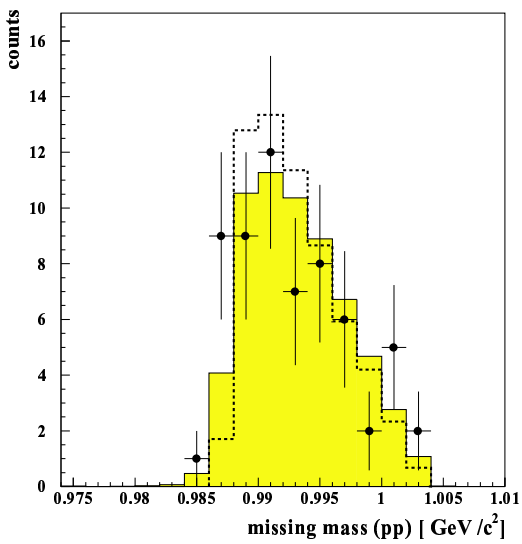

Figure 1: Experimental spectrum of the K^+K^- invariant mass measured for the reaction $pp \to ppK^+K^-$ at a beam momentum of 3.356 GeV/c (data points). Width of the bins corresponds to the experimental resolution of the mass determination (FWHM $\approx$ 2 MeV). Shaded area and dashed line show Monte-Carlo simulation under assumption of the direct and resonance production, correspondingly [29].

Since there exists no experimental determination of the close to threshold total cross section for the production of f_0 and a_0 mesons, before the presentation of the COSY-11 measurement, we will estimate an expected order of magnitude for the considered values at the excess energy Q = 5 MeV at which there exists theoretical predictions [30] for the K^+K^- production based upon the one-pion exchange model and the Breit-Wigner prescription for the f_0 resonance. The calculation shows that the production of $K\bar{K}$ pair through the f_0 resonance ($pp \to ppf_0(980) \to ppK^+K^-$) contributes at Q = 5 MeV, with respect to the K^+K^- threshold, by factor of 20 to 100 less than the nonresonant creation, depending on the set of parameters. Extrapolating [28] the measured cross sections of the $pp \to ppK^+K^-$ reaction [28, 31] to Q = 5 MeV one obtained the value of 0.08 nb. Thus combining the above information and additionally taking into account that the branching ratio of f_0 meson decay into K^+K^- is about 2 % [30], one expects that very close to threshold at Q = 5 MeV (with respect to the ppK^+K^-

final state) the f_0 meson should be produced with the cross section in the order of $0.08\,\mathrm{nb} * 50/20 = 0.2\,\mathrm{nb}$. However, the branching ratio of f_0 decay into $K\bar{K}$ pairs is not well established [9] and may be much smaller than the above assumed value of 2 %. Naively one would expect it to be very small, since due to the energy conservation only a few per cent of the resonance can decay into strange particles and moreover only a fraction of that part will decay into a K^+K^- pair.

In case of the $NN \to NNa_0$ reaction the total cross section was estimated using an effective Lagrangian approach taking into account the one-pion exchange mechanism and the production via t-channel exchanges with $\pi\eta$ and πf_1 mesons [32]. The assumption of the positive interference between s- and u-channel of the one-pion exchange results in the value of 20 nb at $\mathrm{Q} = 5\,\mathrm{MeV}$. However, in the calculations an exchange of heavier mesons was not taken into account. In addition it should be noted that a different choice of coupling constants and cut-off parameter $\Lambda_{\pi NN}$ would easily change the expected cross section by a factor of five in either direction.

The above appraisement indicates that at a few MeV above the production threshold a total cross section for the $pp \to ppa_0(f_0)$ reactions is expected to be in the order of 1 nb to 100 nb.

The study of short-living (broad) particles in the $pp \to ppX$ reaction requires special care when the energy available in the center of mass is close to the sum of the masses of protons and the average mass of the meson ($\sqrt{s} = 2 \cdot m_p + m_0$) [33]. As already mentioned due to the broad mass distribution of such particles the notion of the reaction threshold is not well defined. It is naturally a matter of scale whether a given resonance is considered as a broad one. Experimentally, by broad resonance we define a particle with its full width Γ at half maximum of the mass distribution (spectral function) being much larger than the experimental accuracy of the mass determination, or with a width such broad that the acceptance of the detection system changes significantly over the resonance mass range. Both criteria apply for the measurements performed and discussed in the present contribution.

In the following we will propose a definition of the total cross section as a function of the excess enery $\mathrm{Q} = \sqrt{s} - 2 \cdot m_p - m_X$, which is valid also when Q is small compared to the width Γ of the produced meson.

Performing the measurement with the total centre-of-mass energy $\sqrt{s}$ close to the sum of the average mass of the produced meson plus the mass of the two protons, different mass ranges of the meson are populated with different excess energies: $\mathrm{Q}\,(m) = \sqrt{s} - (2 \cdot m_p + m)$ (see figure 2a). This

implies that the observed mass distribution appears to be different from the one which would be determined at an excess energy much larger than the average mass m_0 ($\sqrt{s} - 2 \cdot m_p \gg m_0$). Neglecting dynamical effects, in case of large $\sqrt{s}$ the mass distribution can be roughly approximated by the Breit-Wigner function, as shown in figure 2a.

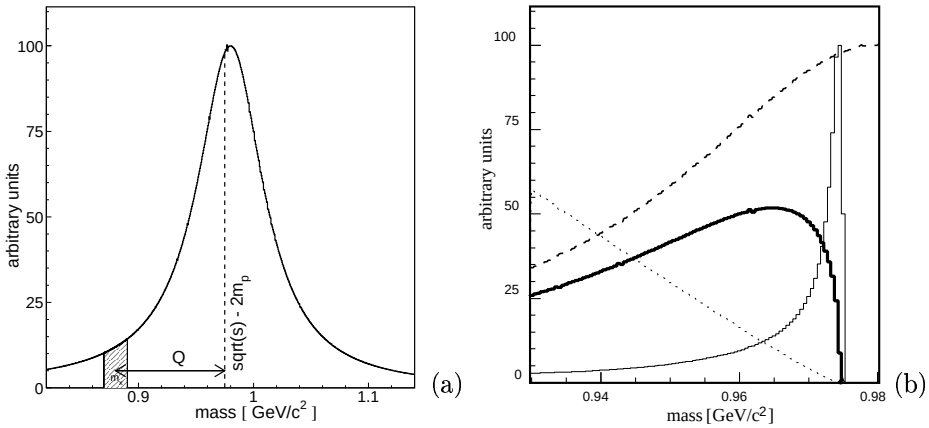

Figure 2: **(a)** Breit-Wigner distribution with the mean value of $m_0 = 980\,\mathrm{MeV/c^2}$ and the width equal to $\Gamma = 70\,\mathrm{MeV/c^2}$. If the measurement would be performed with the $\sqrt{s}$ as depicted by the dashed line then the mass m_x would be measured with the centre-of-mass excess energy equal to Q.
(b) Simulations: The horizontal axis denotes the mass of the produced system X via the $pp \to ppX$ reaction. The long-dashed line denotes the Breit-Wigner distribution, the same as shown in figure 2a. The thin solid line represents the efficiency of the COSY-11 detection system for the simultaneous detection of outgoing protons from the $pp \to ppX$ reaction. The short–dashed line shows the decrease of the phase space volume with the increase of the created mass. The phase space volume was weighted by the proton-proton FSI enhancement factor taken from [34]. The thick solid line results as a convolution of the above described distributions. This simulated line corresponds to a missing mass spectrum of the $pp \to ppX$ reaction if X would be a particle with the mass and width equal to $980\,\mathrm{MeV/c^2}$ and $70\,\mathrm{MeV/c^2}$, respectively, and the outgoing protons would be measured by means of the COSY-11 detection system.

The measurements of the $pp \to ppX$ reactions, reported here, have been performed by means of the COSY-11 detection system [35]. A thick solid line in figure 2b shows the expected missing mass distribution simulated for the total centre-of-mass energy $\sqrt{s}$ equivalent to a maximal produced mass ($\sqrt{s} - 2\,m_p$) smaller than the average mass of the simulated meson. The shape of this curve results from convoluting the meson spectral density

(long-dashed line) with both (i) the decrease of the phase space volume with decreasing excess energy Q weighted by the proton-proton FSI enhancement factor [34] (short-dashed line) and with (ii) the efficiency of the COSY-11 detection system for the simultaneous registration of the two outgoing protons from the $pp \to ppX$ reaction (thin solid line).
The number of observed events per mass bin dN/dm can be written as:

$$\frac{dN}{dm}(m, \mathrm{Q}) = \frac{d\sigma}{dm}(m, \mathrm{Q}) \cdot L \cdot Eff(\mathrm{Q}), \tag{1}$$

with L and Eff, denoting the integrated luminosity, and the efficiency of the COSY-11 detection system, respectively. Note that, as proven by the extensive Monte-Carlo simulations, the COSY-11 efficiency is in a good approximation independent of the produced mass and depends on the excess energy Q only. The cross section $d\sigma/dm$ for the creation of a mass m is expressed by:

$$\frac{d\sigma}{dm}(m, \mathrm{Q}) = |M|^2(\mathrm{Q}) \cdot SD(m, m_0, \Gamma) \cdot V_{ph}(\mathrm{Q}) \cdot FSI_{pp}(\mathrm{Q}) \tag{2}$$

$$\frac{d\sigma}{dm}(m, \mathrm{Q}) = \sigma_{primary}(\mathrm{Q}) \cdot SD(m, m_0, \Gamma), \tag{3}$$

where $M(\mathrm{Q})$ stands for the matrix element accounting for the production mechanism, and the second term SD denotes the spectral density of the produced meson with the average mass and width equal to m_0 and Γ, respectively. The $V_{ps}(\mathrm{Q})$ and $FSI_{pp}(\mathrm{Q})$ represent the phase space volume available to the outgoing particles and the proton-proton FSI enhancement factor, respectively. The term $\sigma_{primary}(\mathrm{Q})$ combines all excess energy dependent factors and could be referred to as a primary production cross section of producing a mass bin of the resonance which is by value of Q smaller than the maximum kinematically available mass. It should be noted that all factors in equations 1 and 2 depend on the excess energy Q only, except the spectral density which is a function of the created mass m. This means that the number of events per mass bin can be expressed as follows:

$$\frac{dN}{dm}(m = \sqrt{s} - 2m_p - \mathrm{Q}, \mathrm{Q}) = const.(\mathrm{Q}) \cdot SD(m, m_0, \Gamma). \tag{4}$$

Scanning experimentally the resonance by changing the value of $\sqrt{s} = 2m_p + m + \mathrm{Q}$ and keeping in the analysis a constant value of Q allows to reproduce the mass distribution of the created meson, even without knowing exactly the energy dependence of the detection efficiency and other factors. Note that if $\sqrt{s} - 2\,m_p$ is in the range of the broad resonance (see figure 2a) then

not all parts of the resonance can be created. Thus, it is not obvious from such a single measurement how to extract the total cross section. However, by scanning the resonance with different values of $\sqrt{s} - 2\,m_p$ one can define the total cross section at a given excess energy Q as an integral over the whole resonance region of the differential cross section $d\sigma/dm(m, \mathrm{Q})$ keeping in the integration Q as a constant, thus:

$$\sigma(\mathrm{Q}) = \int_{2m_p}^{\infty} \frac{d\sigma}{dm}(m{=}\sqrt{s} - 2\,m_p - \mathrm{Q}, \mathrm{Q})\; d\sqrt{s} \tag{5}$$

Please note that if the spectral density function is normalized to unity than $\sigma(\mathrm{Q})$ is directly equal to the primary cross section $\sigma_{primary}(\mathrm{Q})$. This can be inferred by substituting equation 3 in equation 5.
Assuming that similar to the production process for pseudoscalar mesons the value of $|M|^2$ will be constant with small values of Q [36], one expects that the energy dependence of $\sigma(\mathrm{Q})$ from equation 5 will be determined by the Q-dependence of the phase space and the dominant proton-proton FSI.

In the following we will present the analysis of the measurements which were primordially devoted to production studies of the η' meson in proton-proton collisions [37]. The maximum mass ($\sqrt{s} - 2\,m_p$) available in these experiments covered a range from 959.6 MeV to 981.4 MeV. This is the region close the the average mass of the $f_0(980)$ and $a_0(980)$ masses, and hence the signal from production of these mesons should indeed influence the overall observed missing mass spectra. Figure 3 presents one of the missing mass distributions extracted from the experimental data taken at total centre-of-mass energy equivalent to the maximum created mass of M = 972 MeV.

The shape of the "background" below the clear η' peak differs from the shape of the missing mass distribution simulated for the Breit-Wigner like resonance shown as a thick solid line in figure 2b. This is due to the fact that the experimental missing mass spectrum comprises also contributions from non-resonant multi–pion and $\pi\eta$ production. Thus, taking also into account the well known contribution originating from the η' production, one can generally extend equation 4 to:

$$\begin{aligned} \frac{dN}{dm}(m, \mathrm{Q}) &= const.(\mathrm{Q}) \cdot SD(m, m_0, \Gamma) + \\ &+ \frac{dN}{dm}(multi - \pi, \pi\eta, \sqrt{s}) + \frac{dN}{dm}(\eta', \sqrt{s}). \end{aligned} \tag{6}$$

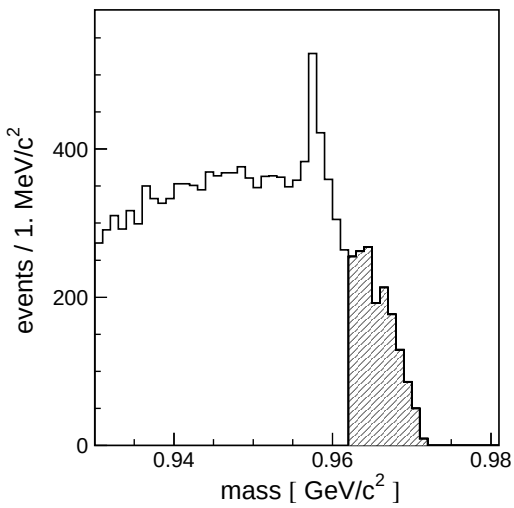

Figure 3: **Experiment:** Missing mass distribution determined for the $pp \to ppX$ reaction at 14 MeV excess energy above the threshold for the η' meson production [37]. Maximum at 958 MeV/c^2 corrsponds to the production of the η' meson. The shaded area denotes the part of the spectrum used in the present analysis.

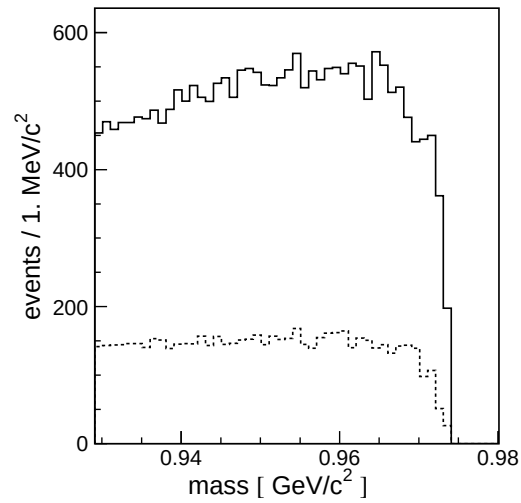

Figure 4: **Simulations:** Missing mass distributions for the reactions $pp \to pp2\pi$ (dashed line) and $pp \to pp3\pi$ (solid line). Please note, that the shape of these spectra differ from each other and both are different from the missing mass distribution shown in figure 2b.

Simulated distributions for the case of the direct 2π and 3π creation are shown in figure 4. One can observe that their shapes differ (i) from each other and (ii) again from the one determined experimentally. The latter discrepancy can be attributed at least qualitatively to contributions of the productions of the $f_0(980)$ and/or $a_0(980)$ mesons to the experimental spectrum.

A mass bin corresponding to $\mathrm{Q} = 5\,\mathrm{MeV} \pm \Delta\mathrm{Q}$ with $\Delta\mathrm{Q} = 5\,\mathrm{MeV}$ was chosen in the analysis for each of the seven measurements under investigation (see as an example the shaded area in figure 3). The number of events per this mass bin has been calculated for seven measurements and after the correction for the detection efficiency has been normalized to the corresponding integrated luminosity:

$$\begin{aligned}\Delta N(\sqrt{s}) &= \frac{1}{L}\int_{Q=0\ MeV}^{Q=10\ MeV} \frac{dN}{dm}\frac{1}{Eff(\mathrm{Q})}\,dm \qquad (7)\\ &= \int_{Q=0\ MeV}^{Q=10\ MeV} \sigma_{primary}\cdot\ SD(\sqrt{s}-2m_p-\mathrm{Q},m_0,\Gamma)\,dm\\ &+ \int_{Q=0\ MeV}^{Q=10\ MeV}\left(\frac{d\sigma}{dm}(multi-\pi,\pi\eta,\sqrt{s})+\frac{d\sigma}{dm}(\eta',\sqrt{s})\right)\,dm\end{aligned}$$

Subsequently, the well known values of $d\sigma/dm(\eta',\sqrt{s})$ [37] were subtracted from the above defined $\Delta N(\sqrt{s})$:

$$\Delta N'(\sqrt{s}) = \Delta N(\sqrt{s}) - \int_{Q=0\ MeV}^{Q=10\ MeV}\frac{d\sigma}{dm}(\eta',\sqrt{s})\,dm \qquad (8)$$

Further, in order to account for the contribution from the multi-pion and $\pi\eta$ production we subtracted from each $\Delta N'(\sqrt{s})$ the value determined for the lowest measured energy. The result is shown in figure 5a, where the variable Δ at the vertical axis reads:

$$\Delta = \Delta N'(\sqrt{s}) - \Delta N'(\sqrt{s}_{lowest} = 2\cdot m_p + 959.6\,\mathrm{MeV}) \qquad (9)$$

On the other hand, assuming changes of the cross section for the non-resonant multi-pion and $\pi\eta$ production to be negligible (which is justified, since the measurements were performed about 560 MeV and 300 MeV above the 3π and $\pi\eta$ thresholds, respectively) the value of Δ can be expressed as follows:

$$\begin{aligned}\Delta &= \sigma_{primary}\cdot\int_{Q=0\ MeV}^{Q=10\ MeV} SD(m,\sqrt{s}-2m_p-\mathrm{Q},\Gamma)\,dm\\ &- \sigma_{primary}\cdot\int_{Q=0\ MeV}^{Q=10\ MeV} SD(m,\sqrt{s}_{lowest}-2m_p-\mathrm{Q},\Gamma)\,dm \qquad (10)\end{aligned}$$

The curves in figure 5a represent calculations performed according to equation 10 approximating the spectral function $SD(m,m_0,\Gamma)$ by the Breit-Wigner distribution. The obtained result demonstrates that the data are

sensitive to the average mass of the created meson or mesons but rather non-sensitive to the width of an assumed Breit-Wigner structure. The latest volume of the Review of Particle Physics [9] shows that the parameters for $f_0(980)$ and $a_0(980)$ mesons are very similar to each other:

$f_0(980): \quad m = 980 \pm 10, \qquad \Gamma = 40 \text{ to } 100$

$a_0(980): \quad m = 985.2 \pm 1.5, \quad \Gamma = 50 \text{ to } 100$

and therefore we can not distiguish between these two resonances in a missing mass analysis from the proton-proton interaction.

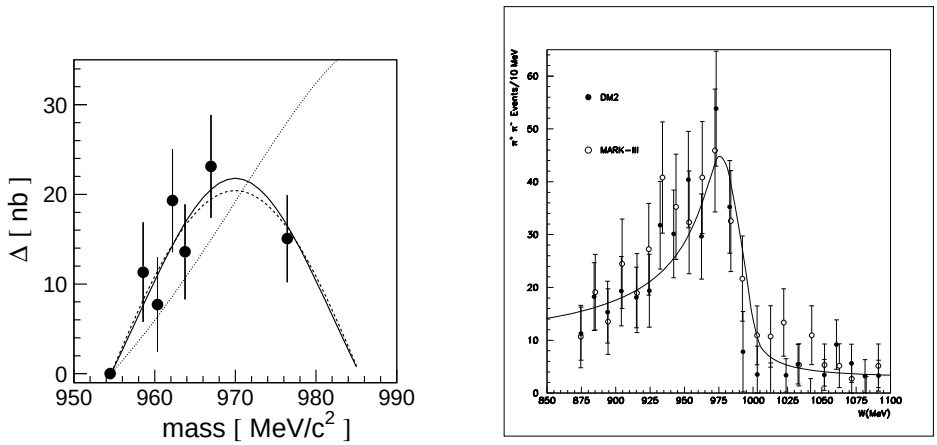

(a) (b)

Figure 5: **(a)** Points denote number of events, measured at the 10 MeV upper bin of the missing mass spectrum for the $pp \to ppX$ reaction, as depicted by the shaded area in figure 3, normalized to the integrated luminosity. The value obtained at 959.6 MeV/c^2 was subtracted from each point. The x-axis denotes the mass corresponding to Q = 5 MeV. For example the point corresponding to the spectrum of figure 3 ($\sqrt{s} - 2\,m_p = 972$ MeV) is plotted at a mass value of 967 MeV/c^2. Lines show the result of simulations of the $pp \to ppX$ reaction, with X being the Breit-Wigner type meson resonance of the following parameters:
(dotted line) mass 990 MeV/c^2, width 65 MeV/c^2, and $\sigma_{primary} = 750$ nb,
(solid line) mass 970 MeV/c^2, width 40 MeV/c^2, and $\sigma_{primary} = 400$ nb,
(dashed line) mass 970 MeV/c^2, width 65 MeV/c^2, and $\sigma_{primary} = 1200$ nb.
(b) $\pi^+\pi^-$ event distribution in the $J/\Psi \to \phi\pi^+\pi^-$ decay around the f_0 mass. Data were taken by DM2 [38] and MARK-III [39] collaborations. Solid line depicts the result of the calculations of [40]. Courtesy of J.A. Oller.

A fit to the resonance like structure of figure 5a results in values of: $m = 970$, $\Gamma = 65$ and $\sigma_{primary} \approx 400$ nb (PRELIMINARY). It is worth to

note, that the obtained structure is in line with the measurements of the $\pi^+\pi^-$ invariant mass distribution of the J/Ψ decay into $\phi\pi^+\pi^-$ system as shown in figure 5b.

This result encourages us for further investigations. We plan to perform a similar analysis with the data taken during the measurements of the K^+K^- [28] and ϕ [41] meson production. This will allow us to extend the mass range of figure 5a up to 1043 MeV.

In conclusion, the factorization ansatz of equation 2 leads to a simple definition of the differential cross section. For the example of the production of the $f_0(980)$ and/or $a_0(980)$ mesons we discuss the notion of the reaction threshold in case of broad resonances where the available phase space volume for a given mass bin changes significantly.

Our present investigation indicates that assigning to the observed enhancement a Breit-Wigner form, a total cross section introduced in equation 5 is in the order of 400 nb (PRELIMINARY). It must be kept in mind that this estimation depends on the assumption that the total cross sections for the non-resonant multi-pion and $\pi\eta$ production change much less than by 400 nb when the $\sqrt{s}$ for the $pp \to ppX$ reaction changes from $2836.1 = 2\,m_p + 959.6\,\mathrm{MeV}$ to $2857.9 = 2\,m_p + 981.4\,\mathrm{MeV}$. The values corresponds to the lowest and largest $\sqrt{s}$ of the reported measurements, respectively.

The obtained value of the total cross section is much larger than expected from the existing theoretical estimations, which however take into account only a part of the possible production mechanisms. In case of f_0, for example, one could consider also a production via an excitation of baryonic resonaces. PDG reports a few N^* resonances around 1700 MeV with the width of $50 - 250$ MeV, which decay predominantly into the $N\pi\pi$ channel.

Acknowledgement. We would like to thank J.A. Oller for comments to the first version of the manuscript.

References

[1] R. Jaffe, Phys. Rev. **D 15** (1977) 267.

[2] D. Morgan, M.R. Pennington, Phys. Rev. **D 48** (1993) 1185.

[3] F. Kleefeld et al., e–Print Archive: hep–ph/0109158.

[4] J. Weinstein, N. Isgur, Phys. Rev. **D 41** (1990) 2236.

[5] Z.S. Wang, S. Krewald, J. Speth, Nucl. Phys. **A 684** (2000) 429c.

[6] D. Lohse et al., Nucl. Phys. **A 516** (1990) 513.

[7] O. Krehl, R. Rapp, J. Speth, Phys. Lett. **B 390** (1997) 23.

[8] J. Haidenbauer, contribution to these proceedings.

[9] D.E. Groom et al., Eur. Phys. J. **C 15** (2000) 1.

[10] J.A. Oller, E. Oset, J.R. Peláez, Phys. Rev. **D 59** (1999) 074001.

[11] B.S. Zou, D.V. Bugg, Phys. Rev. **D 48** (1993) R3948.

[12] N.A. Törnqvist, Phys. Rev. Lett. **49** (1982) 624.

[13] R. Kamiński, L. Leśniak, B. Loiseau, Phys. Lett. **B 413** (1997) 130.

[14] R. Kamiński, L. Leśniak, B. Loiseau, Eur. Phys. J. **C 9** (1999) 141.

[15] R. Kamiński, L. Leśniak, B. Loiseau, Acta Phys. Polon. **B 31** (2000) 2467.

[16] D. Alde et al., Z. Phys. **C 66** (1995) 375; Phys. Lett. **B 397** (1997) 350; Eur. Phys. J. **A 3** (1998) 361.

[17] D. Barberis et al., Phys. Lett. **B 462** (1999) 462.

[18] D. Barberis et al., Phys. Lett. **B 453** (1999) 325.

[19] A. Breakstone et al., Z. Phys. **C 31** (1986) 185.

[20] E.M. Aitala et al., Phys. Rev. Lett. **86** (2001) 765; Phys. Rev. Lett. **86** (2001) 770.

[21] R.R. Akhmetshin et al., Phys. Lett. **B 462** (1999) 371.

[22] R.R. Akhmetshin et al., Phys. Lett. **B 462** (1999) 380.

[23] K. Ackerstaff et al., Eur. Phys. J. **C 4** (1998) 19.

[24] P. Abreu et al., Phys. Lett. **B 449** (1999) 364.

[25] K. Ackerstaff et al., Eur. Phys. J. **C 5** (1998) 411.

[26] J.B. Gay et al., Phys. Lett. **B 63** (1976) 220.

[27] S. Teige et al., Phys. Rev. **D 59** (1998) 012001.

[28] C. Quentmeier et al., Phys. Lett. **B 515** (2001) 276.

[29] C. Quentmeier, doctoral thesis, Westfälische Wilhelms-Universität Münster, Germany (2001).

[30] E.L. Bratkovskaya et al., Eur. Phys. J. **A 4** (1999) 165.

[31] F. Balestra et al., Phys. Lett. **B 468** (1999) 7.

[32] E.L. Bratkovskaya et al., e–Print Archive: nucl–th/0107071.

[33] C. Hanhart, A. Kudryavtsev, Eur. Phys. J. **A 6** (1999) 325.

[34] G. Fäldt, C. Wilkin, Phys. Lett. **B 382** (1996) 209.

[35] S. Brauksiepe et al., Nucl. Instr. & Meth. **A 376** (1996) 397.

[36] P. Moskal et al., Phys. Lett. **B 482** (2000) 356.

[37] P. Moskal et al., Phys. Lett. **B 474** (2000) 416.

[38] A. Falvard et al., Phys. Rev. **D 38** (1988) 2706.

[39] W.S. Lockman, in *Hadron '89, Proceedings of the 3rd International Conference on Hadron Spectroscopy*, Ajaccio, France, edited by F. Binon et al. (Editions Frontières, Gif-sur-Yvette, 1989) 109.

[40] U.-G. Meißner, J.A. Oller, Nucl. Phys. **A 679** (2001) 671.

[41] M. Wolke, contribution to these proceedings.

Theoretical aspects of the reactions $pp \to ppK^+K^-$ and $pp \to ppa_0/f_0$[1]

Johann Haidenbauer

Institut für Kernphysik - Theorie, Forschungszentrum Jülich, Germany

Abstract: Meson–exchange models for $\pi\pi$ and $\pi\eta$ scattering, developed by the Jülich group, are reviewed. In these models the scalar meson resonances $f_0(980)$ and $a_0(980)$ can be understood as $K\bar{K}$ threshold effects. The relevant structures in the data can be described without introducing genuine $(q\bar{q})$ scalar meson states. Implications of such a model on the reactions $NN \to NNf_0/a_0$ and $NN \to NNK\bar{K}$ are discussed.

1 Introduction

The understanding of the structure of hadrons is one of the most challenging unsolved problems in medium–energy physics. With increasing experimental information about the different members of the meson and baryon spectra it becomes more and more important to develop a consistent understanding of the observed mesons and baryons from a theoretical point of view.

In the meson sector this has been done quite successfully — for the low lying pseudoscalar, vector and tensor mesons — within the framework of the simple quark model assuming the mesons to be quark-antiquark $(q\overline{q})$ states grouped together into nonets. For the scalar mesons, however, several questions still remain to be answered, most of them being related to the nature of the experimentally observed mesons $f_0(980)$ and $a_0(980)$. On the other hand, scalar mesons are particularly interesting; e.g., the lowest lying glueball is expected in the 1.5 GeV region with quantum numbers 0^{++} and a detailed understanding of the scalar meson spectrum is necessary to identify glueball candidates. In the light of this situation the structure of the scalar mesons $f_0(980)$ and $a_0(980)$ was investigated by the Jülich group within a realistic meson–exchange model [1]. It turned out that all relevant data could be described in terms of the $\pi\pi - K\bar{K}$ and $\pi\eta - K\bar{K}$ dynamics alone. The structures associated with the $f_0(980)$ and $a_0(980)$ emerge as $K\bar{K}$ threshold effects.

[1] Invited talk

In principle, the reactions $NN \to NNf_0/a_0 \to NNK\bar{K}$ can be investigated at the COSY accelerator in Jülich. This opens the possibility to obtain additional information about those scalar mesons. Of particular interest is, of course, whether such experiments would allow to provide stringent information on the structure of the $f_0(980)$ and $a_0(980)$ mesons, which can be used to discriminate between the various scenarios discussed in the literature, cf. below.

2 Meson–meson scattering

Recently we have developed meson–exchange models for $\pi\pi$ and $\pi\eta$ scattering and we have used them for investigating the nature of the meson resonances $f_0(980)$ and $a_0(980)$ [1]. These models are based on an effective meson Lagrangian utilizing the symmetries of the QCD–Lagrangian as guideline. In particular we use the non–linear σ–model with vector mesons introduced as gauge–bosons [2, 3]. The resulting potential for meson–meson scattering contains t–channel vector–meson exchanges $(\rho, K^*, \omega, \phi)$ as well as s–channel pole diagrams $(\rho, f_0(1400), f_2(1270))$ and is iterated in a three–dimensional scattering equation of Blankenbecler–Sugar type. For details of this procedure the reader is referred to ref. [1].

2.1 $\pi\pi$ scattering and the nature of the $f_0(980)$ resonance

In a long standing controversial discussion the $f_0(980)$ has been described as, for example, a conventional $q\overline{q}$ meson [4], a $K\overline{K}$ molecule [5] or a multiquark state [6]. In addition, several ways have been proposed to discriminate between those models in order to finally decide about the structure of this meson. The first test for any model should be a comparison with experimental data on $\pi\pi \to \pi\pi$ and $\pi\pi \to K\overline{K}$ scattering. Fig. 1 shows that our model is able to produce very good agreement with experimental data on $\pi\pi \to \pi\pi$ in all relevant partial waves and over a wide range of energy. In particular we note that t–channel ρ exchange is the sole contributor to $JI = 02$ and 22, and, as can be seen in the dotted curve in fig. 1, provides a substantial part of the low energy $JI = 00$ interaction. This suggests that the spin–isospin structure provided by the t–channel meson exchanges arising from a Lagrangian with effective meson degrees of freedom is substantively correct.

In particular we are able to describe the structure appearing around 1.0 GeV in the isoscalar $\pi\pi$ S–wave which is assigned to the f_0 meson. In our model this resonance like behavior is generated dynamically by the strong attraction arising from ρ, ω and ϕ exchange in the $K\overline{K}$ channel and we

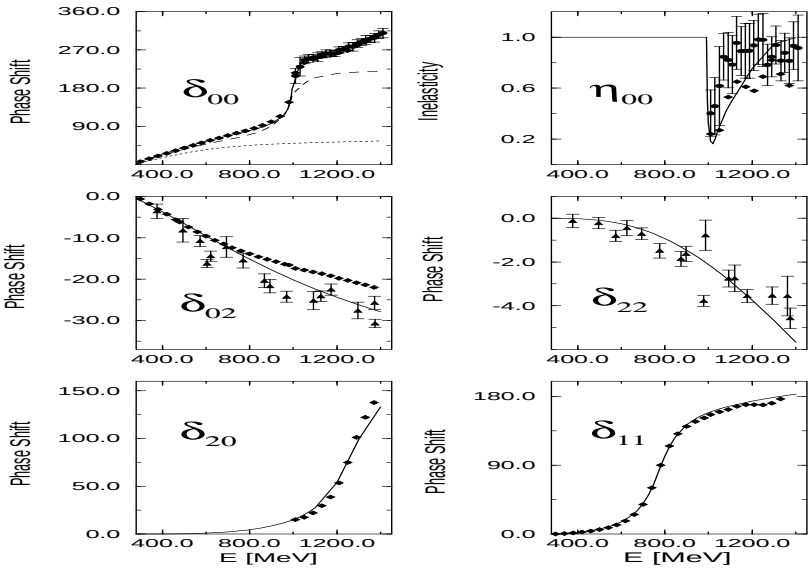

Figure 1: Results of the modified Jülich $\pi\pi$ interaction model. Data are referenced in [1]. The solid line shows the result of our full model. For the dashed line in δ_{00} we have excluded the ϵ s–channel pole diagram. The dotted line contains only t– and u–channel ρ exchange.

therefore do *not* need a genuine scalar resonance with mass around 1.0 GeV (c.f. fig. 1). On the other hand, it is definitely necessary to include a heavy scalar particle, namely the ϵ with mass around 1.4 GeV, to describe the experimental data beyond 1.0 GeV (see the solid line in fig. 1). This particle may be interpreted as the member of the scalar nonet; i.e., it effectively parameterizes the effect of both the isoscalar singlet and octet contributions and any other higher mass states present in the scalar–isoscalar spectrum.

In order to make statements about the nature of the $f_0(980)$ a more detailed analysis of the predictions of our model close to $K\overline{K}$ threshold is required. Fig. 2a therefore compares results of our calculation with experimental data on the $\pi\pi \to K\overline{K}$ channel. The figure shows data obtained from three different direct measurements of $\pi\pi \to K\overline{K}$ cross sections with results inferred from elastic $\pi\pi \to \pi\pi$ scattering (References can be found in [1]). As can be seen from the figure, the $K\overline{K}$ production cross sections are rather poorly known experimentally. Our calculation agrees reasonably well with the most recent data of ref. [7] (shown using open circles in fig. 2a). Quite typically, a model based on a $q\overline{q}$ structure for the $f_0(980)$ would yield

smaller cross sections producing agreement with the older analyses. To finally decide about the nature of the f_0 it is therefore definitely necessary to improve the experimental information on $K\overline{K}$ production.

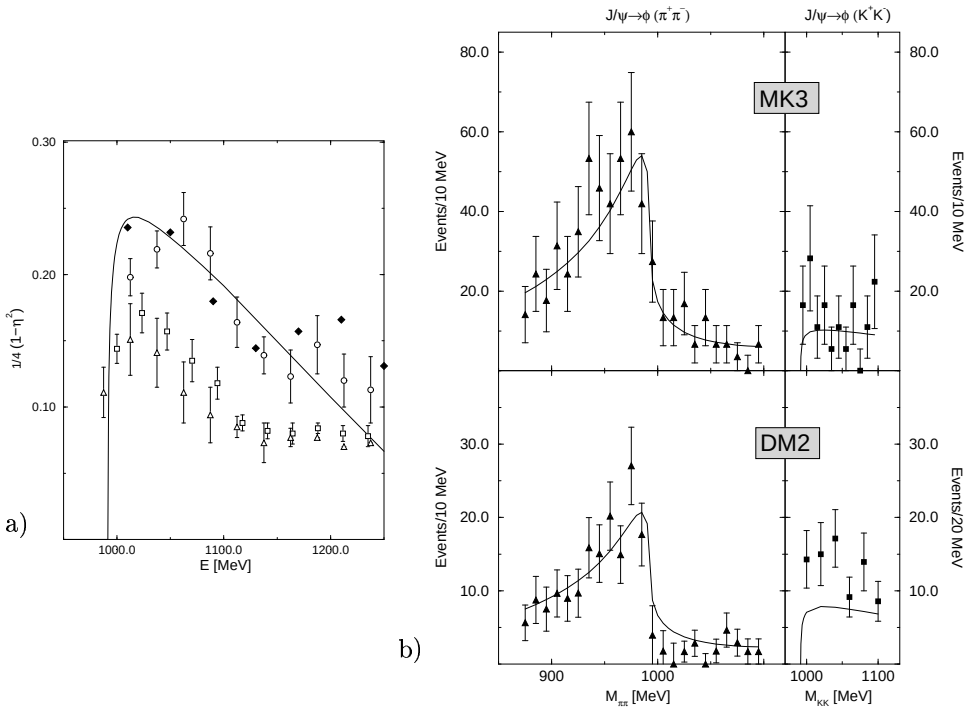

Figure 2: (a) Results of the modified Jülich $\pi\pi$ interaction model compared with data on the $\pi\pi \to K\overline{K}$ channel in terms of $\frac{1}{4}(1-\eta^2)$. Data are referenced in [1]. (b) Fit to $J/\psi \to \phi\pi\pi/\phi KK$ data. The upper panel shows the fit to data of ref. [8] and the lower panel to ref. [9] (The theoretical curves in the lower panel compared to the upper one differ only by an overall normalization factor taking into account the different normalization of the DM2 and MK3 data).

The fact that the $\pi\pi/K\overline{K}$ amplitude is not fully constrained by the available data on meson–meson scattering has already been discussed by Morgan and Pennington [10]. To extend the set of experimental data and to be able to decide about the structure of the f_0 they have investigated the role of the decay $J/\psi \to \phi\pi\pi/\phi K\overline{K}$. Though a recent discussion [11, 12] has shown that this data does not enable one to make a definitive statement about the nature of the f_0, J/ψ decay remains a very valuable addition to an analysis of the $\pi\pi/K\overline{K}$ scattering amplitude. We have calculated the corresponding mass distributions using our meson–exchange model and

compared them with experimental data (Fig. 2b). The figure shows that our model is able to reproduce this data quite well. Moreover, the quality of the fit is comparable in quality with those of alternative models [11, 12] leading to the conclusion that the bound state structure of the f_0 is definitely not disfavored by the J/ψ data.

Analyzing the pole structure of the $\pi\pi$ scattering amplitude (see ref. [1] for details of the sheet structure etc.) we find three poles of physical relevance in the complex plane. Looking at smaller energies, we find a very broad pole at complex energy $(\mathrm{Re}E, \mathrm{Im}E) = (387, \pm 305)\,\mathrm{MeV}$. This pole is the origin of the large $\pi\pi$ S–wave phase shifts below 1.0 GeV (see δ_{00} in fig. 1); following ref. [12] we denote it $\sigma(400)$. It should be mentioned, however, that this pole does *not* correspond to a real physical σ meson but is just a manifestation of the strong attraction between the two pions (this correlation between two pions turns out to be quite important for πN scattering, c.f. sec. 3).

Looking at higher energies, we find the poles generated by the ϵ s–channel diagram necessary to describe data above 1.0 GeV. This pole defines the parameters of a genuine scalar particle which effectively includes the singlet and the octet member of the scalar nonet. We denote it by $f_0(1400)$ although it is more likely an effective parameterization of two scalar resonances, such as $f_0(1400)$ and $f_0(1590)$. Both poles, $\sigma(400)$ and $f_0(1400)$ form a background to the $f_0(980)$.

In the most interesting energy region around $K\overline{K}$ threshold we find a single pole (on sheet II) at $(1015, \pm 15)\,\mathrm{MeV}$ which clearly has to be assigned to the f_0 meson and to the corresponding structure in $\pi\pi$ data. In the zero $\pi\pi/K\overline{K}$ coupling limit the pole moves back to the real axis below $K\overline{K}$ threshold $[(985, 0)\,\mathrm{MeV}]$ which clearly demonstrates the bound state nature of the f_0 within our model. From the pole position we obtain

$$\mathrm{m}_{f_0} = 1015\,\mathrm{MeV}; \qquad \Gamma_{f_0} = 30\,\mathrm{MeV}, \tag{1}$$

which is a rather high value for the f_0 mass compared to other models [10] and turns out to be a consequence of the bound state structure within our model.

2.2 $\pi\eta$ scattering and the nature of the $\mathrm{a}_0(980)$ resonance

Next we turn our attention to the $\pi\eta$ channel and the structure of the a_0. For details of the model the reader is again referred to ref. [1] but it should be mentioned that the entire $\pi\eta$ scattering amplitude is obtained with the addition of only one new parameter compared to the $\pi\pi$ case. Since we

want to extend the concepts applied to the $\pi\pi$ interaction *consistently* to the $\pi\eta$ system the $K\overline{K}$ interaction required for a $\pi\eta/K\overline{K}$ coupled–channel approach is taken to be exactly the same as for the $\pi\pi$ case (projected now onto isospin $I = 1$). However, the important ρ exchange between two kaons becomes repulsive for isospin I=1 destroying the $K\overline{K}$ bound state we found for I=0. Fig. 3 demonstrates that we nevertheless obtain a

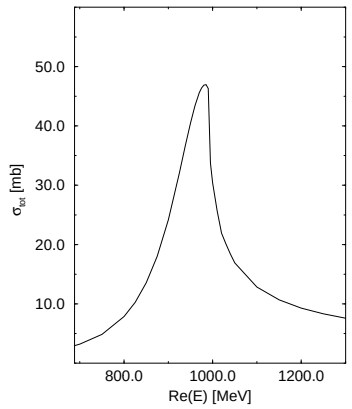

Figure 3: The $\pi\eta$ cross section for our full model.

resonance–like structure close to $K\overline{K}$ threshold when we calculate the $\pi\eta$ cross section within our model. The resonance parameters naively derived from the cross section by Breit–Wigner fitting are in reasonable agreement with experimental data ($m_{a_0} \simeq 990\,\mathrm{MeV}$; $\Gamma_{a_0} \simeq 110\,\mathrm{MeV}$ compared with, e.g., $m_{a_0} = 984 \pm 4\,\mathrm{MeV}$; $\Gamma_{a_0} = 95 \pm 14\,\mathrm{MeV}$ found in [13]). Moreover, we find a single pole corresponding to this structure at $(990, \pm 101)\,\mathrm{MeV}$ (on Sheet II). Since this pole is still present when the direct $K\overline{K}$ interaction is turned off (though at a different position) the only remaining conclusion concerning the origin of this pole and therefore about the nature of the a_0 must be that of a dynamically generated coupled–channel effect.

In summary, we evaluated realistic meson–exchange models for $\pi\pi$ and $\pi\eta$ scattering which are in good agreement with the available experimental data sets. We obtain a consistent understanding of the scalar mesons $f_0(980)$ *and* $a_0(980)$ within the same framework and found the interesting result that their underlying structure is quite different.

3 Remarks on the reaction NN → NNf$_0$/a$_0$ → NNK$\overline{\text{K}}$

The main two issues for the study of f_0 and/or a_0 production in the reaction $NN \to NNK\bar{K}$ are:

1. How can one distinguish those $K\bar{K}$ pairs that emerge from the decay of the f_0 (a_0) mesons from such $K\bar{K}$ pairs that are produced in an uncorrelated way?

2. Is there a clear signal between $K\bar{K}$ pairs that emerge from the decay of a genuine f_0 (a_0) meson and those that are produced by strong $\pi\pi - K\bar{K}$ correlations?

With regard to the former topic some exploratory investigations have been presented in ref. [14]. We would like to concentrate here on the latter aspect. Specifically, we want to examine whether and to which extent strong correlations in the $K\bar{K}$ system as they are induced by the formation of an f_0 and/or a_0 meson (if we think in terms of genuine scalar mesons in the quark–model picture) or by the strong interaction in the $\pi\pi - K\bar{K}$ system (if we think in terms of the Jülich model) have an influence on the $K\bar{K}$ invariant mass spectrum. We assume that the $K\bar{K}$ production proceeds via a "fusion diagram" like depicted in fig. 6 of ref. [14], i.e. via the elementary reaction $\pi\pi \to (f_0) \to K\bar{K}$. The amplitude for this reaction is taken from the Jülich model [1] described in the previous section. In order to study the effects of a genuine f_0 meson an alternative model, presented in ref. [15], is employed in which the structure in the $\pi\pi$ $JI = 00$ phase shifts is not generated by a $K\bar{K}$ bound state (as in the original Jülich model) but by a pole diagram with properly adjusted bare mass and coupling constant. The amplitude of this model would roughly correspond to a Flatté representation of the f_0 meson.

Results for the $K\bar{K}$ invariant mass spectrum for two different excess energies (Q = 5 MeV and Q = 30 MeV) are shown in fig. 4 and compared to the 4–body phase space behaviour. Note that all results are normalized in such a way that they coincide with the experimental K^+K^- production cross section at Q = 17 MeV presented in ref. [16].

Evidently, at the excess energy of Q = 5 MeV (left) the results look very similar — except for the overall normalization. At Q = 30 MeV (right), however, the model calculations show significant differences from the pure phase space. Specifically, the maxium values of the distributions are shifted to lower invariant masses. This shift is noticeably larger for the $\pi\pi - K\bar{K}$

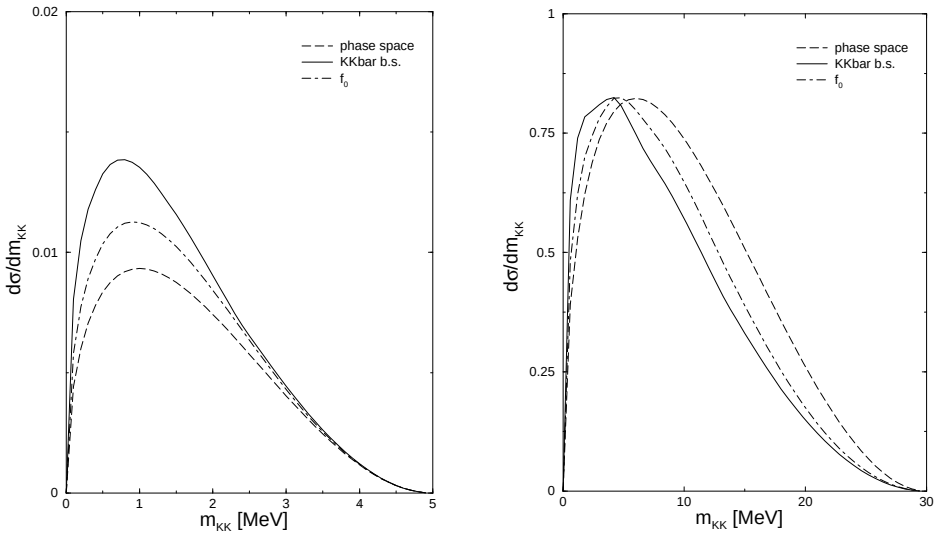

Figure 4: Invariant mass spectrum of the $K\bar{K}$ system for the reaction $NN \to NNK\bar{K}$. The dashed line is the phase space behavior. The solid line is the prediction based on the $\pi\pi - K\bar{K}$ model of the Jülich group. The dash-dotted curve shows the results for a genuine f_0 meson.

model, i.e. the model were the f_0 meson is interpreted as a $K\bar{K}$ bound state, as compared to the model with a genuine f_0 state. Thus, we can conclude that the invariant mass spectrum is definitely sensitive to the structure of the f_0 meson. But, certainly, one has to admit that the effects are not very large and therefore high precision experiments are required in order to obtain conclusive results.

References

[1] G. Janssen, B.C. Pearce, K. Holinde, and J. Speth, Phys. Rev. **D 52** (1995) 2690.

[2] S. Weinberg, Phys. Rev. **166** (1968) 1568.

[3] M. Bando, T. Kugo, and K. Yamawaki, Nucl. Phys. **B 259** (1985) 493.

[4] D. Morgan, Phys. Lett. **B 51** (1974) 71.

[5] J. Weinstein and N. Isgur, Phys. Rev. **D 41** (1990) 2236.

[6] R.L. Jaffe, Phys. Rev. **D 15** (1977) 267.

[7] S.J. Lindenbaum and R.S. Longacre, Phys. Lett. **B 274** (1992) 492.

[8] W. Lockman, in *Hadron '89, Proceedings of the 3rd International Conference on Hadron Spectroscopy*, Ajaccio, France, edited by F. Binon et al. (Editions Frontières, Gif-sur-Yvette, 1989) 109.

[9] A. Falvard et al., Phys. Rev. **D 38** (1988) 2706.

[10] D. Morgan and M.R. Pennington, Phys. Rev. **D 48** (1993) 1185.

[11] D. Morgan and M.R. Pennington, Phys. Rev. **D 48** (1993) 5422.

[12] B.S. Zou and D.V. Bugg, Phys. Rev. **D 50** (1994) 591.

[13] A. Armstrong et al., Z. Phys. **C 52** (1991) 389.

[14] E.L. Bratkovskaya et al., Eur. Phys. J. **A 4** (1999) 165.

[15] O. Krehl, diploma thesis, Jülich 1996, unpublished.

[16] C. Quentmeier et al., Phys. Lett. **B 515** (2001) 276.

Near Threshold K^+K^- Meson–Pair Production in Proton–Proton Collisions

A. Khoukaz, T. Lister, C. Quentmeier, R. Santo

Institut für Kernphysik, Westfälische Wilhelms-Universität, Münster, Germany

Abstract: The near threshold total cross section and angular distributions of K^+K^- pair production via the reaction $pp \to ppK^+K^-$ have been studied at an excess energy of Q = 17 MeV using the COSY-11 facility at the cooler synchrotron COSY. The obtained cross section as well as an upper limit at an excess energy of Q = 3, MeV represent the first measurements on the K^+K^- production in the region of small excess energies where production via the channel $pp \to pp\Phi \to ppK^+K^-$ is energetically forbidden.

1 Introduction

Studies on the kaon-pair production are stimulated by the continuing discussion on the nature of the scalar resonances $f_0(980)$ and $a_0(980)$, which have been interpreted as conventional $q\bar{q}$ states [1], qq-$\bar{q}\bar{q}$ states [2] or as $K\bar{K}$ molecules [3, 4]. Furthermore, exclusive K^- production data are also of special interest in the context of sub-threshold kaon production experiments in nucleus-nucleus interactions, which are expected to probe the antikaon properties at high baryon density.

At the cooler synchrotron COSY [5] near threshold measurements on the reaction $pp \to ppK^+K^-$ have been performed at the internal beam facility COSY-11 [6], using a hydrogen cluster target [7] in front of a C-shaped COSY-dipole magnet, acting as a magnetic spectrometer. Tracks of positively charged particles, detected in a set of two drift chambers, are traced back through the magnetic field to the interaction point, leading to a momentum determination. The velocities of these particles are accessible by a time-of-flight path behind the drift chambers, consisting of scintillation hodoscopes in a distance of $\sim$ 9.3 m. By measuring the momentum and the velocity, a particle identification of the positively charged ejectiles is possible and the four momentum vectors can be completely reconstructed. This yields a full event reconstruction for the reaction type $pp \to ppK^+X$

($X = K^-$) by detecting both outgoing protons as well as the K^+ meson and identifying the X-particle using the missing mass method. Additionally, a silicon pad detector allows to detect the hit position of outgoing K^- mesons.

2 Results

The reaction channel $pp \to ppK^+K^-$ has been studied using the COSY-11 spectrometer at incident proton beam momenta of $\mathrm{p}_{beam} = 3.311\,\mathrm{GeV/c}$ and $3.356\,\mathrm{GeV/c}$, corresponding to excess energies of $\mathrm{Q} = 3\,\mathrm{MeV}$ and $17\,\mathrm{MeV}$ [8]. At the higher excess energy an unambiguous detection of events from the ppK^+K^- reaction is possible, leading to a total number of $\mathrm{N} = 61^{+0}_{-5}$ accumulated K^+K^- events. Due to the high precision of the experimental facility a K^- missing mass resolution of FWHM $\sim 2\,\mathrm{MeV/c^2}$ was achieved.

The accessibility of the four-momentum vectors of all ejectiles from ppK^+K^- events allows to study angular distributions of the particles or systems of particles. Monte-Carlo simulations on the free $pp \to ppK^+K^-$ reaction, considering the pp FSI and the Coulomb interaction, have been performed to determine the acceptance of the detection system in order to obtain acceptance corrected kinematical distributions. The overall detection efficiencies for events from the non-resonant K^+K^- production, requiring the detection of both protons and the K^+ meson, were determined to be $\epsilon\,(3\,\mathrm{MeV}) = \left(6.4 \cdot 10^{-2}\right)^{+43\%}_{-28\%}$ and $\epsilon\,(17\,\mathrm{MeV}) = \left(7.4 \cdot 10^{-3}\right)^{+10\%}_{-13\%}$. These quantities take into account the kaon decay, detection and track reconstruction efficiencies as well as the influence of the error in the absolute excess energies, which are known with a precision of $\Delta\mathrm{Q} = 1\,\mathrm{MeV}$, caused by the uncertainty in the determination of the absolute COSY beam momentum ($\Delta\mathrm{p/p} = 10^{-3}$). In fig. 1 the angular distributions in the center of mass system relative to the beam direction for the extracted ppK^+K^- events are shown for both outgoing protons (a), the K^+K^- system (b), the K^+ mesons (c) and the K^- mesons (d). Within the statistical errors the measured distributions of the protons and the kaons show no significant deviation from an isotropic emission.

The luminosity was determined by comparing the differential counting rates of elastically scattered protons with data recorded by the EDDA collaboration [9]. The integrated luminosities were extracted to be $\int L\,dt = 0.84\,\mathrm{pb}^{-1} \pm 1\,\%\,(\mathrm{stat.}) \pm 5\,\%\,(\mathrm{syst.})$ at $\mathrm{Q} = 3\,\mathrm{MeV}$ and $\int L\,dt = 4.50\,\mathrm{pb}^{-1} \pm 1\,\%\,(\mathrm{stat.}) \pm 5\,\%\,(\mathrm{syst.})$ at $\mathrm{Q} = 17\,\mathrm{MeV}$, corresponding to a mean luminosity of $L = 2 \cdot 10^{30}\,\mathrm{cm}^{-2}\,\mathrm{s}^{-1}$.

In fig. 2 the present result at $\mathrm{Q} = 17\,\mathrm{MeV}$ (filled symbol) and a data

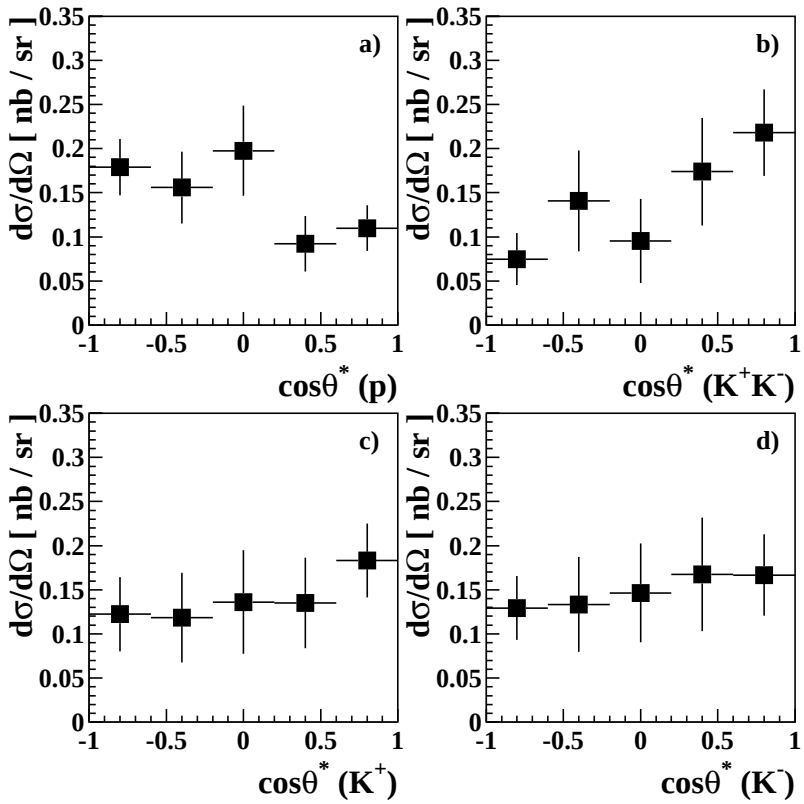

Figure 1: Angular distributions in the overall CMS relative to the beam direction of the extracted ppK^+K^- events for both outgoing protons (a), the K^+K^- system (b), the K^+ mesons (c) and the K^- mesons (d).

point from the DISTO collaboration [10], excluding the contribution from the Φ, are plotted as function of the excess energy. These data represent the available world data for the K^+K^- production via the reaction channel $pp \to ppK^+K^-$ in the near threshold region (threshold: $\mathrm{p}_{beam} = 3.30175\,\mathrm{GeV/c}$).

The total cross section at an excess energy of $\mathrm{Q} = 17 \pm 1\,\mathrm{MeV}$ was determined to be $\sigma = \left(1.80 \pm 0.27^{+0.28}_{-0.35}\right)$ nb, including statistical and systematical errors [8]. The upper limit at $\mathrm{Q} = 3\,\mathrm{MeV}$ was determined to be $\sigma < 0.16\,\mathrm{nb}$ on the basis of a confidence level of 95 % [8].

Fig. 2 shows parametrizations on the K^+K^- cross sections assuming different production processes. The solid line, representing a fit to the data points on the basis of a four-body S-wave phase space expectation including the proton-proton final state interaction (FSI) [8], describes the data points

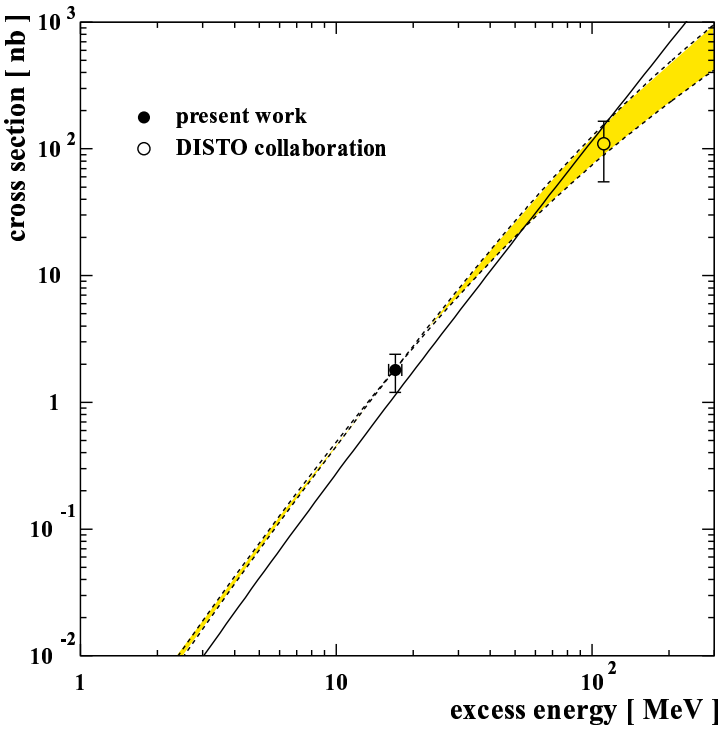

Figure 2: Total cross sections for the free K^+K^- pair production in proton-proton collisions. The curves are described in the text.

adequately within the error bars. Therefore, the total cross section data points are consistent with a description based on the free ppK^+K^- production with no distinct effects of higher partial waves or strong K^+K^- final state interactions. Although not suggested by our previously discussed results, one can calculate the cross section for the $pp \to ppf_0(980) \to ppK^+K^-$ channel, leading to a value of $\sigma\,(pp \to ppf_0 \to ppK^+K^-) = 1.84 \pm 0.29^{+0.25}_{-0.33}$ nb. The dashed lines present three-body phase space calculations for the ppK^+K^- final state via the excitation of the broad f_0 resonance including the pp FSI and normalized to this $\sigma\,(pp \to ppf_0 \to ppK^+K^-)$. Here we assumed the $f_0(980)$ to be a Breit-Wigner distribution with a mass of m = 980 MeV/c^2. The effect of the large uncertainty about the width of the $f_0(980)$ resonance (Γ = 40 MeV/c^2 to 100 MeV/c^2 [11]) is indicated by the dashed area. Nevertheless, within the error bars also this description is

consistent with the measured data. Consequently, the two data points are in agreement with both the assumption of a non-resonant as well as a resonant production via the f_0, always neglecting effects of higher partial waves.

References

[1] D. Morgan, M. R. Pennington, Phys. Rev. **D 48** (1993) 1185.

[2] R. Jaffe, Phys. Rev. **D 15** (1977) 267.

[3] J. Weinstein, N. Isgur, Phys. Rev. **D 41** (1990) 2236.

[4] D. Lohse et al., Nucl. Phys. **A 516** (1990) 513.

[5] U. Bechstedt et al., Nucl. Instr. & Meth. **B 113** (1996) 26; R. Maier, Nucl. Instr. & Meth. **A 390** (1997) 1.

[6] S. Brauksiepe et al., Nucl. Instr. & Meth. **A 376** (1996) 397.

[7] H. Dombrowski et al., Nucl. Instr. & Meth. **A 386** (1997) 228.

[8] C. Quentmeier et al., Phys. Lett. **B 515** (2001) 276; doctoral thesis, Westfälische Wilhelms-Universität Münster, Germany (2001).

[9] D. Albers et al., Phys. Rev. Lett. **78** (1997) 1652.

[10] F. Balestra et al., Phys. Lett. **B 468** (1999) 7.

[11] D.E. Groom et al., *The Review of Particle Physics*, Eur. Phys. J. **C 15** (2000) 1.

Energy Dependence of the pp $\rightarrow$ ppK$^+$K$^-$ Total Cross Section Close to Threshold

M. Wolke and A. Sibirtsev

Institut für Kernphysik, Forschungszentrum Jülich, Germany

Abstract: In order to study the energy dependence of the total $pp \rightarrow ppK^+K^-$ cross section below the Φ production threshold, measurements have been performed at the COSY–11 installation at two excess energies Q in addition to the recently published value at Q = 17 MeV. While data taking has been quite successful at an excess energy of 28 MeV, due to experimental problems the integrated luminosity reached at Q = 10 MeV may not allow to deduce a total cross section value.
The status of the analysis is presented and further theoretical motivation is given for a measurement very close to the elementary antikaon production threshold.

1 Introduction

Close to threshold, the energy dependence of the total cross section for reactions $pp \rightarrow ppX$, where X denotes a single meson or a mesonic system being produced, is determined by phase–space behaviour modified by final state interactions (FSI) of the outgoing particles, predominantly the strong proton–proton FSI. Any deviations from the expected behaviour might be attributed to either changes in the primary production amplitude or effects of final state interactions, i.e. in the kaon–nucleon, antikaon–nucleon or kaon–antikaon subsystems in case of the ppK^+K^- final state.

It should be noted, that possible interpretations of scalar resonances in the 1 GeV/c^2 mass range crucially depend on the strength of the poorly known kaon–antikaon interaction [1]: Within the framework of the Jülich meson exchange model, the $K\overline{K}$ interaction determines both scale and shape of $\pi\pi \rightarrow K\overline{K}$ cross sections. First exploratory calculations on $K\overline{K}$ production in proton–proton scattering in view of the nature of scalar resonances are presented in [2].

K^+K^- Production Studies at COSY–11

Recently, a first value of the total cross section for the reaction $pp \to ppK^+K^-$ below the Φ production threshold at an excess energy of 17 MeV has been published by the COSY–11 collaboration [3, 4].

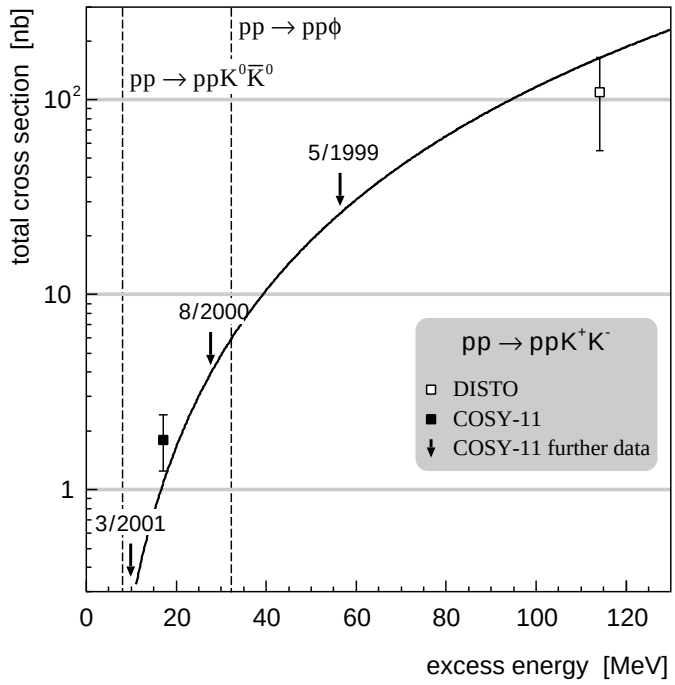

Figure 1: Total cross section for K^+K^- production in proton–proton scattering close to threshold. Data are from the DISTO collaboration (open symbol [5]) and COSY–11 (filled symbol [3, 4]) and include both statistical and systematical errors. The solid line corresponds to an energy dependence of the total cross section based on four–body phase space modified by proton–proton FSI [6], fitted to the COSY–11 and DISTO data. Arrows denote further COSY–11 measurements, the dashed lines indicate the $K^0\overline{K^0}$ and Φ production thresholds, respectively.

In order to study the energy dependence of the total cross section, further measurements [7, 8] have been performed at excess energies of Q = 10 and Q = 28 MeV above the K^+K^- production threshold in March 2001 and August 2000, respectively (Figure 1). For a report on a study of feasibility on K^+K^- production above the Φ threshold see [9].

Preliminary Results at Q = 28 MeV

In August 2000, data have been taken at an excess energy of Q = 28 MeV (p_{beam} = 3.390 GeV/c) for a total running time of 13 days and 5 hours. To identify (ppK^+K^-) final states, three–track events with two identified protons and one additional positively charged particle have been analyzed. The invariant mass of the latter is calculated by combining the reconstructed momentum and the time–of–flight between the nominal target position and the S1 scintillator, with the time of the event at the target being inferred from tracing back the two proton trajectories.

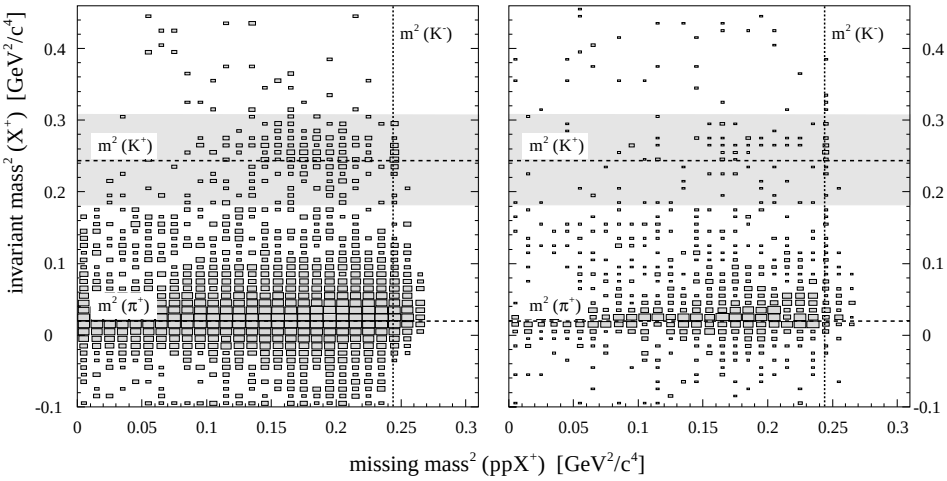

Figure 2: Invariant mass squared of a third positively charged particle in addition to two identified protons versus missing mass squared with respect to the assumed (ppK^+) subsystem at an excess energy of 28 MeV (p_{beam} = 3.390 GeV/c) without (left, logarithmic scale) and with (right, linear scale) the additional requirement of a registered hit in the negative particle detection system.

On the scale of the invariant mass, in addition to the dominant pion contribution a kaon signal within the expected resolution (shaded area in figure 2) is obvious. Within the range of identified kaons, an enhancement is clearly visible close to the kaon mass on the scale of the missing mass with respect to an identified (ppK^+) subsystem, as expected for ppK^+K^- final states. The ppK^+K^- consistent signal remains when requiring an additional hit in the scintillator of the dedicated negative particle detection system mounted inside the dipole gap, while both $pp\pi^+X$ events and ppK^+X events

associated with lower values of the missing mass are effectively reduced in number.

Preliminary missing mass distributions with respect to the detected (ppK^+) subsystem, i.e. projections of figure 2 within the range of identified kaons, are presented in figure 3.

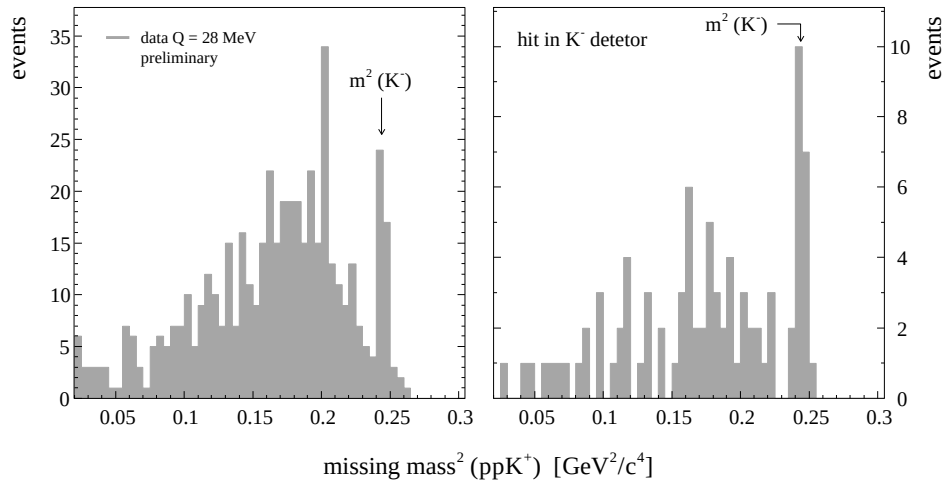

Figure 3: Missing mass squared with respect to an identified (ppK^+) subsystem at an excess energy of 28 MeV ($p_{beam} = 3.390$ GeV/c) without (left) and with (right) the additional requirement of a registered hit in the negative particle detection system.

A signal at the expected position of the charged kaon mass is evident and stands out of a broad background structure (Figure 3 left), which in case of the recently published data at Q = 17 MeV has been well reproduced by contributions from misidentified pions and the excitation of the hyperon resonances $\Lambda\,(1405)$ and $\Sigma\,(1385)$ [3]: In the latter case one of the identified protons may originate from the weak decay of a previously produced hyperon Y via $pp \to pK^+Y \to pK^+pX$ where X denotes a system of one or more undetected particles. In consequence, the missing mass with respect to the identified (ppK^+) subsystem may shift to values too small for a ppK^+K^- hypothesis.

Requiring an additional hit in the negative particle detection system leads to independent proof, with a drastic suppression of the background structure in the region of lower missing masses and a clean signal at the K^- mass (Figure 3 right), the latter with a reduction quantitatively in good agreement with Monte Carlo simulations. Although measured and

expected hit positions of the associated K^- have not yet been compared at this preliminary stage of the analysis, the final result is expected to be as free of background as shown for the measurement at Q = 17 MeV (Figure 3 in [3]). A value of the total $pp \to ppK^+K^-$ cross section at Q = 28 MeV has to await the analysis of proton–proton elastic scattering data measured simultaneously.

Preliminary Results at Q = 10 MeV

Data at an excess energy of 10 MeV with respect to the ppK^+K^- threshold have been taken during 15 days and 20 hours out of a three week beam time in March 2001. However, several hardware problems at the cluster target resulted in a luminosity determined online, which fell short of standard values by roughly one order of magnitude.

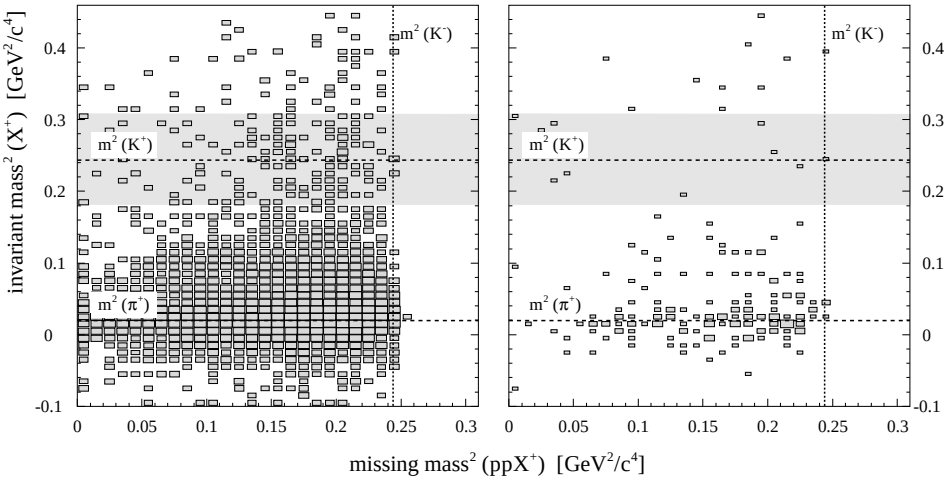

Figure 4: Invariant mass squared of a third positively charged particle in addition to two identified protons versus missing mass squared with respect to the assumed (ppK^+) subsystem at an excess energy of 10 MeV (p_{beam} = 3.333 GeV/c) without (left, logarithmic scale) and with (right, linear scale) the additional requirement of a registered hit in the negative particle detection system.

The distribution of the invariant mass of a third positively charged ejectile in addition to two identified protons is shown as a function of the missing mass with respect to the assumed (ppK^+) subsystem in figure 4. In comparison to the result presented for the measurement at Q = 28 MeV (Fig. 2),

the dominant pion signal appears to be significantly broader, and, consequently, kaons are not as well separated from the pion background (Fig. 4 left). This might still be accounted for by timing shifts of the S1 scintillator, which have not yet been corrected at the present stage of the analysis. However, within the expected resolution of the kaon mass, few candidates for a (ppK^+K^-) final state remain. Requiring an additional hit in the scintillator of the K^- detection system, the number of events consistent with a K^+K^- production hypothesis reduces to one (Fig. 4 right). Note, that statistics with an additional K^- consistent hit only cover three–quarter of data taking, as the scintillator was damaged towards the end of the beam time [1].

In figure 5 preliminary results for the missing mass with respect to a (ppK^+) subsystem are given for events with an identified positively charged kaon (shaded area in figure 4) in addition to two detected protons in the final state.

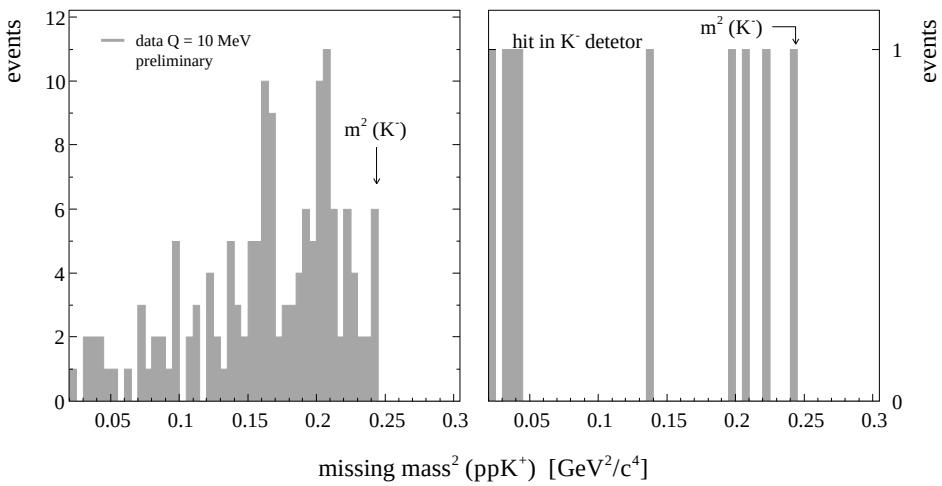

Figure 5: Missing mass squared with respect to an identified (ppK^+) subsystem at an excess energy of 10 MeV ($p_{beam} = 3.333$ GeV/c) without (left) and with (right) the additional requirement of a registered hit in the negative particle detection system.

Without requiring a K^- consistent hit, six events remain compatible

[1] In the final analysis the K^- consistency of hits in the negatively charged particle detection system will be checked by means of the highly granulated silicon pad detector and the results will cover the whole period of data taking independently of any hardware damage of the respective scintillator.

with a ppK^+K^- hypothesis, however, as mentioned above, only one event exhibits a hit in the dedictated K^- scintillator. Thus, in view of the rather low statistics in result of the low integrated luminosity reached during the March 2001 beam time, including the response of the silicon pad detector inside the dipole in the analysis appears to be crucial for a final answer, whether the data taken so far allow to extract a total cross section value at all.

A determination of the total cross section very close to the antikaon production threshold below the previously published data, i.e. for example at $Q = 10\,\mathrm{MeV}$, is especially motivated by very recent theoretical investigations, which will be outlined in the subsequent section.

Physical Motivation

The detailed experimental studies of the reactions $pp \to pp\eta$, $pp \to pp\omega$ and $pp \to pp\eta'$ indicate three following general features:

First, the total η, ω and η' production cross sections σ show very similar dependences on the excess energy, defined as $Q = \sqrt{s} - 2\,m_N - m_X$ with s, m_N and m_X being the squared invariant collision energy and the nucleon and meson masses, respectively.

Second, at $100 \leq Q \leq 1000\,\mathrm{MeV}$ the energy dependence of the total cross section is dominated by three–body phase space ($\sigma \propto Q^2$).

Third, the deviation of data from an Q^2 dependence below $100\,\mathrm{MeV}$ arises from the interaction between the final state protons and possibly between the final state proton and meson. The latter was clearly observed in case of the $pp \to pp\eta$ reaction.

The features listed above can be well illustrated by the data [10, 11, 12, 13, 14, 15] on the reaction $pp \to pp\eta'$, where the possible effect due to the $p\eta'$ final state interaction (FSI) is expected to be almost negligible. Figure 6a) shows the data available for the $pp \to pp\eta'$ cross section as a function of excess energy Q. The dashed line indicates the phase space dependence as $\sigma \propto Q^2$, which apart from the normalization constant reproduces the data at $Q > 100\,\mathrm{MeV}$. The solid line shows the calculations [16, 17] without pp FSI, which explicitly follows the phase space dependence. The dotted line in figure 6a) indicates the effect due to the pp FSI.

Now, the very recent $pp \to ppK^+K^-$ measurement by COSY–11 [3] as well as the DISTO result [5] are shown in figure 6b). The data are in a reasonable agreement with the theoretical calculations without FSI [18] shown by the solid line. In contrast to the η, ω and η' production, the

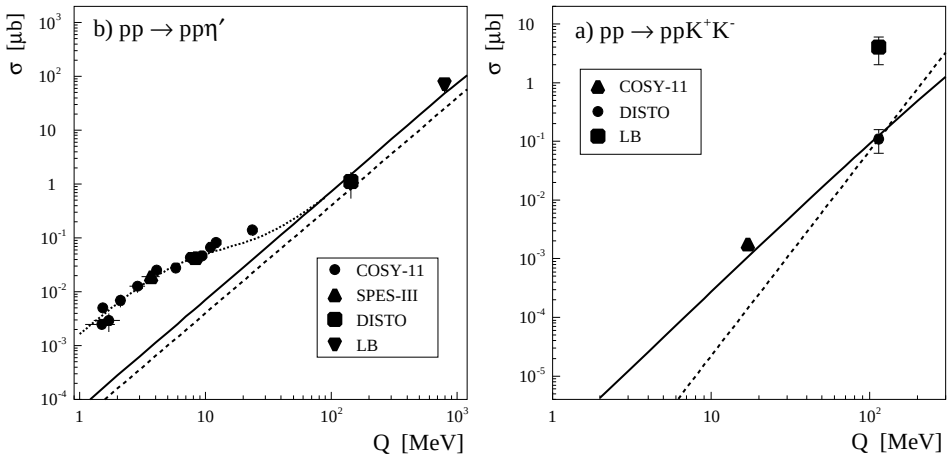

Figure 6: a) The $pp \to pp\eta'$ cross section as a function of excess energy. The data are from [10, 11, 12, 13, 14, 15], the dashed line shows the phase space Q^2–dependence, the solid line indicates calculations without FSI [16, 17], the dotted line shows the parameterization of the pp FSI. b) The $pp \to ppK^+K^-$ cross section. The data are from [3, 5, 15], the solid line shows the calculations of [18], the dashed line indicates the phase space $Q^{7/2}$–dependence.

calculations for the $pp \to ppK^+K^-$ reaction substantially deviate from the 4–body phase space dependence given as $Q^{7/2}$ and shown by the dashed line in figure 6b).

This nontrivial energy dependence of the $pp \to ppK^+K^-$ cross section can be understood in terms of the scattering diagrams shown by figure 7a-b). In that case the energy dependence of the $pp \to pp\eta'$ and $pp \to ppK^+K^-$ cross section is driven by the energy dependence of the relevant scattering amplitudes.

The $\pi^0 p \to \eta' p$, $K^- p \to K^- p$ and $K^+ p \to K^+ p$ scattering amplitudes squared $|\mathrm{M}|^2$ can be evaluated from experimental data [15] on relevant cross sections as

$$\frac{\mathrm{d}\,\sigma}{\mathrm{d}\,\Omega} = \frac{1}{64\,\pi^2\,s}\,\frac{\mathrm{q}_f}{\mathrm{q}_i}\,|\mathrm{M}|^2, \tag{1}$$

where s is squared invariant energy of the interacting particles, while q_i and q_f are their momenta in the initial and final states, respectively, taken in the center of mass system.

Now, figure 7c) shows the data [15] on the $\pi^- p \to \eta' n$ and $\pi^+ n \to \eta' p$ amplitudes squared that almost do not depend on the invariant πN collision

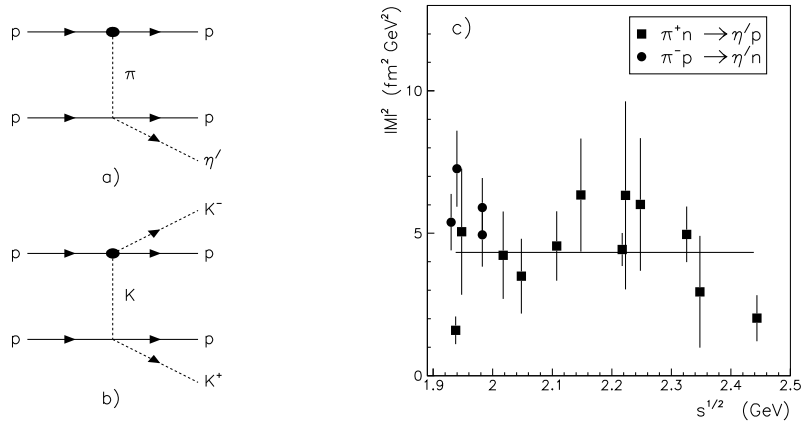

Figure 7: a-b) The scattering diagrams for the reactions $pp \to pp\eta'$ and $pp \to ppK^+K^-$. c) The squared amplitude for the $\pi N \to \eta' N$ scattering as a function of the πN invariant collision energy. The solid line shows a fit by a constant value.

energy and can be well fitted by a constant value, shown by the solid line.

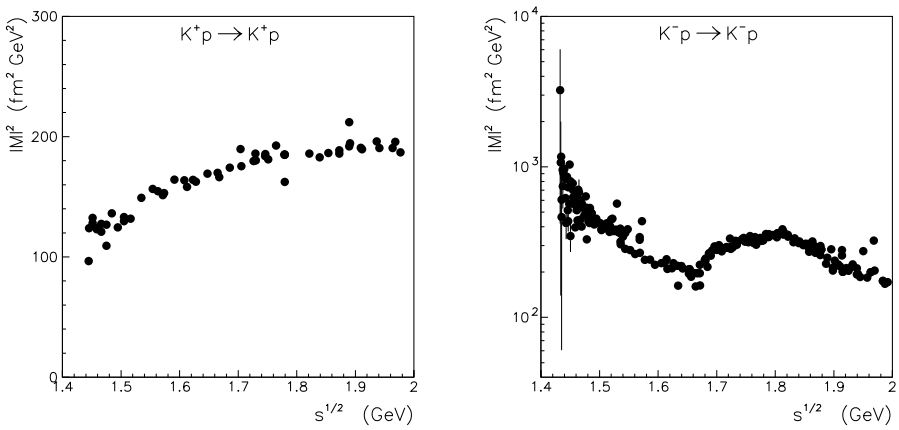

Figure 8: The $K^+p \to K^+p$ and $K^-p \to K^-p$ scattering amplitudes squared as a function of the KN invariant collision energy.

In opposite, the $K^+p \to K^+p$ and $K^-p \to K^-p$ scattering amplitudes [15] indicate a substantial energy dependence, as illustrated by figure 8.

Obviously, it is necessary to collect more $pp \to ppK^+K^-$ data in order to clarify whether such reaction dynamics lead to the deviation of the near threshold K^+K^- production cross section from a trivial phase space $Q^{7/2}$–dependence.

Moreover, by comparing the recent COSY–11 result [3] with the calculations shown by the solid line in figure 6b) one might detect no room for the FSI. The calculations were performed neglecting FSI. Note that the three body reaction with η, ω and η' production indicate strong FSI at excess energies $Q \leq 100$ MeV. It is not clear whether the absence of the FSI effect in the $pp \to ppK^+K^-$ reaction can be explained by partial compensation of the pp and K^-p interaction in the final state or because of an additional degree of freedom given by the 4–body final state. In the latter case the FSI can be more pronounced at energies very close to the $pp \to ppK^+K^-$ reaction threshold and it would be of specific interest to measure the cross section at Q below that 17 MeV data point investigated recently by COSY–11 [3].

Furthermore, it might be possible that the presence of two pairs of strongly interacting particles as pp and K^-p in the final state could no longer be considered by the factorization in terms of two–body different interactions and one would be faced with the four–body problem. In that case the $pp \to ppK^+K^-$ measurements provide a unique opportunity to get insight into the problem experimentally.

References

[1] O. Krehl, R. Rapp, J. Speth, Phys. Lett. **B 390** (1997) 23.

[2] J. Haidenbauer, contribution to these proceedings.

[3] C. Quentmeier et al., Phys. Lett. **B 515** (2001) 276.

[4] A. Khoukaz, T. Lister, C. Quentmeier, R. Santo, contribution to these proceedings.

[5] F. Balestra et al., Phys. Rev. **C 63** (2001) 024004.

[6] G. Fäldt, C. Wilkin, Z. Phys. **A 357** (1997) 241.

[7] M. Wolke et al., *Threshold Kaon Production in the Proton–Proton Interaction at COSY–11*, COSY–Proposal No. 61, May 1998.

[8] M. Wolke, C. Quentmeier et al., *Energy Dependence of the $pp \to ppK^+K^-$ Total Cross Section Close to Threshold*, COSY–Proposal No. 61.2, May 2000.

[9] M. Wolke, contribution to these proceedings.

[10] F. Hibou et al., Phys. Lett. **B 438** (1998) 41.

[11] P. Moskal et al., Phys. Rev. Lett. **80** (1998) 3202.

[12] P. Moskal et al., Phys. Lett. **B 474** (2000) 416.

[13] P. Moskal et al., Phys. Lett. **B 482** (2000) 356.

[14] F. Balestra et al., Phys. Lett. **B 491** (2000) 29.

[15] A. Baldini, V. Flaminio, W.G. Moorhead, D.R.O. Morrison, *Total Cross–Sections for Reactions of High Energy Particles*, ed. by H. Schopper, Landolt-Börnstein, *New Series* **I/12**, Springer, Berlin (1988).

[16] A. Sibirtsev, W. Cassing, Eur. Phys. J. **A 2** (1998) 333.

[17] V. Baru, J. Haidenbauer, A. Kudryavtsev, P. Moskal, J. Speth, C. Hanhart, Eur. Phys. J. **A 6** (1999) 445.

[18] A. Sibirtsev, W. Cassing, C.M. Ko, Z. Phys. **A 358** (1997) 101.

Total Cross Section of the Reaction pp → ppΦ at Threshold

M. Wolke

Institut für Kernphysik, Forschungszentrum Jülich, Germany

Abstract: As a study of feasibility data on close–to–threshold Φ production in proton–proton scattering have been taken at the COSY–11 facility. Despite a sizeable detection probability suggested by cross section estimations and studies of the detection efficiency, within the limited statistics of the present data set no unique signal of Φ production can be deduced. Experimental results and theoretical interpretations of Φ production both in nucleon–nucleon collisions and nucleon–antinucleon annihilation are discussed and the status of the preliminary analysis is presented.

1 Introduction

Within the quark model the Φ meson is an (almost) ideally mixed $s\overline{s}$ state, whereas the nucleon is composed only of u– and d–quarks. According to the OZI rule [1] [1], Φ production in the nucleon–nucleon interaction would be forbidden as a process with disconnected quark lines, if the Φ was a pure $s\overline{s}$ state.

However, due to a small deviation from ideal mixing ($\delta_V = 3.7°$ [3]) the Φ meson is allowed to couple to the nucleon through its $\left(u\overline{u} + d\overline{d} \right)$ admixture. Quantitatively, the naive OZI rule results in a suppression of Φ compared to ω production in hadronic interactions

$$R = \frac{\sigma\,(A\,B \to \Phi\,X)}{\sigma\,(A\,B \to \omega\,X)} = \tan^2(\delta_V) \approx 4.2 \times 10^{-3} \tag{1}$$

after phase space corrections, where A, B and X denote hadronic systems consisting only of light quarks [4]. Any significant deviation might be interpreted as a hint for a strangeness component in the nucleon. A significant contribution of strange sea quarks to the nucleon wave function is suggested by results on the $\Sigma_{\pi N}$ term in pion nucleon elastic scattering [5],

[1] for a review see [2].

on the nucleon's structure function in deep inelastic scattering with polarized muons [6] and, more recently, on charm production in deep inelastic neutrino scattering [7].

Large violations of the OZI expectation (1) have been found in $p\overline{p}$ annihilation experiments by the ASTERIX, Crystal Barrel and OBELIX collaborations at LEAR (as reviewed in [8]). However, deviations are predominantly found in $p\overline{p}$ annihilation at rest as compared to higher energies, and seem to be restricted to S–wave annihilations. Furthermore, the results are strongly dependent on the final state: While the $\Phi\,\pi$ and $\Phi\,\gamma$ channels exceed the OZI value by a factor of 20 and 100, respectively, little or no effect is seen in the $\Phi\,\pi\,\pi$ and $\Phi\,\eta$ final states.

These data have been interpreted as "shake–out" and "rearrangement" of a negatively polarized $s\overline{s}$ Fock space component of the proton wave function [8], which also accounts for large double $\Phi\,\Phi$ cross sections [9] in $p\overline{p}$ annihilation measured at the JETSET experiment [10]. However, OZI–allowed two–step processes via intermediate $K\overline{K}$ or $\Lambda\overline{\Lambda}$ states have been shown to describe available data from $p\overline{p}$ annihilation without any strangeness in the nucleon [11, 12, 13, 14, 15, 16].

In nucleon–nucleon scattering, effects of competing two step processes for Φ production are expected to be of minor importance [17, 18]. Furthermore, in close–to–threshold Φ production the entrance channel must be in a $^3\mathrm{P}_1$ state due to parity and angular momentum conservation, and it is the spin triplet fraction in $p\overline{p}$ annihilation which is strongly correlated to the Φ meson yield [19]. Thus, cross section ratios for Φ and ω production in proton–proton scattering should clearly indicate possible OZI violations and probe the $s\overline{s}$ component of the nucleon.

The exclusive production ratio has been determined in the reaction $pp \to pp\Phi/\omega$ at a beam momentum of 3.67 GeV/c corresponding to an excess energy of 82 MeV with respect to the Φ threshold by the DISTO collaboration at SATURNE [20]. After phase space corrections, the observed ratio exceeds the OZI expectation by an order of magnitude, while data at excess energies larger than 1.6 GeV [21] show an enhancement smaller by a factor of three. At least to this extent, one boson exchange models [22, 23, 24] underestimate the absolute value of the Φ production cross section measured at the DISTO experiment. However, when comparing to the ω production cross section at the same excess energy — reducing uncertainties due to the available phase space, partial wave amplitudes and effects of the proton–proton final state interaction (FSI) — the excess over the OZI prediction reduces to a factor of five.

In the DISTO results, Φ production at an excess energy of 82 MeV ap-

pears to be dominated by S–wave relative to the nucleon–nucleon system. However, the angular distribution of the proton–proton system is found to deviate significantly from isotropic emission at this beam energy with evidence for a P–wave contribution in the final state [20]. Consequently, Φ production at 82 MeV above threshold partly proceeds via the $^1S_0$ and $^1D_2$ spin singlet entrance channels. Thus, the influence of the spin triplet entrance channel, prerequisite to a "rearrangement" of an $s\bar{s}$ component in the nucleon wave function [8], might be diluted in the presently available data and would be expected to be more prominent in data closer to the production threshold.

Recently, within the framework of a relativistic meson exchange model, nucleonic and meson–exchange currents have been taken into account explicitly to study vector meson production in nucleon–nucleon scattering [25, 26, 27]. Angular distributions of the produced mesons are expected to differ depending on the dominant production mechanism [25]. This allows to isolate the nucleonic current contribution, and to determine the ΦNN coupling directly. The experimentally observed isotropic Φ angular distribution [20] clearly favours a dominant $\Phi\rho\pi$ meson exchange contribution over the nucleonic current, which would result in a $\cos^2\Theta$ behaviour. The value of the Φ coupling to the nucleon presently extracted from the DISTO data is consistent with the OZI expectation and still has large uncertainties, due to the lack of more and precise data in the threshold region [27].

2 Close–to–threshold Φ Production at COSY–11

The reaction $pp \to pp\Phi$ has been measured in May 1999 as a study of feasibility [28] at the COSY–11 installation [29]. Data have been taken for a total running time of 3 days and 22 hours at a beam momentum of $p_{beam} = 3.481\,\mathrm{GeV/c}$, i.e. at excess energies of 24 MeV and 56 MeV to the Φ and K^+K^- production thresholds, respectively.

Figure 1 shows the available data on associated strangeness production in the $1\,\mathrm{GeV/c^2}$ mass range via $pp \to pp\Phi$ and the non–resonant ppK^+K^- final state. Assuming the energy dependences to be dominated by three– and four–body phase space, respectively, modified by the proton–proton final state interaction [32] and normalizing to the existing data, total cross section estimations can be derived: At $3.481\,\mathrm{GeV/c}$ the cross section for the reaction $pp \to pp\Phi$ exceeds with a value of $\approx 45\,\mathrm{nb}$ the exclusive non–resonant K^+K^- production by a factor of two. Considering a branching fraction $\Gamma\,(\Phi \to K^+K^-) = 49.2\,\%$ [3] the expected ratio of detected

ppK^+K^- events at COSY–11 for $p_{beam} = 3.481\,\mathrm{GeV/c}$ from resonant compared to non–resonant production is expected to be given by the ratio of detection efficiencies, which has been determined by means of Monte Carlo simulations to be $\approx 70\,\%$[2].

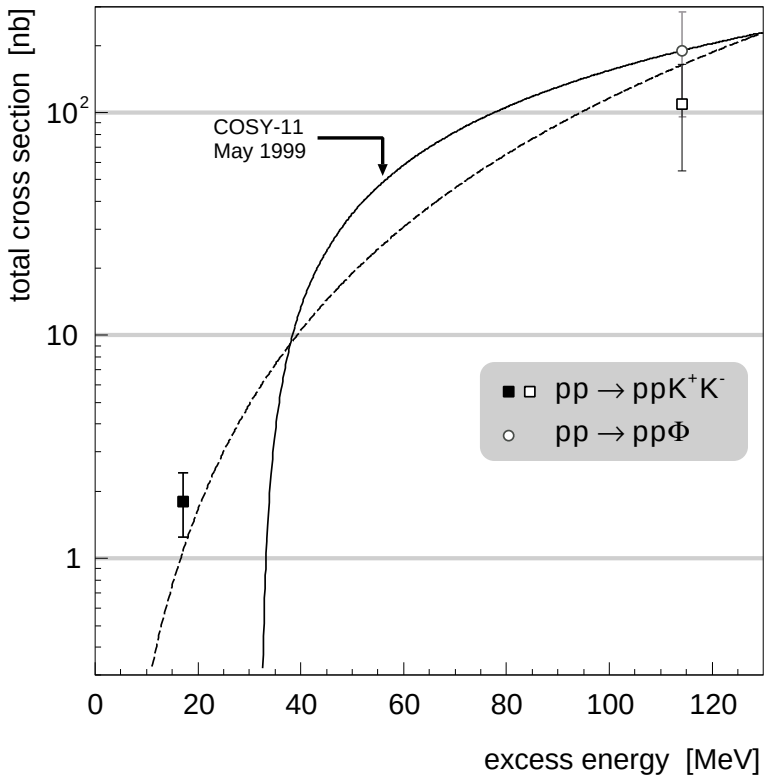

Figure 1: Total cross section for Φ and K^+K^- production in proton–proton scattering close to threshold. Data are from the DISTO collaboration (open symbols [20]) and COSY–11 (filled symbol [30, 31]) and include both statistical and systematical errors. The solid and dashed line correspond to energy dependences of the total cross sections based on three– and four–body phase space modified by proton–proton FSI [32] for Φ (normalized to the DISTO data point) and K^+K^- production (fitted to the COSY–11 and DISTO data), respectively.

Assuming an average luminosity of $2 \times 10^{30}\,\mathrm{cm}^{-2}\mathrm{s}^{-1}$ an overall efficiency of $\approx 0.14\,\%$ for the detection of a (ppK^+) final state from non–resonant

[2]including geometrical acceptance, kaon decay, and reconstruction efficiency

production results in an expected number of ≈ 20 and ≈ 15 events during the total measuring time from non–resonant K^+K^- and resonant $\Phi \to K^+K^-$ production, respectively.

3 Status of the analysis

With the complete four–momentum information of all charged particles in the final state being available at the COSY–11 installation, the reaction $pp \to pp\Phi \to ppK^+K^-$ can be discriminated against non–resonant K^+K^- production via the invariant mass of the charged kaon pair, which is to equal the produced mass of the Φ meson (figure 2).

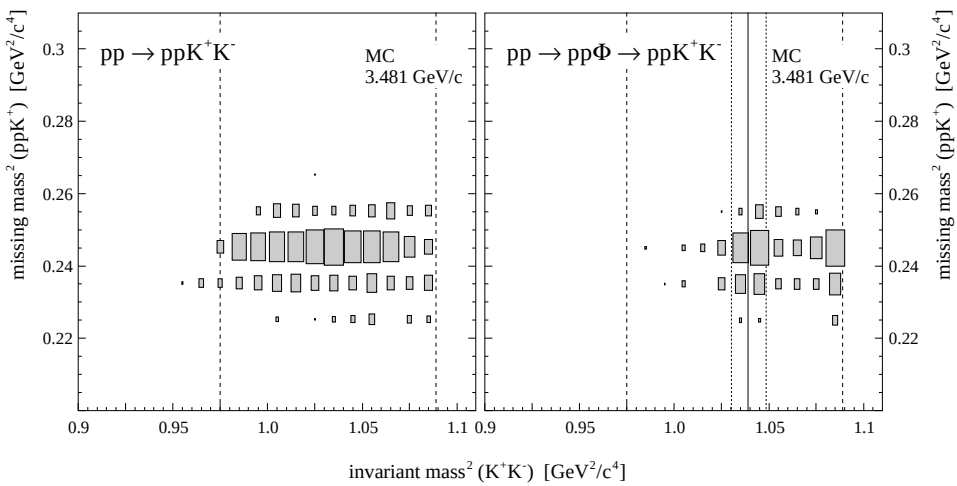

Figure 2: Missing mass squared with respect to an identified (ppK^+) subsystem versus invariant mass squared of the associated K^+K^- meson pair from Monte Carlo simulations at a beam momentum $\mathrm{p}_{beam} = 3.481\,\mathrm{GeV/c}$ taking into account proton–proton final state interaction for non–resonant K^+K^- (left) and resonant $\Phi \to K^+K^-$ production (right). Dashed lines mark the kinematical limits of K^+K^- production at this beam momentum given by $(2\,\mathrm{m}_K)^2$ and $(\sqrt{s} - 2\,\mathrm{m}_p)^2$, respectively. The solid line denotes the mass of the Φ meson squared, its finite width $\Gamma_\Phi = 4.458\,\mathrm{MeV}$ [3] is indicated by the dotted lines (right picture).

While non–resonant production results in a rather flat distribution with respect to the invariant mass of the K^+K^- pair given by four–body phase space modified by the proton–proton final state interaction, a pronounced

signal at the Φ mass is obvious for the resonant $\Phi \to K^+K^-$ production. However, from the finite width of the Φ meson, and due to both the geometrical acceptance of the COSY–11 installation and the effects of the proton–proton FSI favouring (pp) systems of low invariant mass within the distribution of detected events, the resonant distribution exhibits an increase towards the (high) kinematical limit.

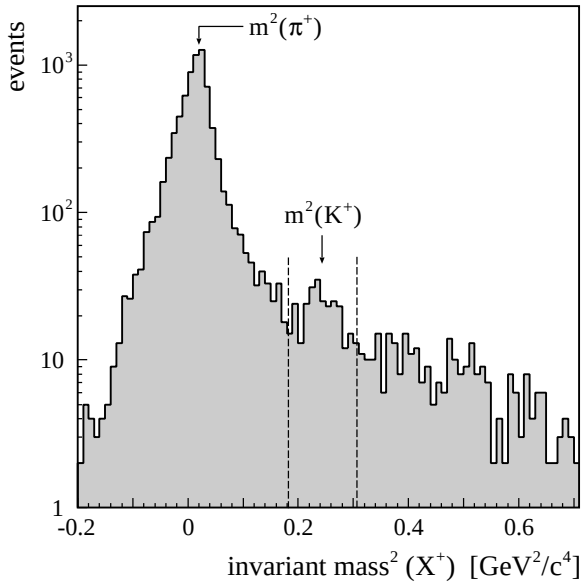

Figure 3: Squared invariant mass of a third positively charged ejectile associated with two identified protons at 3.481 GeV/c. Arrows denote literature masses of π^+ and K^+ [3], dashed lines indicate the cut position used in the following for the K^+ identification.

The analysis of experimental data focuses on the identification of two protons and a positively charged kaon in the final state: Figure 3 exhibits a clear signal of identified kaons in the invariant mass squared of a third charged ejectile in addition to two identified protons on a tail of the dominant pion contribution.

The invariant mass distribution is shown versus the missing mass of the identified (ppK^+) subsystem in figure 4. On the scale of the invariant mass, positively charged kaons appear rather well separated from the dominant pion signal (left picture of figure 4, note the logarithmic scale). A group of 39 events with an identified (ppK^+) subsystem (shaded areas in figure 4) stands out close to the K^- mass — within limits determined from Monte Carlo simulations (figure 2) — as expected for a ppK^+K^- final state.

Requiring an additional hit in the dedicated K^- scintillator mounted inside the dipole gap cleans the spectrum especially in the regions of $(pp\pi^+)$ events and lower missing mass values (right picture of figure 4). Within the resolutions expected for the invariant mass in the kaon mass range and for

the missing mass with respect to an identified (ppK^+) subsystem ten events in total remain consistent with a ppK^+K^- final state.

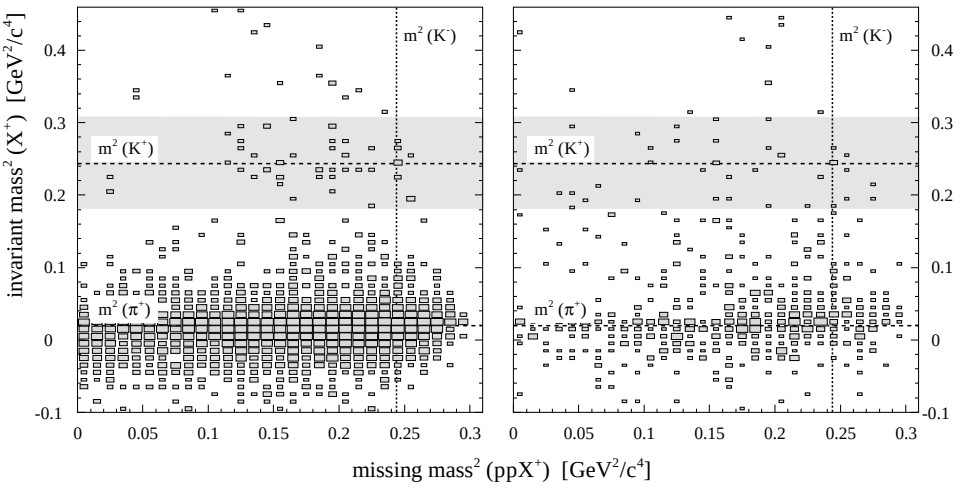

Figure 4: Invariant mass squared of a third positively charged particle in addition to two identified protons versus missing mass squared with respect to the assumed (ppK^+) subsystem without (left picture, logarithmic scale) and with (right, linear scale) requiring an additional hit in the dedicated K^- scintillator inside the dipole gap. Dashed lines indicate literature masses [3], the dashed area corresponds to the cut on the K^+ mass of figure 3.

The missing mass with respect to the (ppK^+) system is shown in figure 5 as a function of the invariant mass of the produced (K^+K^-) pair. Without requiring a detected signal of the K^- in the dedicated scintillator, a slight enhancement close to the Φ mass is obvious (left picture, compare figure 2). However, the signal disappears when demanding an additional K^- consistent hit, although the detection efficiencies of 54 % and 46 % for non–resonant K^+K^- production and the reaction $pp \to pp\Phi \to ppK^+K^-$, respectively, are comparable. In case of an additional K^- consistent hit statistics are obviously too low to draw further conclusions at present (figure 5, right picture).

The total number of candidates for a ppK^+K^- final state falls short of the estimations based on total cross section and acceptance studies by a factor of two. This might be easily accounted for by the integrated luminosity, which so far has not been determined accurately.

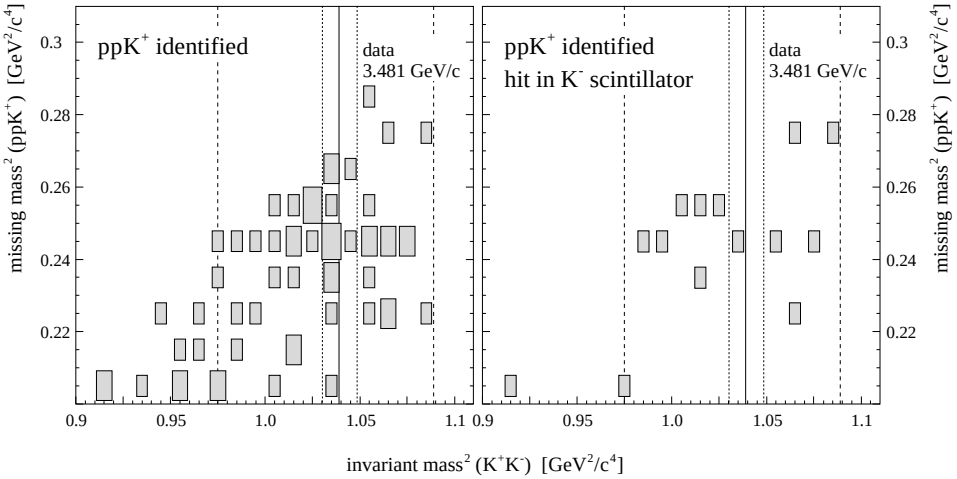

Figure 5: Missing mass squared with respect to the identified (ppK^+) subsystem versus invariant mass squared of the corresponding (K^+K^-) meson pair without (left picture) and with (right) requiring an additional hit in the dedicated K^- scintillator inside the dipole gap. Lines are the same as in figure 2.

The preliminary result presented in figures 4 and 5 might still change in the final analysis, as corrections for possible timing instabilities of the relevant scintillation detectors and thus of the reconstructed invariant masses have to be included.

4 Conclusion

The study of feasibility performed at the COSY–11 facility on the reaction $pp \to pp\Phi \to ppK^+K^-$ shows clear signatures of identified (ppK^+K^-) final states. A discussion of the absolute number of detected events must await a determination of the integrated luminosity, presently falling below estimations based on typical luminosities by a factor of two. Statistics turn out to be too low to give unequivocally evidence of Φ production and to discriminate versus non–resonant K^+K^- production. However, at least the data set should allow to determine an upper limit on the reaction $pp \to pp\Phi$ at a beam momentum of $\mathrm{p}_{beam} = 3.481\,\mathrm{GeV/c}$ and thus on the Φ/ω ratio in proton–proton scattering from the analysis of ω production at the same excess energy [33].

References

[1] S. Okubo, Phys. Lett. **5** (1963) 165; G. Zweig, Report CERN–TH–412 (1964); J. Iizuka, Prog. Theor. Phys. Suppl. **37–38** (1966) 21.

[2] H. Lipkin, Int. J. Mod. Phys. **E 1** (1992) 603.

[3] D.E. Groom et al., Eur. Phys. J. **C 15** (2000) 1.

[4] H. Lipkin, Phys. Lett. **B 60** (1976) 371.

[5] T.P. Cheng, R.F. Dashen, Phys. Rev. Lett. **26** (1971) 594; T.P. Cheng, Phys. Rev. **D 13** (1976) 2161; J. Gasser, H. Leutwyler, M.P. Locher, M.E. Sainio, Phys. Lett. **B 213** (1988) 85; J.Gasser, H.Leutwyler, M.E. Sainio, Phys. Lett. **B 253** (1991) 252.

[6] J. Ashman et al., Phys. Lett. **B 206** (1988) 364; Nucl. Phys. **B 328** (1989) 1; P. Amaudruz et al., Phys. Lett. **B 295** (1992) 159.

[7] T. Adams et al., Workshop on Physics with Electron Polarized Ion Collider – EPIC'99, Bloomington, Indiana, 8–11 Apr 1999, Proc. ed. by L.C. Bland, J.T. Londergan, A.P. Szczepaniak, World Scientific, Singapore (2000) 337 and e–Print Archive hep–ex/9906038; V. Barone, C. Pascaud, F.Zomer, Eur. Phys. J. **C 12** (2000) 243 and references therein.

[8] J. Ellis, M. Karliner, D.E. Kharzeev, M.G. Sapozhnikov, Phys. Lett. **B 353** (1995) 319; Nucl. Phys. **A 673** (2000) 256.

[9] C.B. Dover, T. Gutsche, M. Maruyama, A. Faessler, Prog. Part. Nucl. Phys. **29** (1992) 87.

[10] M. Macri et al., Nucl. Phys. **A 558** (1993) 27c.

[11] M.P. Locher, Y. Lu, B.S. Zou, Z. Phys. **A347** (1994) 281.

[12] O. Gortchakov, M.P. Locher, V.E. Markushin, S. von Rotz, Z. Phys. **A 353** (1996) 447.

[13] V.E. Markushin, M.P. Locher, Eur. Phys. J. **A 1** (1998) 91.

[14] D. Bazatu, F.M. Lev, Phys. Lett. **B 329** (1994) 143; Phys. Rev. **C 51** (1995) R2893.

[15] A.V. Anisovich, E. Klempt, Z. Phys. **A 354** (1996) 197.

[16] V. Mull, K. Holinde, J. Speth, Phys. Lett. **B 334** (1994) 295.

[17] P. Geiger, N. Isgur, Phys. Rev. **D 54** (1996) 1; Phys. Rev. **D 55** (1997) 299.

[18] U.–G. Meißner, V. Mull, J. Speth, J.W. van Orden, Phys. Lett. **B 408** (1997) 381.

[19] A.M. Bertin et al., Phys. Lett. **B 388** (1996) 450.

[20] F. Balestra et al., Phys. Rev. **C 63** (2001) 024004.

[21] V. Blobel et al., Phys. Lett. **B 59** (1975) 88; R. Baldi et al., Phys. Lett. **B 68** (1977) 381; M.W. Arenton et al., Phys. Rev. **D 25** (1982) 2241; S.V. Golovkin et al., Z. Phys. **A 359** (1997) 435.

[22] A. Sibirtsev, Nucl. Phys. **A 604** (1996) 455; A. Sibirtsev, W.Cassing, Eur. Phys. J. **A 7** (2000) 307.

[23] W.S. Chung, G.Q. Li, C.M. Ko, Phys. Lett. **B 401** (1997) 1.

[24] A.I. Titov, B. Kämpfer, V.V. Shklyar, Phys. Rev. **C 59** (1999) 999.

[25] K. Nakayama, A. Szczurek, C. Hanhart, J. Haidenbauer, J.Speth, Phys. Rev. **C 57** (1998) 1580.

[26] K. Nakayama, J.W. Durso, J. Haidenbauer, C. Hanhart, J. Speth, Phys. Rev. **C 60** (1999) 055209.

[27] K. Nakayama, contribution to these proceedings.

[28] G. Schepers et al., *Study of ω and Φ production at COSY–11*, COSY Proposal No. 78, Nov 1998.

[29] S. Brauksiepe et al., Nucl. Instr. & Meth. **A 376** (1996) 397.

[30] C. Quentmeier et al., Phys. Lett. **B 515** (2001) 276.

[31] A. Khoukaz, contribution to these proceedings.

[32] G. Fäldt, C. Wilkin, Z. Phys. **A 357** (1997) 241.

[33] G. Schepers, D. Grzonka, contribution to these proceedings.

First ideas for experiments beyond 'COSY–11'

D. Grzonka

Institut für Kernphysik, Forschungszentrum Jülich, Germany

Abstract: A possible direction for long term future activities of the COSY–11 collaboration is given. For the continuation and extension of the studies performed at COSY–11 a new internal facility with detection systems for charged and neutral particles is needed.
A few reaction channels are briefly discussed to demonstrate the need for such a new facility.

1 Introduction

COSY–11 was designed as a first generation experiment for threshold studies. There is no doubt that it worked successfully, however, due to the usage of the dipole magnet as a spectrometer the gap hight limits the geometrical acceptance. At Q-values of a few MeV, depending on the reaction channel, the efficiency decreases to the percent level which prevents COSY–11 from performing some relevant and interesting experiments of the physics goal of COSY–11 within a reasonable beam time when exceeding the threshold region. In such situations very often the desire for a new facility came up, something called 'Super COSY–11', a new internal facility incorporating the advantages of the present COSY–11 installation but increasing the capability to measure with high precision interesting channels in an intentional exclusive way.

2 General motivation for a new facility

The recent precise data from COSY and other machines in the medium energy regime have triggered a lot of theoretical activities in this field. Much more work has to be done on the theoretical side but also further dedicated complementary experimental results are needed to support or to reject particular considerations.

In various reaction channels it became clear that more differential observables like angular or Dalitz plot distributions and more selective studies concerning the spin and isospin degrees of freedom are necessary to distinguish between different model descriptions.

To perform such studies within reasonable beam times a detection system with a full solid angle coverage also at higher excess energies is required. Additionally to charged particles also γ's and neutrons have to be detected in this new facility. This will make more exclusive measurements posssible. The missing mass technique presently used at COSY–11 is limited to reaction channels with only one unobserved particle and has the disadvantage of an unavoidable physical background. For example the study of η and η' meson production would result in much cleaner event samples if an event tag would be possible with the decay γ's.

3 Examples of reaction channels

There are a lot of interesting reaction channels for such a new facility. One important topic is the strangeness production where the Λ/Σ hyperon studies could be continued. This programme will of course include the investigation of the excited hyperons $\Lambda(1405)$ and $\Sigma(1385)$ whose structure is presently under discussion. Of course the meson production would be continued attaching importance to the vector meson production and detailed studies of the broad $f_0(980)$ and $a_0(980)$ resonances or mesonic states. Also for investigations of the again broad nucleon resonances the detection of charged and neutral decay particles in a 4π system would allow detailed analyses.

To be more specific at least a few reaction channels for which such a new facility is needed have to be briefly discussed.

3.1 Hyperon production

The hyperon production in the reaction channels $pp \to pK^+\Lambda$ and $pp \to pK^+\Sigma^0$ has been measured at COSY–11 close to threshold [1, 2], and at higher excess energies at the TOF spectrometer [3]. Besides total cross section data partly also angular and Dalitz plot distributions as well as polarisation observables have been extracted.

Nevertheless more data are needed to develop appropriate theoretical models for the description of the hyperon production. As an example let's take the measured cross section ratio of Λ/Σ production with the unexpected high value of about 28 close to threshold compared to the value 2-3

at high excess energies [2]. This could be explained in terms of a destructive interference between K and π exchange amplitudes [4] but also alternative approaches are available [5, 6] which base on other exchange mesons including nucleon resonances. The measurement of other isospin components in the reaction channel $NN \to NKY$, like $pp \to p\Sigma^+K^0$, could clarify the situation. The identification of the Σ^+ and the K^0 via their main decay channels ($\Sigma^+ \to p\pi^0$, $n\pi^+$, $K^0 \to \pi^+\pi^-$, $\pi^0\pi^0$, $\pi^+\pi^-\pi^0$) requires the detection of γ's and neutrons.

Furthermore by controlling the spin degrees of freedom more detailed informations of the reaction mechanisms are accessible. For instance the spin transfer coefficients show a different behaviour if pion or kaon exchange is dominant [7].

3.2 Elastic Λp scattering

The theoretical description of the hyperon production needs a good knowledge of the hyperon–nucleon interaction as a basic input for the calculations. The elementary NN ineraction is well known due to the extended data base of the elastic NN interactions but for the YN interaction the situation is much worse due to the rather limited data set. Partly data on the YN system are accessible via Dalitz plot analysis of a 3 body exit channel like $pp \to pK^+\Lambda$ but the production mechanism disturbs this information by filtering certain partial waves. The direct study of the YN elastic scattering would be the optimum approach to a YN data base. Unfortunately a direct hyperon beam is not available and the lifetime of hyperons is rather short. Therefore an experimental access to YN elastic scattering data has to be a sequence of hyperon production e.g. $pp \to pK^+Y$ with a subsequent use of the produced hyperon as a beam particle hitting another nucleon $Yp \to Yp$. For a Λ hyperon with its $c\tau$ of 7.89 cm such a sequence could be performed with a spatially separated second target with useful reaction rates. A sketch of the setup is given in fig. 1. A rough estimate using reasonable numbers for cross sections, luminosity and detection efficiency gives event rates of about 100 per hour. Therefore a dedicated setup could allow such studies at an internal target experiment at COSY but for more precise statements a detailed treatment has to be done including a check if an external target station would be more suitable.

These studies require high resolution tracking systems with large acceptance close to the target.

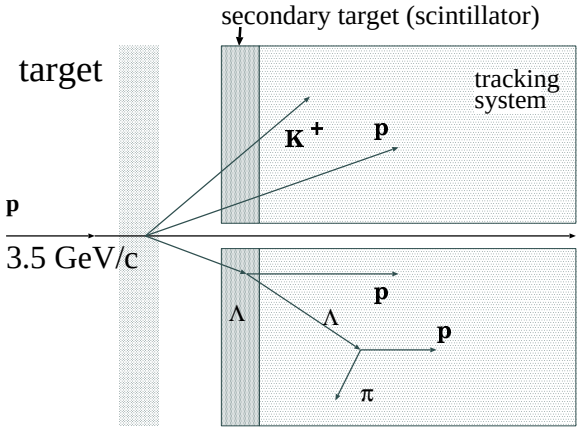

Figure 1: Sketch of the experimental setup to measure Λp elastic scattering.

3.3 Vector meson production

Another field of actual interest is the vector meson production (ρ, ω, Φ). For low Q-values ($\leq 100\,\mathrm{MeV}$) some data are available for the pp induced ω and Φ production from measurements at SATURNE [8, 9] and COSY–TOF [10]. An extension of the data base for vector meson production is desirable for the understanding of the reaction mechanism and the extraction of the NNV coupling constants.

By detecting the decay products of the vector mesons a high selectivity and background reduction is achievable. The production of the ρ meson with its two pion decay could be well distinguished from the ω production with the dominant decay chanels $\omega \to \pi^+\pi^-\pi^0$ and $\omega \to \gamma\pi^0$. Also here a γ detection system is required to perform detailed analyses.

4 Concept of the new facility

The measurements of all the Λ/Σ hyperon channels including their decay channels, as well as detailed studies of the vector meson production require a detection system with the general feature of measuring charged and neutral particles with a close to full solid angle coverage in the laboratory system. Up to now such a system is not existing at COSY. For the future of the experimental studies at COSY such a new internal detection system is strongly required. Without going into detail the new facility has to include: polarized $\vec{H}$ ($\vec{D}$) target, tracking detectors (Si-μstrip, drift chambers, scintillating

fibres), magnetic field, scintillator hodoscopes, γ detector, neutron detector and, depending on the proposed studies further special components for dedicated studies like $\Lambda p \to \Lambda p$. To simplify the determination of polarisation observables the setup has to be rotationally symmetric.

In general there is no doubt that a high acceptance detection system for charged and neutral particles is necessary for the future of COSY. But to make this point more clear the proposal for such a facility should include a few topics like the hyperon and vector meson production with a very detailed consideration of the physics. Therefore the first step towards a 'SUPER COSY–11' is the preparation of a detailed physics programme which clearly shows the need for such a facility before we go into detail concerning the detection system.

References

[1] J. Balewski et al., Phys. Lett. **B 388** (1996) 859, J. Balewski et al., Phys. Lett. **B 420** (1998) 211, J. Balewski et al., Eur. Phys. J. **A 2** (1998) 99.

[2] S. Sewerin et al., Phys. Rev. Lett. **83** (1999) 682.

[3] R. Bilger et al., Phys. Lett. **B 420** (1998) 217.

[4] A. Gasparian et al., Phys. Lett. **B 480** (2000) 273.

[5] A. Sibirtsev et al., e–Print Archive: nucl-th/0004022 (2000).

[6] R. Shyam, G. Penner, U. Mosel, Phys. Rev. **C 63** (2001) 022202.

[7] F. Balestra et al., Phys. Rev. Lett. **83** (1999) 1534.

[8] F. Balestra et al., Phys. Rev. **C 63** (2001) 024004.

[9] F. Hibou et al., Phys. Rev. Lett. **83** (1999) 492.

[10] S. Abd El–Samad et al., Phys. Lett. **B 522** (2001) 16.

Future Aspects of Physics at COSY

W. Oelert

Institut für Kernphysik, Forschungszentrum Jülich, Germany

Abstract: At the extended collaboration meeting of the COSY–11 experiment I would like to present a comprehensive but brief summary of physics which could be done out of the tradition of the COSY–11 activities. It is obvious that the discussion gets the more ambiguous the more I try to talk about the far future. I hope I can convince you that COSY and COSY-11 produced creditable results and in fact, do have a stake in the future.

The success of physics at COSY is largely due to input from different persons, institutions and agencies. We would not have the success we are having if there would not be the strong support from the COSY staff, the Forschungszentrum Jülich infrastructure and directorates, the International Büro of the BMBF, the Verbundforschung of the BMBF and last not least the active collaborations between different partners. One of those partners are the people from the Cracow institutions both from the Institute of Physics of the Jagellonian University and from The Henryk Niewodniczañski Institute of Nuclear Physics.

The success of the COSY–11 experiment is documented in eleven publications, four papers in Nucl. Instr. & Meth., eight Diploma – and eight PhD – theses as well as one Habilitation [1].

The physics of COSY–11 centers around i) open strangeness production at threshold via the reactions: $pp \to pK\Lambda/\Sigma$ and $pp \to ppKK$ and ii) flavour neutral meson production at threshold in p–p and p–d or d–p scattering. In addition, first initiatives with a polarized proton beam seem to show very promising results. Neutron induced measurements are under preparation.

Still let me remind you that since its beginning of first experiments in April 95 COSY–11 used 278 days (3/4 of a year) of beam time which means lots of effort from the accelerator crew, the funding agencies, the Research Centre Jülich and the COSY–11 collaboration members themselves.

As a consequence I would like to stress that our research is very expensive. We certainly should be aware of that and each member of the collaboration should somehow draw his own conclusions. I myself would suggest that such conclusions are:

- Not every thing that can be measured should be measured, we need good reasons for doing what we do. We should want what we want.
- We should realize what we can do and should not waste time with things undoable for us.
- We should ask ourselves whether the understanding of physics profits from our particular experiment, whether we – or at least somebody else – can interpret the results of our experiment.
- If we decided to do something, we should do it right, professionally and up to date.
  We should be excited, we should be convinced and – after all – we should have fun in what we are doing.

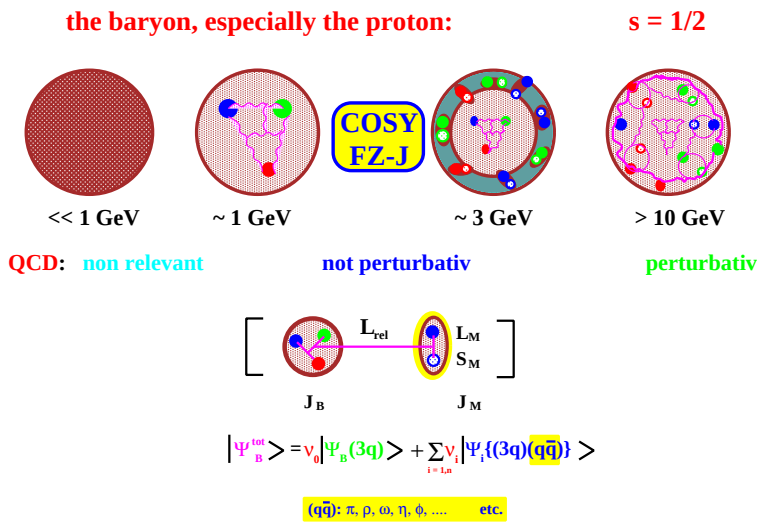

Figure 1: Simple picture of the structure of the nucleon at different energies.

Experiments at and with the proton is the main framework of physics at COSY–11.

At low–energy scattering (short wavelength, $\lambda \approx$ R) the proton looks like a diffuse charged object with a radius of about R = 1 fm and no internal structure visible. At high energy-scattering ($\lambda \ll$ R) the sub–structure of the proton is obvious, charge distributions and structure functions can be determined and separated in contributions from valence– and sea–quarks.

COSY — with its momentum at 3 GeV/c ($\lambda \approx 0.1$ fm) — is just the intermediate link between the two extreme regions of particle or nuclear physics at high– and low–energy scattering, as schematically demonstrated in figure 1. Especially the energy range of COSY makes it rather questionable, whether COSY is the right place to contribute to the physics of glueballs, which is done nowadays at several places. Further, since the glue couples strongly to $\bar{q}q$ pairs their signature is by far not easy to be understood. However, I would like to stress the possibility of effects from glue which might be identified at COSY.

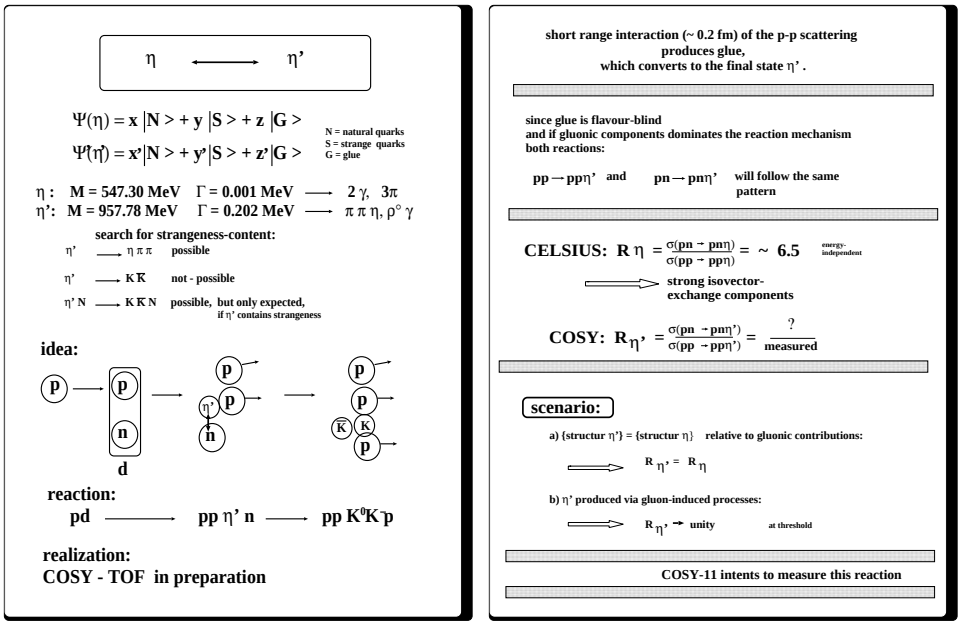

Figure 2: Two suggestions for investigations to follow the question of the η and η' content.

With figure 2 I remind you of two suggestions — which resulted in accepted proposals at COSY — which have the aim of determining the structure of the not yet understood content of the η and especially the η' mesons.

The left side of the figure is a suggestion from TOF (E. Roderburg et al.). The aim is to study the decay of η' into two K-mesons. Since the mass of the η' is too low to do so in a free decay the recoil on the neutron of the deuteron target must be used. Strong indications of a strangeness content are given, if an η' decay into two K-mesons would be observed.

At the right side of figure 2 I repeat the suggestion of COSY–11 (P. Moskal et al.) based on a publication of Bass, Wetzel und Weise [2] where the ratio of η' production on the neutron *vs.* the one on the proton should give indications of the gluonic content of the η' meson. If it is identical or close to the respective ratio of the η production (which has been extracted from measurements at CELSIUS, at COSY and at SATURNE and results in a value of $R_\eta = 6.5$) then η and η' are supposed to have very similar structures. If, however, the ratio approches unity, gluonic components might be responsible for this observation due to the flavour blindness of gluons.

SU(4) - multiplets:

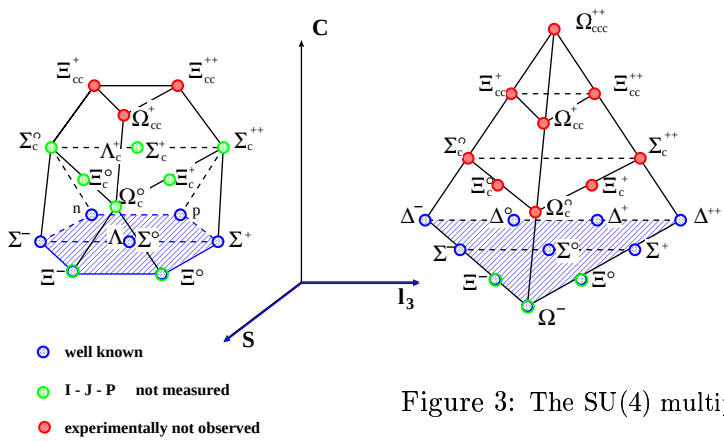

Figure 3: The SU(4) multiplets of the baryon.

Beside these activities I regard the investigations of COSY–11 concerning the open strangeness as very important for many considerations in particle physics and astronomy. Let me point out explicitly the studies of the lowest possible energy channel $pp \to ppK^+K^-$ where exciting results approach as well as the surprisingly different cross section at threshold for the Λ and Σ^0 production. Here further studies have to be done and COSY–11 certainly has an interesting future for the upcoming years. Lots of theoretical papers were initiated by this research.

Additional reaction channels, which are complementary and therefore serve for the systematic interpretation should be given here without further comments, COSY–11 knows about the difficulty of doing such experiments but the collaboration has the chance to study at least some of them:

$$pp \to nK^+\Sigma^+, \qquad pp \to pK^0\Sigma^+, \qquad pp \to nK^+K^+\Xi^0,$$
$$pd \to dK^+K^+\Xi^-, \quad pd \to pK^+K^+\Xi^-n, \quad pd \to nK^+K^+\Xi^0n.$$

Especially in view of the poorly known excited states of baryons, see figure 3, the not yet analysed excitation of the interesting $\Lambda(1405)$ baryon resonance awaits to be done.

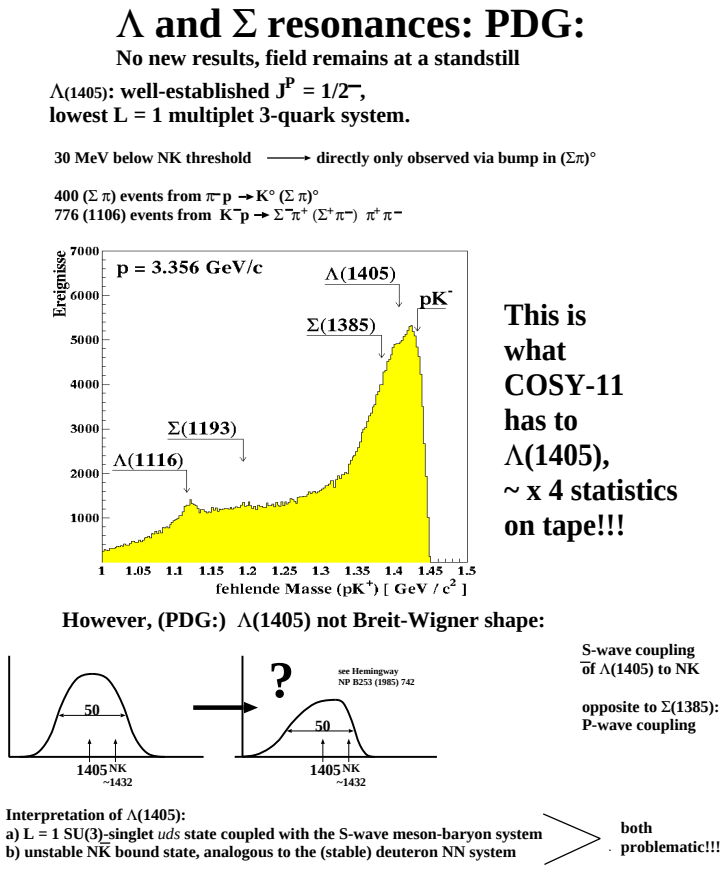

Figure 4: Information on the exitation of the $\Sigma(1385)$ and $\Lambda(1405)$ taken by COSY–11.

COSY–11 took such data — see figure 4 — as a by–product from the intensive $pp \to ppK^+K^-$ investigations. The collaboration has information on tape which should be looked at carefully since it is interesting physics.

As mentioned already I think that COSY–11 and most of the other experiments at COSY will have a brilliant future continuing their present program and concentrating on essential physics questions to be answered.

But how about the future five years from now? Here the COSY community should not worry since the Research Centre Jülich just decided i) to build a new injector for COSY that should improve the present beam features by an order of magnitude, especially for the polarized beam and ii) to re–open the positions of two directors from the IKP. These are clear signs that we can count on further support of the FZ Jülich – a lucky situation! In the copy of the transparency (figure 5) — which is marked by my name since it is my personal view point and not an official statement — I try to give a possible scenario of what might be happening in the medium range future at COSY–Jülich.

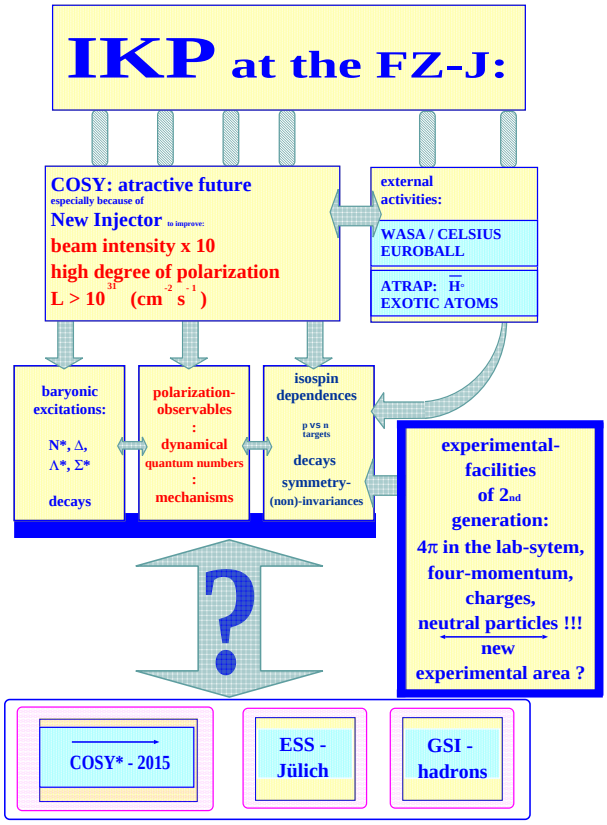

Figure 5: Personal view of the possibilities of the near and far future of COSY and IKP.

By far the strongest and most intensive activity of the IKP — and the cooperating external institutes — is at COSY. During the build–up of the new injector we will have the chance to complete our studies on threshold production and strangenes dissociation. Having the injector in operation a new area will start, where I personally see the following three topics as interesting physics:

- Study of baryonic excitations as: $N^*, \Delta, \Lambda^*, \Sigma^*$ and their decays.
- Determination of dynamical quantum numbers in experiments with polarized beams.
- Isospin dependences and symmetry braking investigations.

All these topics are fundamental questions of todays physics. But we should be aware of the fact that such experiments need experimental facilities of the second generation which in turn needs ideas, innovations, enthusiasm of people and after all money. The present experimental facilities at COSY have all their specific advantages but do not serve for all information needed. We do have the — at least nearly — 4π detectors EDDA and TOF but they have no charge determination and no neutral particle identification; we do have COSY–11, ANKE and Big Karl but they are far from being a 4π detection system for both charged and neutral particles. A second generation facility should overcome these lacks of experimental information for all observables of a reaction. Certainly there are lots of examples of detection systems which would provide such capability, however, based on the principle design of COSY–11, which was extended to the facility ANKE, I dream of two essential changes as depicted in figure 6:

- the target area should be totally surrounded by detection systems, which appears to be feasible using modern micro–detection systems, and
- change of the magnet to a "scintillating magnet" by replacing each other iron sheet to a scintillator sheet and read them out in groups via photomultipiers.
  This suggestion certainly needs a lot of R & D work in order to construct a realistic calorimeter, but it might be worth trying so — at least.

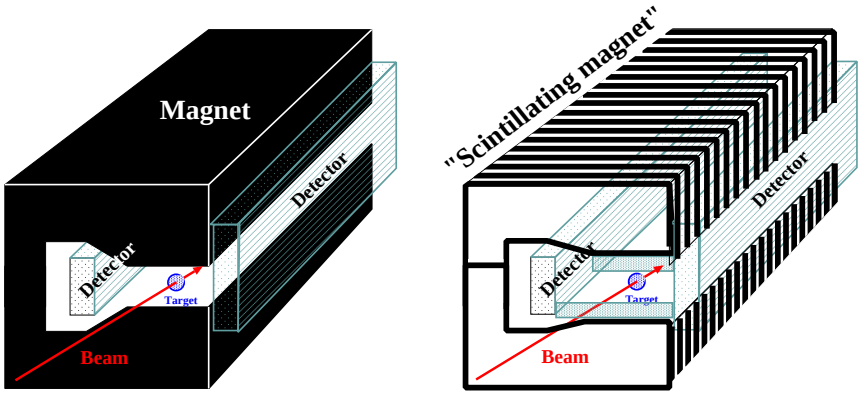

Figure 6: Suggestion for a "Scintillating Magnet".

Coming back once more to my view point of the IKP within the FZ Jülich, as shown in figure 5, I would like to draw your attention to the far future. The FZ Jülich is applying to be the host of a new European Spallation Source (ESS) and the GSI wants to build a new wide ranged hadron facility. Both are developments which should be of great interest to us, though the profile of the IKP will certainly change if one or even both of these events will happen.

At the ESS new physics can be invented, different from our present work, but interesting in the sense that Jülich could probably contribute to the active field of neutrino physics. I am not at all an expert in this field, but talking to experts I see here a certain exciting possibility.

If — on the other hand — GSI will succeed in getting a new hadron facility lots of physics which presently is been done at COSY and which has been done by many physicists of the COSY community at the low energy antiproton ring (LEAR) — which is closed down since the end of 1996 — can be continued and further developed at this wonderful machinery.

And COSY and the hadron physics at Jülich?

Would it not be thinkable, that — after the decisions on possible new facilities at Jülich and GSI — there is room for a new COSY*, with proton beam momenta in the range of 25 GeV/c? As pointed out, for the near future the physics at COSY is on a safe ground. In the far future — say around the year 2015 — a new accelerator should be realistic, if hadron physics should continue at Jülich.

I will not go in detail here what could be done with such kind of facility. In my presentation I mentioned several possibilities and showed yet not published but very interesting results of the PS185 collaboration using the antiproton beam at LEAR with a polarized target. These data are especially interesting since they indicate that none of the present theoretical predictions are able to reproduce the observations made. A challenge for new interpretations. A challenge for us to continue on this road of physics with polarization and spin structure observables.

At the end, I would like to mention explicitly the exciting physics case of producing simultaneously systems of three strange–quarks and three anti-strange-quarks [3].

		Q-value [GeV/c]	
$\bar{p}p \longrightarrow$	$\bar{\Omega}\Omega$	4.9	Ω: {sss}
$pp \longrightarrow$	$\bar{\Omega}\Omega$ pp	13.6	
$pp \longrightarrow$	$\Phi\Phi\Phi$ pp $\Phi\Phi\omega$ pp $\Phi\omega\omega$ pp	12.0	Φ: $\{\bar{s}\, s\}$
	$\omega\omega\omega$ pp	8.5	ω: $1/\sqrt{2}$ $\{\bar{u}u + \bar{d}d\}$

$\Omega\,\bar{\Omega}$ *vs* $\phi\phi\phi$		
content:	3 x s plus 3 x $\bar{s}$	3 x $s\bar{s}$
mass:	2 x 1.672 = 3.344 GeV/c²	3 x 1.020 = 3.060 GeV/c²
Isospin:	0	0
J:	2 x 3/2 → 0, ..., 3	3 x 1 → 1, ..., 3

Figure 7: On the difference between the $\Omega\bar{\Omega}$ and the $\Phi\Phi\Phi$ systems.

These six quarks can either form an $\Omega\bar{\Omega}$ system with mass 3.345 GeV/c^2 or a three ϕ–meson system with mass 3.058 GeV/c^2. Two systems with very similar masses. From results of PS185 we would infer that the two $J^P = 3/2^+$ $\Omega\bar{\Omega}$ objects will be created in a totally spin symmetric way. We can learn a lot if we measure the spin correlation of the three $J^P = 1^-$ ϕ–mesons.

Let me stop at this point. I hope I could convince you that it is to a large extent in our hands to continue with the exciting, interesting and innovative physics. We should continue to be as productive as we have been during the past years, we should want what we want. We have good and serious indications and proofs that the Research Centre Jülich further supports our activities. We have extraordinary support from our funding agencies, especially from the "Internationales Büro des BMBF an dem DLR" and we have a very good collaboration with our friends here in Cracow.

We thank the Jagellonian University for the sanction of our activities and the support given to the physicists of the Physics Institute.

We thank our Cracow colleagues and friends for their great hospitality. In this spirit I would like to close with a picture I showed already at several occasions, which shows that COSY and our work at COSY–11 combines Cracow and Jülich.

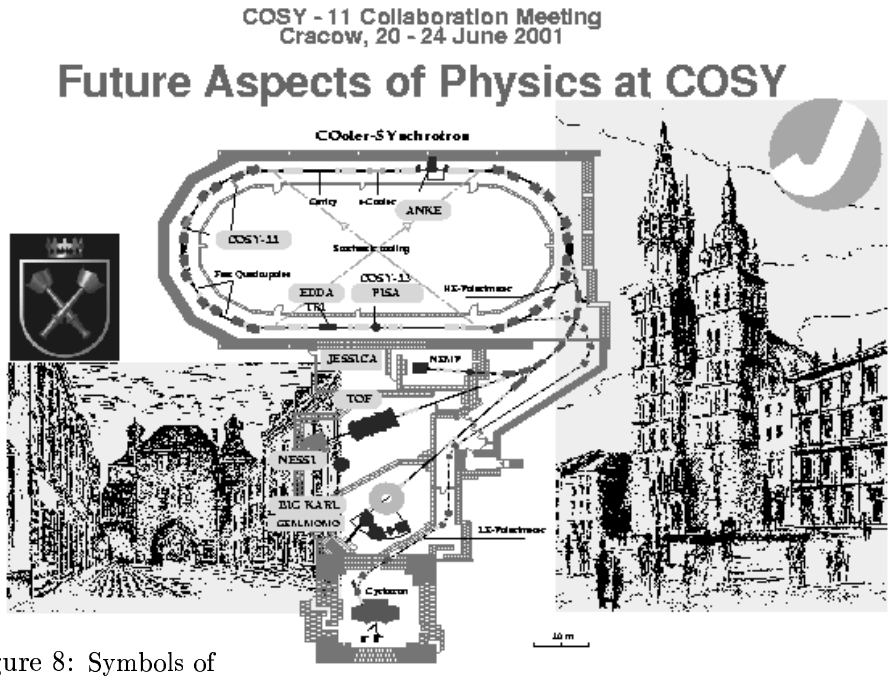

Figure 8: Symbols of Cracow (city and Jagellonian University) and Jülich (city and Research Centre) around COSY.

References

[1] COSY–11 Collaboration, see COSY–11 Home Page please: http://ikpe1101.ikp.kfa-juelich.de.

[2] S.D. Bass, S. Wetzel, W. Weise, Nucl. Phys. **A 686** (2001) 429.

[3] W. Oelert, Nucl. Phys. **A 639** (1998) 13c.